

CRUSTAL STRUCTURE ALONG THE CENTRAL SUNDA MARGIN, INDONESIA

Dissertation

zur Erlangung des Doktorgrades
der Mathematisch-Naturwissenschaftlichen Fakultät
der Christian-Albrechts-Universität zu Kiel

vorgelegt von

Heidrun Kopp

Kiel, 2001

Referent: Prof. Dr. E. R. Flüh
Koreferent: Prof. Dr. W. Rabbel
Tag der mündlichen Prüfung: 14. Mai 2001

Zum Druck genehmigt: Kiel, den

Der Dekan
gez. T. Bauer

TABLE OF CONTENTS

ABSTRACT

ZUSAMMENFASSUNG

1	INTRODUCTION	1
2	TECTONIC EVOLUTION OF WESTERN INDONESIA	5
3	CENOZOIC ARC-TRENCH SYSTEM	11
3.1	Oblique to Frontal Subduction	11
3.2	Lower Trench Slope Morphology	15
3.3	Seismotectonics of the Sunda Arc	18
4	CRUSTAL STRUCTURE OF THE JAVA MARGIN FROM SEISMIC WIDE-ANGLE AND MULTICHANNEL REFLECTION DATA	27
4.1	Introduction	27
4.2	Geodynamic Setting	28
4.3	Seismic Data	29
4.3.1	Modelling	34
4.4	Interpretation	37
4.4.1	OBH Profile SO138-05 And Coincident MCS Profile SO137-03 ...	37
4.4.2	OBH Profiles SO138-06 And SO138-07	43
4.4.3	Gravity Modelling	53
4.5	Discussion	54
4.5.1	Oceanic Crust	54
4.5.2	Structure of the Accretionary Domain And Outer High	55
4.5.3	Forearc Domain	57
4.6	Conclusions	58

5	CRUSTAL STRUCTURE OF THE CENTRAL SUNDA MARGIN AT THE ONSET OF OBLIQUE SUBDUCTION	63
5.1	Introduction	63
5.2	Geodynamic Setting	65
5.3	Seismic Data	66
5.4	Interpretation	77
	5.4.1 Sumatra Transect	77
	5.4.2 Strike Lines SO138-02 And SO138-03	84
	5.4.3 Sunda Strait Transect	87
	5.4.4 Gravity Modelling	92
5.5	Discussion	95
	5.5.1 Igneous Oceanic Crust And Subducted Plate	95
	5.5.2 Structure of the Accretionary Domain And Outer High	99
	5.5.3 Forearc Domain	100
5.6	Conclusions	102
6	BSR OCCURRENCE ALONG THE SUNDA MARGIN AND ITS LINKAGE TO FLUID FLOW: NEW INSIGHTS FROM THE GINCO AND RAMA PROJECTS	107
6.1	Introduction	107
6.2	Possible Methane Sources And BSR Formation	107
6.3	The RAMA Data Acquisition	108
6.4	Interpretation	109
6.5	Discussion And Conclusions	113
7	TRANSTENSIONAL BASINS IN THE SUNDA STRAIT	119
7.1	Introduction	119
7.2	Geodynamic Setting	122
7.3	Morphology of the Sunda Strait Graben From High Resolution Bathymetry	123

7.4	Stratigraphy of the Upper Sediment Layers	124
7.5	OBH Profile SO138-08	124
7.6	Discussion And Conclusions	126
8	DISCUSSION AND CONCLUSIONS.	129
	APPENDIX A: MCS SEISMICS.....	i-x
	APPENDIX B: MINISTREAMER DATA	i-iii

ACKNOWLEDGEMENTS

CURRICULUM VITAE

ABSTRACT

The Sunda collision zone marks the eastern boundary of the Indian ocean along the Indonesian archipelago, where oceanic crust is subducted beneath the islands of Sumatra and Java. Collision along this accretionary margin is orthogonal off Java and increasingly oblique off Sumatra, giving rise to the Sumatra and Mentawai strike-slip faults.

A grid of seismic reflection and refraction profiles was acquired across the subduction zone and within Sunda Strait and the forearc region. A combined interpretation of these data sets for the first time provides an exact structural model of the subduction complex. The interpretation of the wide-angle data is based on a forward-modelling technique, incorporating geological information gained from the time-migrated sections of the multichannel seismics. A number of additional geophysical methods were employed to sustain the results gained from the seismic data, including gravity modeling, synthetic data generation, and bathymetric data interpretation.

The interpretations presented in this work allow to draw a detailed structural image of the margin. The main structural features forming the margin include an active frontal accretionary prism, a well-developed outer high and a distinct forearc basin. Seismic velocities of the outer high are moderate to a depth of more than 15 km, clearly indicating a sedimentary composition, which has long been debated.

These structural units are recognized on all dip lines crossing the collision complex. They are not significantly influenced by the increasing subduction obliquity, as believed previously, but develop from the presence of a core buttress, which underlies the forearc domain. This region of increased rock strength compared to the material found seaward of it is for the first time recognized in the domains of frontal and of oblique subduction of the Sunda margin and represents the main factor causing the evolution of the forearc structures. In addition, the nature of the forearc basin basement off Sumatra and off Java, which has long been enigmatic, is established from the seismic and modeling results: Continental crust is underlying the basin off Sumatra, whereas off western Java the underlying crust displays a more oceanic nature, as is supported by gravity and synthetic data modeling. The configuration of the descending plate underneath the subduction zone is documented to a

depth of more than 35 km by the refraction data, indicating an increasing slab dip from Sumatra to Java.

Additional investigations of Sunda Strait which marks a physiographic and tectonic break at the point of directional change of the subduction zone, reveal its close connection to the convergent setting of the adjacent arc. An evolutionary model for the past 5 Ma has been developed from the seismic and bathymetry data, revealing the transtensional nature of the basin found in prolongation of the dextral Sumatra fault.

ZUSAMMENFASSUNG

Die Sunda Konvergenzzone bildet die östliche Grenze des Indischen Ozeans entlang des indonesischen Archipels, längs derer aktive Subduktion unter Sumatra und Java stattfindet. Die Plattenkollision verläuft orthogonal vor Java und weist einen zunehmenden Schrägheitsgrad vor Sumatra auf, aus dem die Sumatra- und Mentawai-Transformstörungen resultieren.

Ein Netz von reflexions- und refraktionsseismischen Profilen wurde über der Subduktionszone, sowie innerhalb der Sunda-Straße und des benachbarten Forearc-Bereiches gewonnen. Eine kombinierte Interpretation dieser Datensätze liefert zum ersten Mal ein exaktes Strukturmodell des Subduktionskomplexes. Die Interpretation der Weitwinkeldaten basiert auf einer Vorwärtsmodellierung, die sich auf geologische Horizonte, die in den Steilwinkeldaten identifiziert wurden, stützt. Eine Anzahl weiterer geophysikalischer Methoden, unter anderem Schweremodellierungen, das Erstellen synthetischer Daten, sowie die Interpretation der gewonnenen Meeresbodenbathymetrie, wurde angewandt, um die Ergebnisse, die aus den seismischen Daten gewonnen wurden, auf ein breites Fundament zu stellen.

Die hier erarbeiteten Interpretationen erlauben ein detailliertes strukturelles Abbild der Plattenränder vorzustellen. Die strukturellen Hauptkomponenten der Plattengrenze bestehen aus einem aktiven frontalen Akkretionsprisma, einem mächtigen Äußeren Hoch ('Outer High') und einem deutlich ausgebildetem Forearc-Becken. Die relativ niedrigen seismischen Geschwindigkeiten des Outer Highs bis in Tiefen von 15 km deuten klar auf einen sedimentären Aufbau hin, der bisher umstritten war.

Diese Strukturkomponenten sind im Bereich der gesamten Kollisionszone anzutreffen, wie durch die Linien über den Kollisionskomplex dokumentiert ist. Sie sind hingegen der bisherigen Annahmen nicht maßgeblich durch den erhöhten Schrägheitsgrad der Subduktion beeinflusst, sondern bilden sich aufgrund eines sogenannten 'Core Buttress' aus, das dem Forearc-Bereich unterliegt. Diese Region der im Vergleich zum seewärtigen Material erhöhten Gesteinsstärke konnte zum ersten Mal in den Bereichen frontaler und schräger Subduktion des Sunda-Bogens bestimmt werden und somit auch der Hauptfaktor

für die Entstehung der Forearcstrukturen. Zusätzlich wird aus den seismischen und Modellierungsergebnissen erstmals der lange umstrittene Aufbau des Grundgebirges unterhalb des Forearc-Beckens vor Sumatra und vor Java deutlich: Kontinentale Kruste bildet die Basis des Forearc-Beckens vor Sumatra, während die Kruste im analogen Bereich vor West-Java einen ozeanischen Charakter aufweist, wie durch die Schweremodellierung und die synthetischen Daten bestätigt wird. Die Geometrie der abtauchenden Platte unterhalb der Subduktionszone ist bis in über 35 km Tiefe durch die Refraktionsdaten dokumentiert, die eine erhöhte Plattenbiegung vor Java im Vergleich zu Sumatra aufdecken.

Die zusätzlichen Untersuchungen in der Sunda-Straße, die zwei unterschiedliche tektonische Regionen trennt, zeigen die enge Verbindung dieses Gebietes mit der konvergenten Tektonik des benachbarten Plattenrandes auf. Ein tektonisches Evolutionsmodell für die letzten 5 Millionen Jahre wurde aus den seismischen und bathymetrischen Daten entwickelt und basiert auf dem transtensionalen Charakter des Sunda-Grabens, der in Verlängerung der dextralen Sumatra-Störung liegt.

1. INTRODUCTION

Subduction zones continue to be of major interest to the Earth Sciences Community. This is partly due to their enormous potential for natural hazards, particularly in the form of earthquakes, tsunamis and arc volcanism. Convergent margins also serve as one end-member in a global perspective of the Earth's internal dynamics, as oceanic crust is destroyed here, whereas subduction accretion and arc magmatism are the main global processes responsible for continental crust formation. The Sunda margin subduction zone off western Indonesia (Figure 1.1) is suited particularly well for studying some of the key questions related to the mechanics and development during plate convergence because of significant lateral variations along the arc which also imprint the architecture of the system.

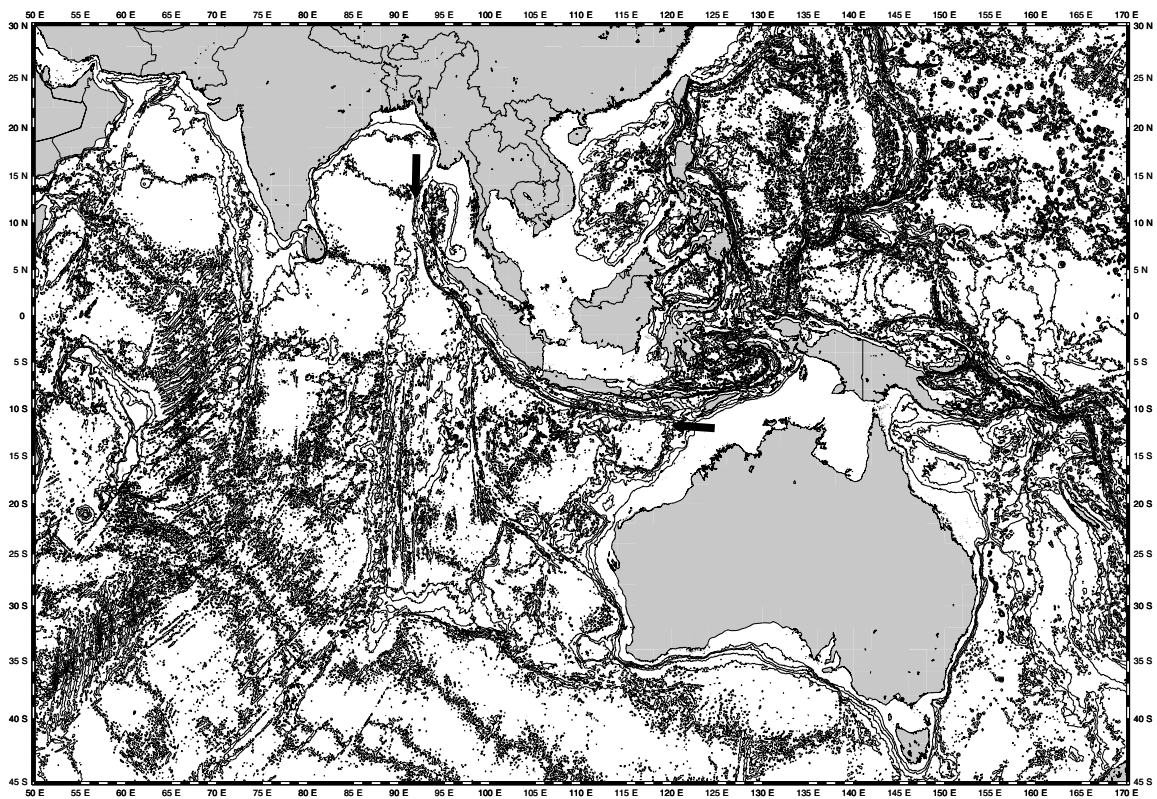


Figure 1.1: Bathymetric map of the Indian ocean and western Pacific. The Sunda margin runs along the islands of Sumatra and Java in Indonesia, as indicated by the arrows, and is characterized by a change in curvature of the trench, as is visible in the bathymetry.

The age of the subducting crust decreases from south-east to north-west, while the sedimentary cover increases in the same direction. One of the key elements within this area is the transition from orthogonal subduction off Java to an oblique collision off Sumatra. Initiation of strain partitioning along the oblique segment is manifested in the Sumatra strike-slip fault, which partially compensates the component of arc-parallel motion (possibly in conjunction with the offshore Mentawai fault zone). The transition between the frontal and oblique subduction regimes is believed to occur within Sunda Strait, causing extension expressed as transtensional basins above the downgoing plate.

Marine investigations of the Sunda trench and forearc region were carried out within the scope of the GINCO project. GINCO is an acronym for Geoscientific *IN*vestigations on the active *CO*nvergence zone between the East Eurasian and Australian Plates along Indonesia. The project aimed at investigating the geological structures of the margin in view of the lateral variation of subduction parameters along the transition zone from Java to Sumatra. A detailed knowledge of the crust and upper mantle was attempted to better evaluate geophysical and geological differences characterizing the various subduction regimes.

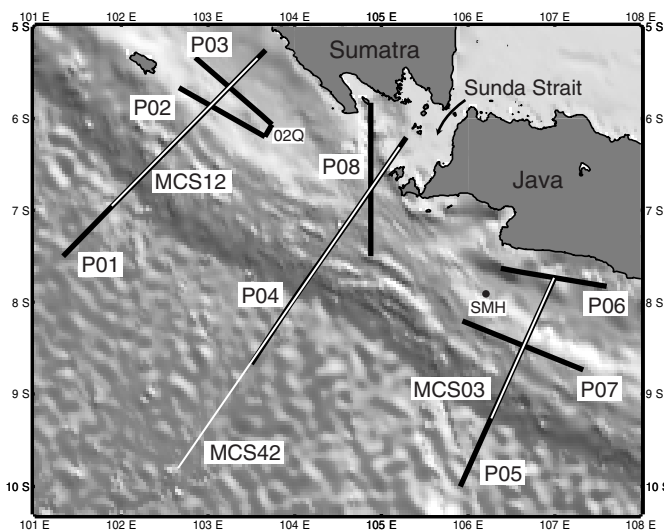


Figure 1.2: Location map of seismic profiles from the GINCO project discussed in this work. P01-P08 denote wide-angle seismic lines (black), along which ministreamer reflection data were recorded simultaneously. The three MCS lines (white) were acquired during a separate leg of RV Sonne. SMH shows the location of the Snail-and-Mussel Hill discussed in Chapter 6.

Three legs of the German RV SONNE (SO137, SO138, and SO139; Nov. 21, 1998 through Feb. 27, 1999) were dedicated to different geophysical methods; seismic data were acquired during the first two cruises and a location map of the lines presented in this work is shown in Figure 1.2. Leg SO137 focused on the collection of multichannel seismic reflection (MCS) data, of which 1015 profile km are discussed in this work. On cruise SO138, certain

profiles of the MCS survey were selected for coincident seismic wide-angle measurements during which 111 ocean-bottom hydrophones (OBH) and ocean-bottom seismometers (OBS) were deployed along 1860 profile km. During wide-angle data acquisition a ministreamer was also operated. The main tasks of the third leg (SO139) comprised geological and geochemical analyses. High resolution bathymetry data were recorded during all legs, whereas magnetic and gravity data collection was restricted to the first two cruises (Beiersdorf, 1999; Flueh, 1999; Reichert, 1999).

Resulting from the unique geological and tectonic setting of the margin, three working areas were chosen for the GINCO project:

- off Java, where normal subduction is occurring
- off Sumatra, where strain partitioning induces a stretching of the forearc sliver and slip along the Sumatra fault system
- off and within Sunda Strait, which forms the juncture between these two subduction regimes.

Based on this regional distinction, the work presented here is structured into several parts:

A short overview of the tectonic evolution of the region precedes an introduction to the Cenozoic arc trench system. The current tectonic setting is investigated employing high resolution bathymetry data. A discussion of the local seismotectonics takes the 1994 Java and 2000 Sumatra earthquakes into consideration. Expanding this regional review, a detailed investigation of the two subduction regimes off Java and off Sumatra is presented in the form of two manuscripts comprising the next two chapters. An analysis of the distribution of bottom simulating reflectors or BSRs, which were detected in all three study areas, employs additional reflection seismic lines acquired by the Scripps Institution of Oceanography. These data were migrated at GEOMAR as part of this thesis and expand the study region to the margin off central Java. In the following chapter, a paper publication examines bathymetric and tectonic features of the Sunda Strait, which shed some light on its evolution.

The closing chapter discusses structural similarities recognized all along the margin and investigates their dependence on the existence of a core buttress identified in the refraction data.

An overview of the seismic data acquisition procedures, processing modules and data flow for the reflection data (MCS and Ministreamer) is given in the appendix. As the complete processing of the refraction data was conducted on board, the OBH processing is not discussed here but is documented in detail in the cruise report for leg SO138. A detailed description of the different processing steps during MCS data processing, including an analysis of the multiple suppression approach employed, is given in Appendix A.

Beiersdorf, H. (edt) and Shipboard Science Party, GINCO3 (SONNE Cruise SO-139): Geo-scientific investigations along the active convergence zone between the Eastern Eurasian and Indo-Australian Plates off Indonesia, *Cruise Report*, BGR, Hannover, 1999.

Flueh, E.R. (edt) and Shipboard Science Party, GINCO2 (SONNE Cruise SO-138): Geo-scientific investigations along the active convergence zone between the Eastern Eurasian and Indo-Australian Plates off Indonesia, *Cruise Report*, Geomar, Kiel, 1999.

Reichert, C. (edt) and Shipboard Science Party, GINCO1 (SONNE Cruise SO-137): Geo-scientific investigations along the active convergence zone between the Eastern Eurasian and Indo-Australian Plates off Indonesia, *Cruise Report*, BGR, Hannover, 1999.

2. TECTONIC EVOLUTION OF THE WESTERN INDONESIAN REGION

The evolution of the large tectonic units of the Indian ocean is well confined by seafloor-spreading isochrons (Müller et al., 1997). Much of the Indonesian region is however characterized by the interaction of several smaller lithospheric plates, the movement of which within the complex is not well constrained. Several continental terranes were identified in SE Asia (Metcalf, 1996), which are entirely allochthonous to central and northern Asia, although there is still some disagreement as to the number of terranes and their boundaries. Comparative studies of paleontology, paleomagnetism and stratigraphy suggest that the various pre-Cretaceous continental terranes were derived from Gondwanaland (Gasparon and Varne, 1995; Nishimura and Suparka, 1997). The evolution of Gondwanaland and Tethys during the Paleozoic and Mesozoic involved the rifting of continental slivers/fragments from northern Gondwanaland and their northwards drift and accretion, accompanied by the opening and destruction of the Tethys ocean system, to form proto-SE Asia (Fig. 2.1) (Metcalf, 1996). The continental terranes are bounded by sutures (representing former oceans), by narrow mobile belts or major fault zones (Fig. 2.2) (McCourt, 1996). The formation of present-day SE Asia involved the progressive suturing of terranes to each other during Late Paleozoic to Cenozoic times and their subsequent disruption, principally caused by the collision of India with Eurasia. The ages of sutures in SE Asia become younger to the south and south-east. It is generally agreed, as shown in Figure 2.2 after Metcalf (1996), that South Tibet, Burma, western Thailand, Malaysia and Sumatra reveal strong geological correlations and formed a geological province, the Sibumasu terrane, which is bounded to the west by the Shan Boundary Fault and the Andaman Sea basin and to the south-west by the Woyla suture in Sumatra (Audley-Charles, 1988; Hutchinson, 1989; Metcalf, 1996; McCourt, 1996). Its eastern boundary is formed by the Raub-Bentong suture in Peninsular Malaysia. The eastern boundary of Sibumasu in North Thailand and Burma is still not clear (Metcalf, 1996). Paleomagnetic data along with Gondwanaland faunas (Cambrian to Lower Permian) with NW Australian affinities on Sibumasu strongly suggest a NW Australian origin for the Sibumasu terrane (Metcalf, 1996; Nishimura and Suparka, 1997). The predicted paleolatitude for Sibumasu, if placed adjacent to NW Australia, would be about 40°S in the Late Carboniferous.

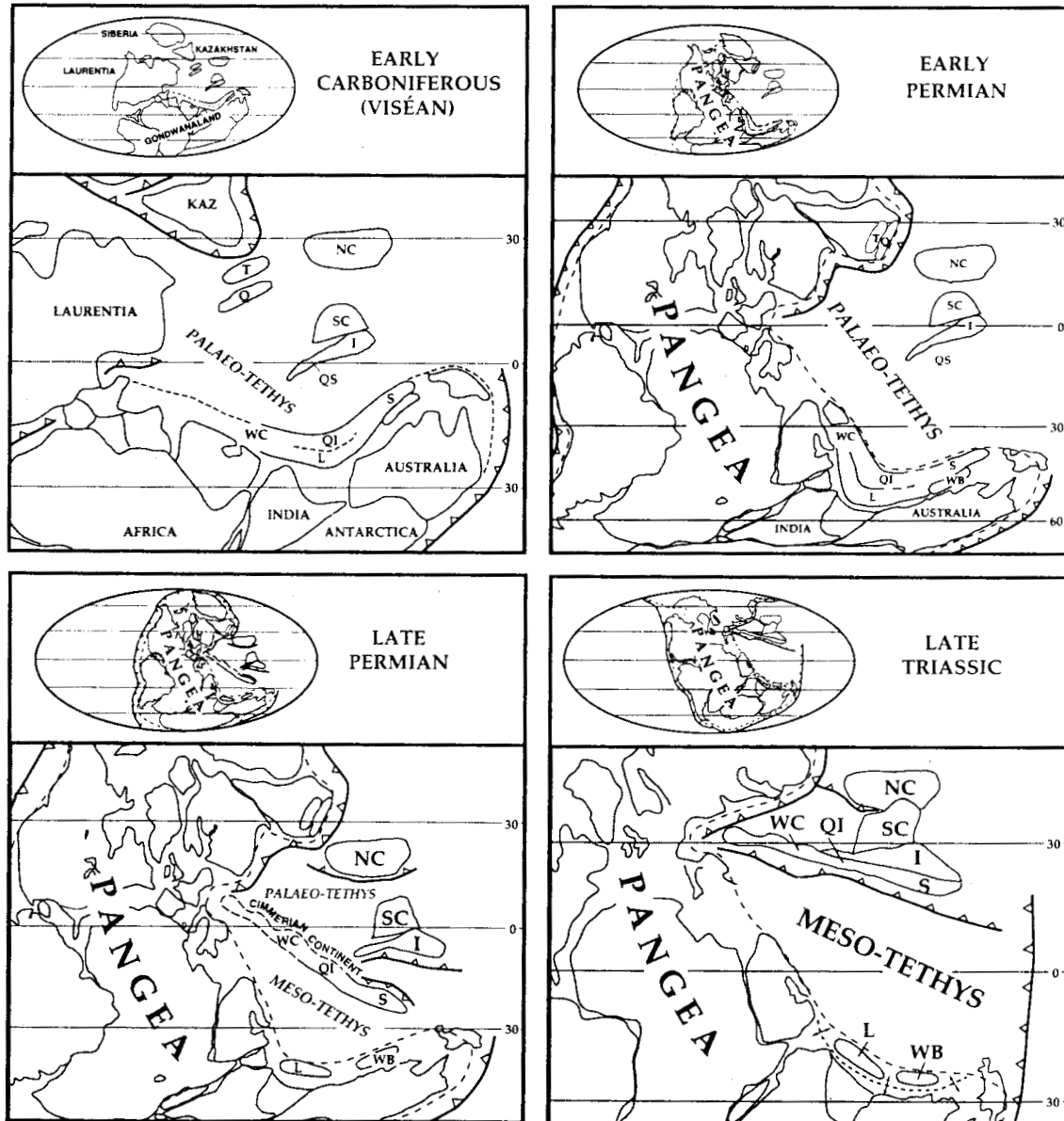


Figure 2.1: Paleographic reconstructions of the Tethyan region for Early Carboniferous, Early Permian, Late Permian and Late Triassic showing the postulated positions of SE Asian terranes. Present day outlines are for reference only. NC: North China, SC: South China, T: Tarim, I: Indochina, Q: Qaidam, WC: Western Cimmerian Continent, Qi: Quiatang, L: Lhasa, S: Sibumasu, WB: West Burma (from Metcalfe, 1996).

A major rifting phase occurred on the northern margin of Gondwana in the Early Permian (Fig. 2.1), as is indicated by the occurrence of calc-alkaline volcanics and granitic plutons of Permo-Triassic age (248-218 Ma), (Nishimura and Suparka, 1997). Paleomagnetic data indicate that Sibumasu travelled rapidly from southern to northern paleolatitudes in Permian times (Metcalfe, 1996), followed by collision of the Sibumasu Block with East Malaya along the Raub-Bentong suture in the earliest Triassic (McCourt, 1996). Metcalfe

(1996) suggested a collision time of Sibumasu with Indochina in the latest Permian or Triassic, but the exact suturing age is still controversial.

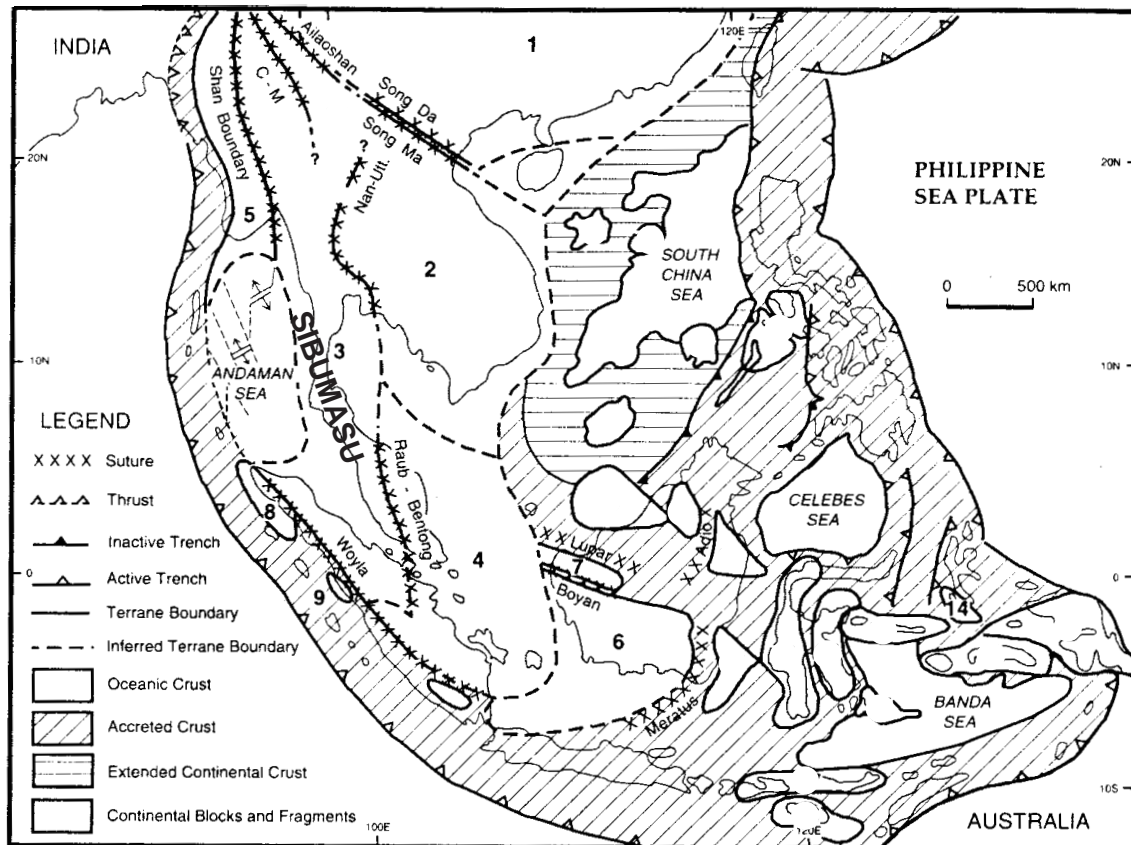


Figure 2.2: Distribution of principal continental terranes and sutures in SE Asia: 1. South China; 2. Indochina; 3. Sibumasu; 4. East Malaya; 5. West Burma; 6. SW Borneo; 7. Semitau; 8. Sikuleh; 9. Natal (after Metcalfe, 1996).

The Late Triassic to Late Jurassic saw renewed rifting on the north-east margin of Gondwanaland, leading to the destruction of the Meso-Tethys (Fig. 2.1). The Woyla terrane split from Gondwana in the Late Jurassic and by Late Cretaceous had accreted to proto-SE Asia. This terrane consisted of several small continental fragments, including the Sikuleh and Natal blocks, now located along the Woyla suture along the south-west margin of Sumatra, as shown in Figure 2.2, which comprises Cretaceous ophiolites and accretionary complex material (Metcalfe, 1996). Stratigraphic similarities with the Exmouth Plateau of the NW Australian shelf and paleomagnetic data from the Sikuleh block suggest paleolatitudes of 26°S for the Late Triassic and 10°S in the Late Mesozoic which is consistent with a NW Australian origin of these terranes (Metcalfe, 1996).

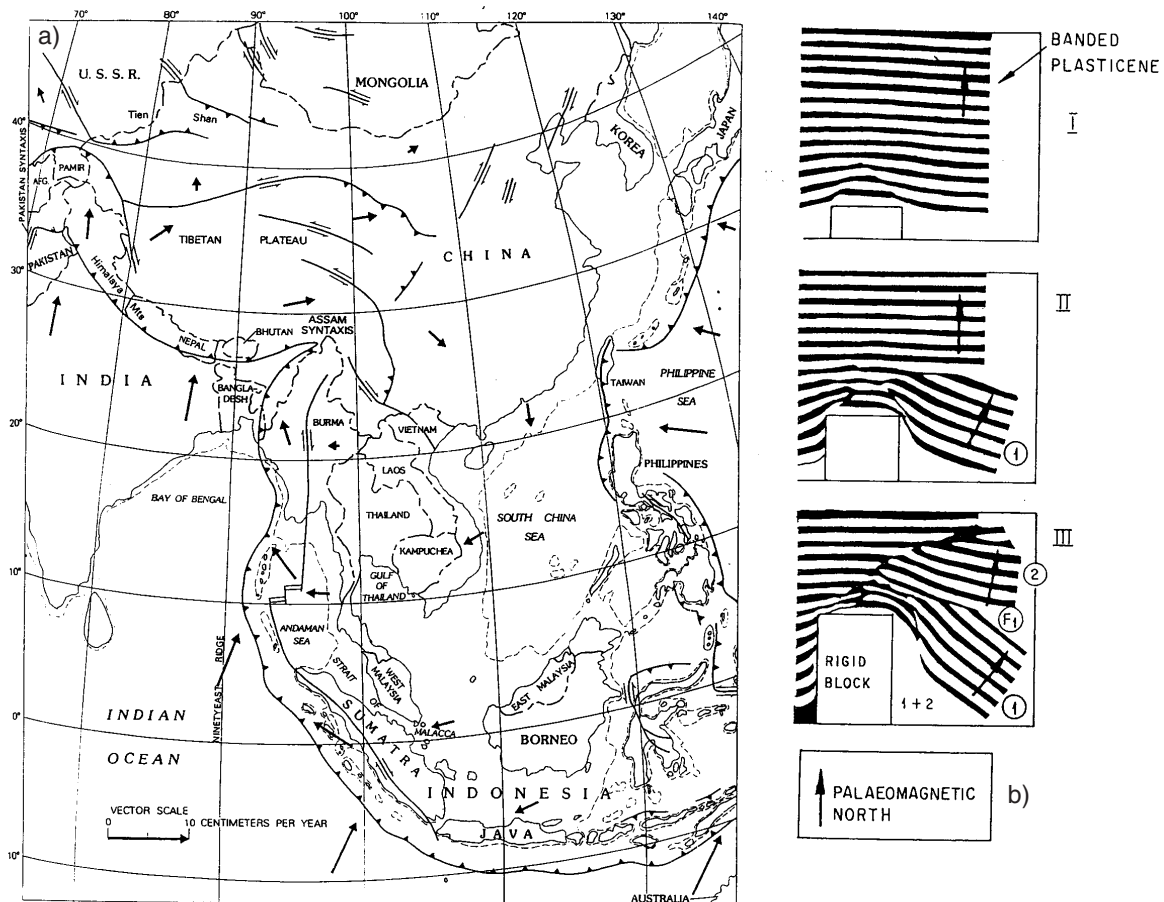


Figure 2.3: a) Some active structures of the Chinese-Indonesian region. Perhaps half the northward motion of India relative to northwest Eurasia is being taken up by underthrusting of the Tibetan Plateau by India and by compressive thickening of the entire continental crust. The other half is compensated primarily by the eastward motion, relative to northwestern Eurasia, of China. Southeast Asia and western Indonesia are swinging clockwise, pivoted near the Assam syntaxis, over the Indian ocean and the northern Bay of Bengal. Large arrows show direction and velocity of motion relative to northwestern Eurasia (from Hamilton, 1979).

b) Three successive stages of an indentation experiment on plasticine (plan view). The free side is on the right. The rigid block is modelled as India. 1 is taken as the Indochina-South-east Asian block, 2 as south China. 1 is the opening of the South China sea and 1+2 as the Andaman Sea. F_1 is the Red River Fault (from Tapponnier, 1982).

The time of initiation of northward subduction of the Izangi Plate, which underlay the Mesozoic Tethys Ocean along the proto-Sunda trench is still enigmatic, but magmatism and ophiolite emplacement date back to the Cretaceous (Widiyantoro and van der Hilst, 1996). Cretaceous subduction complexes around margins of the Eurasian continent are identified in western and central Java and south-western Sulawesi (Nishimura and Suparka, 1997).

The location of these subduction complexes and paleomagnetic measurements indicate that the position of pre-Tertiary subduction was at the front of the Eurasian continent. A waning or cessation of subduction along the proto-Sunda Arc was proposed by Hamilton (1979) for the Late Cretaceous to Early Tertiary, based on the magmatic record. From middle Tertiary times on, subduction of the Indian sea plate occurred again along Sumatra and became connected to the Java Trench during the Late Miocene (10-8 Ma).

The present distribution and geometry of SE Asia is the result of the effects of the collision of Indian and Eurasia, i.e. indentation, extrusion and strike-slip faulting. India collided with the Tethyan margin in Eocene time (Fig. 2.3), about 40 million years ago, and since then has continued to move northward at a velocity of about 5 cm/yr relative to Eurasia. The great Pakistan and Assam syntaxes at west and east corners of the Indian plate indicate northward motion of India relative to the Middle East to the west, and to South-East Asia to the east. About half the northward motion of India relative to north-west Eurasia is being accommodated by continental underthrusting of the Tibetan plateau and by compressive thickening of the entire continental crust (Hamilton, 1979). The other half is compensated primarily by the eastward motion of China, obliquely out of the way of the advancing southern continent, along a complex series of strike-slip faults and other structures. The resulting escape tectonics in south-eastern Asia included clockwise rotation of tectonic units in Indochina and Indonesia, as implied by the plasticine indentation experiments of Tapponnier et al. (1982) presented in Figure 2.3a.

Audley-Charles, M.G., Evolution of the southern margin of Thethys (North Australian region) from early Permian to late Cretaceous, in: Gondwana and Thethys, Audley-Charles, M.G., and A. Hallam (eds), *Geological Society Special Publication* 37, 79-100, 1988.

Gasparon, M., and R. Varne, Sumatran granitoids and their relationship to Southeast Asian terranes, *Tectonophysics*, 251, 277-299, 1995.

Hamilton, W.B., *Tectonics of the Indonesian Region*, USGS Professional Paper, 1078, 1979.

Hutchinson, C.S., *Geological Evolution of South-East Asia*, Clarendon Press, Oxford, 1989.

McCourt, W., M. J. Crow, E. J. Cobbing, and T. C. Amin, Mesozoic and Cenozoic plutonic evolution of SE Asia: evidence from Sumatra, Indonesia, in: Tectonic Evolution of Southeast Asia, R. Hall (edt), *Geological Society of London Spec. Publication* 106, 321-335, 1996.

Metcalfe, I., Pre-Cretaceous evolution of SE Asian terranes, in: Tectonic Evolution of Southeast Asia, R. Hall (edt), *Geological Society of London Spec. Publication* 106, 97-122, 1996.

Müller, D., W. R. Roest, J. Y. Royer, L. M. Gahagan, and J. G. Sclater, Digital isochrons of the world's ocean floor, *Journal of Geophysical Research*, 102, 3211-3214, 1997.

Nishimura, S., and S. Suparka, Tectonic approach to the Neogene evolution of Pacific-Indian Ocean seaways, *Tectonophysics*, 281, 1-16, 1997.

Tapponnier, P., G. Peltzer, A. Y. Le Dain, Armijo-Rolando, and P. Cobbold, Propagating extrusion tectonics in Asia: new insights from simple experiments with plasticine, *Geology*, 10, 12, 611-616, 1982.

Widiyantoro, S., and R. van der Hilst, Structure and Evolution of Lithospheric Slab Beneath the Sunda Arc, Indonesia, *Science*, 271, 1566-1570, 1996.

3. THE CENOZOIC ARC-TRENCH SYSTEM

3.1 Oblique to frontal subduction

The Sunda Arc, which extends over 5600 km between the Himalayan syntaxis in the north-west and the Banda Arc to the east, is a classic convergent or subduction margin with the Indo-Australian plate underthrusting the Eurasian or South-East Asian plate (Fig. 3.1). Changes of orientation of the plate margin result in a change of subduction obliquity from Java to Sumatra. The nature of the transition between these two subduction regimes is of major interest: the forearc basin, which is characteristic for the subduction sectors off Sumatra and off Java, is disrupted south of the Sunda Strait (Fig. 3.1), coinciding with a concave bend of the trench. The change of orientation of the trench near the Sunda Strait imposes a large change in the ratio of parallel to normal slip. Along the western arc this ratio progressively increases toward the Andaman region in the north, whereas along the eastern arc it remains nearly constant at a low rate (Fitch, 1972).

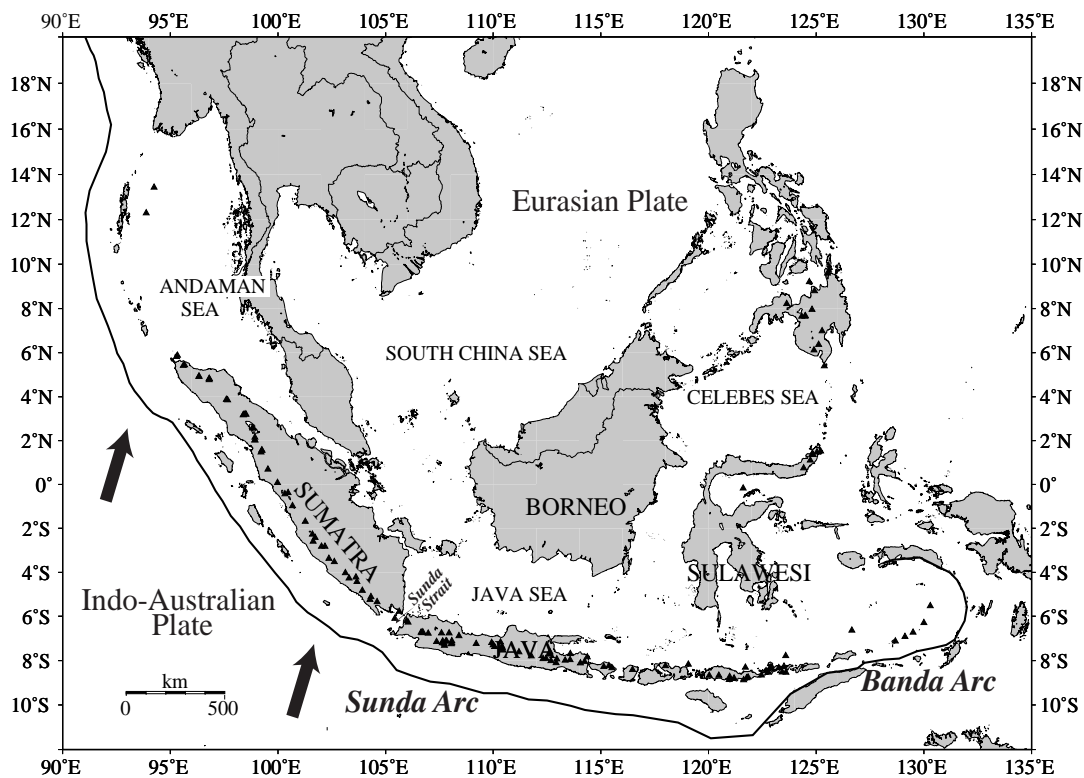


Figure 3.1: Geographic map of Indonesia indicating the trace of the Sunda Arc and Banda Arc subduction zones.

Along Sumatra, oblique subduction induces partitioning of the motion into convergent motion and north-westward strike-slip motion. This partitioning results from the coupling effect between the dipping oceanic slab and the upper plate lithosphere. The coupling can be identified by the study of slip vectors at the subduction zone which indicates the true direction of relative movement of the oceanic slab with respect to the forearc (McCaffrey, 1992). The subduction can thus be resolved into two components, one perpendicular component, calculated at between 5.7 and 7.0 cm/yr, and a transform component of slippage parallel to the trench axis of up to 2.1 cm/yr (Hutchinson, 1989). The lateral movement results in the formation of a microplate sliver, while the movement perpendicular to the margin, mainly taken up by subduction, is also expressed by compressional deformation within the accretionary prism or the forearc. The obliquity of the Sumatra subduction zone is mainly compensated by dextral strike-slip movement along the Sumatra fault (Fig. 3.2), which runs parallel to the long axis of Sumatra and offsets right laterally the Sumatra island, thus forming the Sumatra plate sliver between the trench of the Sunda Arc and the Sumatran fault.

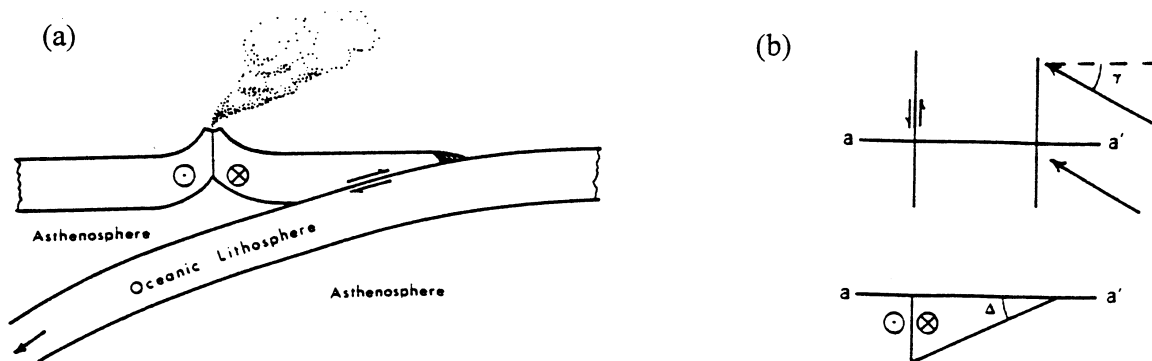


Figure 3.2.: a) illustrates the formation of the transcurrent fault along a thermally-thinned zone coincident with the axis of the magmatic arc. Oblique motion is converted into a subduction zone-transcurrent fault pair northwest of Sunda Strait, where the angle of convergence between the Indian and Eurasian plates becomes markedly oblique.

b) is a cartoon depicting the geometry of a Sunda-style margin. γ and Δ are the angle of convergence and the dip of the Wadati-Benioff zone, respectively (from Fitch, 1972).

It has also been proposed that the Mentawai fault off Sumatra takes part in the compensation (Diament et al., 1992, Malod and Kemal, 1996). Thus at least a fraction of slip parallel to the plate margin results in transcurrent movements on the nearly vertical Sumatra fault, which consists of about 20 separate en echelon segments, extending 1600

km along the volcanic chain of western Sumatra (Newcomb and McCann, 1987). The Sumatran fault has been explained as a lithospheric scale fault zone that cuts the lithosphere vertically down to the asthenospheric wedge (Bellier and Sébrier, 1995). North of Sumatra it extends into the Andaman Basin, where it most likely joins the fracture zones of the back arc spreading center near the Andaman Islands.

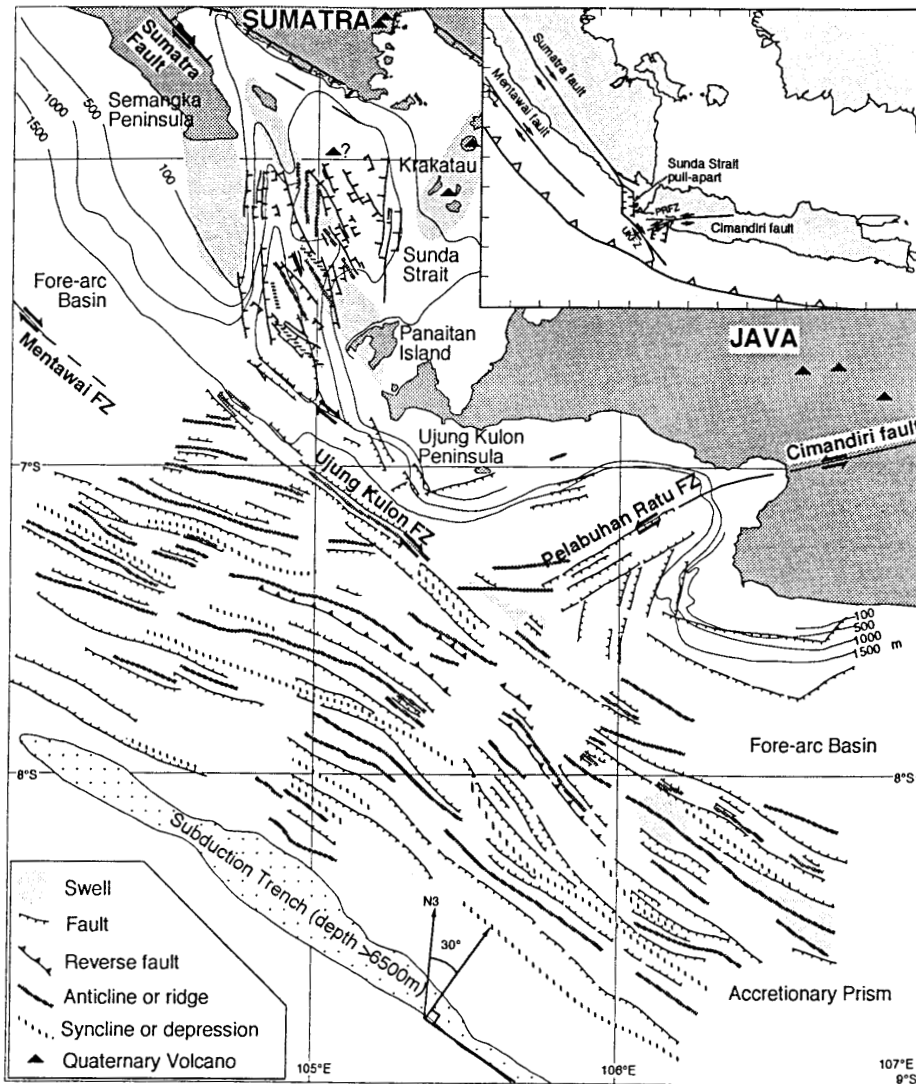


Figure 3.3: Tectonic sketch of the forearc domain south of Sunda Strait. The Sumatra fault is relayed by the Sunda Strait pull-apart basin to the Ujung Kulon fracture zone. The inlay shows a simplified structural map of the Sumatra-Ujung Kulon fault system (from Malod et al., 1995).

The Sumatra fault may be traced into the forearc of south Sumatra and appears to turn into a complex pattern of extensional faults (Huchon and Le Pichon, 1984). The southern end of the Sumatra fault is connected to a large pull-apart basin within Sunda Strait

(discussed in detail in Chapter 7) and has been proposed to be relayed to the Ujung Kulon Fracture Zone off western Java (Fig. 3.3) (Malod et al., 1995). The southeastern extent of this fault zone is still enigmatic as its trace is lost in the outer high south of Sunda Strait, where the concave bend of the trench results in a complex tectonic pattern. A possible continuation of this fault zone along the forearc basin margin off southern Java is discussed in Chapter 4.

It is generally agreed that the northward increase in convergence obliquity along the Sumatran margin leads to a north-westward increase of the forearc motion relative to the upper plate which increases from zero, east of the Sunda Strait, to 45-60 mm/yr, in northern Sumatra; thus the variation in obliquity along the margin produces a variation in slip rate along the Sumatra fault (Bellier and Sébrier, 1995). This results in a longitudinal extension of the forearc sliver plate between the trench and the Sumatra fault. This model may partly explain the discrepancy between extension at the two ends of the Sumatra fault, from more than 460 km in the Andaman Sea (Curry et al., 1978) compared to only 50-70 km in the Sunda Strait (Diament et al., 1992). The exact mechanisms responsible for forearc stretching are still debated and the forearc deformation along Sumatra is yet poorly understood. This is mainly due to the complex role of the offshore Mentawai fault zone (Fig. 3.3), for which an explanation as a lithospheric strike-slip fault and thus as an analogue to the Sumatra fault has been proposed (Diament et al., 1992). The lack of deep penetrating high resolution seismic data from the fault zone makes this interpretation tentative. In the GINCO study area only a small amount of slip or none at all can be expected along the Mentawai fault zone, as the Sunda Strait extension is fully compensated by slip on the Sumatra fault here. Offshore northern Sumatra, the Mentawai fault is relayed and connected to the Sumatra fault by the Batee fault. The slip rate along the Mentawai fault here is also currently still unknown (Malod and Kemal, 1996), though due to the increased slip along the Sumatra fault and a higher factor of stretching of the forearc sliver north of 1°S, a crucial role of the Mentawai fault system must be expected here.

3.2 Lower trench slope morphology

The bathymetric survey conducted during the GINCO cruises yields new insights into the tectonic and deformational processes occurring along the deformation front and adjacent lower trench slope. Figure 3.4 shows the extent of the hydrosweep data which focused on selected areas off Sumatra and off Java.

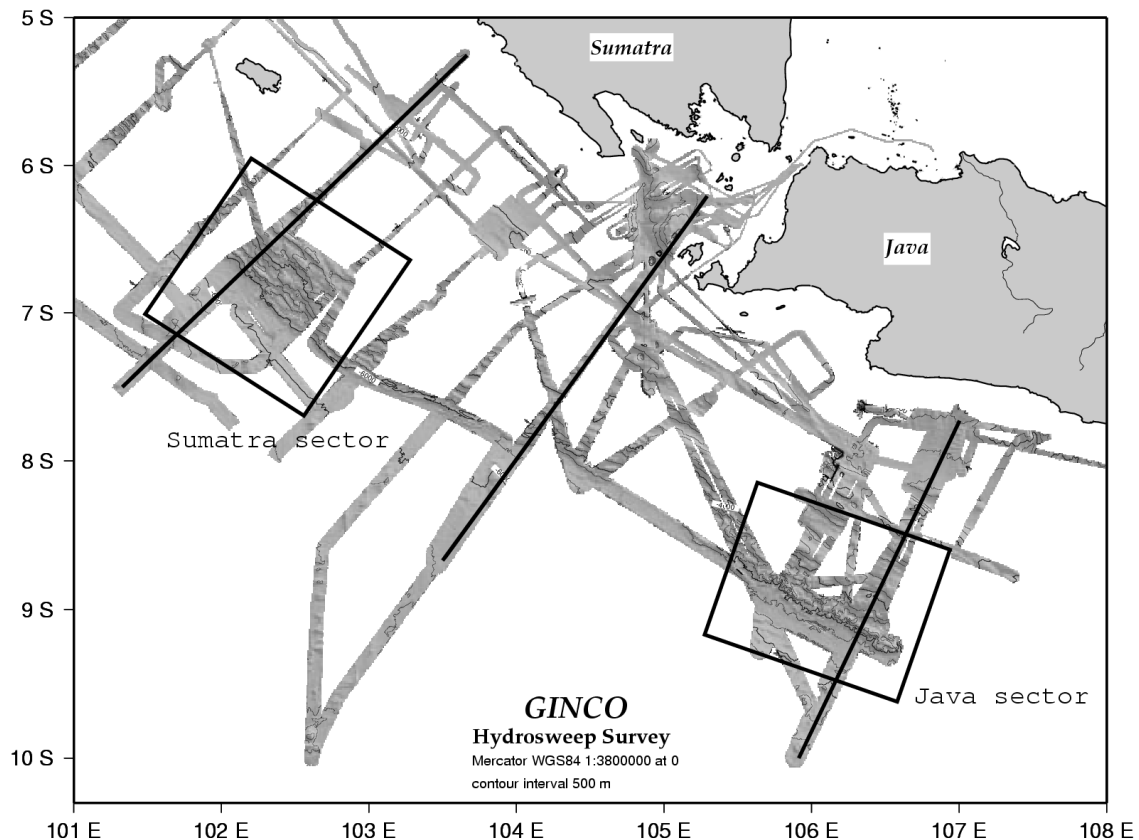


Figure 3.4: Hydrosweep survey conducted during the GINCO project. The Sumatra and the Java sector are indicated by boxes. Black lines depict the location of the seismic refraction dip profiles.

The detailed mapping of the Sumatra sector (Fig. 3.5) reveals a segmentation of the accretionary domain into several parts which display different morphological styles. Large slides in the landward part suggest active tectonism, as does the rough topography of the trenchward section of the prism. The most remarkable feature is a displacement of the deformation front of about 8 km to the southwest whose origin remains enigmatic. Numerous transverse disturbances and faults characterize this part of the wedge where accretion is forming new ridges. A compressional regime, as suggested by GPS measurements (Wilson et al., 1998) and the variation of obliquity will cause a

segmentation of the accretionary complex into different blocks of the forearc domain, resulting in a complex configuration of transform and normal faults as seen in this high resolution bathymetry and reported elsewhere (Malod and Kemal, 1996).

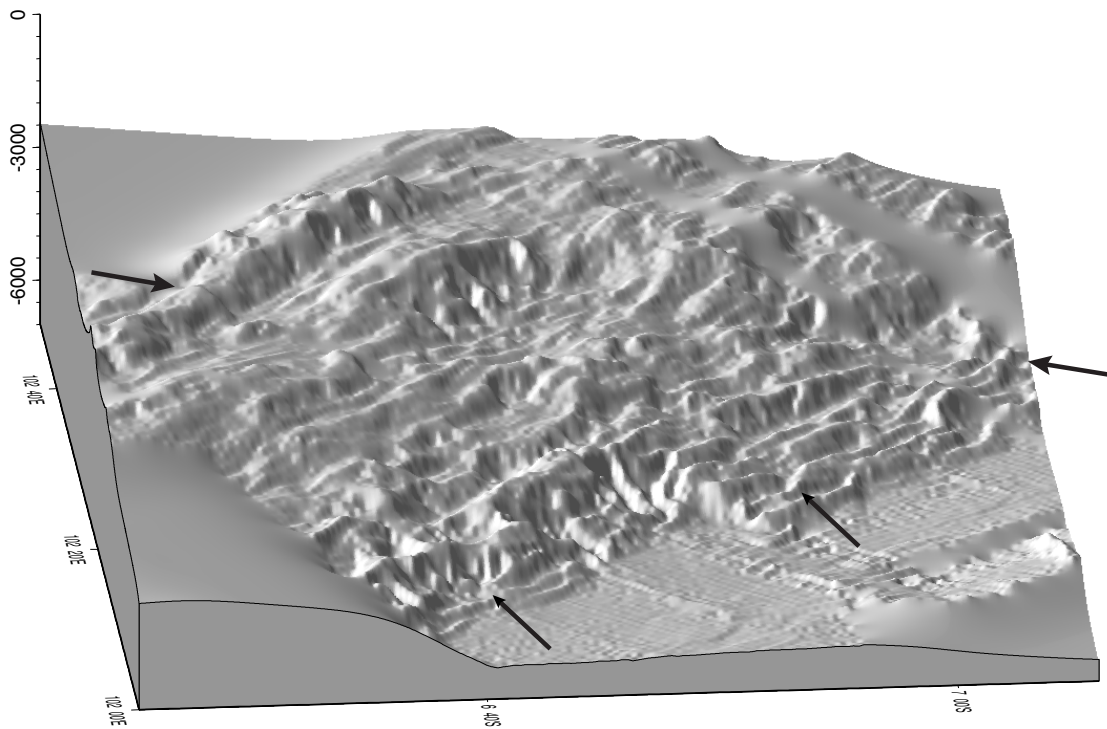


Figure 3.5: Detailed mapping of the lower trench slope and accretionary prism off Sumatra. Location is shown in Fig. 3.4. Tentative identification of faults indicated by arrows.

A comparison of the regimes of frontal and oblique subduction (Fig. 3.6) reveals differences in the morphology of the lower trench slope. The landward part of the accretionary domain in the Java sector shows a smoother seafloor topography than the highly disturbed Sumatran sector, which is dominated by faults and linear breaks as well as large slides. The deformation front along the Sumatran sector is marked by elongated ridges, while along the Javanese sector a more chaotic structure is observed. Here, the width of the actively deforming zone is considerably less than further north.

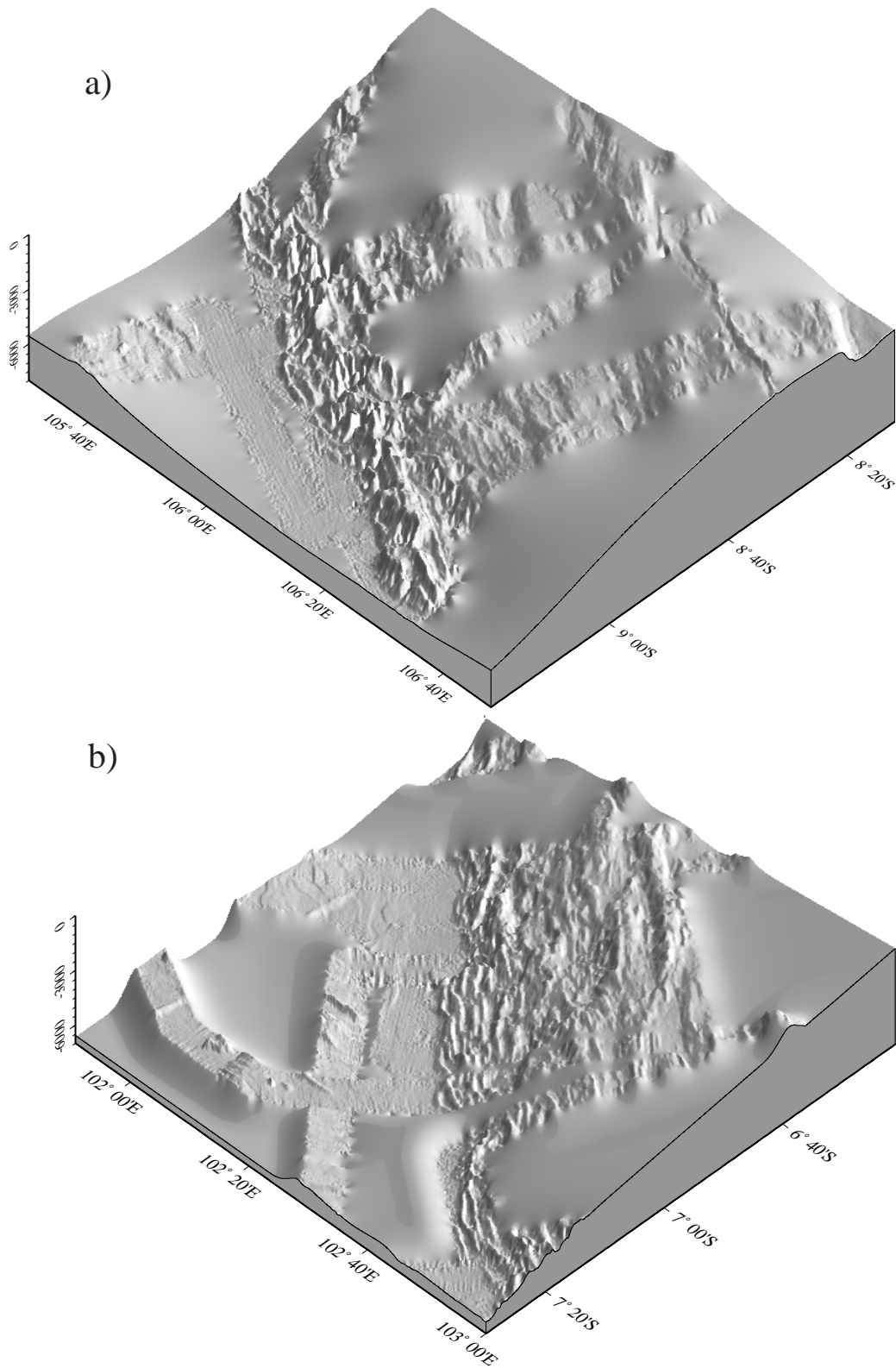


Figure 3.6: Comparison of the lower trench slope morphology in areas of frontal (a) and oblique (b) subduction.

3.3 Seismotectonics of the Sunda Arc

Given the tectonic setting of the Sunda Arc, it can be expected that the junction of the island arc material along the eastern Sunda and Banda Arcs and the continental platform of Sumatra overlies a strongly heterogeneous mantle, as is evident from regional seismicity. The character of subduction related seismicity changes abruptly between east and west of Sunda Strait. Seismicity displays a distinct Wadati-Benioff zone, which exists all the way around the arc (Fig. 3.7), but dramatically changes in depth and pattern (Curry, 1989) (Fig. 3.8). Active andesitic volcanism occurs along most of the arc, and age and thickness of the subducted oceanic lithosphere increases from Sumatra to Java. For young subducting lithosphere (with age less than 70 Ma) the thickness of the elastic lithosphere increases with age (Parsons and Sclater, 1977). Eastward from near Sunda Strait the age of the oceanic crust is over 70 Ma (Hamilton, 1979). The thick slab off Java and further east extends to greater depth and exerts significant slab pull force which supplements the outer bulge

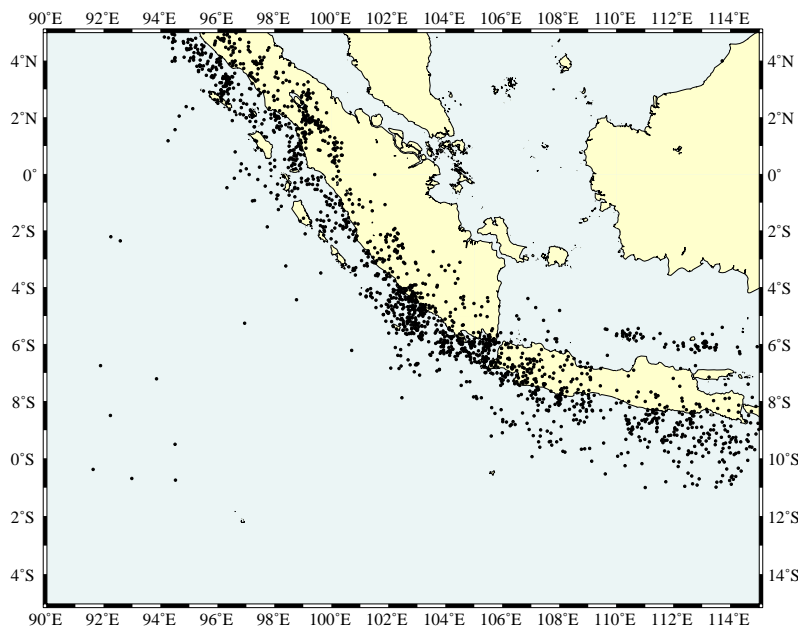


Figure 3.7: Epicenter distribution of earthquakes ($M > 3$) recorded along the Sunda Arc between 1928 and 1994 (maximum depth 700 km) (from Princeton's earthquake catalogue).

bending related extensional stress to cause the tensional earthquakes oceanward off the trench of Java. The increasing dip and depth of penetration of the

Benioff zone (as shown in Fig. 3.8, profiles JJ'-OO') reflect this change. Steplike increase in the depth of the deepest earthquakes from 150 km west of the strait to >600 km east of it suggests that the rate of underthrusting in this region has a similar step-like increase. Fitch (1972) pointed out that an abrupt change in the orientation of the arc near the Sunda Strait can account for such a change in the rate of underthrusting and thus can account for the configuration of the inclined seismic zone beneath this part of the arc in general.

Deep focus earthquakes down to almost 700 km occur underneath Java, but end abruptly near the Sunda Strait (Fig. 3.8). Underneath Java, seismic activity extends

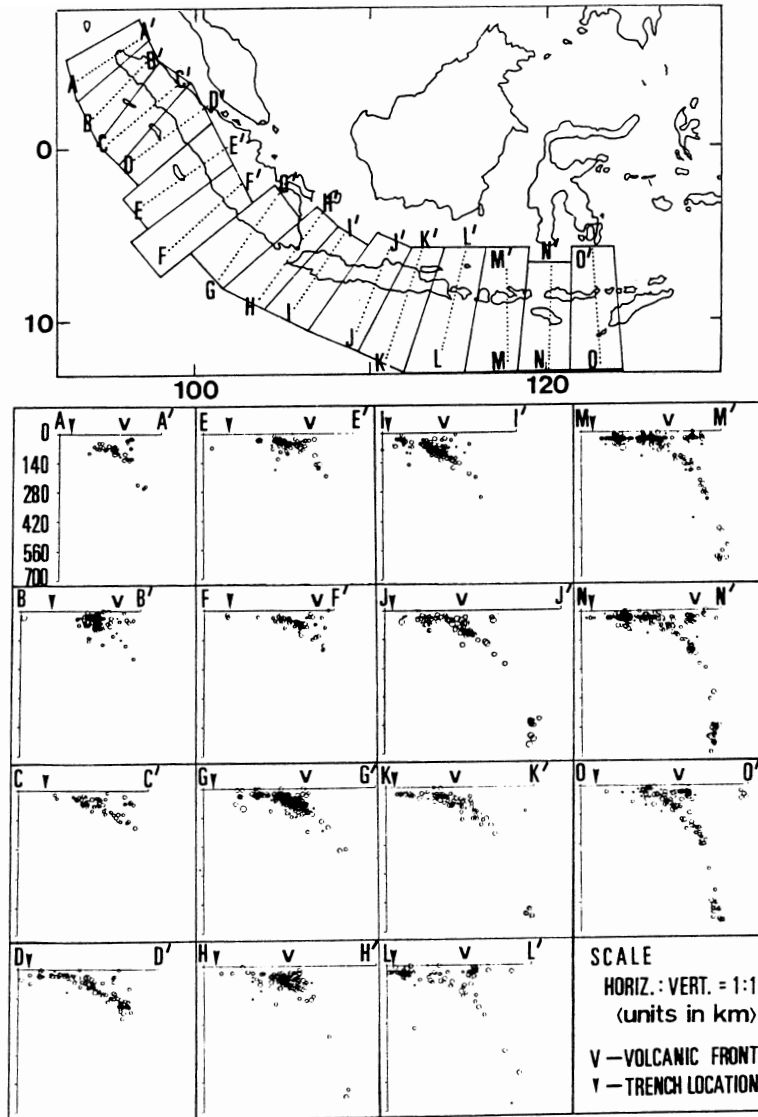


Figure 3.8: Benioff zone structure along the Sunda Arc. Earthquakes reported by 15 or more stations from the ISC Data File (1971-1983) are plotted versus depth. The depth variation of the Benioff zone along the arc ranges from ca. 300 km in northern Sumatra (profile A-A') to ca. 700 km beneath Java (profiles J-J', N-N', K-K', and O-O') (from Curray, 1998).

from the surface to a depth of 670 km. The seismic zone is steeply dipping here at an angle of about 60° . Recent hypocenter determination studies by Schöffel and Das (1999) suggest a southward dipping slab below 500 km depth, in opposite direction to the northward dipping upper part of the slab (Fig. 3.9). Further to the west and north, earthquake foci do not exceed a depth of 300 km. Slab configuration is ambiguous in northern Sumatra while in the south a plane dipping $40\text{-}50^\circ$ is apparent, which has been attributed to the relatively young age of subducted lithosphere.

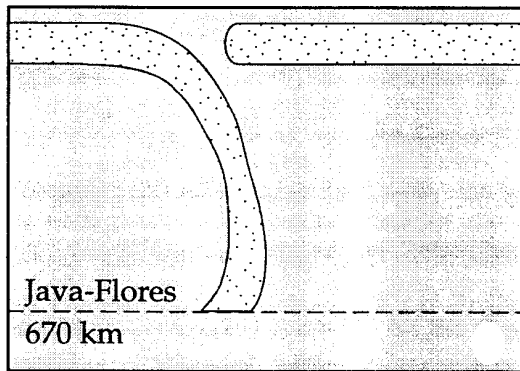


Figure 3.9: Proposed shape of the downgoing slab along the Java-Flores subduction zone (from Schöffel and Das, 1999).

The detection of a positive velocity anomaly in the lower mantle beneath Sumatra (Widiyantoro and van der Hilst, 1996) suggests that the deep part of the slab is detached from the seismogenic slab (Fig. 3.10). This might have been caused by the buoyancy of the young lithosphere and the change to oblique subduction because of the rotation of Sumatra, which reduced flow in the vertical direction and may have combined to temporarily cease subduction, while the deep, old slab continued to sink to larger depths.

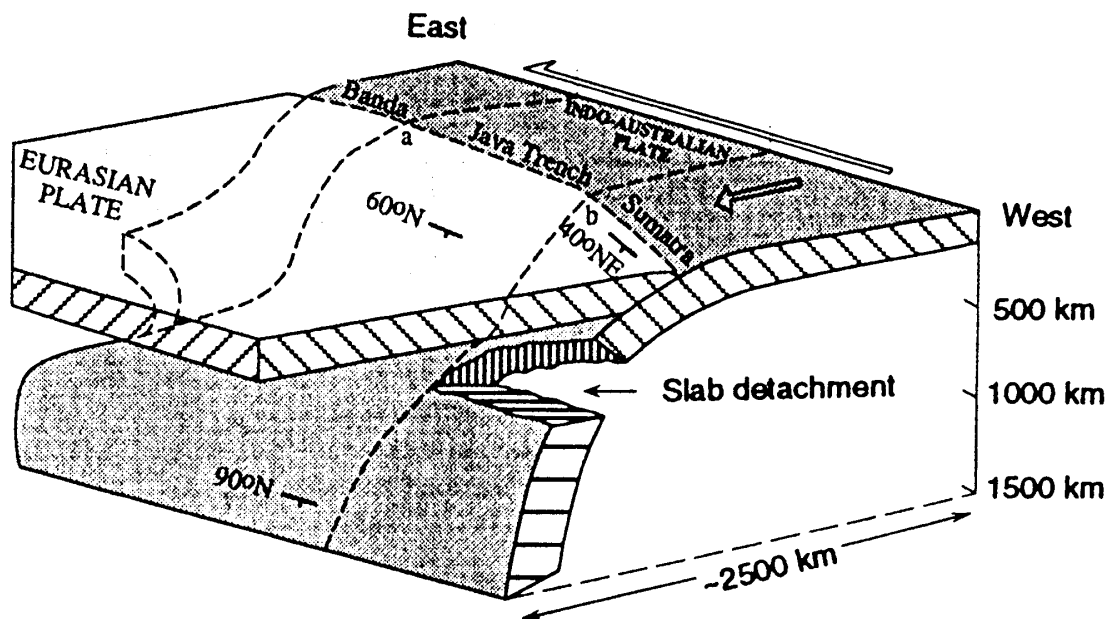


Figure 3.10: Slab structure beneath the Sunda and western Banda arcs. The shallow slab dips in a northeast direction at an angle of ca. 40° below Sumatra and in a north direction at an angle of ca. 60° below Java; the deep slabs sinks almost vertically into the lower mantle. Notice the slab detachment below Sumatra (from Widiyantoro and van der Hilst, 1996).

The shallowest earthquakes (0-20 km) near Sumatra immediately adjacent to the Sunda trench are commonly associated with strain release occurring along the plate boundary. At Sumatra, the interplate seismic coupling is very high, and thus causes the large thrust events. The majority of strong earthquakes in both the historic and instrumental catalogues

of the Sunda Arc ($M_w = 8.75$, in 1833, $M_w = 8.4$, in 1861 and $M_w=8.2$, in 1964) are located in the forearc of Sumatra (Fig. 3.7). At Java, subduction occurs primarily aseismically. It is striking that at Sumatra, although the plates are strongly coupled, the shallow seismicity does not extend far into the continental platform, whereas the whole of Java experiences many such shallow events. The difference in slab penetration between Sumatra and Java cannot completely account for this difference in shallow seismicity inlands of Sumatra and Java. However, the distance from the trench to inland Sumatra (400 km on average) exceeds that of Java (app. 250 km). As a matter of fact, the line of active volcanoes (which usually corresponds to the 120 km depth contour for the inclined seismic zone) passes through the centre (E-W) of Java, whereas for Sumatra it runs close to the Indian ocean coast.

The occurrence of numerous large earthquakes near Sumatra and the almost complete absence of such events near Java (Fig. 3.11) correlate with changes in tectonic style along the arc and support the variation in mode of interplate motion (seismic vs. aseismic). The maximum magnitude of great interplate earthquakes in Sumatra ($M_w = 8.5-9$) contrasts sharply with that of interplate earthquakes in Java ($M = 7.2$). The variation in maximum magnitude of earthquakes in the world's subduction zones is similar to the variation in seismic slip rate (Newcomb and McCann, 1987). In regions that have great earthquakes, seismic slip rates are comparable to the rate of relative plate motion. Sumatra's great earthquakes account for a majority of slip between the two plates. The lack of such events near Java indicates differential motion at the plate margin which is principally being taken up aseismically or by small magnitude earthquakes. Papadimitriou et al. (2001) computed the probability for the occurrence of a intermediate to deep focus mainshock of $M > 7.0$ during the period 1997-2006 for the circum-Pacific region. The probability for a magnitude 7.3 earthquake underneath Java lies at less than 50%.

A strong correlation of earthquake size with both age of the subducted lithosphere and convergence rate has been found (Newcomb and McCann, 1987). High convergence rates and subduction of younger seafloor are associated with regions of great thrust earthquakes (Fig. 3.11), while regions with fewer such events tend to subduct older seafloor at low rates. Convergence rates along the Sunda Arc do not change substantially, but the

difference in age of the subducted lithosphere is almost 100 my between northern Sumatra and eastern Java.

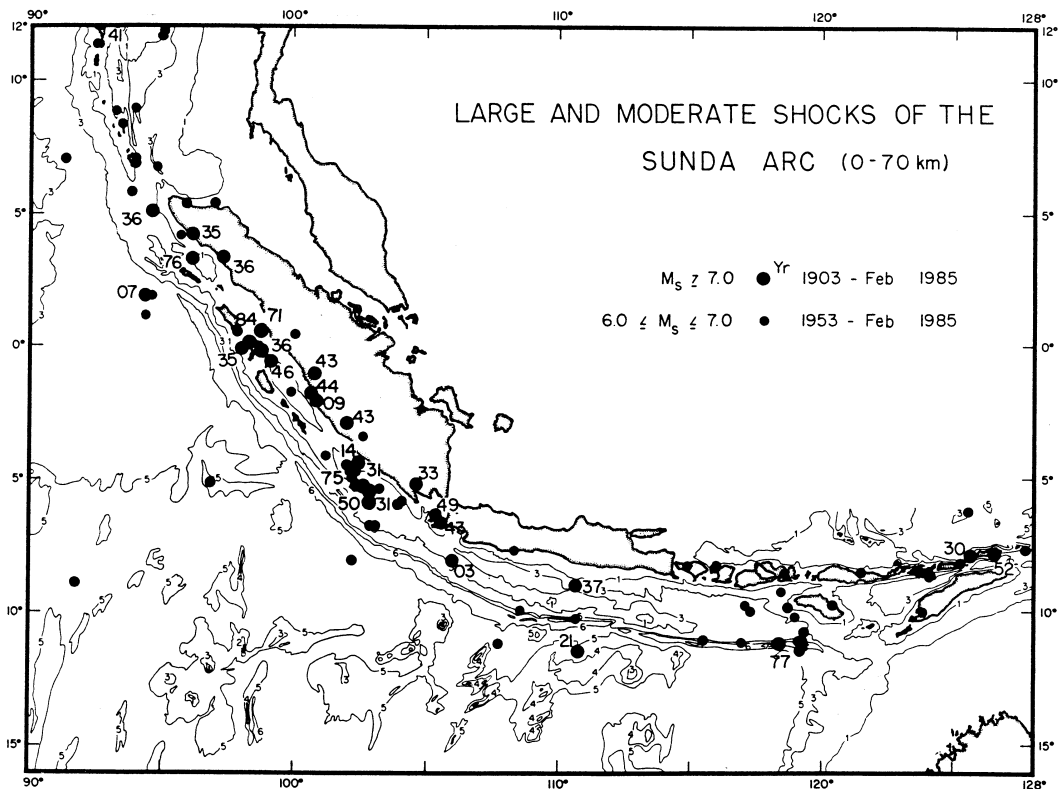


Figure 3.11: Large shallow earthquakes ($M_s > 7.0$, $z < 70$ km) of this century are plotted with the year indicated beside the epicentral location. All events since 1921 have been relocated. The catalogue of large and moderate events was developed by Newcomb and McCann (1987). Large shocks mainly occur along the Sumatran sector of the subduction zone.

The basis for this correlation may be interpreted in terms of the subducted plates' trajectory, where convergence rate controls the horizontal component and slab age controls the vertical component. The average density of an oceanic lithosphere increases as it ages, since more high-density material is incorporated with time. The difference in vertical velocity upon subduction causes changes in coupling along the plate boundary and hence changes in the ability to generate great earthquakes. The vertical force acting on an old and dense subducted plate (like the one beneath Java) will minimize coupling in an interface thrust zone, resulting in an almost entire absence of great thrust earthquakes (Ghose et al., 1990).

The June 1994 Java earthquake:

The 1994 Java Tsunami earthquake poses an exemption to this trend. This large subduction thrust earthquake of magnitude 7.2 caused a devastating tsunami on Java and was the first recorded large thrust earthquake on the Java subduction zone. Its hypocenter was located at a depth of 16 km, consistent with the plate interface geometry (Abercrombie et al., 2000). The area of the main slip collocated with a subducting seamount. Thus the Java thrust earthquake is interpreted as slip over this bathymetric high which poses a locked patch in an otherwise decoupled subduction zone (Abercrombie et al., 2000).

The June 2000 Sumatra earthquake:

An earthquake of magnitude 7.8 occurred on June 4, 2000, close to the Sumatra trench north of GINCO line SO138-01 (Fig. 3.12 and 1.2) at a depth of about 49 km and with a duration of ca. 60 s.

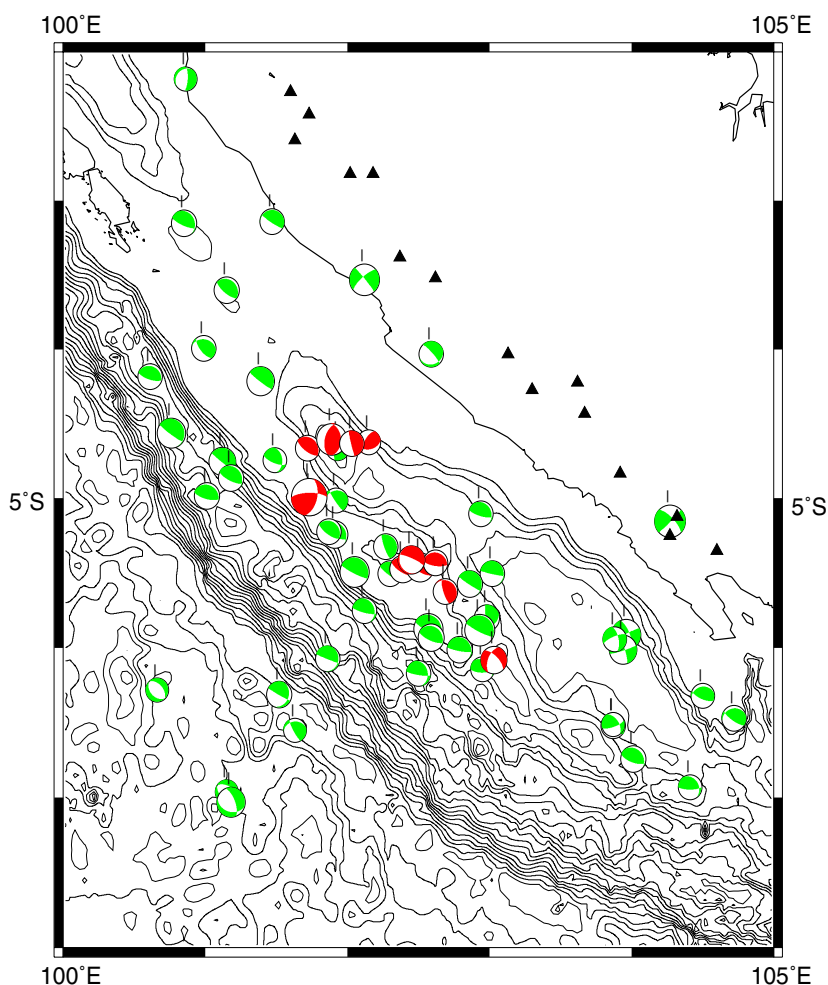


Figure 3.12: Preliminary CMT solutions for the June 4, 2000 earthquake and its aftershocks (dark circles). Light circles depict earthquakes along the margin and the Sumatra fault since 1990.

Relocation of around 30 aftershocks shows that they extend ca. 150 km to the southeast along the subduction zone at depths ranging from 15 km to 90 km (R. Abercrombie, personal communication, Dec. 2000). It is proposed that this earthquake is a

combination of strike-slip in the subducting slab and thrusting on the plate interface resulting from left-lateral stress produced by the effect of the locked Sumatra subduction zone and the unlocked Java trench, as discussed above.

- Abercrombie, R. E., M. Antolik, K. Felzer, and G. Ekström, The 1994 Java Tsunami Earthquake: Slip over a subducting seamount, *Journal of Geophysical Research*, in press, November 2000.
- Bellier, O., and M. Sébrier, Is the slip rate variation on the Great Sumatran Fault accomodated by fore-arc stretching?, *Geophysical Research Letters*, 22, 15, 1969-1972, 1995.
- Curray, J.R., G.G. Shor, Jr., R.W. Raitt, and M. Henry, Seismic refraction and reflection studies of crustal structure of the Eastern Sunda and Western Banda arcs, *Journal of Geophysical Research*, 82, 17, 2479-2489, 1978.
- Curray, J.R., The Sunda Arc: A model for oblique plate convergence, *Netherlands Journal of Sea Research*, 24, 131-140, 1989.
- Diament, M., H. Harjono, K. Karta, C. Deplus, D. Dahrin, M. T. Zan, Jr., M. Gerard, O. Lassal, A. Martin, J. Malod, Mentawai fault zone off Sumatra: a new key to the geodynamics of western Indonesia, *Geology*, 20, 259-262, 1992.
- Ghose, R., S. Yoshioka, and K. Oike, Three-dimensional numerical simulation of the subduction dynamics in the Sunda arc region, Southeast Asia, *Tectonophysics*, 181, 223-255, 1990.
- Fitch, T.J., Plate convergence, transcurrent faults and internal deformation adjacent to Southeast Asia and the Western Pacific, *Journal of Geophysical Research*, 77, 4432-4460, 1972.
- Hamilton, W.B., *Tectonics of the Indonesian Region*, USGS Professional Paper, 1078, 1979.
- Huchon, P., and X. Le Pichon, Sunda Strait and Central Sumatra fault, *Geology*, 12, 668-672, 1984.
- Hutchinson, C.S., *Geological Evolution of South-East Asia*, Claredon Press, Oxford, 1989.
- Malod, J. A., K. Karta, M.O. Beslier, M.T. Zen Jr., From normal to oblique subduction: Tectonic relationships between Java and Sumatra, *Journal of Southeast Asian Earth Sciences*, 12, 85-93, 1995.
- Malod, J. and B. M. Kemal, The Sumatra margin: oblique subduction and lateral displacement of the accretionary prism, in: Tectonic Evolution of Southeast Asia, R. Hall (edt), *Geological Society of London Spec. Publication*, 106, 19-28, 1996.
- McCaffrey, R., Oblique Plate Convergence, slip vectors, and forearc deformation, *Journal of Geophysical Research*, 97, 6, 8905-8915, 1992.
- Newcomb, K.R., and W.R. McCann, Seismic history and seismotectonics of the Sunda Arc, *Journal of Geophysical Research*, 92 421-439, 1987.

- Papadimitriou, E. E., C. B. Papazachos, and T. M. Tsapanos, Test and application of the time- and magnitude predicatable-model to the intermediate and deep-focus earthquakes in the subduction zones of the circum-Pacific belt, *Tectonophysics*, 330, 45-68, 2001.
- Parsons, B. and J. G. Sclater, An analysis of the variation of the ocean floor bathymetry and heat flow with age, *Journal of Geophysical Research*, 82, 5, 803-827, 1977.
- Schöffel, H.-J., and S. Das, Fine details of the Wadati-Benioff zone under Indonesia and its geodynamic implications, *Journal of Geophysical Research*, 104, 6, 13202-14114, 1999.
- Widiyantoro, S., and R. van der Hilst, Structure and evolution of lithospheric slab beneath the Sunda Arc, Indonesia, *Science*, 271, 1566-1570, 1996.
- Wilson, P., J. Rais, Ch. Reigber, E. Reinhard, B.A.C. Ambrosius, X. Le Pichon, M. Kasser, P. Suharto, Abdul Majid, Paduka Awang Haji Othman Bin Haji Yakuub, R. Almeda, and C. Boonphakdee, Study provides data on active plate tectonics in Southeast Asia Region, *EOS Transactions*, 79, 45, 545/548, 1998.

4. CRUSTAL STRUCTURE OF THE JAVA MARGIN FROM SEISMIC WIDE-ANGLE AND MULTICHANNEL REFLECTION DATA

4.1 Introduction

The Sunda Arc off Indonesia is a classic convergent margin that has acted as a type example for many concepts concerning mechanisms of accretion and forearc evolution (Hamilton, 1979; Karig et al., 1980; McCaffrey, 1992; Izart et al., 1994; Malod and Kemal, 1996; Samuel and Harbury, 1996). Several geological parameters, including the curvature of the trench and the age of the subducted plate, change significantly along strike of the margin, thus uniquely placing it in a variety of tectonic settings. The Sunda Arc forms the southern termination of the Indonesian Archipelago where the Indo-Australian plate is subducted underneath the Eurasian plate (Fig. 4.1). Along the arc, the collision system changes from oceanic-continental in Sumatra through transitional in Java to intraoceanic in Bali and Flores (Hamilton, 1988).

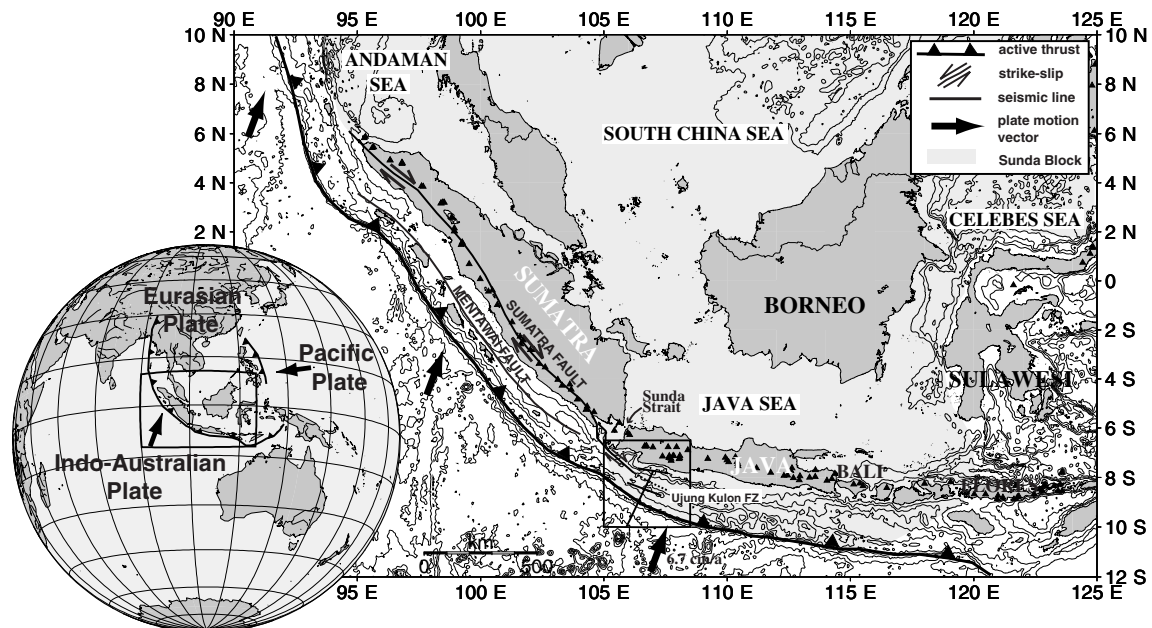


Figure 4.1: Geodynamic setting of the Sunda Arc displaying major tectonic features where the Indo-Australian plate is subducted beneath the Eurasian plate. Plate motion vectors are from the Australia-Eurasia rotation pole after DeMets (1990). The curvature of the Sunda trench results in regimes of frontal subduction off Java and oblique subduction off Sumatra. The study area is located across the margin off western Java. Volcanic distribution is taken from the Smithsonian Global Volcanism Program data set. The Sunda Block (after Wilson et al., 1998) is underlain in grey. The southeastern extent of the Ujung Kulon Fracture Zone indicated by a dotted line is not established.

Despite the long history of scientific investigations along the Sunda Arc, only few limited data exist off Java. To fill this gap, the GINCO Project (Geo-scientific INvestigations along the active CONvergence zone between the eastern Eurasian and Indo-Australian Plates off Indonesia) set out to investigate the crustal structure and plate boundary off Java. Using the RV SONNE during November, 1998 through January, 1999, we collected seismic multichannel reflection (MCS) and wide-angle refraction data across the Sunda subduction zone and forearc domain. In this paper, we report on a coincident MCS/wide-angle seismic profile and two strike-lines from the Java margin. Using these data we can track the downgoing plate from the trench to a depth of 30 km and derive a velocity-depth model across the subduction complex. Additionally, the structure of the Java margin is resolved in considerable detail. Based on our newly acquired seismic data and their interpretation we discuss the crustal structure of the collision zone and present gravity modelling to verify our conclusions. Thus the first detailed cross section of the Sunda Arc margin between Sumatra and Bali is presented.

4.2 Geodynamic Setting

The study area is located off western Java across the Sunda collision zone (Fig. 4.2). The margin represents a typical subduction zone, displaying the outer bulge, a deep trench and large accretionary unit separated from the outer high by a trench slope break, as well as a forearc basin and a volcanic arc further in the hinterland. This sector of the Indo-Australian/Eurasian subduction system has been active since at least Oligocene and evolved after the late Eocene collision of India with Asia (Hamilton, 1988). This collision resulted in a 10° clockwise rotation of southeast Asia accompanied by widespread extension and basin formation in the Indonesian region (Rangin and Pubellier, 1990; Daly et al., 1991). The present plate convergence off western Java and the kinematics of the area are well determined by GPS measurements (Tregoning et al., 1994). The motion of Australia with respect to West Java occurs at 67 mm/yr in a direction N11°E which is orthogonal to the trench. The West Java vector shows a velocity value of 30 mm/yr in a direction N140°E. This has been interpreted as a manifestation of a West Java motion with the distinct Sunda Block (Fig. 4.1) in a northeast direction, as proposed by Wilson et al. (1998). However, the relative motion of the Sunda Block with respect to Eurasia is about 200 mm/yr in a

northeast direction (Wilson et al, 1998), which supports the interpretation of the West Java motion as a result of plate margin deformation.

The age of the incoming plate increases from Sumatra in the west to Flores in the east. Off western Java, the crustal age is estimated to be 96 Ma (Diament et al., 1990). The increase in age is consistent with an increase in plate dip along the arc (Widiyantoro and van der Hilst, 1996), and an increasing depth of seismic activity. West of Sunda Strait, seismicity is not generated beneath 250 km depth (Puspito and Shimazaki, 1995), while underneath Java earthquakes with focal depths of up to 670 km occur. Widiyantoro and van der Hilst (1996) suggest that the plate is continuous across a seismic gap between 350 and 500 km underneath this part of the arc. Sunda Strait (Fig. 4.1) also seems to be a transition zone regarding the morphology of the forearc domain. A distinct forearc basin, divided into several large sub-basins, is present off Sumatra (Moore et al., 1980). It vanishes off Sunda Strait and reappears off Java, where it displays a greater depth and is more continuous than its Sumatran analogue. The outer high is larger in the Sumatran sector where sediment influx on the incoming plate is greater than off Java. Off Java, the outer high is completely submerged and generally 2000-3000 m deep, with isolated highs reaching depths around 1000 m (Moore et al, 1980). The variations in seismicity and forearc morphology are linked to the different tectonic settings resulting from the along-strike change of geophysical parameters discussed above, foremost the age of the subducted plate and the curvature of the trench. Moore et al. (1980) present single-channel reflection profiles south of Java and investigate the trench slope and slope basins. The data show all the morphological elements of a subduction zone (deep trench, slope basins with sedimentary infill, outer high, forearc basin), however, the internal structure is not resolved (Moore et al, 1980). From an early seismic refraction line off central Java, Curray et al. (1977) interpret oceanic crust to be present underneath the forearc basin, but they fail to track the downgoing plate.

4.3 Seismic Data

Seismic wide-angle measurements were conducted during leg SO138 of the German RV SONNE in early 1999 along 3 profiles off western Java (Flueh et al, 1999). Profile 5 is located across strike the Java trench (Fig. 4.2). The profile covers about 80 km of oceanic

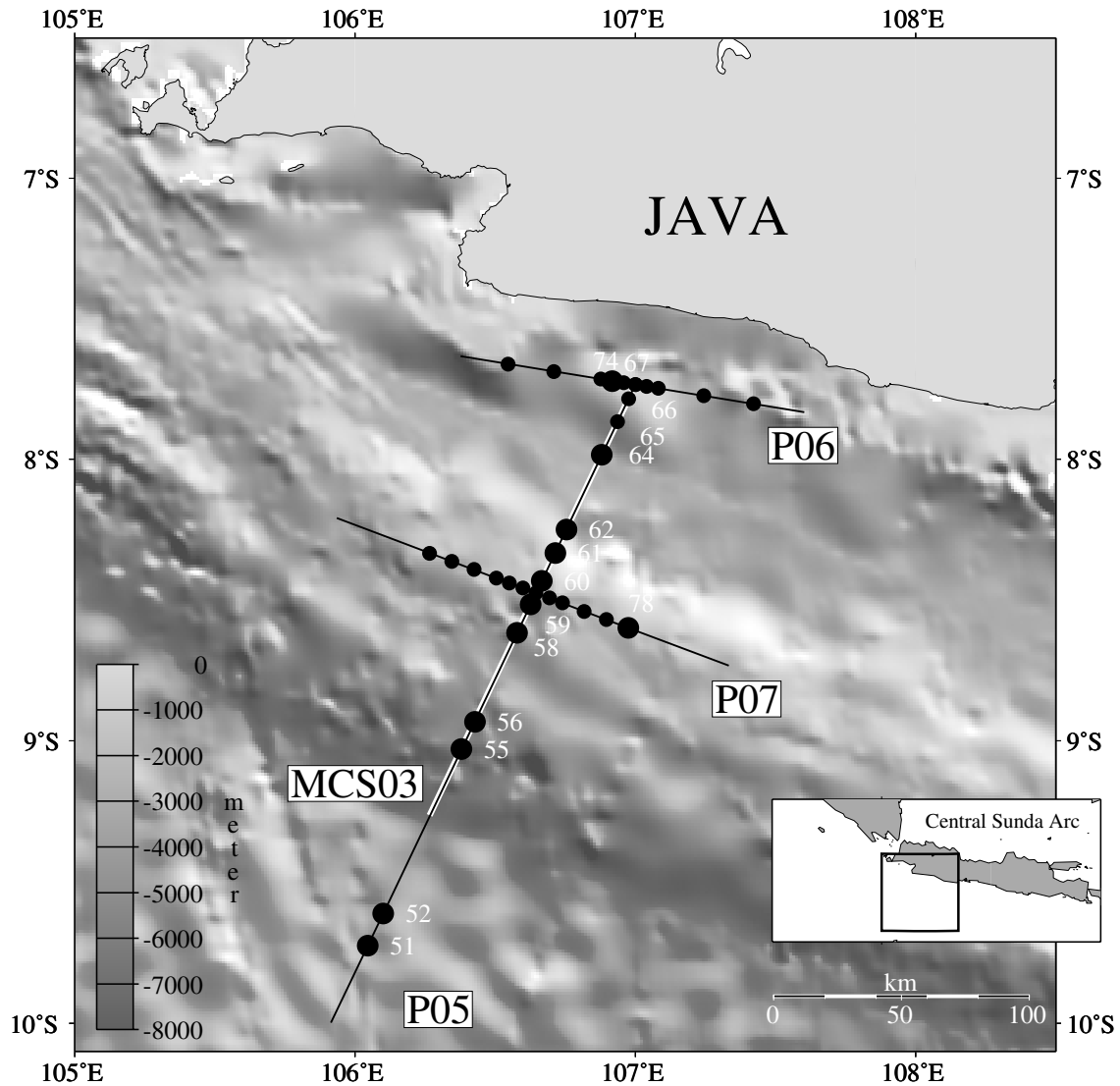


Figure 4.2: Location map of the seismic experiment across the subduction complex off western Java. The seafloor bathymetry is illuminated from the northeast. A total of 35 instruments recorded wide-angle data along 590 profile kilometers. Refraction and reflection seismic data were acquired along the corresponding dip lines P05 and MCS03. Shooting along P05 was extended for about 90 km beyond the end of the MCS line onto the ocean basin. Additional wide-angle data were recorded along the two strike lines which are located along strike the crest of the outer high and the Javanese shelf, respectively.

crust seaward of the trench, the accretionary wedge and outer high as well as the forearc basin and ends on the Javanese shelf. The profile is coincident with MCS Line SO137-03 collected during leg SO137 (Reichert et al, 1999), though the wide-angle shooting was extended seaward 90 km beyond the end of the MCS line to obtain reversed coverage on the oceanic crust. In addition, two cross lines were shot: Profile 7 runs along strike the crest of

the outer high while Profile 6 lies at the north-eastern end of the dip line, close to the shelf break along the northwest boundary of the forearc basin. A total of 39 stations were deployed on the various profiles, mainly the GEOMAR ocean-bottom hydrophones (OBH) (Flueh and Bialas, 1996) and a few ocean-bottom seismometers. Locations are provided in Figure 4.2.

The seismic signals were generated by a tuned set of 20 airguns grouped in two identical linear sub-arrays. The total volume of the array is 51.2 liters (3.124 cu. in.). The shots were triggered in time intervals of 60 s at a speed of 5.5 knots, resulting in an average shot point distance of 167 m. Wide-angle data processing included relocation of the instrument position by analysing the direct arrivals and a low-cut frequency filter. A two-gated predictive deconvolution was applied to the data to improve the temporal resolution. Owing to the broad frequency range contained in the data and to the highly variable seafloor depth along the profiles, a time-dependent and offset-dependent frequency filter was applied. The seismic energy was sufficient to trace signals on the record sections to distances between 60 and 80 km and data quality is good on average. Only selected examples of record sections are shown in the following.

For the MCS data the same source as for the OBH data was used and signals were received along a 3.5 km long streamer with 120 channels and a recording length of 14 s. The shot interval was 50 m and the hydrophone spacing 25 m, resulting in a CMP distance of 12.5 m and a fold of 30. After trace editing and balancing a frequency filter was applied. Special attention was devoted to the f-k domain multiple removal process which is based on move-out differences between primary and multiple events in the CMP gather. A trace interpolation was applied to prevent aliasing before f-k multiple reduction. A two-gated predictive deconvolution further suppressed the multiple and enhanced signal resolution. Due to the significant relief of the seafloor, coherency within the CMP gathers is limited. Thus the demultiple process is inhibited so that multiple energy still remains, especially beneath the outer high. A post-stack time migration was achieved to complete the processing sequence. It was interactively improved using a smoothed velocity field as derived from modelling the wide-angle data. Figure 4.3a displays the southern part of the MCS line, covering the trench and deformation front, which lie at a waterdepth of over 6300 m. The top of the subducted plate is visible for more than 80 km behind the

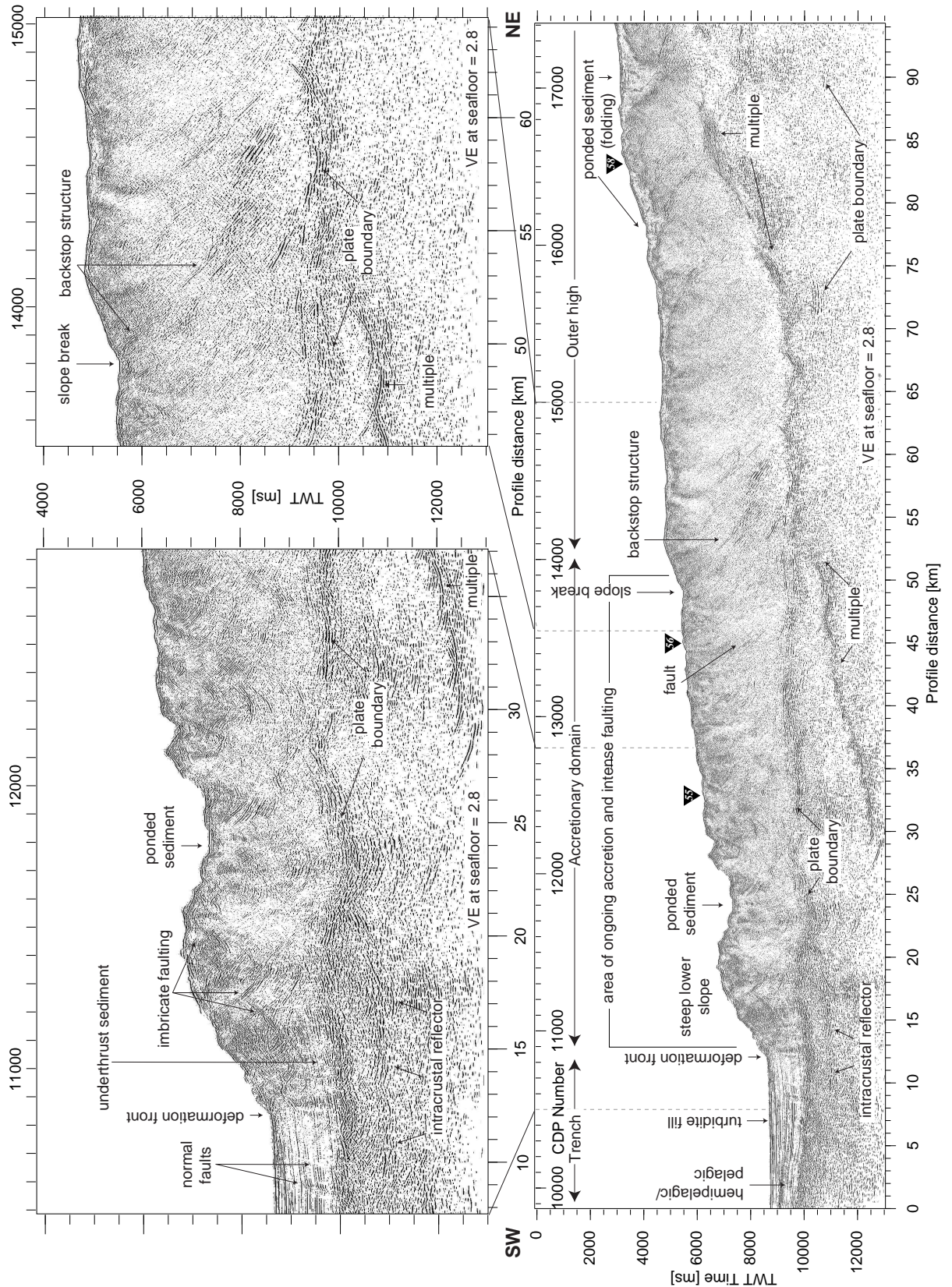


Figure 4.3a: Southwestern part of MCS profile 03 from the trench to the outer high. The active accretionary domain extends from the trench to the backstop structure (CDP 14100). The slope break above the backstop marks the transition from the accretionary domain to the outer high which is characterized by a rough surface basement top underneath a sediment cover. Whereas the accretionary domain is disturbed by many active faults, the seaward part of the outer high shows little tectonic activity. The velocity model presented in Figure 4.5 shows laterally increasing velocities in the accretionary domain and laterally constant velocities underneath the outer high.

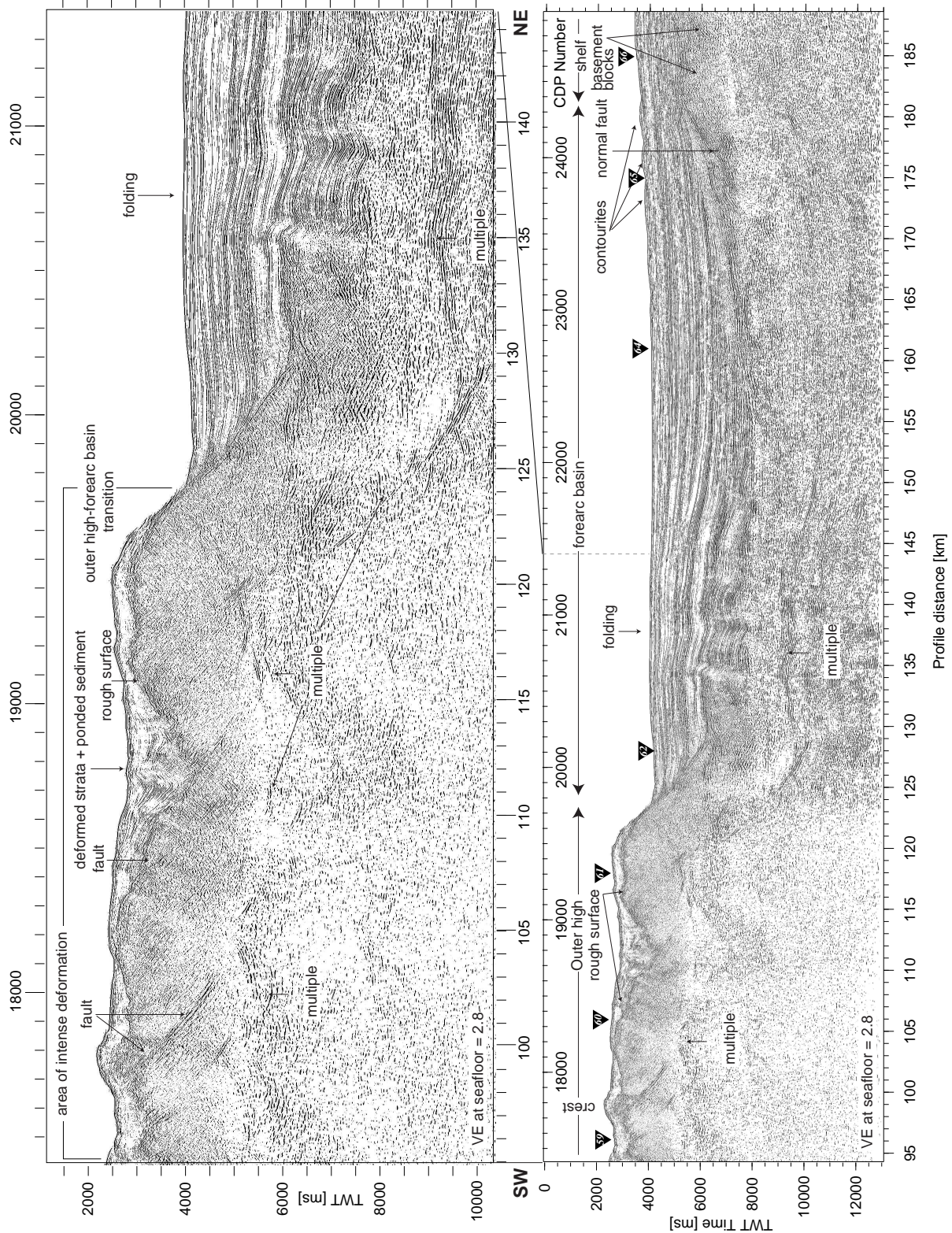


Figure 4.3b: Northeastern part of the MCS profile 03 covering the landward part of the outer high and the forearc basin and shelf onset. Towards the forearc basin, the outer high is undergoing compression as is expressed in intense folding and faulting. The outer high-forearc basin transition is marked by a sharp boundary. Intense folding of the forearc basin sediments is still active; deformation ceases towards the shelf. The wavy seafloor topography between CDP 23000 to 24500 is characteristic of contourites. The shelf is composed of several large basement blocks bounded by large normal faults.

deformation front. The frontal part of the subduction complex is characterized by a distinct topography, which becomes smoother landward of a backstop structure (CDP 14000). A thin sedimentary cover is visible here above a rough surface basement top. Figure 4.3b shows the landward part of the profile from the crest of the outer high to the Java shelf. Thicker sequences of ponded sediment have been trapped in several larger basins above the rough surface. Reflectivity is rather low within the outer high underneath the rough surface. This part is furthermore disturbed by remnants of the seafloor multiple. Further landward, the well resolved sediment infill of the forearc basin onlaps onto the Java shelf and shows some deformation along the seaward part of the basin.

4.3.1 Modelling

To reveal the deep structure of the margin both wide-angle and reflection seismic data were incorporated in an integrated interpretation of both data sets. Due to the different demands concerning the shot interval for wide-angle and multichannel recordings, the OBH and MCS data acquisition were realized independently. If shot along coincident tracks a joint interpretation is feasible. In areas of complex topography this requires accurate navigation. An alignment of the seafloor reflection and the waterdepth (Fig. 4.4) shows good compatibility between the two data sets except for a short part of the line from profile km 100 to 120, where apparently the profiles do not fully overlap.

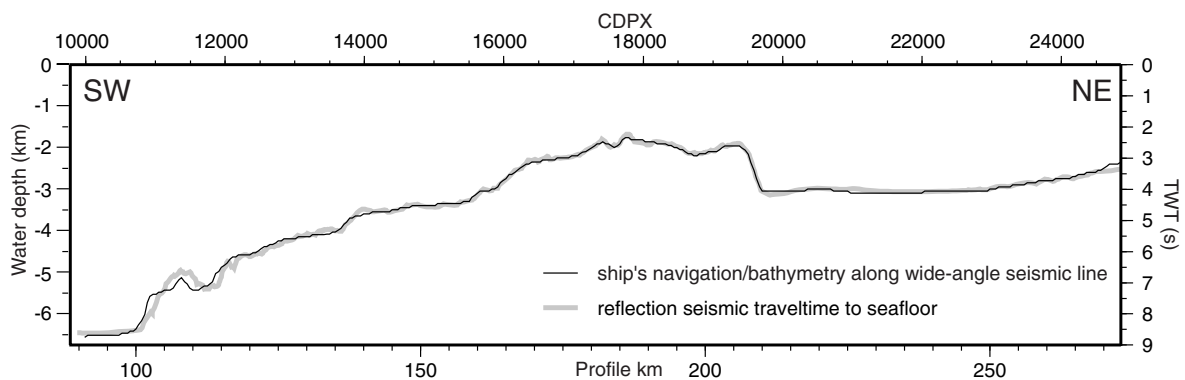


Figure 4.4: Comparison of the seafloor bathymetry along OBH profile 05 to the two-way traveltime to the seafloor of corresponding MCS line 03 to ensure compatibility of the two data sets. The profiles were not acquired simultaneously to meet the different demands concerning the shot interval for wide-angle and reflection data. Equal geometries during data acquisition should yield an identical fit of the bathymetry and travel time to the seafloor for the two lines. This criterion must be fulfilled in order to correlate the two profiles. Good compatibility was achieved along the lines except for a distance of about 20 km landward of the deformation front.

A forward modelling technique (Luetgert, 1992) was chosen for the wide-angle data and the resulting crustal model for all three OBH profiles is shown in Figure 4.5. First arrivals of the OBH data in the near-offset range (<30 km), including refracted waves in the sedimentary section of the outer high and refracted waves through the oceanic crust, could be accurately identified with uncertainties less than ± 50 ms. At larger offsets accuracy declined to about ± 100 ms due to a lower signal-to-noise ratio. Events from the plate boundary are clear and continuous for 30-40 km on several stations underneath the outer high of the dip line, with decreasing amplitudes and clarity further landward at greater depth. Their traveltimes could also be picked with errors varying from ± 50 ms to ± 100 ms. PmP reflections from the oceanic Moho were clearly recorded by stations deployed on the outer high, though the picking accuracy only lies between ± 100 ms and ± 150 ms due to their late arrivals which partially interfere with earlier events and noise.

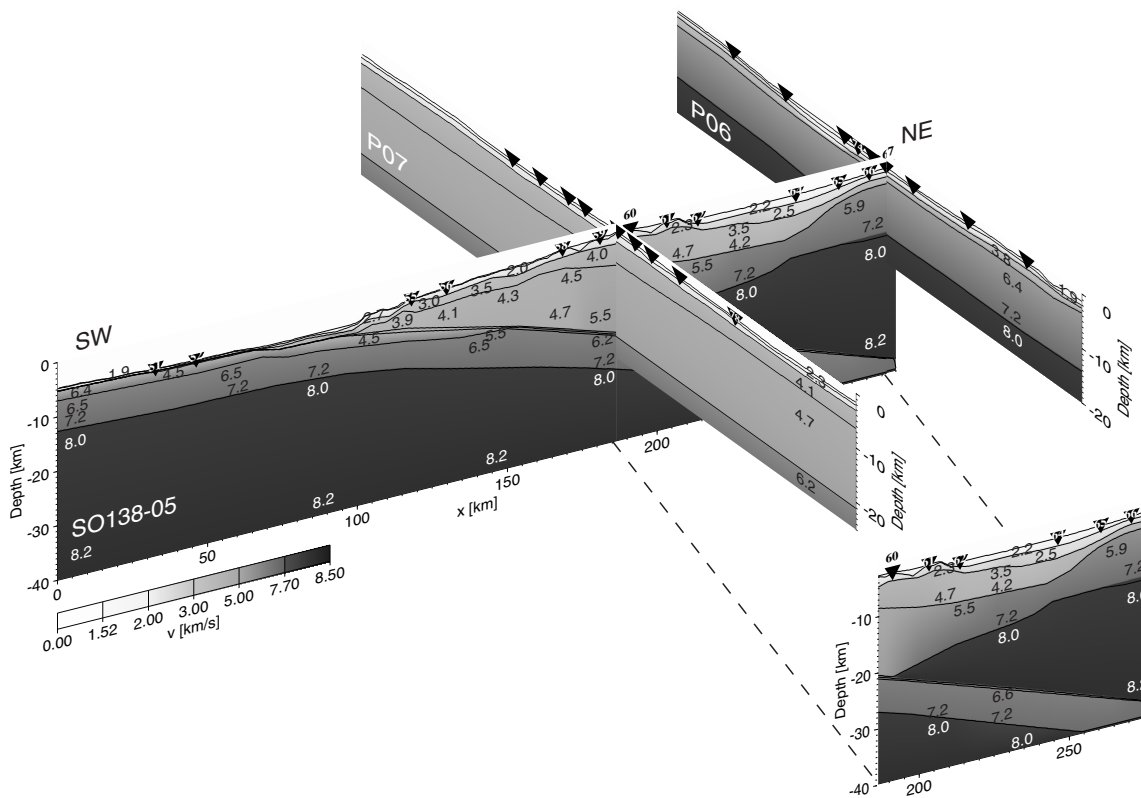


Figure 4.5: 3-D velocity-depth model across the Java subduction zone. The subducted plate is recorded along the dip line SO138-05 and along strike-line 07. The frontal prism shows laterally increasing velocities characteristic of a sedimentary composition (< 4.7 km/s). The massive outer high of about 20 km thickness displays laterally constant seismic velocities, increasing with depth to about 5.5 km/s. The forearc basin carries 4 km of sediment infill. The sediment fill is underlain by a layer displaying velocities increasing from 5.5 to 7.2 km/s above the shallow upper plate Moho. Underneath the shelf velocities are higher, corresponding to the faulted basement blocks identified in the MCS data (Fig. 4.3b). A shallow layer of high velocities is indicative of a mantle upwelling underneath the forearc basin.

Wide-angle data from profile 05 (Fig. 4.5) have a very complex travel time pattern due to the rapid change in water depth and the variable composition of the accretionary complex and outer high. As the energy penetration along the dip line is greatest, we started by modelling this profile first. The velocity tie points were later used to determine the velocity field along the two strike-lines. The velocity model along profile 05 was developed from modelling identified arrivals in the OBH data, incorporating prominent events in the reflection data applying a top-to-bottom approach. The near-vertical-incidence reflections in the MCS data (Fig. 4.3) helped position the rough surface underneath the outer high (Fig. 4.3b, CDP 16000-19700) and the top of the subducted plate near the trench (CDP 10000-17100) as well as the basement underneath the forearc basin and the shelf onset (CDP 20000-24900, see Fig. 4.3).

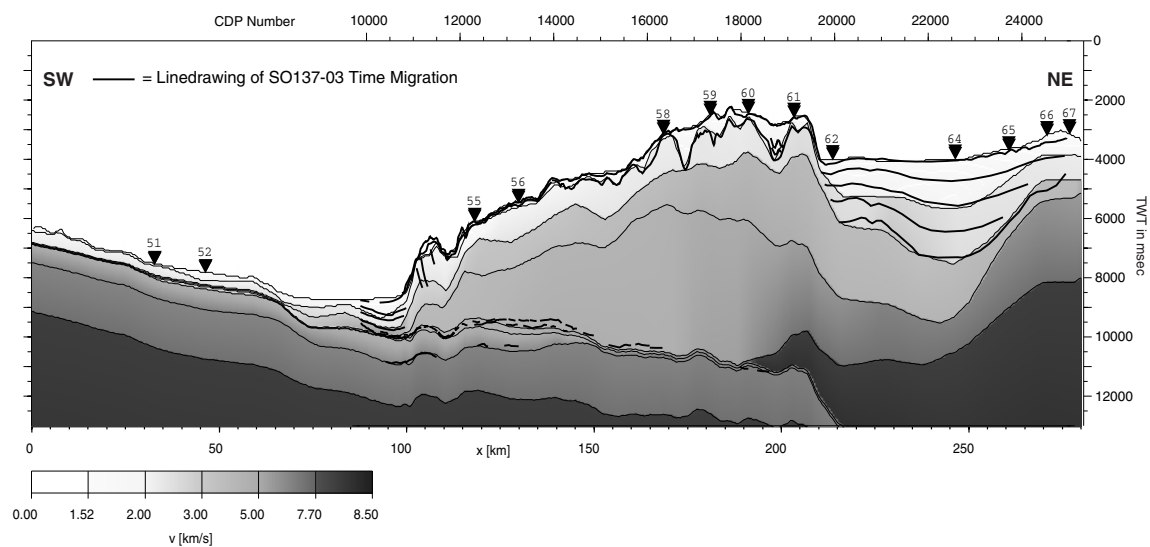


Figure 4.6: Linedrawing of MCS profile 03 plotted on top of the wide-angle velocity model which was converted to a time section in two-way traveltime. A good correlation of the main units in the upper segments of the wide-angle model to the near-vertical incidence reflections of the MCS data was achieved. The MCS recording started in the trench, where several layers of trench infill are resolved above the downgoing plate. The top of the subducted plate is visible for about 80 km underneath the accretionary complex and outer high. An intracrustal reflector was recorded in the MCS as well as the OBH data about 0.8 s below the top of the subducted plate underneath the frontal prism. The outer high displays a rough surface beneath the upper sediment cover, which correlates with a significant velocity change in the wide-angle model. A maximum of 2.8 s of sediment fill is recorded in the forearc basin, onlapping onto the Javanese shelf.

Modelling of the strike-lines yielded basic velocity information of the outer high and the Java shelf, which was tied to the velocity structure of the dip line (Fig. 4.5). Thus further

constraint on the velocity field was achieved. Reflection data recorded by a three channel streamer along the strike-lines 06 and 07 (Flueh et al., 1999) helped model the upper segments of the strike-lines.

Figure 4.6 displays the final wide-angle velocity model of the dip line converted to a time section and overlain by a line drawing of the MCS data. A good correlation of the main reflection horizons with significant velocity changes in the subsurface was achieved.

4.4 Interpretation

4.4.1 OBH Profile SO138-05 and coincident MCS Profile SO137-03

Ocean basin and trench

OBH Line 05 is 280 km long and extends from the Java shelf beyond the end of the MCS profile to the ocean basin (Fig. 4.5). Two instruments (OBH 51 and 52, Fig. 4.7) recorded data on the oceanic crust seaward of the trench, which allowed some insight into the structure of the igneous crust. The incoming plate is covered by 600 m of pelagic and hemi-pelagic sediment and a normal oceanic crust of 7.4 km thickness is observed.

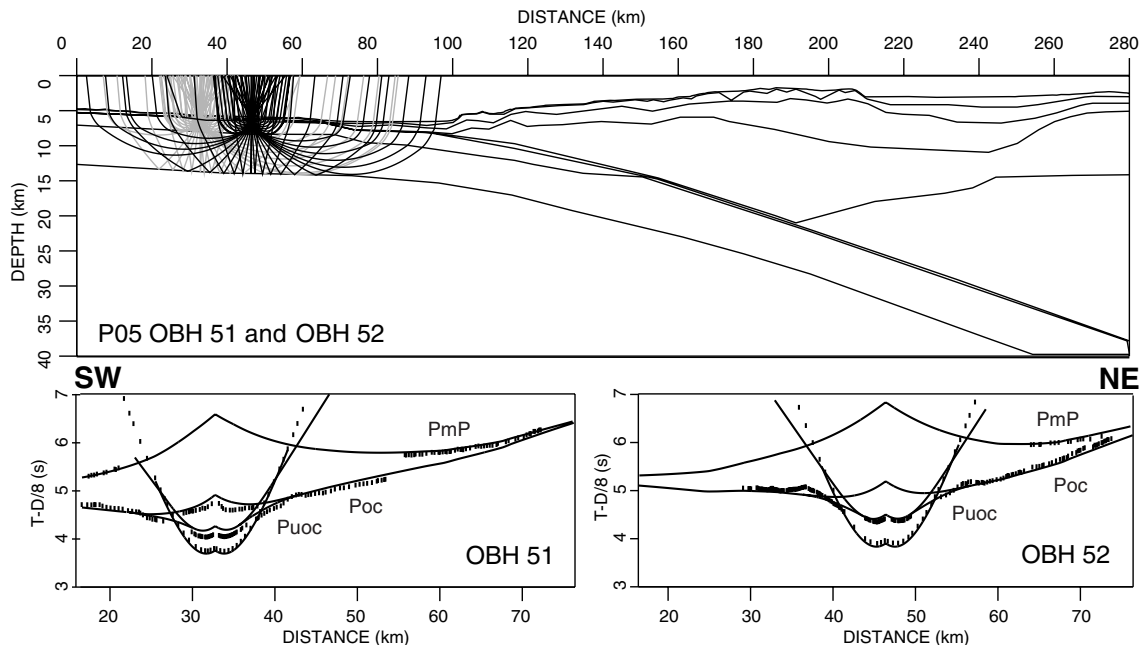


Figure 4.7: OBH 51 and 52 are located on the incoming igneous oceanic crust which shows a thickness of 7.4 km and a normal velocity structure. Puoc indicates refracted waves through the upper oceanic crust (=uoc) and Poc through the lower crust.

The upper oceanic crust of 2 km thickness was modelled with a higher velocity gradient than the lower crust (layer 3), which displays a velocity increase from 6.5 to 7.2 km/s.

Phases Puoc and Poc (Fig. 4.7) are refracted through the upper and lower crust, respectively. The trench sediment fill is inferred from the MCS data (Fig. 4.3a, CDP 9900-10800), in which hemipelagic/pelagic sediment and turbidite fill is resolved. From the south-western end of profile MCS 03 up to about CDP 10800, the trench infill is characterized by near parallel, subhorizontal and landward divergent facies that onlap the basement. Two landward normal faults cutting the pelagic sediment around CDP 10600 and CDP 10700 (Fig. 4.3a blowup) seem to be inactive as they do not disturb the turbiditic fill. Due to the great depth of the trench of over 6.3 km no instruments could be deployed here. Unfortunately one instrument deployed immediately landward of the trench failed to record any data.

Subducted plate

The next two stations (OBH 55 and 56, see Fig. 4.3a) trace the top of the subducted plate as a strong reflection Ptoc (toc denotes top of oceanic crust) and refraction Poc (oc denotes oceanic crust) (OBH 55 and 56 in Figs. 4.8 and 4.9). The plate boundary is also present in the multichannel data, where it occurs as a high-amplitude reflection which can be followed for about 90 km underneath the outer high. This reflection displays a strong lateral coherency (Fig. 4.3a). An intracrustal reflection is recorded about 0.8 s TWT later (Fig. 4.3a). This phase Pioc is also clearly visible in the OBH data (OBH 55 and 56) and is interpreted as the transition from upper to lower crust (ioc denotes intra-oceanic crustal reflector). Whereas phase Pioc is recorded by stations OBH 55 and OBH 56, its presence on the record section of OBH 58 is ambiguous since the arrivals from the subducted plate appear as a strong band of energy which does not clearly resolve the intra-oceanic crustal reflection. Where the intracrustal reflection marks the upper-lower oceanic crust transition on both data sets along the profile we applied a distinct layering for the oceanic crust. Phases indexed uoc (uoc denotes upper oceanic crust) indicate refracted waves through the upper crust (OBH 51 and 52, OBH 55). Starting around profile km 140 this transition is not resolved anymore and thus we applied a single velocity gradient with depth for the subducted plate. OBH 58 records the top of the plate at about 17 km depth at profile km 170 (Ptoc and Poc in Fig. 4.10). The plate boundary is also present on the record section of station 60 (Fig. 4.12). OBH 62 (Fig. 4.13) is the most landward instrument to record it at a depth of 26 km at profile km 215. A strong Moho reflection from the oceanic plate was

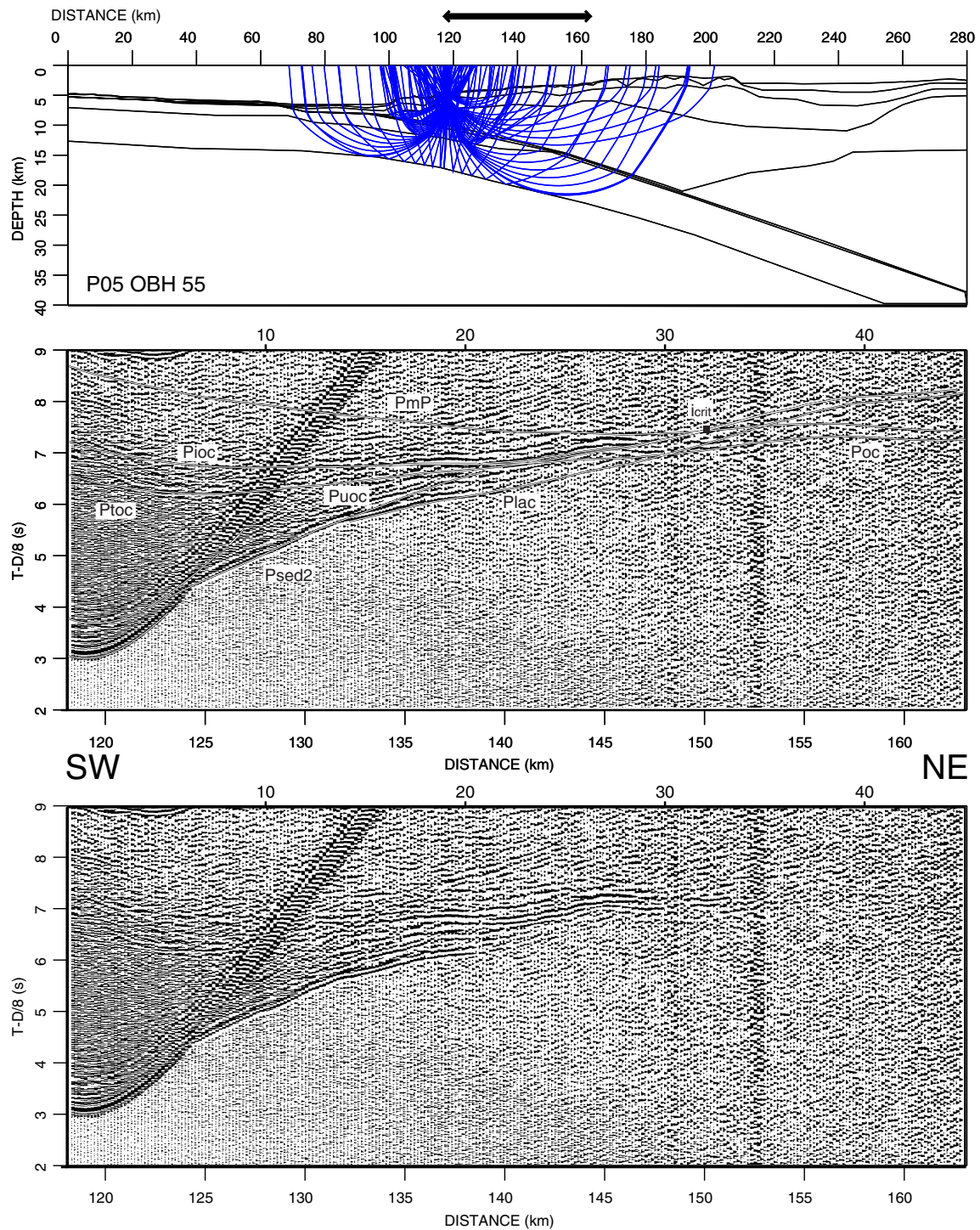


Figure 7.8: OBH 55 is the first station landward of the trench. The upper image displays the raypaths through the model subsurface. The data are shown with overlain traveltimes in the middle image. The top of the subducted plate P_{toc} and an intracrustal reflector P_{loc} are recorded as reflections by stations 55 and 56 (Fig. 7.9). The velocity structure of the accretionary domain is documented by the sedimentary phases P_{sed2} and P_{lac} (=lower accretionary complex). The thick black arrow above the model distance axis signifies the transect displayed in the record section below.

been trapped in between the ridges but no pelagic sediment cover is visible on top of the accretionary unit in the MCS data. The velocity structure of the accretionary domain was determined from refracted waves through the upper sedimentary units (Psed1 and Psed2) and through the lower accretionary complex (Plac; lac denotes lower accretionary complex) mainly from the six OBH stations (55, 56, 58-61) positioned on the accretionary wedge and outer high. The smooth velocity-depth functions are characterized by a positive downward and landward gradient. The upper units show low velocities (2.7-3.0 km/s) (Fig. 4.5) while the lower part of the frontal prism displays seismic velocities from 3.9 to 4.1 km/s, which show little lateral variation for the first 20 km of the frontal prism. This is documented by phases Psed2 and Plac of OBH 56 between OBH-profile kilometers 100 to 120 (Fig. 4.9). Velocities are then increasing laterally by about 0.5 km/s from 20-35 km landward of the deformation front, as is validated by the landward-travelling phases Psed2 and Plac of station 55 (Fig. 4.8), before levelling at an approximate laterally constant value at OBH-profile km 135, which coincides with the position of a backstop structure identified in the MCS data (Fig. 4.3a). The velocity structure of the frontal part of the wedge is also supported by the southwest running phases Psed2 and Plac of OBH 58 and 60 (Figs. 4.10 and 4.12).

Outer high and forearc basin

The backstop structure is identified in the MCS data as a prominent, landward-dipping reflection. It cuts from the seafloor at the trench-slope break almost to the top of the subducted plate (Fig. 4.3a blowup). The backstop marks the transition from the accretionary domain at the front of the subduction complex to the more elevated topography of the outer high.

Landward of the slope break the seafloor topography is smoother than on the accretionary domain and a sediment cover becomes apparent in the MCS data (Fig. 4.3a and b). Underneath this sediment cover a rough surface is clearly visible, forming ridges and troughs in which ponded sediment is trapped. Landward of the slope break roughly between CDP 14000 and CDP 15500 only little evidence for tectonic activity can be recognized. Towards the forearc basin (between CDP 16000 and 19800), compressional forces are active and strata deformation and tectonic activity increase. Recent tectonic movement is documented by folded sedimentary strata and active faults which crop out at

the seafloor (CDP 17700-18000). Folding appears to be still active, as the seafloor sediment is affected (CDP 18800). The transition from the outer high to the forearc basin is characterized by a steep flank (CDP 19500-20000, Fig. 4.3b), dipping about 25° . This transition is extremely sharp and recent deformation is evident in folded forearc sediment 10 km landward of the outer high (CDP 20000-21800, Fig. 4.3b). The thick sedimentary sequence of the forearc basin is well documented by the reflection data. Deformation becomes less intense towards the shelf. The top basement lies at 7.5 s TWT in the center of the basin and is covered by younger sediment. The younger sequences onlap onto these strata. The seismic character of the top basement changes towards the shelf, where high, low-frequency amplitudes prevail. In contrast, in the center of the basin reduced amplitudes trace the gentle relief of the basement top here. The wavy seafloor topography between CDP 23000 and 24500 (Fig. 4.3b) is a possible indication for contourites. Moore et al. (1980) report on canyons cutting the Javanese shelf and extending into the deeper parts of the basin. These canyons would play an important role in terrigenous sediment transport and deposition. Evidence for normal faulting is also found in the Javanese shelf, where large seaward dipping faults occur at CDP 24000 and CDP 22200.

Velocities of the outer high behind the accreting wedge (i.e. within the first 60 km from the deformation front) are still fairly low. They range from 2.2 to about 4 km/s for the upper segments (Psed2), and from 4.4 to 4.6 km/s (Plac) between a depth of 6 km and the top of the subducted plate (OBH 55, Fig. 4.8). Underneath the crest of the outer high velocities gradually increase with depth, reaching values of 5.4-5.5 km/s where the maximum thickness of 20 km of the outer high is observed. Lateral velocity changes are minimal between the backstop and the crest of the outer high at CDP 17800 (OBH 60, Fig. 4.12). However, a completely different velocity structure is recorded landward of the crest and underneath the forearc basin. Increasing deformation as suggested by the MCS data is coincident with laterally increasing velocities in the lower part of the outer high. The strong lateral increase in velocities from the crest of the wedge to the forearc basin which is seen in the blowup in Figure 4.5 is documented by OBH 59 (Fig. 4.11). The upper sedimentary units (Psed1 and Psed2) show velocities of up to 4.7 km/s. The next layer displays velocities increasing from 5.5 km/s to 7.2 km/s. This is established in the transition between phases Psed2 and Plac-oc_{up} of OBH 59, where the lower velocities of phase Psed2 dominate up to a distance of a little less than 20 km. Apparent velocities are

then increasing between 20 and 25 km distance (P_{oc_up}), before decreasing again. This apparent velocity decrease at larger offsets is caused by the forearc basin sediments (P_{sed_fb}), through which the rays travel before hitting the surface. These characteristics in the raypath are also evident in neighboring stations 58 and 60 (Figs. 4.10 and 4.12). About 4 km of sedimentary fill is recorded in the forearc basin (P_{sed_fb} of OBH 64 in Fig. 4.14 and MCS data (Fig. 4.3b)), underlain by a 4 km thick unit displaying velocities from 3.5 to 4.3 km/s. This unit is underlain by the aforementioned high velocity layer with velocities between 5.5-7.2 km/s (Fig. 4.5 blowup) as is documented by phases P_{oc_up} (e.g. OBH 64 in Fig. 4.14 or OBH 66 in Fig. 4.15, P_{oc_up} indicates refracted waves through this oceanic type crust of the upper plate). Velocities of this layer increase laterally towards the Javanese shelf, where they reach velocities of 5.9 km/s at 5 km depth in the shelf. The shelf top appears as refracted phase P_{shelf} and its corresponding near-vertical reflection (e.g. OBH 66 in Fig. 4.15; compare also results from strike-line SO138-06). The lower boundary underneath the shelf and forearc basin is characterized by a velocity step from 7.2 km/s to about 8.0 km/s, as can be deduced from the critical angle i_{crit} of wide-angle reflections PmP_{up} recorded by OBH stations 60-62 (Figs. 4.12, 4.9, and 4.13, PmP_{up} for upper plate Moho reflection). Station 64 (Fig. 4.14) records this event underneath the forearc basin as a reflection (PmP_{up}). Reversed coverage is achieved by stations OBS 66 (Fig. 4.15) and OBH 67 (not shown) which recorded a strong PmP_{up} at 15-16 km depth underneath the forearc basin. The extent of this interface underneath the outer high is not clearly resolved; we extended it to profile km 170 to the downgoing plate, since we do not record any phases from the mantle transition of the subducted slab northeast of profile km 190. The landward continuation of the mantle transition of the upper plate underneath the Java shelf at ca. 15 km depth is validated by strike-line SO138-06.

4.4.2 OBH Profiles SO138-06 and SO138-07

Wide-angle data were recorded along two strike-lines to yield some 3-D constraint on the dip line (Fig. 4.2) and are supplemented by ministreamer reflection data (not shown here) (Flueh et al., 1999). Profile SO138-07 is located 93 km landward of the deformation front along the crest of the outer high. The line displays a very smooth velocity structure along the outer high with little topography variation along-strike. A sediment cover of about 1 km thickness is present above the rough surface, which was also observed on the dip line. Along this strike-line, the topography of the rough surface is much smoother

compared to the dip line. No distinguished basins or ponded sediment are visible in the ministreamer data. The deeper structure is characterized by fairly low velocities. Figure 4.16 shows data from station 78, which recorded phases to a distance of almost 80 km and thus covers almost the complete line. Reverberations of more than 1 second caused by the sedimentary strata are characteristic of all stations, so that later events might be hidden by this energy. Events Psed2 and Plac are present on all stations deployed along this profile, displaying velocities which increase from 4.1 km/s in the upper segments to 5.4 km/s at 20 km depth. While Psed2 was also clearly recorded as a near-vertical reflection, the corresponding phase for Plac is not as apparent in the primary recording but is clearly visible in the multiple (Plac-mul in Fig. 4.16). Several stations along this profile (OBH 78-81, OBH 86) recorded the top of the subducted oceanic plate. It is well imaged on the wide-angle record section of OBH 78 (Fig. 4.16) as refracted wave Poc at offsets greater than -50 km. The corresponding near-vertical reflection Ptoc is less apparent and its onset is not as clearly defined.

Profile SO138-06 is located at a distance of 180 km landward of the deformation front (Fig. 4.2). Energy penetration on this line is limited, but the velocity structure to about 20 km depth is resolved (Fig. 4.5). The data quality of the later arrivals are somewhat poorer than on the other two profiles due to a lower signal-to-noise ratio, which might have been caused by heavier ship traffic or a different current pattern close to shore. The seafloor shows some topography expressed in a trough at the eastern end of the profile. The central part of the line lies in a broad, shallow basin on top of the Java shelf (Fig. 4.5). OBH 74 is positioned near the center of this basin (Fig. 4.17). A maximum of 3 km sediment cover is resolved in the basin, which is consistent with the ministreamer recordings, which resolve ca. 1.4 s TWT of sediment fill (Flueh et al., 1999). The Java shelf is traced underneath the basin by refracted phases P_{shelf} . The very clear vertical reflection (Fig. 4.17) from the shelf top is consistent with results from the dip line (e.g. OBH 66 in Fig. 4.15). The shelf displays a thickness of about 10 km (Fig. 4.5). Here, velocities increase from 5.9 km/s to 7.2 km/s. A weak PmP_{up} documents a shallow Moho at 15 km depth, which is in accordance with the dip line (Fig. 4.17).

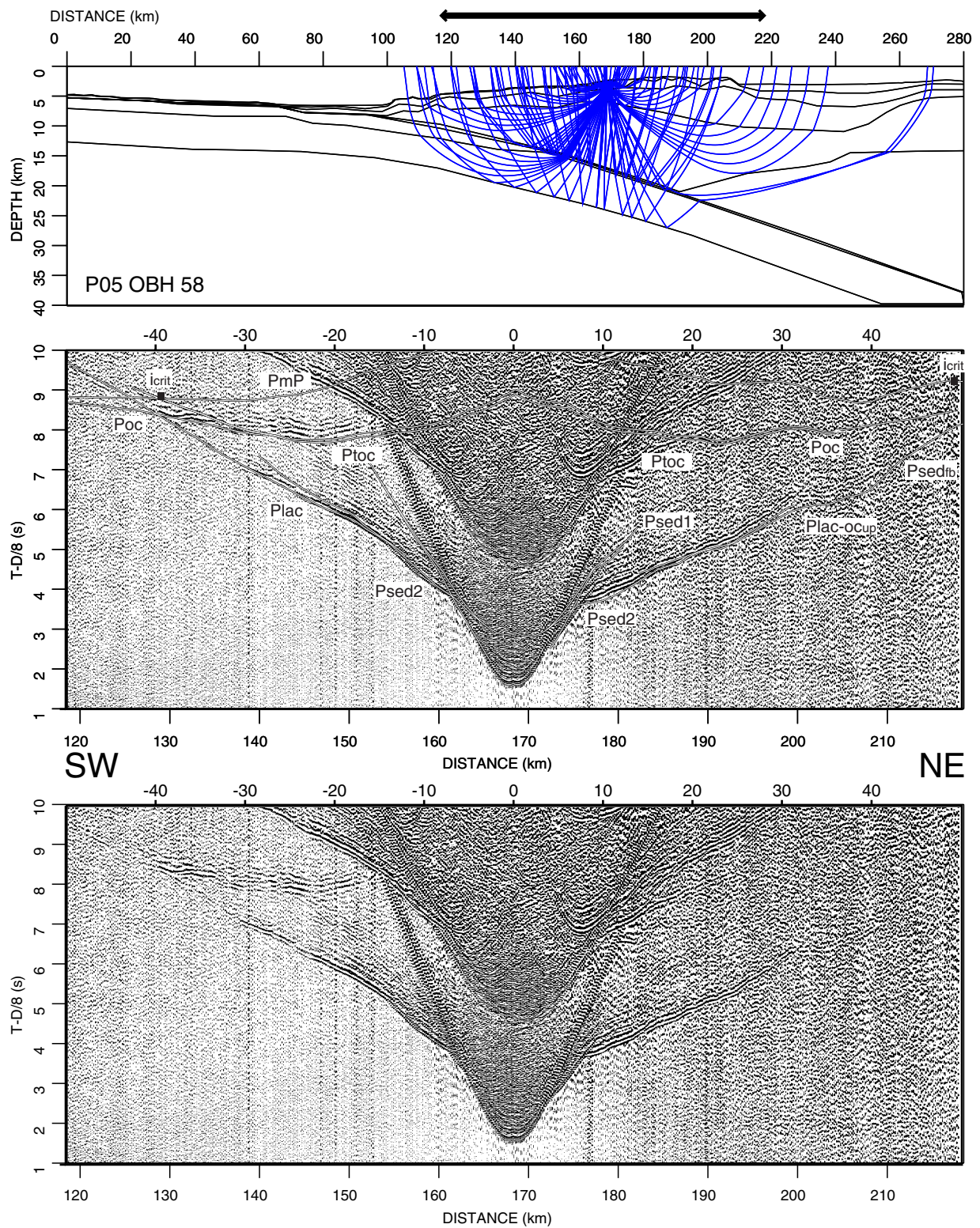


Figure 4.10: Raypaths (upper image) and seismic section for OBH 58. Strong phases P_{toc} and P_{oc} track the downgoing slab. The seaward sedimentary phases P_{sed2} and P_{lac} document the velocity structure in the accretionary domain. Landwards, phase $P_{lac-oc_{up}}$ travels through the lower accretionary complex as well as through the oceanic-type crust underneath the forearc basin, before passing through the forearc basin sediments ($P_{sed_{fb}}$).

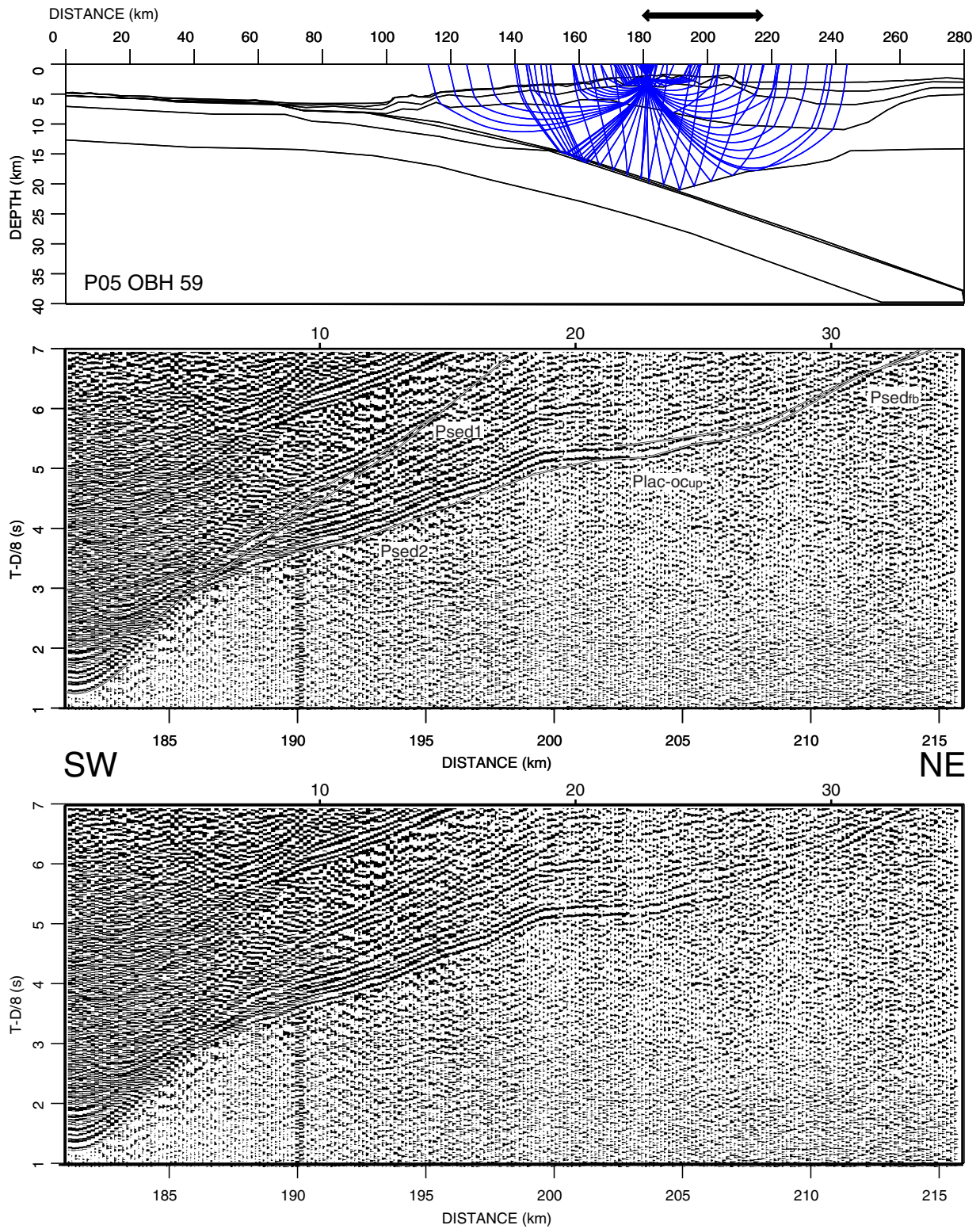


Figure 4.11: OBH 59 is located near the crest of the outer high. Phases P_{sed2} and P_{sedfb} cover the sedimentary sequences of the outer high and forearc basin. Arrivals of $Plac-oc_{up}$ ($lac-oc_{up}$ denotes lower accretionary complex-oceanic-type crust of upper plate) travelled through the layer of high velocities underlying the forearc basin sediments as is documented by the high velocities at 20-25 km offset. At larger offsets velocities decrease again as they travel through the sediment infill of the forearc basin (P_{sedfb}).

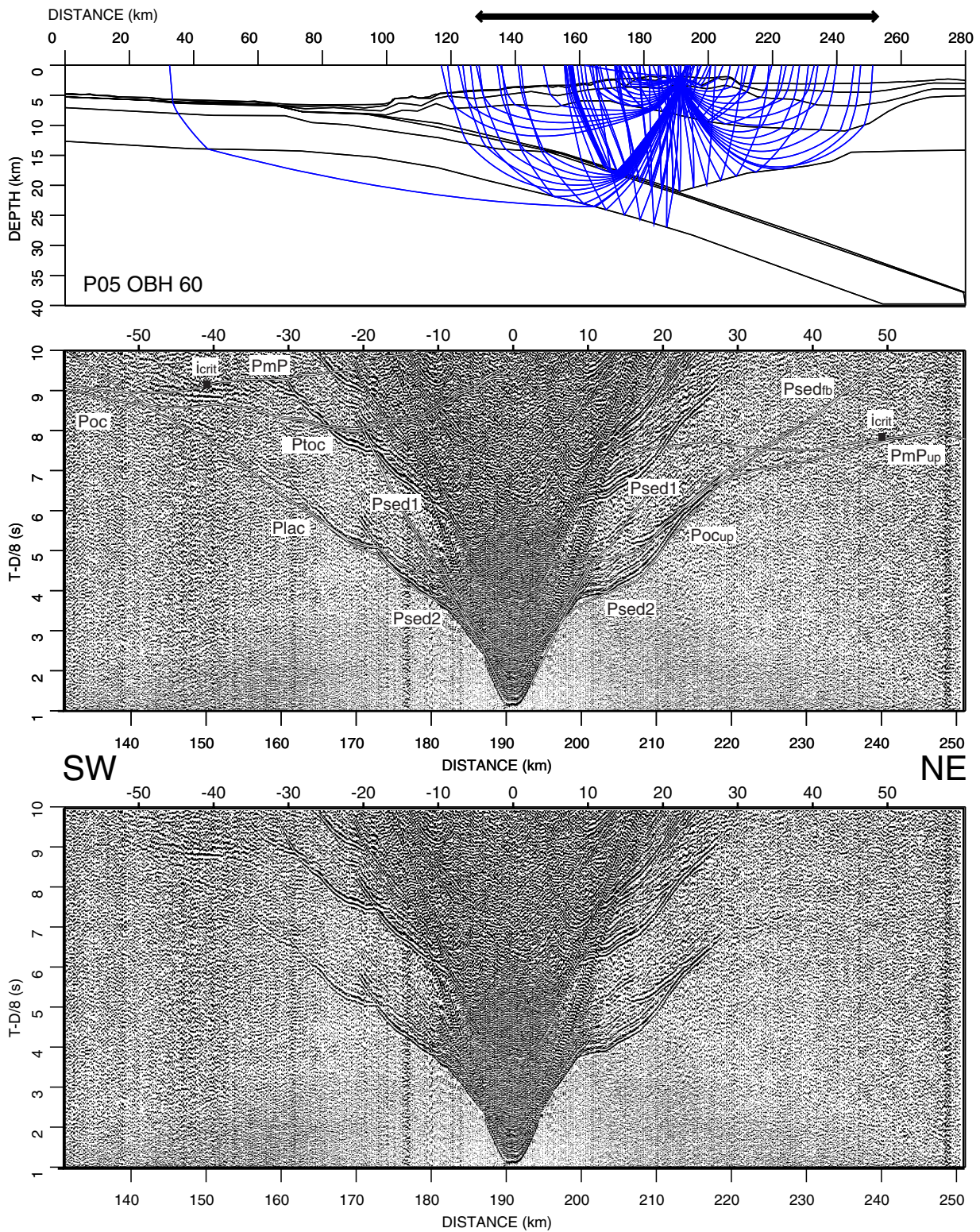


Figure 4.12: Raypaths (upper image) and seismic sections for OBH 60 which covers part of the accretionary domain, the outer high and parts of the forearc basin. Phases P_{toc} and P_{oc} track the subducted slab underneath the outer high. The velocity structure of the accretionary domain is validated by the seaward phases P_{sed2} and P_{lac}. The landward sedimentary phases verify the velocity increase underneath the forearc sediments at an offset range from 9-16 km. The upper plate mantle transition underneath the forearc basin is recorded as wide-angle reflection P_{mP_{up}}.

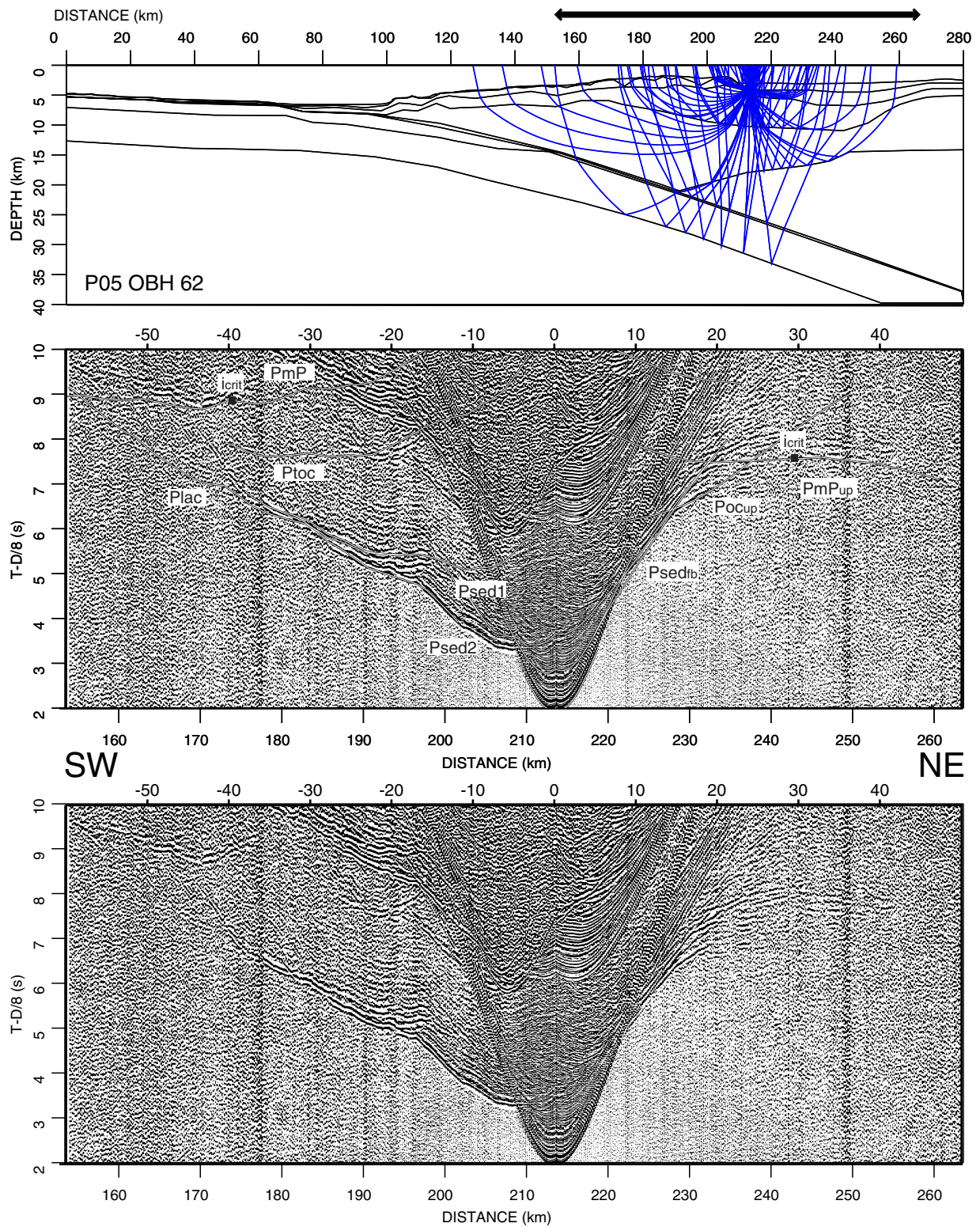


Figure 4.13: OBH 62 is the most landward station recording the top of the subducted plate P_{loc} and the oceanic Moba P_{mP} of the downgoing slab. The upper plate mantle transition underneath the forearc basin is validated by wide-angle reflection $P_{mP_{up}}$ which becomes visible at offsets beyond the critical angle i_{crit} . The mantle velocity underneath the forearc basin is calculated from this critical angle and lies between 7.9 km/s and 8.1 km/s.

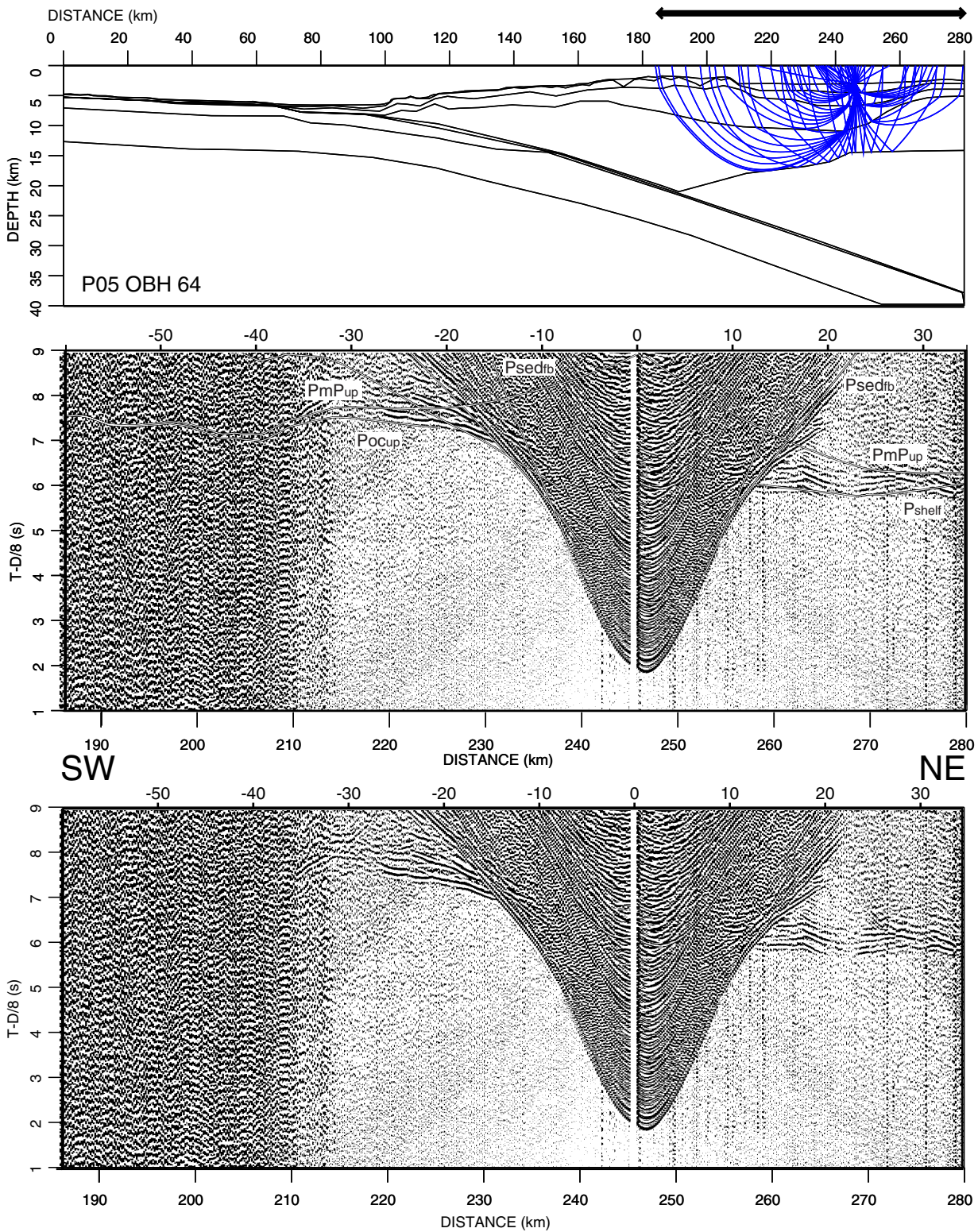


Figure 4.14: OBH station 64 is positioned in the center of the forearc basin. Phases $P_{sed_{fb}}$ denote refracted waves through the forearc basin sediment fill. Phase $P_{oc_{up}}$ documents the oceanic-type crustal layer underneath the basin while P_{shelf} travels through the shelf onset. Reflections $P_{mP_{up}}$ mark the mantle transition underneath the forearc basin.

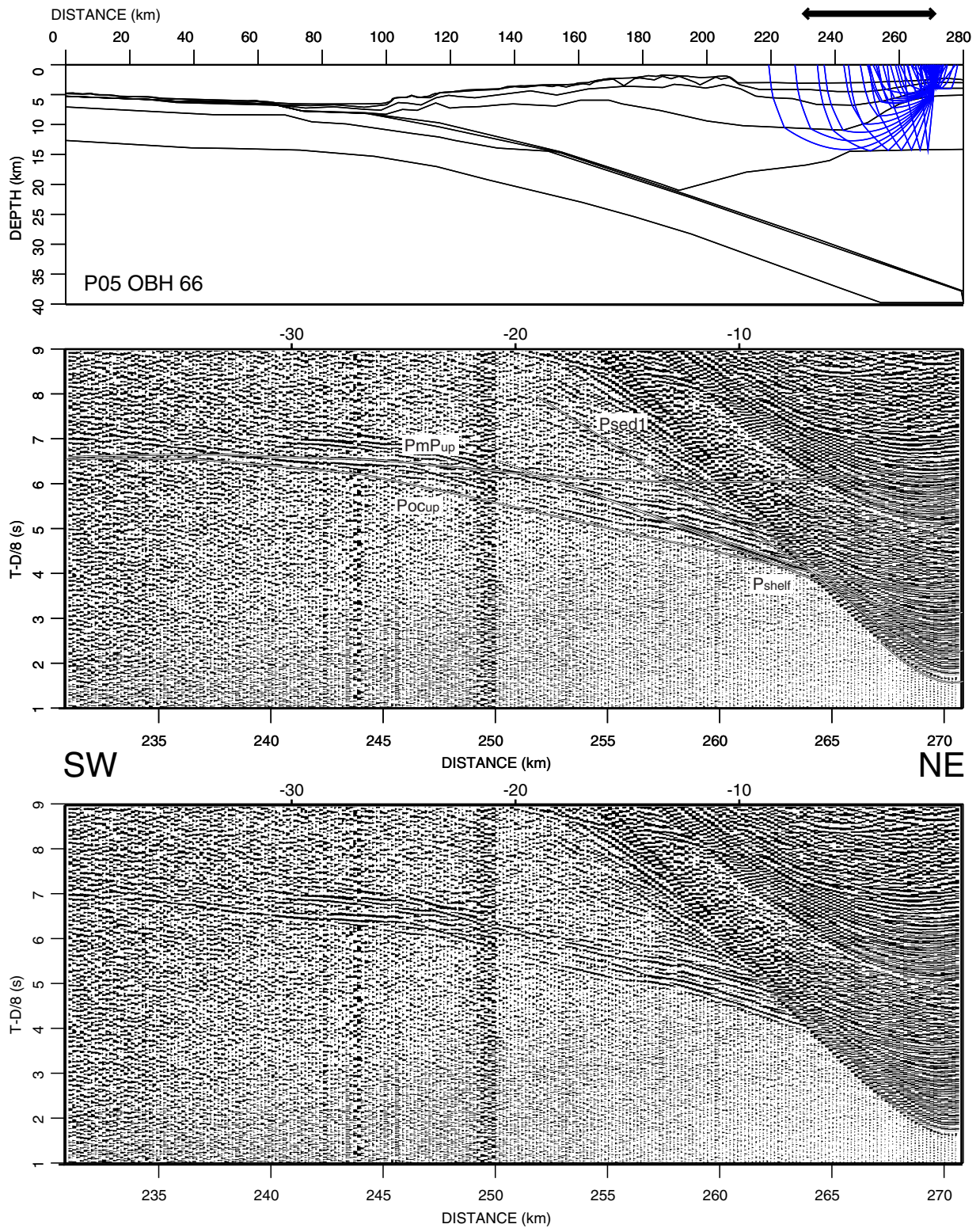


Figure 4.15: OBH station 66 is located on the Java shelf near strike-line S0138-06. Phase $P_{OC_{up}}$ travels through the oceanic-type crustal layer underneath the basin and P_{shelf} through the shelf onset. Reflection $P_{mP_{up}}$ records the upper plate Moba.

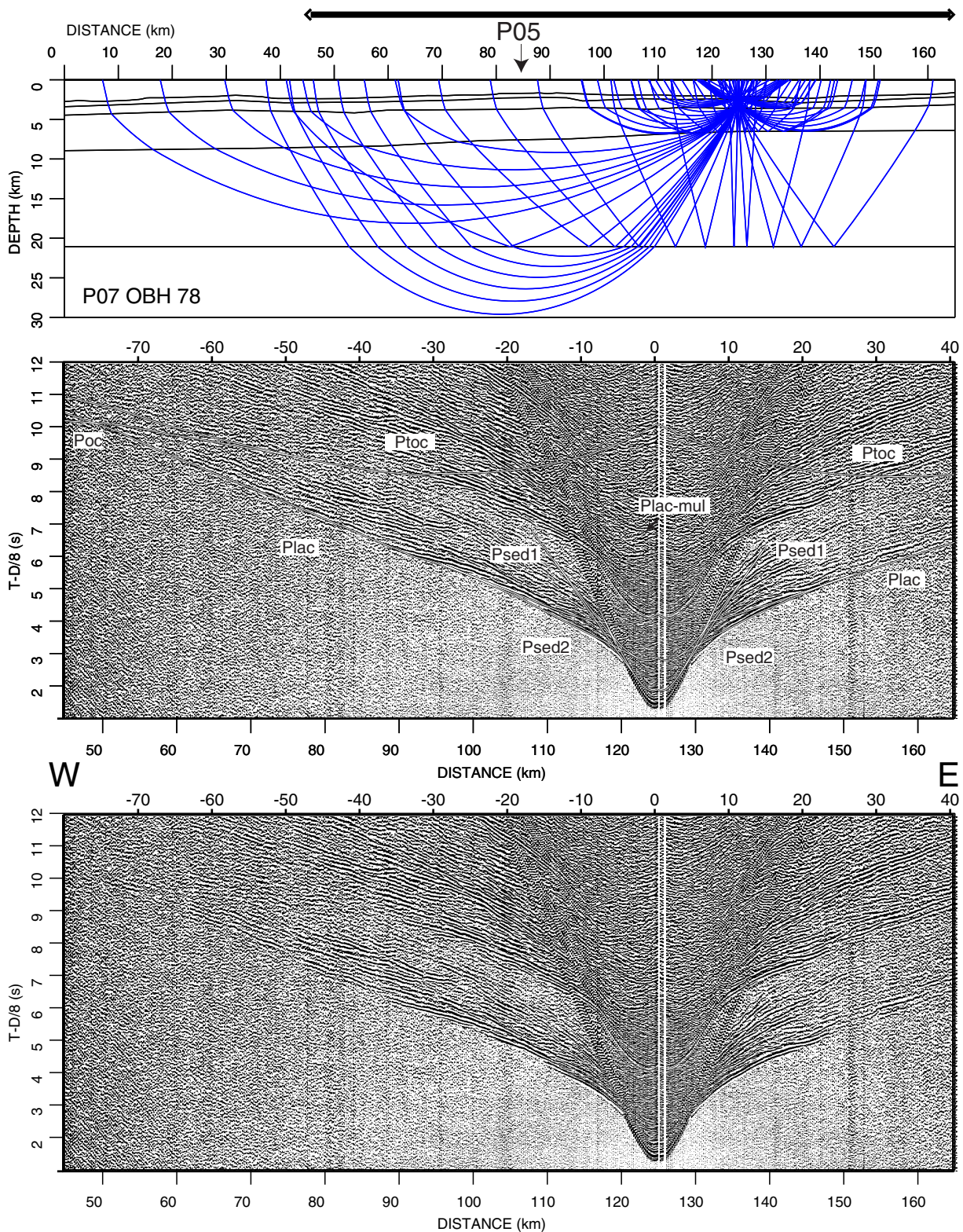


Figure 4.16: Raypaths (upper image) and seismic section for OBH 78. This is the easternmost station along strike-line S0138-07 which runs along the crest of the outer high. The fairly low velocities of the outer high are validated by arrivals P_{sed2} and Plac which can be traced to offsets over 70 km. Reflection P_{toc} from the top of the subducted igneous crust yields some 3D-constraint on the dip of the subducted slab.

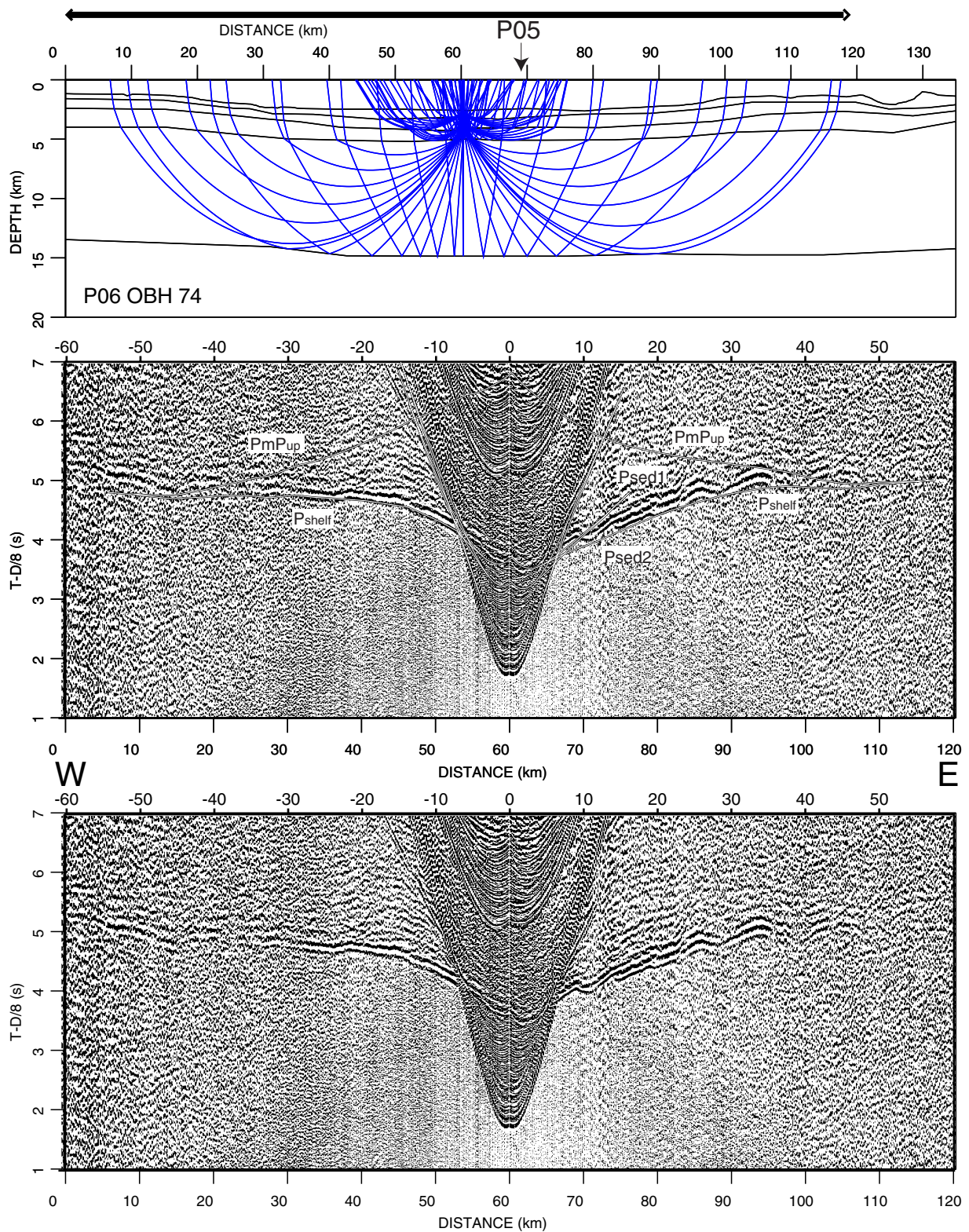


Figure 4.17: OBH 74 is located near the center of strike-line S0138-06 on the Java shelf. Phases P_{shelf} travel through the shelf basement and show velocities of ca. 6-7 km/s. The corresponding near-vertical reflection at 3.8 s is also recorded along the dip line by the stations located on the Java shelf (compare OBH 66 in Fig. 4.15). The weak $P_{mP_{up}}$ yields some constraint on the extent of the upper plate Moho underneath the shelf onset.

4.4.3 Gravity modelling

Further constraint on our model is yielded by gravity calculations for the dip line SO138-05. The gravity model was developed from the structures obtained in the velocity depth model (Fig. 4.5) to which standard constant density values were assigned (Fig. 4.18b). The calculated gravity anomaly is compared to ship data acquired by the BGR during cruise SO138 (thick grey line in Fig. 4.18a) (Heyde et al., 2000). Gravity variations of up to 210 mGal are present along the profile. The trench and the forearc basin are characterized by distinct gravity lows around profile km 90 and 230, as can be expected from the great depth of the trench and the sedimentary infill of the forearc basin, respectively. Our calculations (dark grey line in Fig. 4.18a) fit the observed data (black line in Fig. 4.18a) to within +/-10 mGal along the whole profile and thus, to first-order approximation, the 2-D modelling corresponds adequately to the observed gravity values along the dip line.

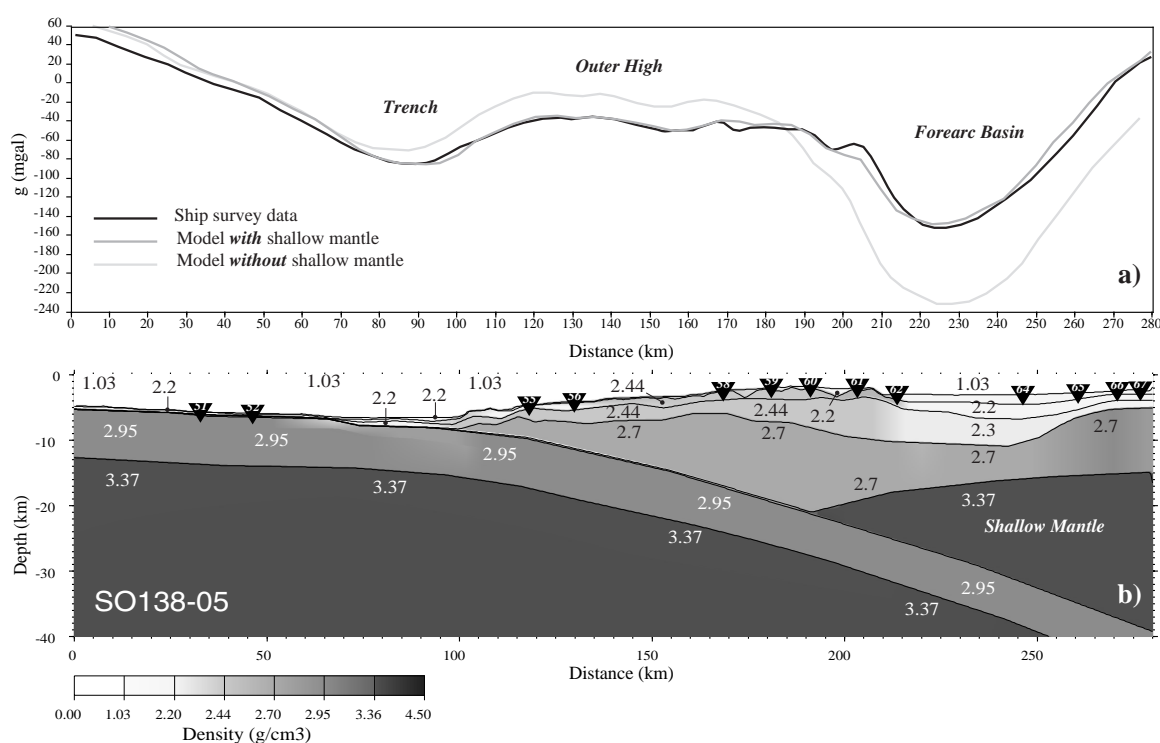


Figure 4.18: Gravity model for dip line SO138-05 (Fig. 4.18b). Density values were assigned to the velocity structures gained from forward modelling of the OBH data. The resulting gravity anomaly (black line in Fig. 4.18a) is compared to ship data acquired during cruise SO138 (Heyde, 2000) (thick grey line in Fig. 4.18a). The gravity calculations support the existence of a shallow mantle underneath the forearc basin. Without a shallow mantle, gravity discrepancies (thin grey line in Fig. 4.18a) of up to 90 mGal are observed.

Without further efforts to ensure an overall superior fit, a detailed match was nonetheless achieved except for the southwestern 30 km of the profile, where the observed gravity data are somewhat lower than the calculated values. Density values between 2.2 g/cm³ and 2.44 g/cm³ were used for the sedimentary strata (Fig. 4.18b). The subducted plate was modelled with a uniform density of 2.95 g/cm³ and the underlying mantle material with density values of 3.37 g/cm³. As no drilling information on the composition of the outer high is available, the deeper segments of the outer high and frontal prism were assumed to have density values of 2.7 g/cm³. These higher values are consistent with the greater overburden here. Assumed mantle densities of 3.37 g/cm³ yield a good fit for the oceanic mantle beneath the igneous oceanic plate and thus were also assumed for the high-velocity material observed underneath the forearc basin where a satisfactory fit is observed. Removing this shallow mantle material and replacing it with densities typical of compacted or metamorphosed sediment of 2.7 g/cm³ as found underneath the Java shelf causes a misfit of up to 90 mGal (light track in Fig. 4.18a). This misfit is too large to be compensated by variations in the density structure of the upper segments or to be caused by 3-D effects. Thus, the gravity data are in favor of the presence of mantle material underneath the forearc basin and a shallow upper plate Moho here.

4.5 Discussion

4.5.1 Oceanic crust

The velocity-depth function of the incoming igneous crust along Profile SO138-05 shows a normal velocity-depth structure comparable with Pacific oceanic crustal samples older than 29 Ma (White et al., 1992). DSDP Hole 211 at 9.78°S and 102.7°E south of southern Sumatra drilled Quaternary and Pliocene pelagic sediment and reached basement. As no Pn was recorded by the stations located on the ocean basin, the mantle velocity is not well defined but is assumed to be 8.0-8.1 km/s. This is in agreement with data derived off central Java (Curry et al., 1977) which show a similar structure of the oceanic crust and mantle seaward of the trench. Line MCS 03 recorded a 1 s TWT thick sedimentary wedge in the trench which corresponds to 1.5 km sediment thickness derived from the OBH data (Fig. 4.6). Trench fill along Java varies considerably and is highest off western Java, where sediment influx to the oceanic plate is still influenced by the Bengal fan (Moore et al., 1980). Some turbidite fill originating from axial sediment transport is resolved in the data.

This material may have been transported over hundreds of kilometers along the Sumatra-Java trench system. Near the deformation front the trench fill is already affected by minor deformation and uplift as the sediments are pushed towards the toe of the accretionary wedge.

As the crust enters the trench it starts bending gently by 3.5° (Fig. 4.19). The top of the subducted plate is traced by a number of stations as its dip increases underneath the outer high to 7° . Strike-line SO138-07 along the crest of the outer high yields some 3D constraint on the position of the slab as it is imaged at 21 km depth. As no local earthquake or tomographic studies exist, the slab configuration can only be correlated to global data, whose locations however are not detailed enough in this area to yield any conclusive information.

From beneath the deformation front to at least 50 km underneath the accretionary wedge an intracrustal reflector is recognized and interpreted as the upper to lower crust transition. Seaward of the deformation front and at greater depth this reflection is not well constrained as it is not resolved here.

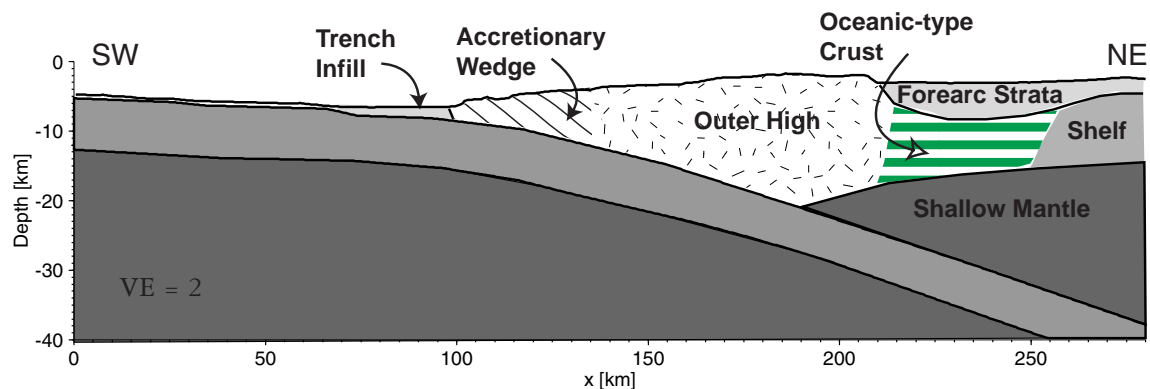


Figure 4.19: Major tectonic units of the Sunda margin. The shallow mantle underneath the forearc basin is validated by wide-angle seismic data and gravity modelling. It underlies a layer of elevated velocities which is interpreted as altered oceanic-type crust. Towards Java, the shelf onset is covered by coincident profiles SO138-05 and MCS Line SO137-03 as well as strike-line 06.

4.5.2 Structure of the accretionary domain and outer high

The accretionary domain is defined as the seawardmost forearc material which is actively deformed at present. It extends from the deformation front to the slope break 37 km landward (Fig. 4.19). A strong backstop reflection separates the accretionary unit from the

outer high. Geomorphologically, the accretionary domain is characterized by a series of bathymetric highs, the most pronounced being the distinct ridge just landward of the deformation front (CDP 10800-11700) (Fig. 4.3a). This ridge displays a quite chaotic seismic character, indicating that some deformation and tectonic activity is currently occurring at the toe of the accretionary prism. Several imbricate thrust faults are recognized, most of which cut the seafloor and are still active. As the trench fill sediments are accreted and underthrust beneath this accretionary ridge, uplift is expressed in intense faulting. It remains unclear how much sediment is transported in a bypass channel beyond the active backstop structure. We interpret the frontal prism as evidence for ongoing accretion, resulting in the variable seafloor topography of accretionary ridges and a high degree of deformation and faulting. The velocity model supports this interpretation as lateral velocity changes occur up to the location of the backstop structure. The fairly low (<4.6 km/s) velocities are representative of young accreted sediment. A different situation emerges landward of the slope break. Tectonic activity in the seaward part of the outer high is less profound compared to the accretionary domain. Reflectivity within the outer high underneath the rough surface is limited in the reflection data. Velocities show little lateral variation but increase moderately with depth (<5.5 km/s) due to material compaction. These velocities are supported by the results of strike-line SO138-07 and are roughly in accordance with existing refraction data from central Java (Curry et al., 1977). As no drilling information is available for the Java subduction complex (the closest drill holes are located within Sunda Strait on the Java shelf) the composition of the outer high basement is not known. Our velocity results indicate a sedimentary origin, possibly metamorphosed near the base, however drilling information is needed to verify this assumption.

Whereas the seaward part of the outer high shows little evidence for active deformation, the landward part towards the forearc basin is experiencing ongoing activity. Several large faults are recognized (e.g. around CDP 17800 or 18400), which seem to be still active as they affect the seafloor. The rough surface is more distinctly expressed towards the forearc domain, where its geomorphology forms several basins of increasing depth resulting from the steepening of the old accreted strata now forming the backstop. Sediment ponded in these basins is highly deformed. The folded strata affect the seafloor (e.g. around CDP 18800) and tectonic compressional activity is still ongoing.

4.5.3 Forearc domain

Compression also affects the seaward part of the forearc basin where large folds involving all sedimentary units cause a slight uplift of the seafloor. This remarkable pattern of large scale folding and the pronounced unconformity at the outer high-forearc basin transition compose the most striking aspect of the forearc basin structure. Landward of the depocenter deformation of the sedimentary strata ceases. The nature of the outer high/forearc transition remains open. Malod and Kemal (1996) propose that the dextral strike-slip movement along the Sumatra fault is relayed to the south by the Ujung Kulon fracture zone (Fig. 4.1) which runs from the Sunda Strait transtensional basin (Lelgemann et al., 2000) along the northern transit of the outer high and fringes the forearc basin south of Java. Its southeastern extent is however not well established and thus an interpretation of the outer high/forearc transition observed here as a strike-slip fault or continuation of the Ujung Kulon fracture zone, which is suggested by the seismic signal and the presence of the large basin, lies beyond the scope of this data set.

The dip line covers the southwesternmost part of the Java shelf (Fig. 4.19), which is composed of large downfaulted basement blocks rotated to the northeast. Existing multichannel data off central Java show a similar pattern (van der Werff, 1995). Well data on the Java shelf north of Java island indicate that the shelf basement consists of late Oligocene volcanic rocks (Bolliger and de Ruiter, 1975). Mesozoic-Paleogene mélangé and intrusives related to an older active plate margin may also compose the basement (van der Werff, 1995). The velocity layer underneath the forearc basin displays a 5-7 km thick unit with velocities increasing laterally towards the Java shelf. The higher velocities of the shelf correlate to the basement blocks indicating a composition of metamorphosed pyroclastic sediment drilled in the Sunda Strait (Lelgemann et al., 2000). Underneath the forearc basin however this unit is more oceanic in character. Velocities increase from 5.5 km/s to 7.2 km/s. Similar results were reported off central Java (Curry et al., 1977) where a layer of variable velocity and thickness underlying the forearc basin is interpreted as altered oceanic crust. We favor an interpretation of this unit underneath the forearc basin as an oceanic-type crust (Fig. 4.19). The base of this unit marks a crust-mantle transition, as the seismic and gravity data support the existence of mantle material here (Fig 19). One possible explanation for oceanic-type crust positioned underneath the forearc basin would be an

interpretation as remnant pieces of older oceanic crust. The subduction of the former Tethys ocean coincided with the opening of the Indian ocean by rapid seafloor spreading during Cretaceous to middle Eocene times (Daly et al., 1991; Packham and Harbury, 1996). After the complete subduction of Tethys incipient northward subduction of the Indian ocean along the newly formed Sunda trench was initiated (Rangin et al., 1990), accompanied by a renewal of volcanic arc activity (Packham and Harbury, 1996). The Tethys suture zone which crosses western Java (Rangin et al., 1990) represents the remaining fragment of this ocean and marks the trace of the subducted Tethys ocean. Without drilling and age information however an interpretation and evaluation of the oceanic crust found underneath the forearc basin cannot be well established and remains open.

4.6 Conclusions

The combined analysis and interpretation of the wide-angle and reflection seismic data, together with the results of the 2D gravity modelling have allowed us to identify the major structural elements of the West Java margin at shallow and deep crustal levels (Fig. 4.19). The structure of the subduction complex was resolved in detail by the reflection data and together with the velocity information gained from the wide-angle data the following conclusions can be drawn:

- 1) The data clearly define a gently dipping Indian Plate that subducts at the trench at about 3.5° and increases gradually to 7° beneath the outer high. The incoming igneous oceanic crust shows a thickness of 7.4 km and a velocity structure that lies within the range of values obtained for similar oceanic settings. The configuration of the descending slab is supported by the results of strike-line SO138-07 which tracks the subducted plate at 21 km depth and by the gravity modelling conducted along the dip line.

- 2) The seaward part of the margin is occupied by a 35 km wide and 7 km deep accretionary wedge. Accretion is ongoing as is suggested by the intense faulting and indicated by the existence of accretionary ridges in the frontal part of the margin. This is further supported by the velocity structure, which is characterized by low velocities (4.6 km/s at 7 km depth) and a lateral positive velocity gradient. The landward termination of

the active accretionary domain is marked by a slope break and corresponding backstop structure, which represent a major structural break.

3) The massive outer high is ca. 75 km wide and 20 km deep. Velocities are moderate underneath the outer high, displaying a downward positive gradient and reaching velocity values of 5.5 km/s at 20 km depth. The material composition of the outer high is not known. The velocity model presented here makes an igneous or ophiolitic composition unlikely. A sedimentary composition, possibly containing metamorphosed material at its base, is coherent with the moderate velocities found here, but would need to be justified by drilling information. The seaward part of the outer high shows little evidence for tectonic activity. The reflection data failed to resolve any details underneath the rough surface basement top. Strata deformation caused by compression increases towards the forearc basin and is expressed in intense folding of the ponded sediment on the outer high and of the forearc sediment fill. The cause of these compressional forces remains unexplained.

4) One crucial aspect of the study regards the nature of the forearc basement. A layer of elevated velocities was found underneath the forearc basin and shelf onset. Underneath the forearc basin, the layer displays an oceanic-type velocity structure, whereas underneath the shelf the higher velocities (>5.9 km/s) are attributed to rotated basement blocks of metamorphosed pyroclastic sediment which were identified in the MCS data. The base of this layer displays a velocity step from 7.2 km/s to ca. 8.0 km/s as is deduced from the refracted waves through this segment and from the critical angle of the rays reflected from this boundary. The shallow upper plate Moho underneath the forearc basin is supported by the 2D gravity modelling which expects high density material here. A possible source for oceanic-type crust might be remnant fragments of former oceanic crust that has been altered and might be related to the subduction of the former Tethys ocean. Drilling and age information as well as local earthquake data would help to further unravel the tectonic evolution of the margin.

- Bolliger, W., and P.A.C. De Ruiter, Geology of the south central Java offshore area, *Proc. Indon. Petr. Ass., 4th Ann. Convention*, 67-82, 1975.
- Curry, J. R., G. G. Shor, R. W. Raitt, M. Henry, Seismic refraction and reflection studies of crustal structure of the eastern Sunda and western Banda Arcs, *Journal of Geophysical Research*, 82, 17, 2479-2489, 1977.
- Daly, M.C., M.A. Cooper, I. Wilson, D.G. Smith, B.G.D. Hooper, Cenozoic plate tectonics and basin evolution in Indonesia, *Marine and Petroleum Geology*, 8, 2-21, 1991.
- DeMets, C., R. G. Gordon, D. F. Argus, S. Stein, Current plate motions, *Geophysical Journal International*, 101, 425-478, 1990.
- Diament, M., C. Deplus, H. Harjono, M. Larue, O. Lassal, J. Dubois, V. Renard, Extension in the Sunda Strait (Indonesia): a review of the Krakatau programme, *Oceanologica Acta Special Volume*, 10, 31-42, 1990.
- Flueh, E.R. and J. Bialas, A digital, high data capacity ocean bottom recorder for seismic investigations, *Int. Underwater Systems Design*, 18, 3, 18-20, 1996.
- Flueh, E.R. (edt) and Shipboard Science Party, GINCO2 (SONNE Cruise SO-138): Geo-scientific investigations along the active convergence zone between the Eastern Eurasian and Indo-Australian Plates off Indonesia, *Cruise Report*, Geomar, Kiel, 1999.
- Hamilton, W., Tectonics of the Indonesian region, *U.S. Geological Survey Professional Paper* 1078, 1979.
- Hamilton, W., Plate tectonics and island arcs, *Geological Society of America Bulletin*, 100, 1503-1527, 1988.
- Heyde, I., H. A. Roeser, B. Schreckenberger, Gravimetric measurements and their interpretation, *GINCO Final Report*, Part I, BGR, Hannover, 2000.
- Huchon, P., and X. Le Pichon, Sunda Strait and Central Sumatra fault, *Geology*, 12, 668-672, 1984.
- Izart, A., B. Mustafa Kemal, J. A. Malod, Seismic stratigraphy and subsidence evolution of the northwest Sumatra fore-arc basin, *Marine Geology*, 122, 109-124, 1994.
- Karig, D.E., G. F. Moore, J. R. Curry, M. B. Lawrence, Morphology and shallow structure of the lower trench slope off Nias Island, Sunda Arc, in: The tectonic and geologic evolution of Southeast Asian seas and islands, D. Hayes (edt), *Geophysical Monograph*, 23, 179-208, 1980.
- Lelgemann, H., M.-A. Gutscher, J. Bialas, E. R. Flueh, W. Weinrebe, C. Reichert, Transtensional basins in the western Sunda Strait, *Geophysical Research Letters*, 27, 21, 3545-3548, 2000.
- Luetgert, J., MacRay-Interactive two-dimensional seismic raytracing for the Macintosh, *U.S. Geological Survey Open File Report*, 92-356, 1992.
- Malod, J. A., and B. M. Kemal, The Sumatra margin: oblique subduction and lateral displacement of the accretionary prism, in: Tectonic evolution of Southeast Asia, R. Hall and D. Blundell (edts), *Geological Society Special Publication*, 106, 19-28, 1996.
- Malod, J. A., K. Karta, M.O. Beslier, M.T. Zen Jr., From normal to oblique subduction: Tectonic relationships between Java and Sumatra, *Journal of Southeast Asian Earth Sciences*, 12, 85-93, 1995.
- McCaffrey, R., Oblique plate convergence, slip vectors, and forearc deformation, *Journal of Geophysical Research*, 97, B6, 8905-8915, 1992.
- Moore, G. F., J. R. Curry, D. G. Moore, D. E. Karig, Variations in geologic structure along the Sunda fore arc, Northeastern Indian Ocean, in: The tectonic and geologic evolution of Southeast Asian seas and islands, D. Hayes (edt), *Geophysical Monograph*, 23, 145-160, 1980.

- Packham, G., Cenozoic SE Asia: reconstructing its aggregation and reorganization, in: Tectonic evolution of Southeast Asia, R. Hall and D. Blundell (eds), *Geological Society Special Publication*, 106, 123-152, 1996.
- Puspito, N. T., and K. Shimazaki, Mantle structure and seismotectonics of the Sunda and Banda arcs, *Tectonophysics*, 251, 215-228, 1995.
- Rangin, C., L. Jolivet, M. Pubellier, A simple model for the tectonic evolution of southeast Asia and Indonesia region for the past 43 m.y. , *Bull. Soc. Geol. France*, 6, 889-905, 1990.
- Rangin, C., and M. Pubellier, The quest for Tethys in the western Pacific. 8 paleogeodynamic maps for Cenozoic time, *Bull, Soc. Geol. Fr.*, 8, 907-913, 1990.
- Reichert, C. (edt) and Shipboard Science Party, GINCO1 (SONNE Cruise SO-137): Geo-scientific investigations along the active convergence zone between the Eastern Eurasian and Indo-Australian Plates off Indonesia, *Cruise Report*, BGR, Hannover, 1999.
- Samuel, M. A., and N. A. Harbury, The Mentawai fault zone and deformation of the Sumatran forearc in the Nias area, in: Tectonic evolution of Southeast Asia, R. Hall and D. Blundell (eds), *Geological Society Special Publication*, 106, 337-351, 1996.
- Tregoning, P., F. K. Brunner, Y. Bock, S. S. O. Puntodewo, R. McCaffrey, J. F. Genrich, E. Calais, J. Rais, C. Subarya, First geodetic measurement of convergence across the Java Trench, *Geophysical Research Letters*, 21, 19, 2135-2138, 1994.
- White, R.S., D. McKenzie, R.K. O'Nions, Oceanic crustal thickness from seismic measurements and Rare Earth Element inversions, *Journal of Geophysical Research*, 97, B13, 19681-19715, 1992.
- van der Werff, W., Forearc development and early orogenesis along the Eastern Sunda/Western Banda arc (Indonesia), *Phd Thesis*, Amsterdam, 1995.
- Widiyantoro, S., and R. van der Hilst, Structure and evolution of lithospheric slab beneath the Sunda Arc, Indonesia, *Science*, 271, 1566-1570, 1996.
- Wilson, P., J. Rais, C. Reigber, E. Reinhart, B. A. C. Ambrosius, X. Le Pichon, M. Kasser, P. Suharto, Dato' Abdul Majid, Dato' Paduka Awang Haji Othman Bin Haji Yaakub, R. Almeda, C. Boonphakdee, Study provides data on active plate tectonics in Southeast Asia region, *EOS Transactions*, 79, 45, 545-549, 1998.

5. CRUSTAL STRUCTURE OF THE CENTRAL SUNDA MARGIN AT THE ONSET OF OBLIQUE SUBDUCTION

5.1 Introduction

The central Sunda margin along the southern termination of the Indonesian Archipelago (Fig. 5.1) presents a prime target for investigations on the variation of forearc structures related to an increasing obliquity of plate collision. The curvature of the trench is the main characteristic of this subduction complex, resulting in regimes of frontal subduction off Java to oblique subduction off Sumatra which becomes subparallel towards the Andaman Sea (Fig. 5.1) (Fitch, 1972; Hamilton, 1979; Moore et al., 1980; Huchon and Le Pichon, 1984). The region poses an archetype example for the partitioning of the convergent motion into a component of thrusting at the trench and a component of arc-parallel strike-slip motion, resulting in a lateral displacement of the forearc platelet along the dextral Sumatra strike-slip fault and possibly along the Mentawai fault zone which runs along the outer border of the forearc basin (Diament et al., 1992; Malod and Kemal, 1996). The increasing obliquity in the Sumatra area induces decoupling of the downgoing slab from the upper plate by strain partitioning (Malod and Kemal, 1996). As can be deduced from the analysis of slip vectors, decoupling off Sumatra is not fully complete (McCaffrey, 1991; McCaffrey, 1992; McCaffrey, 1996). Geodetic observations show a high degree of coupling of the forearc domain to the downgoing slab in the south, decreasing to the north (Prawirodirdjo et al., 1997). Decoupling by strain partitioning alone can thus not fully explain the difference in the amount of extension in the Sunda Strait (<100 km) and the Andaman Sea (>400 km) (Bellier and Sébrier, 1995; McCaffrey, 1996). Additional stretching of the forearc domain could account for this discrepancy and is coherent with an increase in slip rate along the Sumatra Fault (Bellier and Sébrier, 1995). The mechanism of the forearc stretching is still not fully understood as is the role of the Mentawai Fault zone. The tectonic differences and dynamics along the 5600 km long Sunda Arc also result from the variation of several other geological parameters, including the age of the subducted plate and the thickness of the incoming sediment cover (Curry et al., 1977; Hamilton, 1979; Moore et al., 1980). The Sunda margin has been the locus for a series of scientific investigations (McCaffrey, 1992; Izart et al., 1994; Malod and Kemal, 1996; Samuel and Harbury, 1996), however, only scarce seismic data covers the transition zone from oblique to frontal subduction off southern Sumatra and the Sunda Strait (Fig. 5.1). A detailed

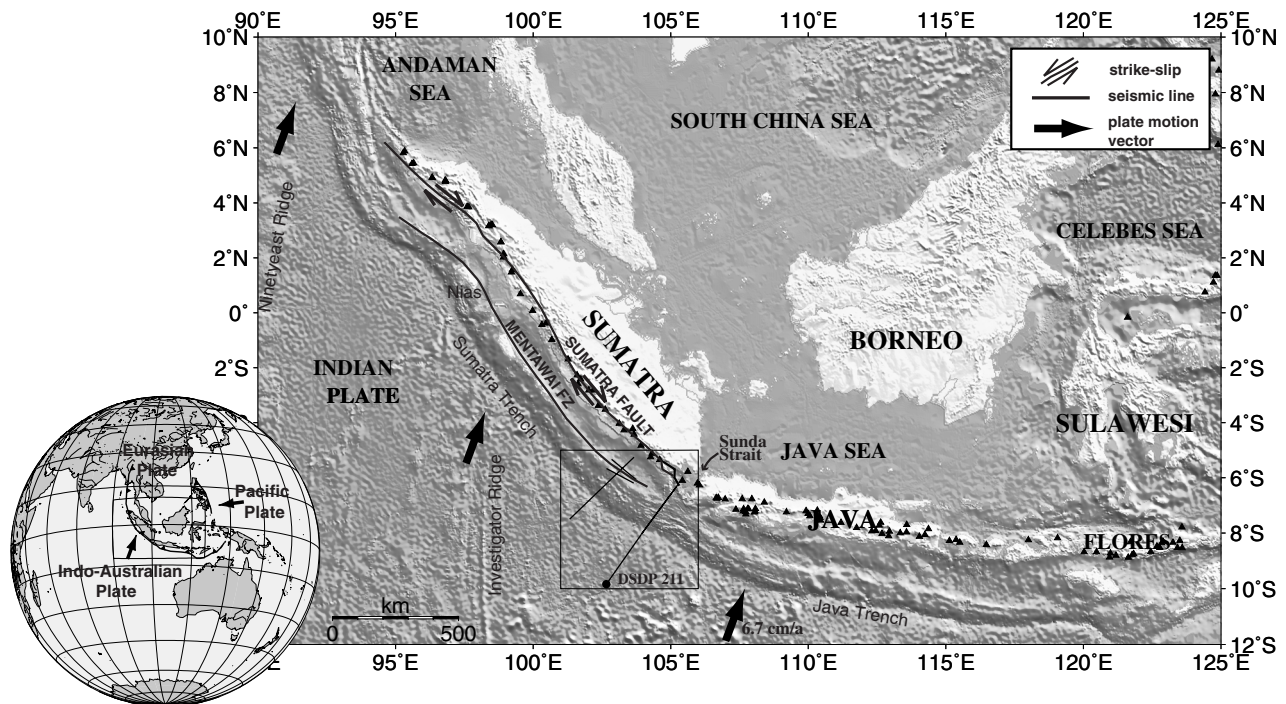


Figure 5.1: Bathymetric map of western Indonesia where the Indo-Australian plate is thrust underneath Eurasia along the Sumatra and Java trench system. The change in orientation of the Sunda margin causes an increase in subduction obliquity to the northwest. Subduction is frontal off Java and oblique off Sumatra where strain partitioning leads to the initiation of the Sumatra strike-slip fault and possibly the Mentawai transpressional fault. The study area is located at the juncture of these two subduction regimes as indicated by the box. Plate motion vectors are from the Australia-Eurasia rotation pole after DeMets (1990). Volcanic distribution is taken from the Smithsonian Global Volcanism Program data set; bathymetric information is extracted from the Topex data set.

investigation of this progression was the aim of the project GINCO (Geo-scientific INvestigations along the active CONvergence zone between the eastern Eurasian and Indo-Australian Plates off Indonesia) during which we collected seismic multichannel reflection (MCS) and wide-angle refraction data across the Sunda subduction zone and within the forearc domain using the RV SONNE during November, 1998 through January, 1999. We present here the interpretation of two seismic lines off southern Sumatra and off Sunda Strait along which coincident MCS and wide-angle seismic data were acquired. In addition, we discuss two wide-angle strike-lines covering the forearc domain off Sumatra which yield some 3D-constraint on the derived velocity-depth model. Along the two wide-angle dip lines the downgoing plate is tracked from the trench to a depth of more than 30 km which is supported by supplementary gravity modelling. Moreover, the structure of the Sunda margin is resolved in considerable detail by the MCS data. The velocity structure of the forearc domain is derived from forward raytracing of the two-strike lines, complemented by

comparisons with synthetic data. Based on these newly acquired seismic data and their interpretation we present a detailed cross-section and discuss the crustal structure of the subduction zone off southern Sumatra and off Sunda Strait.

5.2 Geodynamic Setting

The Sunda Arc marks the collision zone where the Indo-Australian plate is thrust underneath the Eurasian plate (Fig. 5.1). The subduction system has been active since at least Oligocene and evolved after the late Eocene collision of India with Eurasia (Hamilton, 1988). The present day kinematics of the Sunda margin (Fig. 5.1) are described to the first order by global plate motion solutions (NUVEL-1 and NUVEL-1A) (DeMets et al., 1990; DeMets et al., 1994). Additional GPS measurements determine the motion of Australia with respect to West Java at 67 mm/yr in a direction N11°E, which is orthogonal to the trench (Tregoning et al., 1994).

The investigated area is positioned across the Sunda collision zone off southern Sumatra and off Sunda Strait (Fig. 5.2). Located at the point of directional change of the trench, Sunda Strait marks a transition zone between orthogonal subduction off Java and oblique subduction off Sumatra. Sunda Strait is located at the southern termination of the Sumatra Fault (Malod et al., 1995) and has evolved under a transtensional regime, as is evident from seismic investigations (Diament et al., 1990; Lelgemann et al., 2000) and from local seismicity (Harjono, 1991). The age of the incoming plate increases from Sumatra in the west to Flores in the east (Fig. 5.1). Off southern Sumatra, the plate age is about 90 Ma (Widiyantoro and van der Hilst, 1996). The increase in age is consistent with an increase in plate dip along the arc (Widiyantoro and van der Hilst, 1996), and an increasing depth of seismic activity. Underneath the Sumatran part of the arc, seismicity does not exceed 250 km in depth (Puspito and Shimazaki, 1995), while further east seismic activity up to 670 km depth occurs. The width and elevation of the accretionary complex and outer high increases to the north of Sumatra (Moore et al., 1980), where sediment influx on the incoming plate is greater than off Java. Parts of the outer high are exposed subaerially in an island chain (e.g. Pulau Enggano in Fig. 5.2) which parallels the Sumatra trench (Moore et al., 1980). The island of Nias (Fig. 5.1) provided the focus for a number of geophysical and geological investigations. Early studies (Moore et al., 1980) interpreted Nias as part of the subduction complex which had been uplifted due to the accretion of thick Bengal fan

sediments which reached the area in Middle to Late Miocene. More recently, Samuel et al. (1995) interpret Nias as the results of inversion of extensional sub-basins. Early refraction studies around Nias (Kieckhefer et al., 1980) covered a wedge and outer high of about 20 km thickness which composes Nias island. Velocities are moderate (<5 km/s), increasing towards the forearc basin. The nature of the forearc basin basement is assumed to be continental. Off Sumatra, a distinct forearc basin is divided into several large sub-basins (Moore et al., 1980). The seismic stratigraphy of the forearc domain has been determined around Nias from reflection seismic data and borehole information (Beaudry and Moore, 1981; Beaudry and Moore, 1985; Izart et al., 1994). Expanding the work of Beaudry and Moore, Izart et al. (1994) propose a Paleogene uplift of the Sumatra margin followed by Miocene subsidence which increases during the Pliocene and Quaternary.

5.3 Seismic Data

Seismic multichannel reflection data were collected during leg SO137 of the German RV SONNE (Reichert, 1999). Profile SO137-12 is located off southern Sumatra, approximately 75 km southeast of the island of Enggano (Fig. 5.2) and extends from the Sunda trench to the Sumatra shelf. A second line (SO137-42) covers the subduction complex further southeast off Sunda Strait and extends about 250 km seaward of the trench onto the ocean basin. The data were recorded along a 3 km long streamer with a maximum of 120 channels and a recording length of 14 s. Along both lines coincident wide-angle data were acquired (profiles SO138-01 and SO138-04 in Fig. 5.2) during the next leg of RV SONNE (Flueh, 1999). Both OBH-lines are extended about 100 km seaward of the trench to obtain reversed coverage on the oceanic crust. In addition, two wide-angle strike-lines were shot across OBH-profile 01: Profile 02 covers the landward part of the outer high at the transition to the forearc basin while line 03 runs along strike the depocenter of the forearc basin. Along the various profiles a total of 50 stations were deployed, consisting mainly of the GEOMAR ocean-bottom hydrophones (OBH) (Flueh and Bialas, 1996) with a few ocean-bottom seismometers. Instrument locations are provided in Figure 5.2. The same seismic source was applied during both legs and signals were generated by a tuned set of 20 airguns grouped in two identical linear sub-arrays. The total volume of the array is 51.2 liters (3.124 cu. in.). For the multichannel reflection recordings a shot interval of 50 m and a hydrophone spacing of 25 m were chosen, resulting in a CMP distance of 12.5 m and a maximum fold of 30. Processing included frequency filtering after an amplitude

balancing and trace editing of the shot gathers. A primary focus during data processing was laid on multiple removal, which was achieved in the f-k domain based on move-out differences between primary and multiple events in the CMP gather. A trace interpolation was applied to prevent aliasing before f-k multiple reduction.

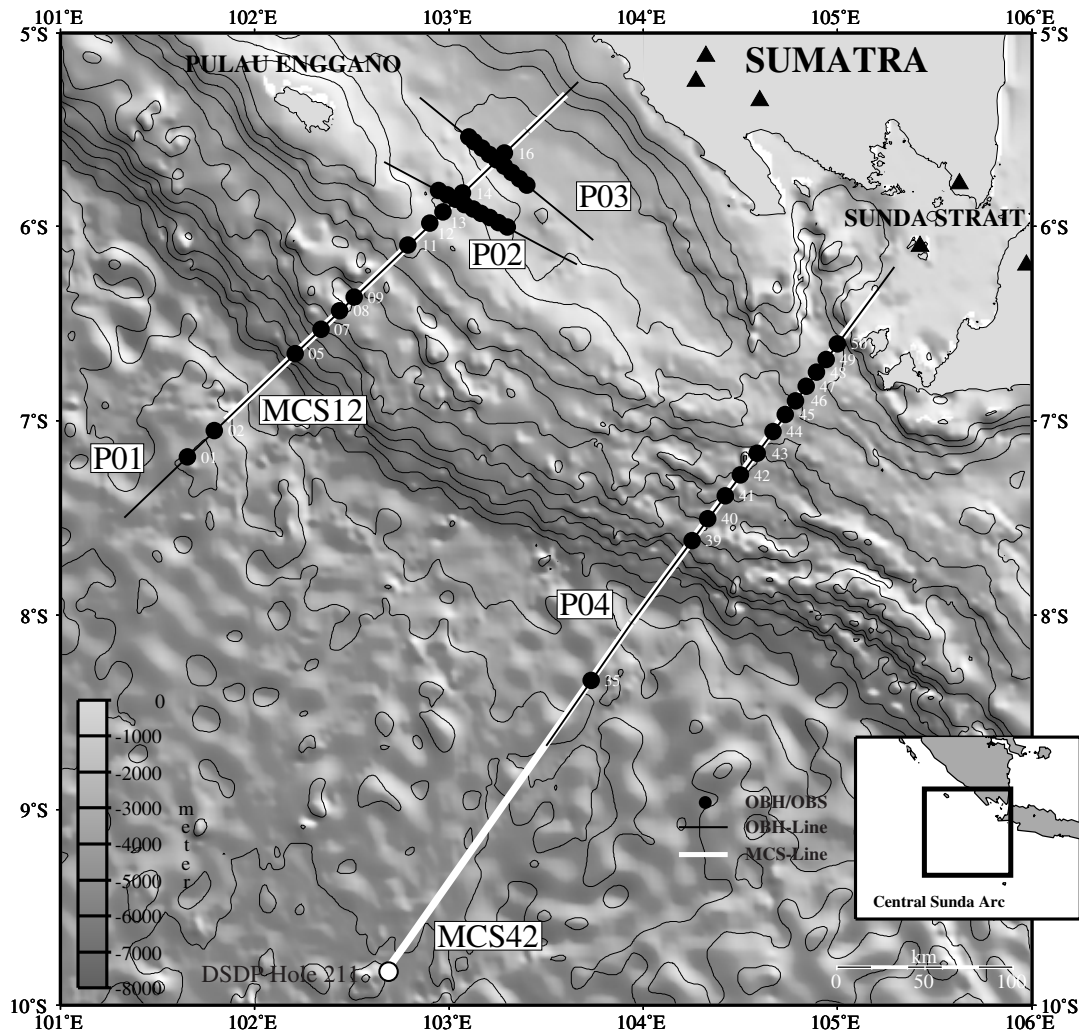


Figure 5.2: Location map of the seismic survey across the plate margin off southern Sumatra and off Sunda Strait. The seafloor bathymetry is illuminated from the northeast. A total of 50 instruments recorded wide-angle data along 950 profile kilometers. Refraction and reflection seismic data were acquired along the corresponding dip lines P01 and MCS12 as well as along P04 and MCS42. Shooting along MCS42 was extended for about 250 km beyond the trench onto the ocean basin. Additional wide-angle data were recorded along the two strike lines P02 and P03 which are located along strike the crest of the outer high and the Sumatra forearc basin, respectively.

An enhanced signal resolution and further multiple suppression was achieved by a two-gated predictive deconvolution. However, the demultiple process is inhibited due to limited energy coherency within the CMP gathers resulting from the highly variable

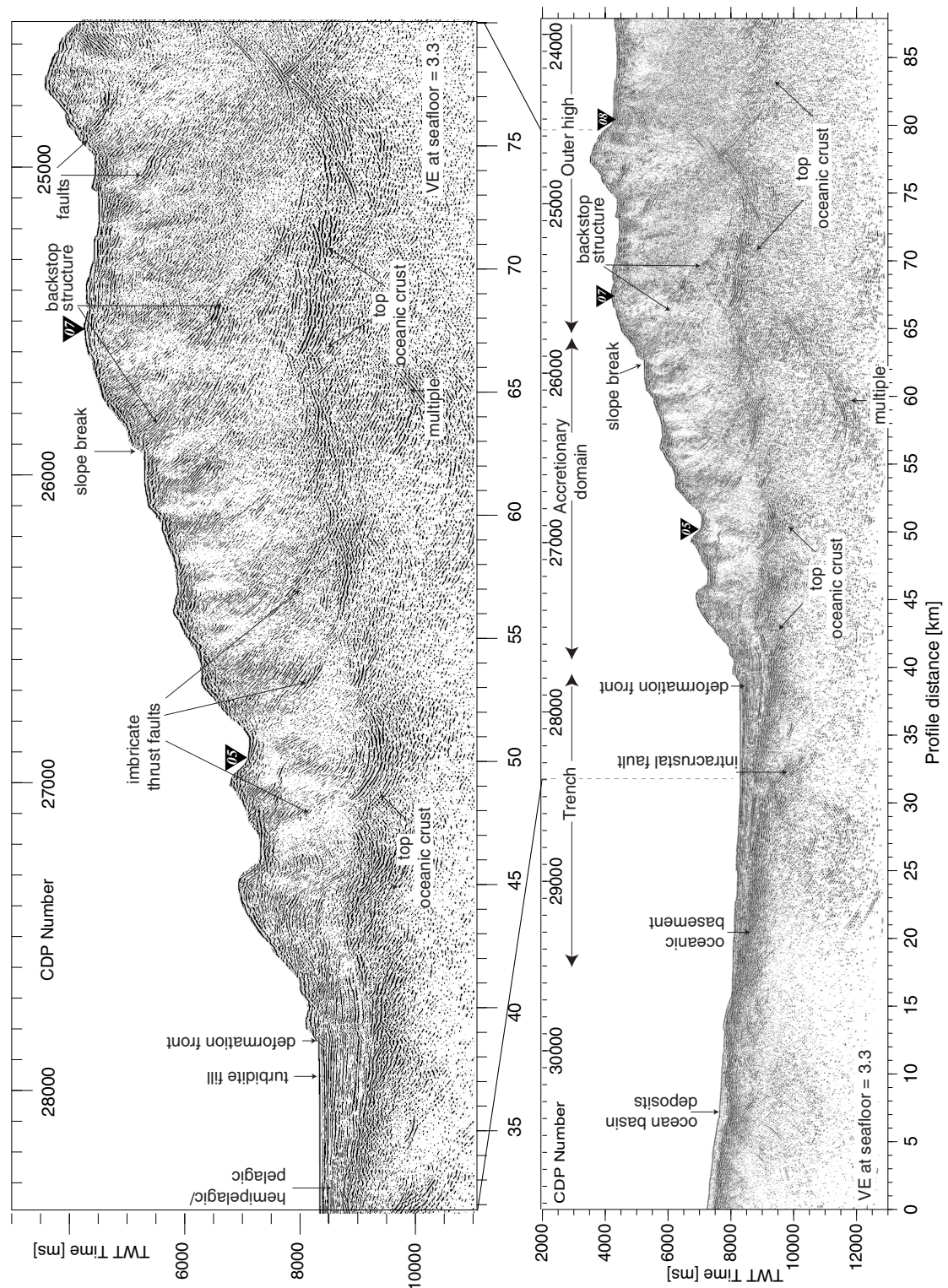


Figure 5.3a: Seaward portion of MCS profile 12 off southern Sumatra. The active accretionary domain extends from the trench to the slope break marking the backstop structure between CDP 25000 and CDP 26000. The accretionary prism is characterized by intense faulting leading to a chaotic seismic signature. The top of the subducted plate can be followed from the trench to underneath the outer high in Figure 5.3b. The subducting oceanic crust is cut by several large landward dipping faults. The corresponding velocity-depth model presented in Figure 5 shows a locally thickened oceanic crust seaward of the trench and laterally increasing velocities in the accretionary domain.

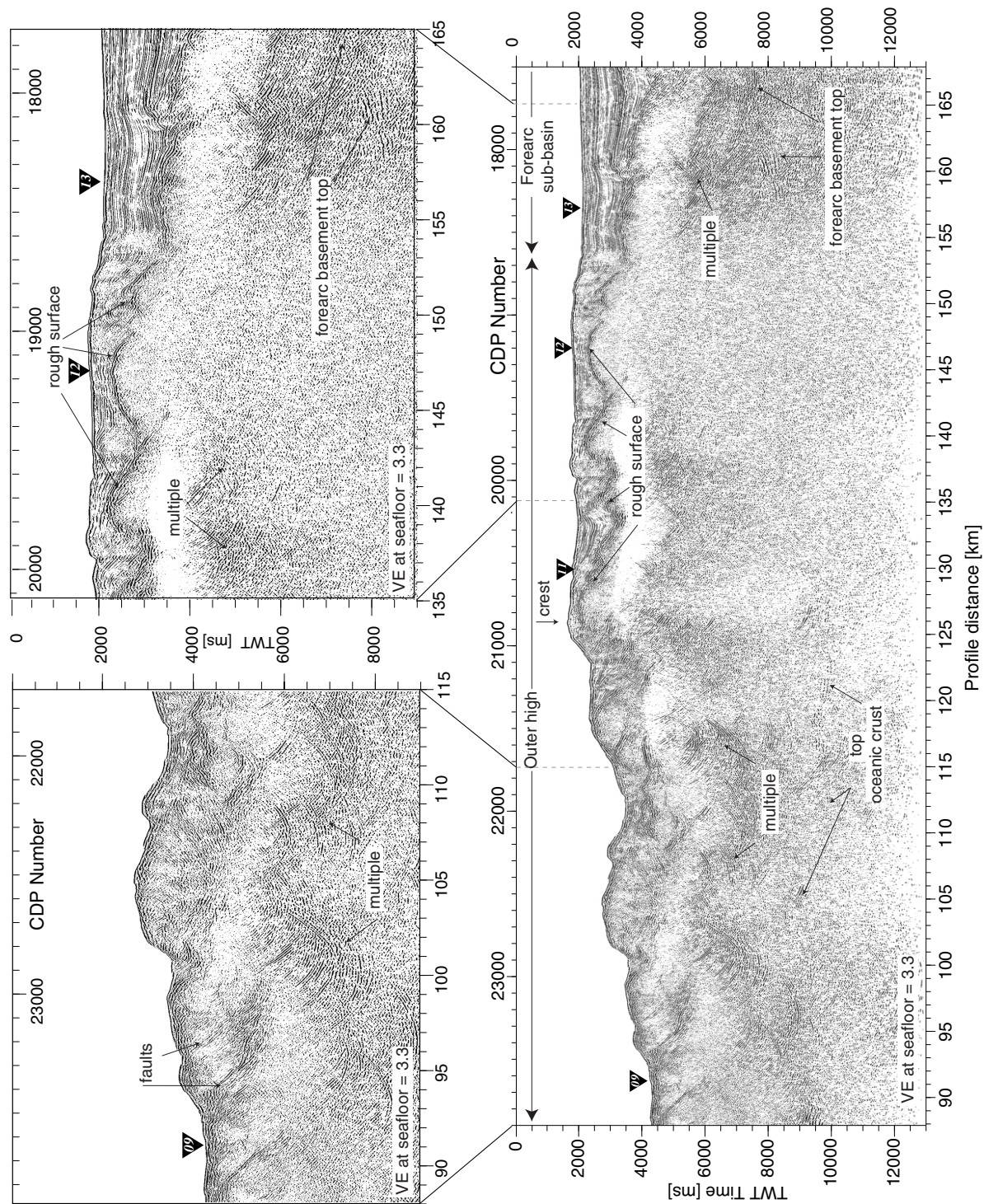


Figure 5.3b: Central transect of MCS line 12 across the outer high and the seaward forearc sub-basin. The rough surface basement top inhibits reflectivity within the outer high. Pondered sediments are trapped in several basins created by the basement top, which deepen towards the forearc basin. Tectonic activity is evident in several faults across the outer high. The top of the subducted plate can be traced to around profile kilometer 120.

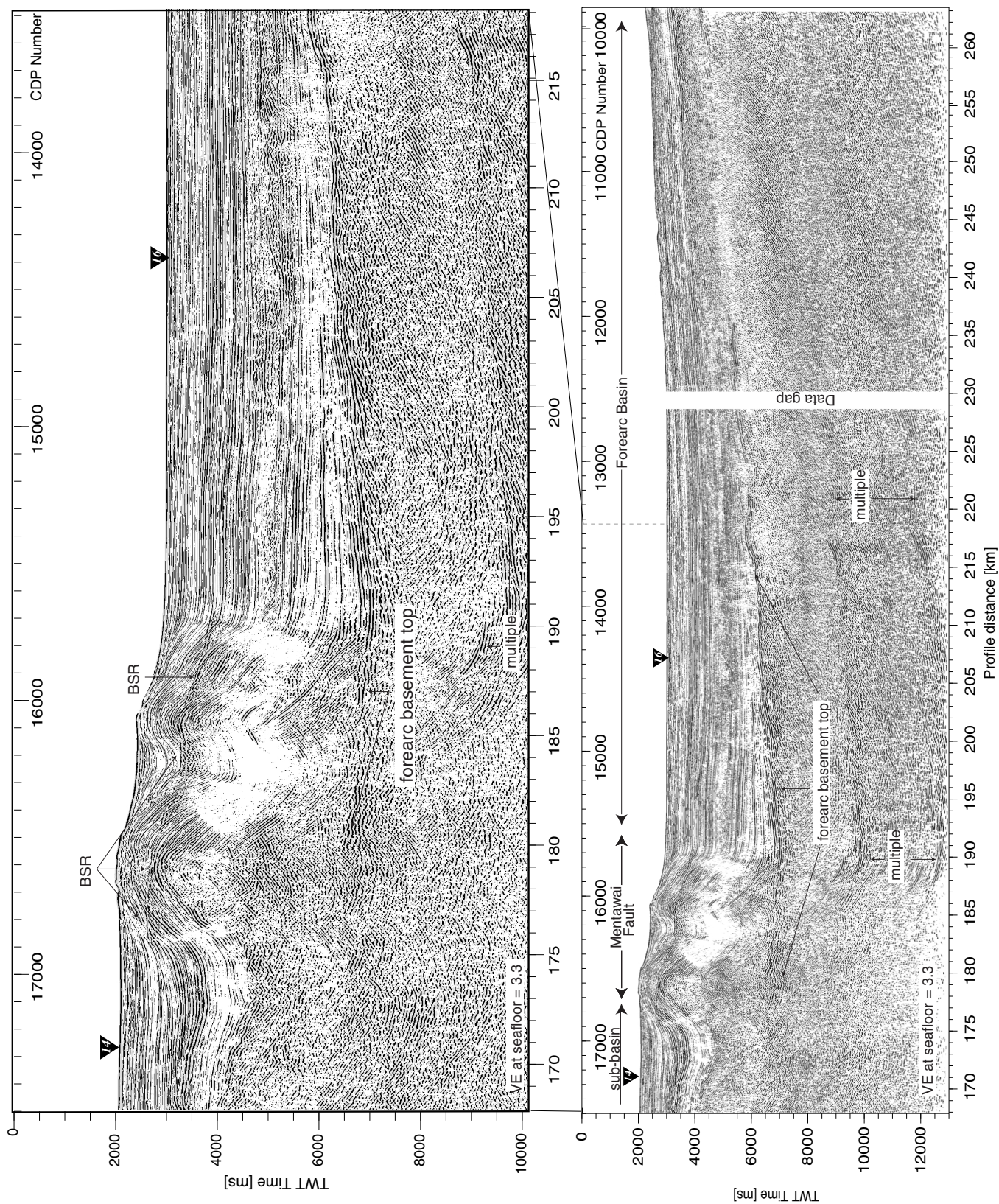


Figure 5.3c: Landward part of MCS line 12 covering the forearc basin which shows a maximum of 5 km of sediment fill. The Mentawai Fault zone represents a major structural break, separating a smaller sub-basin (CDP 16900-18700) carrying about 3 km of sediment from the main basin. Elevation in seafloor depth across the fault zone is about 600 m.

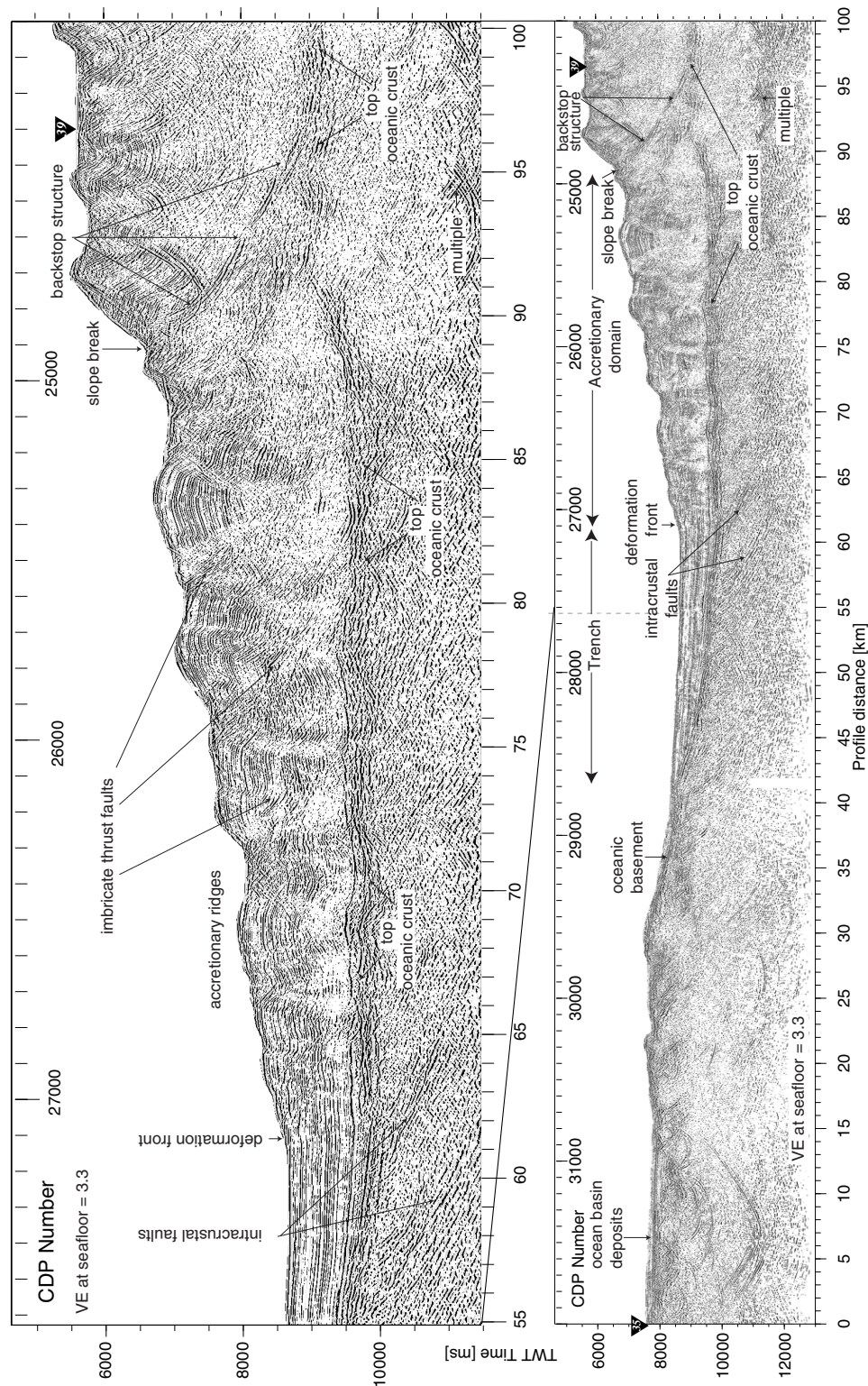


Figure 5.4a: Part of MCS line 42 covering the trench and the active accretionary domain. The seaward portion of the profile extends for 250 km onto the ocean basin, only 35 profile kilometers located seaward of the trench are displayed here. The accretionary prism is bounded by the deformation front and the active backstop structure, which cuts through near the top of the subducted plate. The dextral plate is followed for over 100 km landward of the deformation front. Several accretionary ridges are recognized on top of the subducted oceanic crust, bounded by imbricate thrust faults. Landward dipping intracrustal faults are found beneath the trench (CDP 26800-27600).

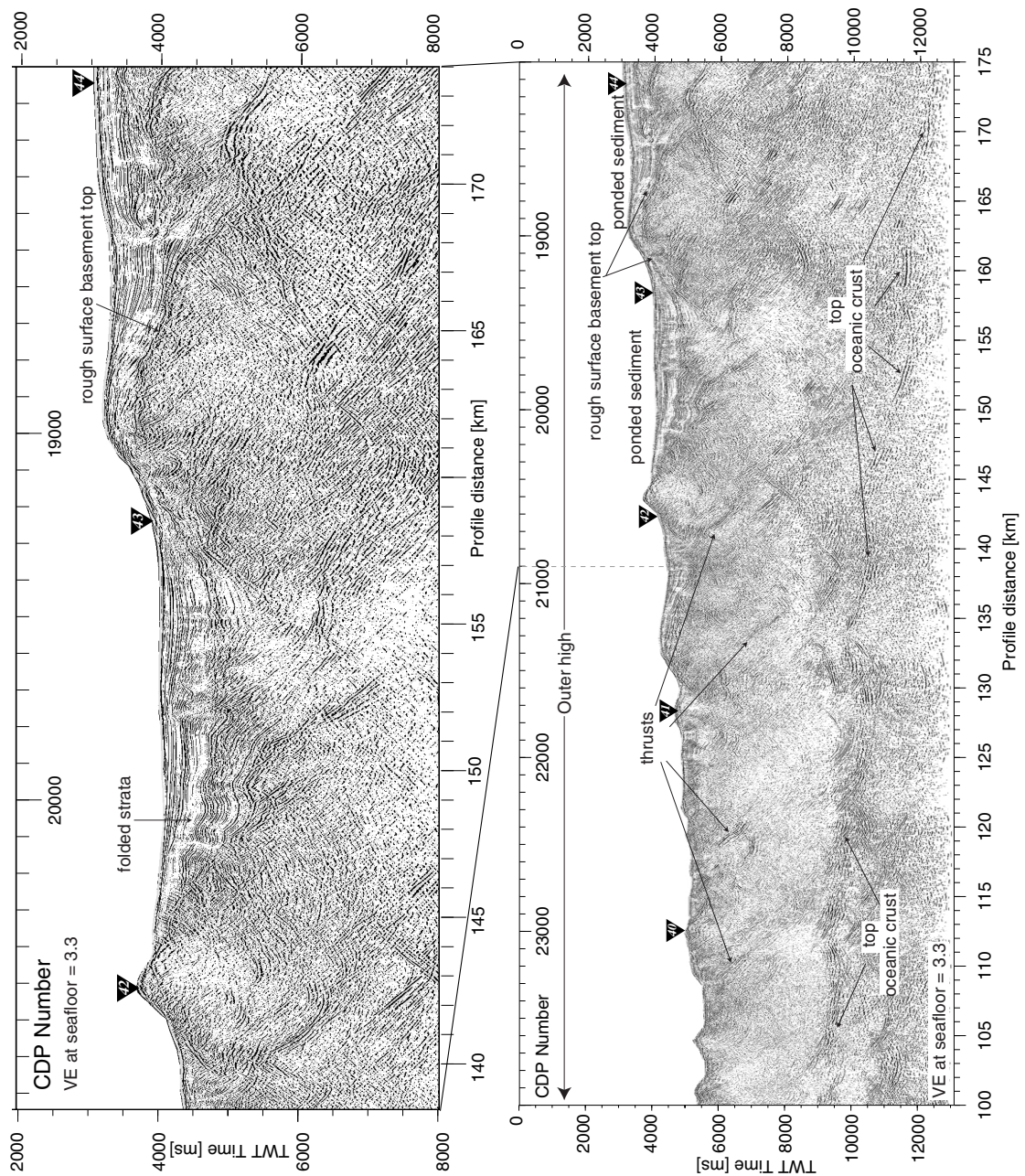


Figure 5.4b: Central part of MCS line 42 across the outer high, underneath which the top of the subducted plate is recognized. A rough surface basement top is identified landwards of CDP 21300. Active faulting still characterizes this part of the subduction complex. The outer high region is not as well expressed as on profile 12 off southern Sumatra. The corresponding velocity depth model displayed in Figure 5.6 shows laterally constant seismic velocities of moderate values.

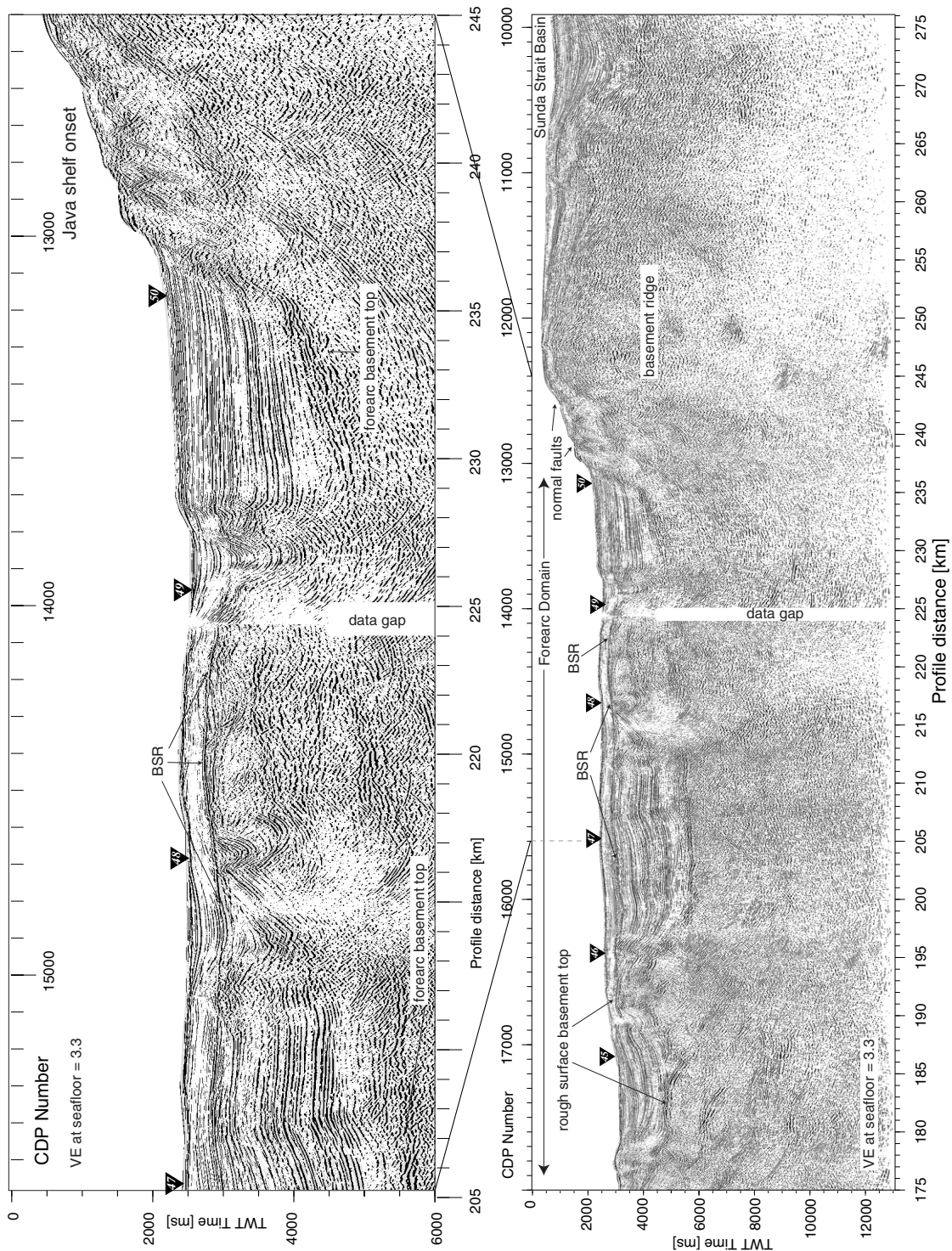


Figure 5.4c: Northeastern part of profile MCS 42 covering the forearc domain and the southern entrance to Sunda Strait. A distinct forearc basin, as found off Sumatra and off Java, is absent here, though large amounts of sediment have accumulated. Especially the older sedimentary sequences are affected by tectonic activity whereas the younger strata is comparably less disturbed. The onset of the Java shelf around CDP 13000 is marked by a steep seafloor elevation showing only a thin sedimentary cover seaward of a sedimentary basin (CDP 10000-11500) located within Sunda Strait. The basement ridge is characterized by high seismic velocities as presented in Figure 5.6.

seafloor topography. Multiple energy still remains, especially underneath the outer high, where significant seafloor depth variations occur. A post-stack time migration is included in the processing sequence. A smoothed velocity field derived from the wide-angle data modelling served as a starting model for the migration process.

For the wide-angle data recording shots were triggered in time intervals of 60 s at a speed of 5.5 knots, resulting in an average shot point distance of 167 m. Wide-angle data processing included relocation of the instrument position by analysing the direct arrivals followed by a low-cut frequency filter. A two-gated predictive deconvolution was applied to the data to improve the temporal resolution. A time- and offset-dependent filtering was chosen to account for the broad frequency range contained in the data as well as for the significant seafloor depth variation. The seismic energy was sufficient to trace signals on the record sections to distances between 60 and 80 km and data quality is good on average. Only selected examples of record sections are shown in the following.

Fig. 5.3a displays the southwestern part of MCS line SO137-12, covering the trench and deformation front, which exhibit a waterdepth of approximately 6750 m. The top of the subducted plate is visible for more than 80 km landward of the deformation front. The topography between the deformation front and a backstop structure which was recognized around CDP 25500 displays several distinct ridges and troughs in which small amounts of recent sediment are trapped. The backstop structure coincides with a clear slope break at the seafloor. Landward of the slope break, recent sediment accumulations become visible above a rough surface basement top (Fig. 5.3b). They thicken towards the forearc sub-basin (landward of CDP 18600). Little internal structure is resolved underneath the rough basement top where the data is further obscured by remnants of the seafloor multiple. Figure 5.3c shows the landwardmost part of the profile from the northeastern part of the outer high to the Sumatra shelf. The Mentawai fault zone is about 15 km wide and divides the forearc basin into a seaward sub-basin and the landward main basin. It consists of two anticlinal folds between CDP 15800 and 16900. A bottom simulating reflector (BSR) is recognized. In the forearc basin the thick sediment infill is well resolved as it onlaps onto the Sumatra shelf. The sedimentary sequences show little deformation in the basin. The basement top of the forearc shows some reflectivity (unconformity?) and can be traced underneath the Mentawai Fault Zone.

Fig. 5.4a displays the southern part of profile SO137-42, with only the first 40 km seaward of the trench shown. The seafloor between profile km 15-40 shows some topography and no pelagic sediment cover can be recognized here. Landward of the trench a number of ridges above the top of the downgoing plate are present between the deformation front and a slope break that defines the backstop structure (CDP 24600). The top of the subducted plate can be traced throughout Figure 5.4b, to a distance of more than 110 km landward of the deformation front. The upper segments of the outer high are disturbed by a number of faults creating a ridge and trough morphology. Some faults cut through near the top of the subducted oceanic plate. Also on this profile, a sedimentary cover is visible landward of the backstop structure. A distinct forearc basin, as is seen on profile 12, is absent on this line. The sedimentary units thicken towards the Java shelf (Fig. 5.4c) and gain a similar thickness as on line 12. A strong BSR mimicks the seafloor between CDP 14000 and 17000. The sediments onlap onto the pronounced Java shelf, which steeply rises about 1200 m in elevation to 200 m waterdepth. Within Sunda Strait the shelf shows substantial sedimentary infill in a small basin (CDP 10000-11500), whereas little sediment can be recognized further seaward until CDP 13000.

Modelling

An integrative approach using both the wide-angle as well as the reflection data was chosen to reveal the deeper structure along the transects. Data acquisition of the two data sets was conducted during two subsequent cruises to meet the different demands concerning the shot interval for wide-angle and multichannel recordings.

A forward modelling technique (Luetgert, 1992) using a top-to-bottom approach was applied to derive the velocity-depth models (Figs. 5.5 and 5.6), using both first and later arrivals. The MCS data helped to model the upper segments of the dip lines. The two strike-lines P02 and P03 (see Fig. 5.2) were later tied to the dip line SO138-01 and thus further constrained the velocity field along the Sumatra transect. Uncertainties in identifying first arrivals from refracted waves through the upper sections of the outer high and forearc domain and from refracted waves through the oceanic crust ranged from less than +/-50 ms for arrivals in the near-offset range (<30 km) to about +/-100 ms at larger offsets due to a poorer signal-to-noise ratio. PmP reflections from the oceanic crust-mantle

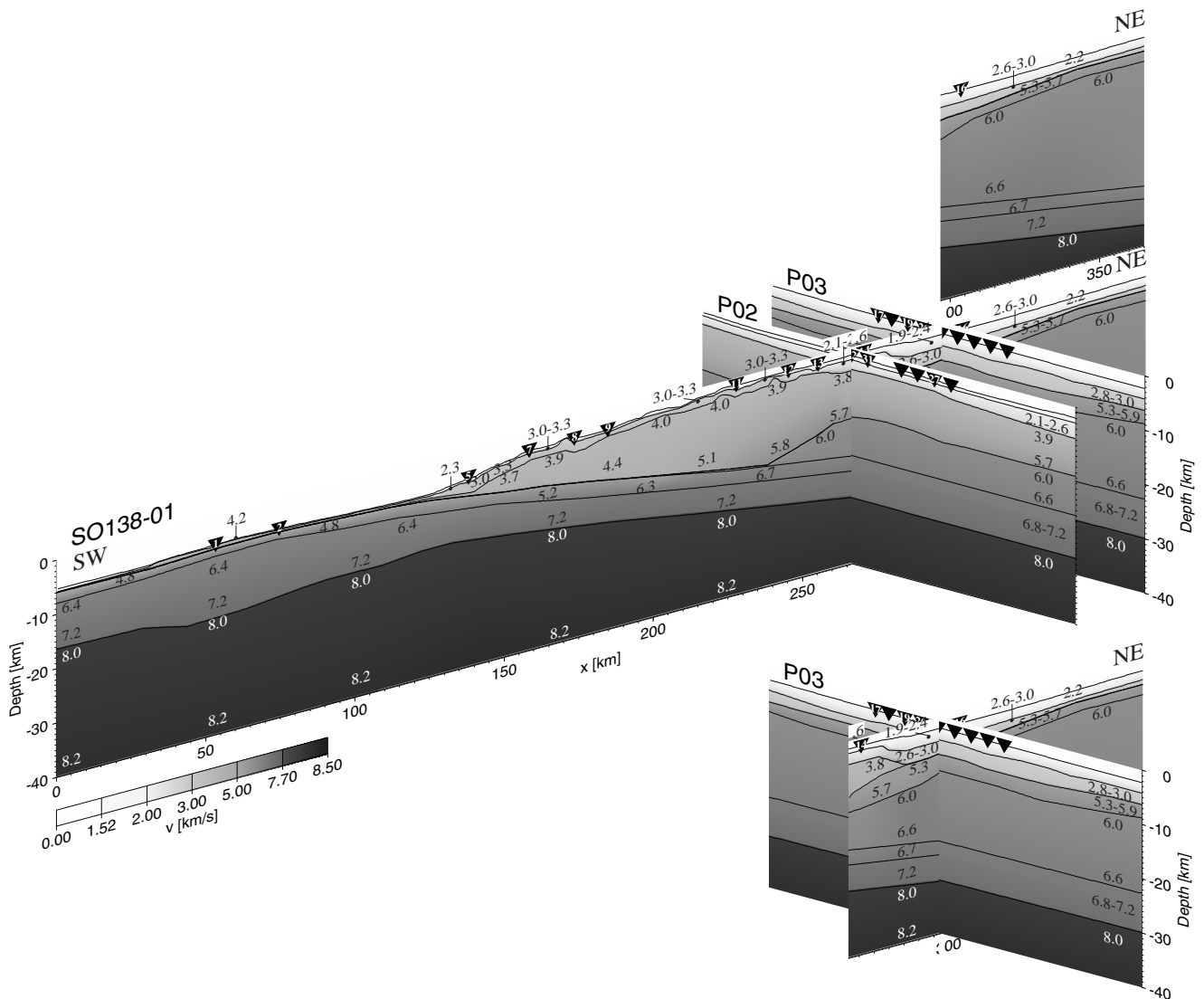


Figure 5.5: 3-D velocity-depth model across the Sumatra subduction zone. The blowups show the covered section of the dip line. The dip of the subducted plate is verified to a depth of over 30 km as it is recorded along the dip line SO138-01 and along strike-lines 02 and 03. The massive outer high separates the active accretionary domain from the forearc basin and displays moderate velocities reaching 5.8 km/s at almost 20 km depth. The velocity structure underneath the forearc basin is indicative of continental crust.

boundary are present on a number of stations on the outer high and ocean basin as well as in the forearc domain on profile 04.

Due to their late arrival times these events could only be picked with accuracies less than ± 100 ms. Both dip lines (01 and 04) show a fairly complex velocity field reflecting

the rapid change in water depth and the variable composition and compaction of the accretionary complex and outer high (Figs. 5.5 and 5.6).

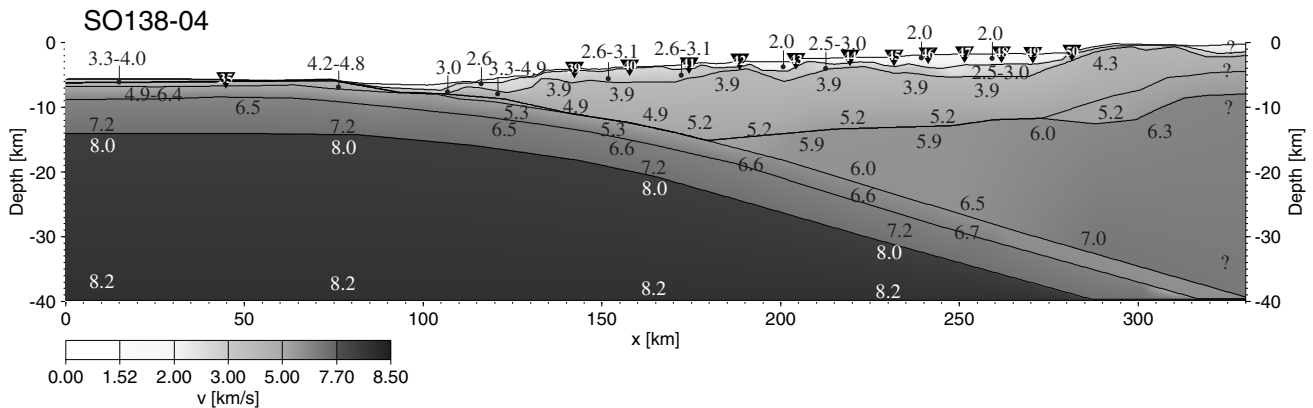


Figure 5.6: 2-D velocity depth model along refraction line SO138-04 of the Sunda Strait transect. The subduction complex and forearc domain show a laterally homogeneous velocity structure manifested in an approximately 9 km thick layer composing the lower accretionary complex. Laterally increasing velocities are found within the active accretionary prism. The leading edge of the upper plate shows decreased velocities compared to Sumatra. The Java shelf around profile kilometer 300 is located within Sunda Strait, where a shallow basement with velocities exceeding 4.3 km/s is found.

The position of the rough surface basement top, which is present along both dip lines, as well as the depth of the basement underneath the forearc domain and the top of the subducted plate were identified from the MCS data and are also prominent wide-angle reflections. Comparison of the main reflection horizons with major velocity changes of the final wide-angle models along the two profiles are shown in Figure 5.7. During modelling the main horizons identified in the MCS data were incorporated by simulation of an 'exploding reflector'.

5.4 Interpretation

5.4.1 Sumatra transect

The 360 km long OBH profile 01 crosses the trench and accretionary domain, as well as the outer high and the southernmost Sumatra forearc sub-basin. A prominent feature traversed by this line is the Mentawai Fault zone which borders the seaward part of the forearc basin and lies in between the two strike-lines (Fig. 5.2).

More than 500 m of hemi-pelagic and pelagic ocean basin deposits are visible on the incoming crust for the first 20 km seaward of the trench, as determined from the time-converted velocity-depth model shown in Figure 5.7. The oceanic basement shows some

topography, which in parts has not been fully smoothed by the sedimentary cover (e.g. around CDP 29800 in Fig. 5.3a). Two instruments are deployed seaward of the trench (OBH 01 and OBH 02), which record a 2 km thick upper crust, displaying velocities

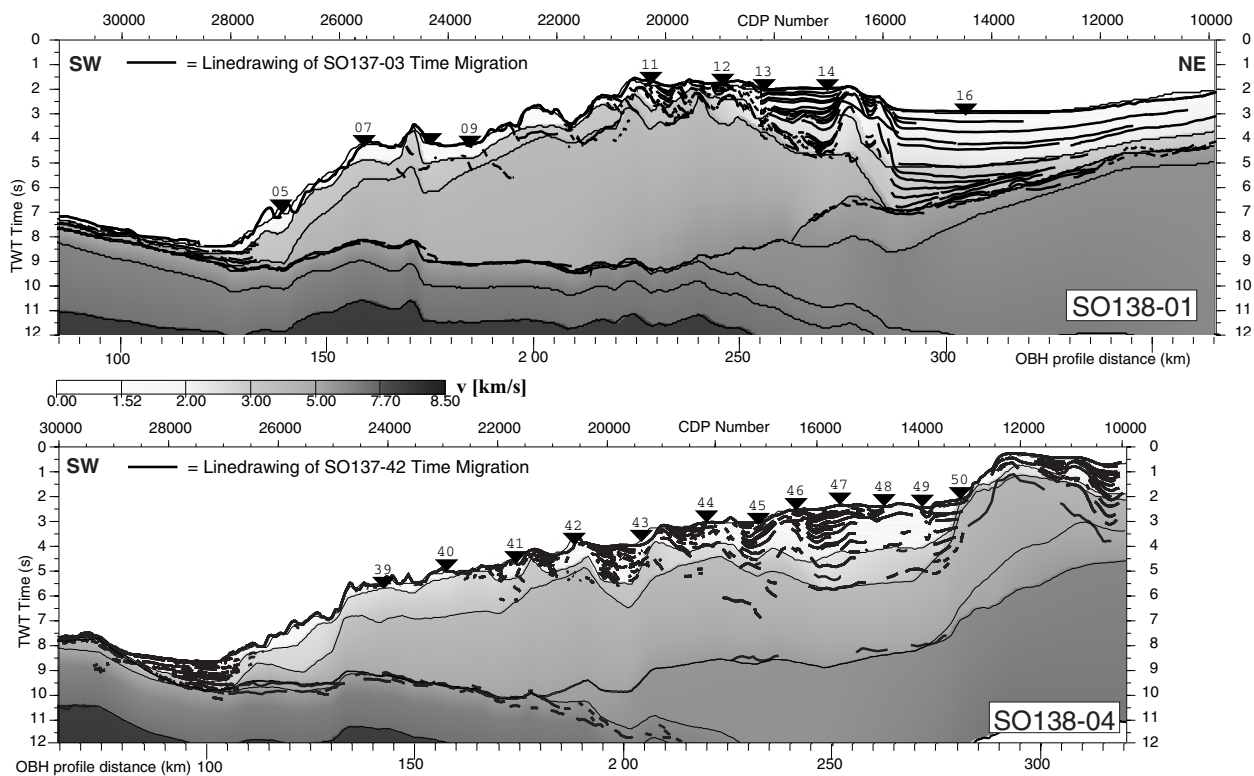


Figure 5.7: Time-converted sections of the velocity depth models gained from the two dip lines are overlain by linedrawings of the corresponding reflection lines. The modelling of the upper segments of the velocity depth sections is based on the results gained from the MCS data. A good correlation of the main units could be achieved. The top of the subducted plate is clearly identified in both data sets as is the basement top underneath the forearc domains. The large sedimentary basin northeast of the Java shelf onset is recognized in the MCS data, but not constrained by the wide-angle survey.

increasing from 4.8 km/s to 6.3 km/s. Phases Poc ('oc' denotes oceanic crust) record a locally thickened lower crust with velocities increasing from 6.4 km/s to 7.2 km/s. The highly variable Moho depth is imaged in the clear PmP and Pn phases recorded by stations 01 and 05 (Fig. 5.8). As the shooting terminates 30 km seaward of the trench, the extent of crustal thickening is not well constrained. Mantle velocities underneath the ocean basin are determined at 8.0 km/s by reversed Pn observations. Several landward dipping faults in the oceanic basement are visible underneath the sediment cover (Fig 3a), some of which cut deep into the oceanic crust (CDP 28400). The up to 1.1 km thick trench fill consists of turbiditic sequences above pelagic/hemi-pelagic sediment infill. The trench infill is

characterized by near parallel, subhorizontal and landward divergent facies that onlap the basement.

The top of the oceanic plate can be traced as a strong reflection in the MCS data for 80 km landward of the deformation front underneath the active accretionary domain and parts of the outer high. The reflection displays a high lateral coherency (Figs. 5.3a and b) but is somewhat inhibited further landward by remnants of the seafloor multiple. Several OBH stations deployed on the active accretionary domain and outer high (OBH 05-09) record the top of the plate as it is thrust underneath the upper plate. OBH 05 (Fig. 5.8) covers the accretionary domain as well as the trench and parts of the oceanic basin. The top of the subducted plate is recorded as event P_{toc} ('toc' denotes top of oceanic plate) underneath the accretionary prism. The high apparent velocities of the P_{mP} and P_n phases at southwestern offsets greater than 25 km are caused by the Moho undulations observed seaward of the trench. Station 07 (Fig. 5.9) traces the top of the subducted slab as a strong vertical reflection underneath the outer high at 0 to 9 km offset and as a refraction P_{oc} at greater offsets. Underneath the trench the top of the plate is recorded at about 7 s, but interferes with the strong sedimentary phases at offsets less than 20 km. A weaker Moho reflection is recorded at 22 km depth beyond the critical angle i_{crit} at about 30 km offset to the northeast. From the trench to underneath the crest of the outer high the reflection from the top of the subducted plate (P_{toc}) and its corresponding refraction P_{oc} as well as the Moho reflection (P_{mP}) are recorded by station OBH 08 (Fig. 5.9). Beyond the critical angle i_{crit} the mantle transition causes high amplitudes up to 50 km offset underneath the outer high. The clearest P_{mP} reflections are observed on the record sections of stations 12 and 13. OBH 12 (Fig. 5.10) constrains the plate dip underneath the outer high, where a strong wide-angle P_{mP} is observed at 35-50 km offset to the southwest along profile km 195 to 208. Station 13 (Fig. 5.10) tracks the Moho to a depth of approximately 25 km. Underneath the forearc basin, both the top of the plate as well as the mantle transition unfortunately interfere with the strong multiple of the basement here (e.g. positive offsets on OBH13 in Fig. 5.10) so that they cannot be clearly identified.

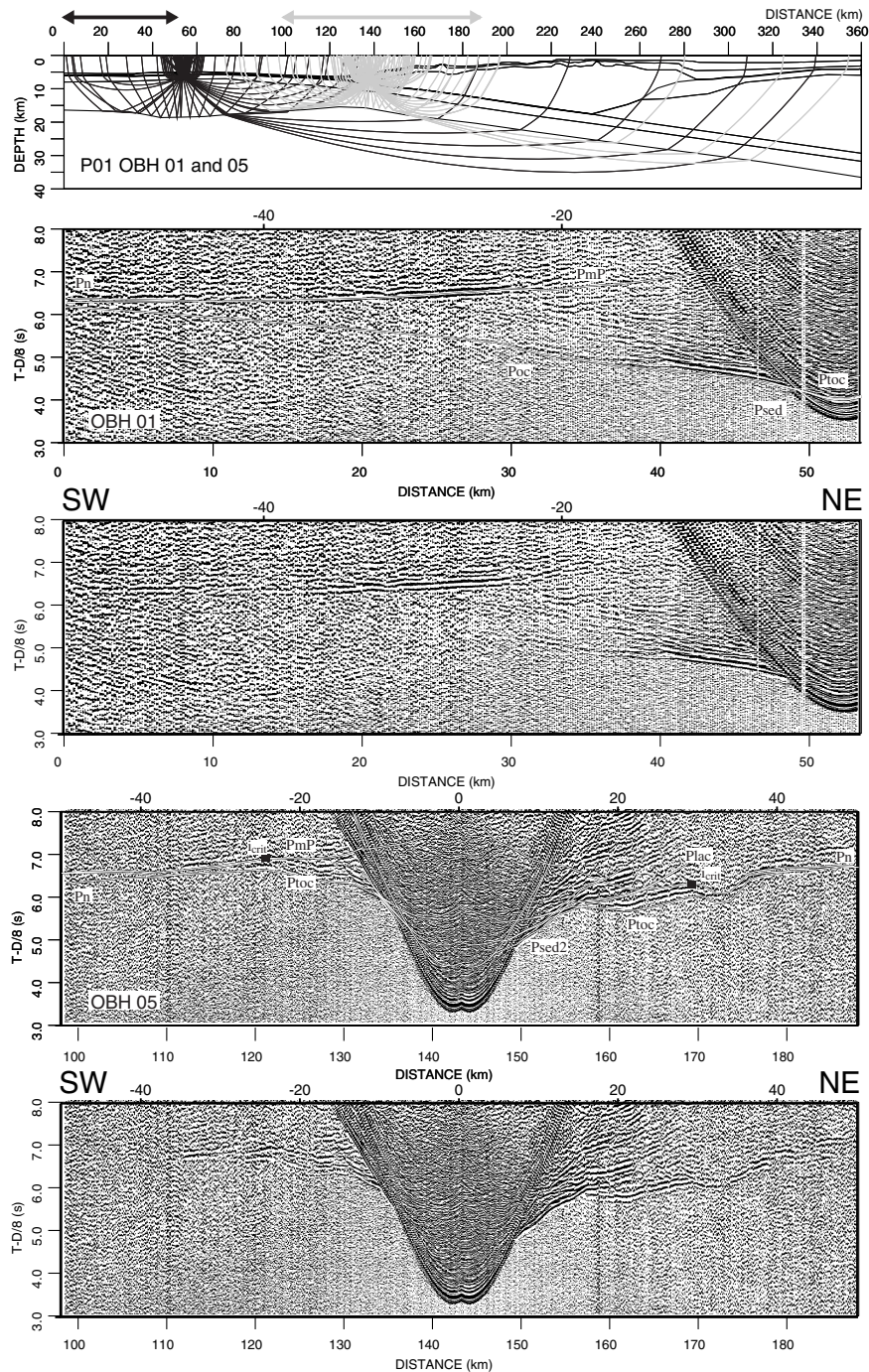


Figure 5.8: Data sections from two stations deployed along the dip line SO138-01. The upper image displays the raypaths through the model subsurface for both stations. Thick arrows indicate the offset displayed in the data records of the corresponding stations. The data are shown with overlain modelled traveltimes in the upper images, whereas the pure dataset is displayed in the lower sections. OBH 01 is located on the incoming plate and records a local thickening of theigenous oceanic crust. Mantle phases (PmP and Pn) record normal upper mantle velocities of 8.0 km/s. Station 05 is the first station landward of the deformation front documenting the downthrusting of the oceanic plate underneath the trench. Phase PtoC is the reflection from the top of the plate which shows a normal thickness of 7.5 km here as gained from the recorded mantle transition. The landward travelling phase Plac runs through the lower accretionary complex beneath the upper sedimentary layers recorded by phase Pscd2. The offset of the critical angle is marked by a black square.

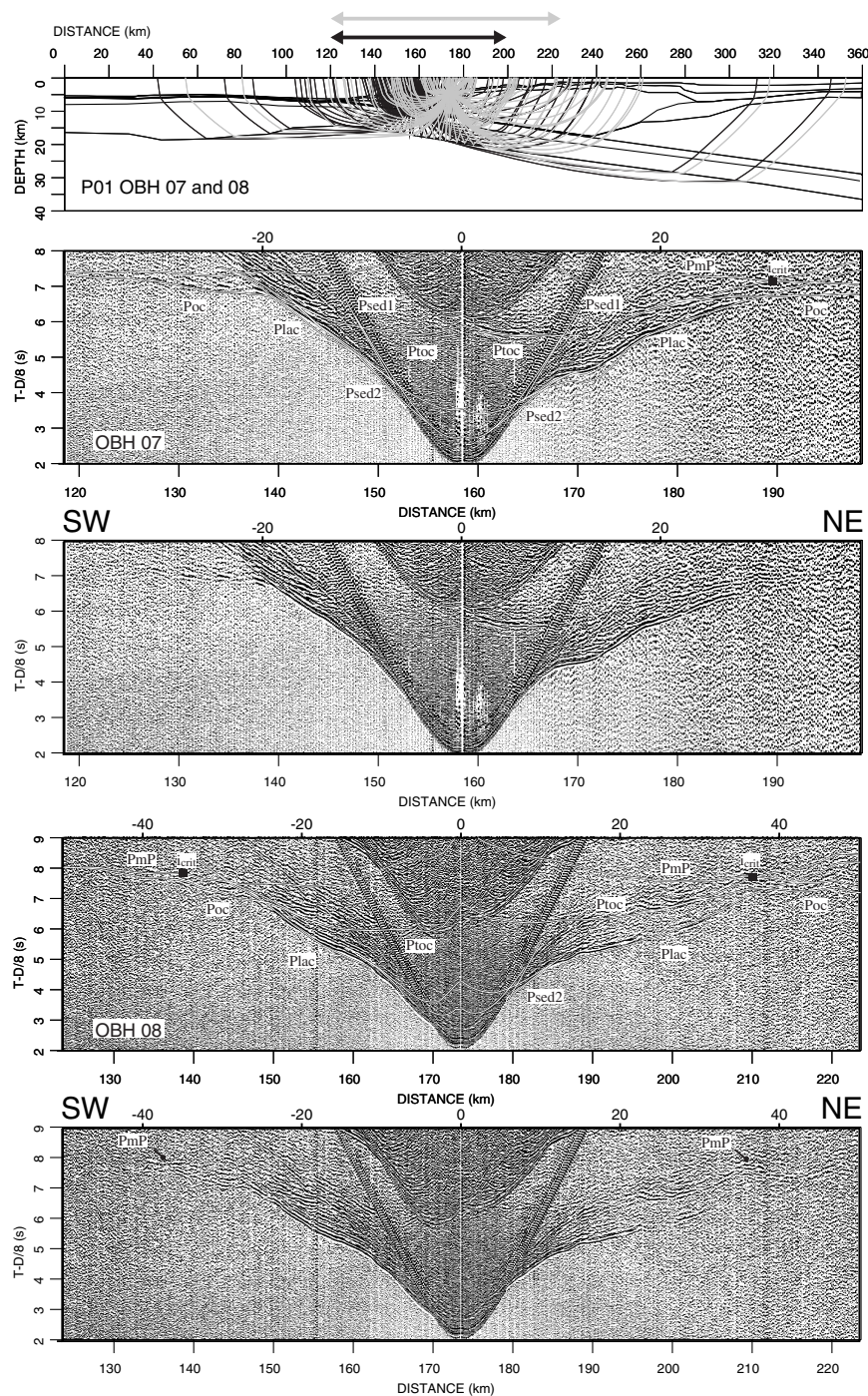


Figure 5.9: OBH 07 of profile P01 is deployed on the outer high. The velocity structure of the outer high is documented by the sedimentary phases Psed1 and Psed2 for the upper segments and by phase Plac for the lower accretionary complex. The top of the subducted plate is recorded by reflection Ptoc and its corresponding refraction Poc. A strong vertical reflection Ptoc from the subducted slab is present at positive offsets. High amplitudes caused by the mantle reflection PmP are visible beyond the critical angle to the northeast. OBH 08 also records the mantle transition as reflections PmP beyond the critical angle.

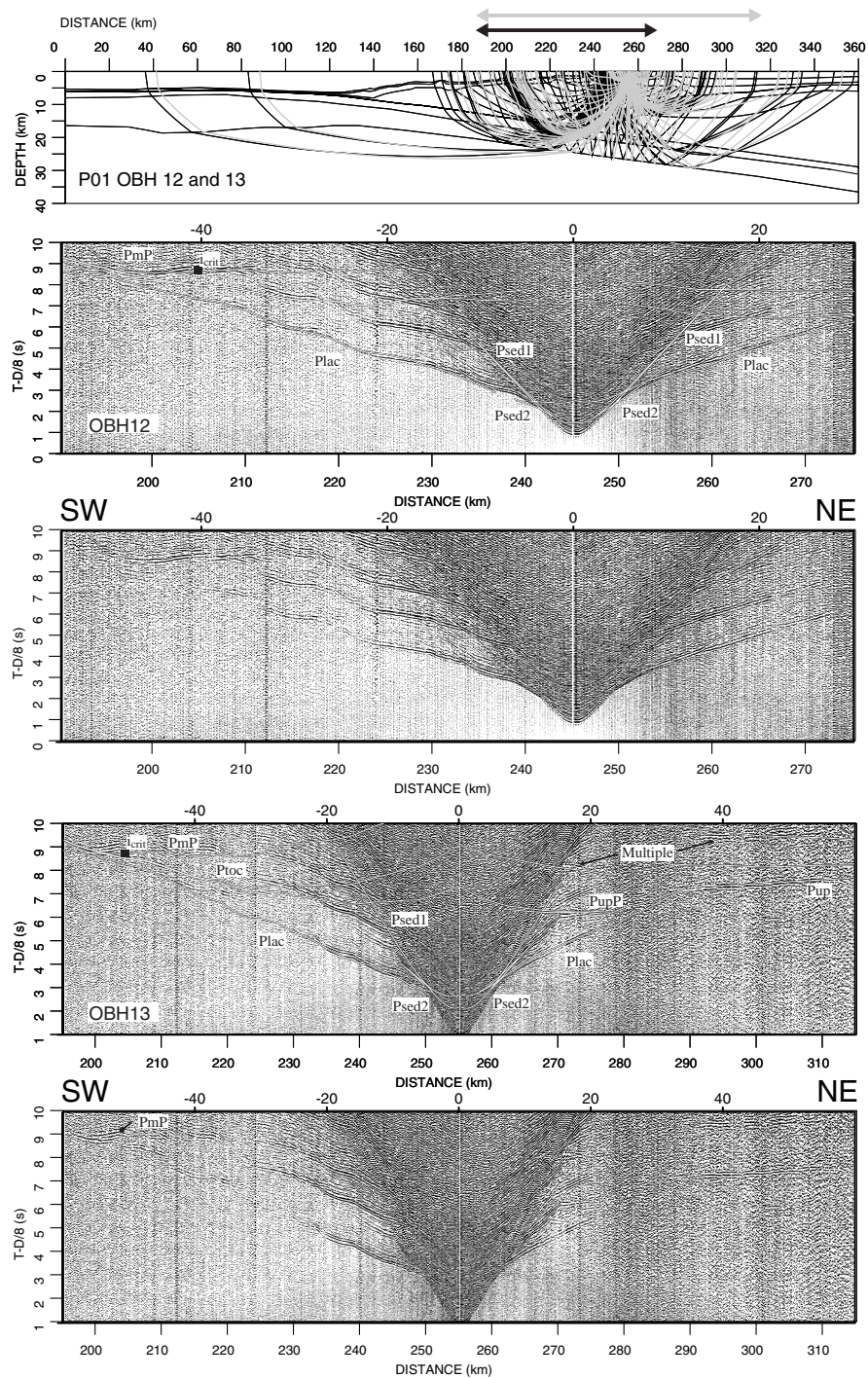


Figure 5.10: OBH stations 12 and 13 are the most landward stations located on the outer high. Both instrument recordings reflect the smooth velocity structure of the outer high recorded by the sedimentary phases Psed1/2 and Plac. The oceanic Moho is recorded by seaward travelling phases PmP. Underneath the forearc basin the leading edge of the upper plate is recorded by reflection PupP and the corresponding refraction Pup of OBH 13.

The velocity structure of the active accretionary prism and the outer high were mainly determined from stations 05-13. Phases Psed1 and Psed2 (Figs. 5.8 through 5.10) are refracted through the upper sedimentary layers on the accretionary prism and outer high above the rough surface basement top which was identified from the MCS data. The lower part of the accretionary complex is covered by refracted phases Plac ('lac' denotes lower accretionary complex). The backstop structure which marks the transition from the active accretionary prism to the outer high is observed in the MCS data (Fig. 5.3a), where it appears as a pronounced, landward-dipping reflection which runs from the seafloor slope break down near the top of the subducted plate. This transition from the active accretionary domain to the outer high also is evident in the velocity structure: at the frontal part of the accretionary complex between the deformation front at profile km 39 and the backstop structure velocities increase laterally from ca. 3.0 km/s to over 4.0 km/s (Fig. 5.5). Beyond the backstop structure in the outer high, velocities remain constant from the slope break to the crest of the outer high. Here, velocities increase slowly with depth and reach values of 5.8 km/s at 18 km depth. This smooth velocity field of the outer high is manifested in phases Plac recorded by the stations on the outer high (e.g. OBH 08 in Fig. 5.9, OBH 12 and OBH 13 in Fig. 5.10). The seafloor topography of the active accretionary prism is characterized by two pronounced accretionary ridges around CDP 27300 and 27000; small recent ridges are recognized immediately landward of the deformation front at profile km 40 (Fig. 5.3a). The rugged seafloor topography of the active accretionary wedge prevails along the seaward part of the outer high until the crest at CDP 21000. The accretionary prism is disturbed by a number of imbricate thrust faults (Fig. 5.3a) which appear as long elongated landward-dipping reflections cutting from the seafloor deep through the wedge. A high degree of deformation expressed in large faults (e.g. near CDP 23700 and 25100) is also characteristic for the seaward part of the outer high (Fig. 5.3a and b). Landward of the crest, a pelagic sediment cover becomes visible and ponded sediment is trapped in several basins formed by the rough surface basement top (Fig. 5.3b). The seaward part of the forearc basin is characterized by a pronounced anticline (Fig. 5.3c) which marks the position of the Mentawai Fault zone between CDP 15700 and 16900. Folding here is still active and involves the entire sedimentary strata and crops out at the seafloor as a large, 15 km wide bulge. The Mentawai Fault zone splits off a smaller sub-basin from the main forearc basin. A maximum of 5 km sediment infill is recorded in the main basin, compared to approximately 3 km seaward of the Mentawai anticline in the sub-

basin; the variation in seafloor depth between the two basins equals almost 600 m. A clear BSR is visible crossing the anticline, but is difficult to trace in the subparallel strata of the forearc basin and sub-basin (Fig. 5.3c). The sedimentary units in the forearc basin show little deformation as they progressively thin towards the northeastern end of the profile. Seismic velocities increase from about 1.9/2.0 km/s to 3.0 km/s in the sedimentary strata (Fig. 5.5). The underlying basement top is found at approximately 6 s TWT where the basin is deepest near the Mentawai Fault (Fig. 5.3c). The basement top, which is marked by a high amplitude, low frequency band of energy, continues underneath the anticlinal feature and is still traceable underneath the sub-basin landward of the Mentawai Fault Zone. Towards the Sumatra shelf the seismic signature of the basement top changes significantly at profile distance 240 km (Fig. 5.3c). A two kilometer thick layer with velocities increasing from 5.3-5.7 km/s is found in the basement (Fig. 5.5), underneath which higher velocities, ranging from 6.0 km/s to about 6.6 km/s at greater depth, dominate. This lower unit is evident in phases PupP (the reflection from the upper plate) (OBH 13 in Fig. 5.10) and the corresponding refracted wave Pup ('up' denotes upper plate) and extends underneath the outer high where it forms the leading edge of the overridding plate.

5.4.2 Strike lines SO138-02 and SO138-03

The seismic grid was extended by two strike lines to gain additional constraints on the configuration of the subducted plate, which was recorded by instruments along both lines. Profile SO138-02 lies along strike the aforementioned sub-basin, about 140 km landward of the deformation front and comprises 9 instrument locations (Fig. 5.2). The line shows some topographic variation, amounting to about 1 km seafloor elevation difference along the profile. The velocity-depth model which was achieved with the incorporation of ministreamer reflection data recordings (not shown here) (Flueh, 1999), shows a substantial variation in sediment thickness of the upper sequences, which increase from about 2 km to almost 4 km at the southeastern end of the profile. As is evident from the reflection data, strong deformation of the sedimentary strata occurs as folding and partial stacking of the sequences is observed. Compressional tectonic activity is ongoing and the entire upper sedimentary units as well as the seafloor are affected. Phases Psed1 and Psed2 travelling through these units (Fig. 5.11) represent velocities ranging from less than 2.0 km/s at the top to 2.6 km/s in the lower parts (Fig. 5.5). The underlying 7-9 km thick unit of the lower

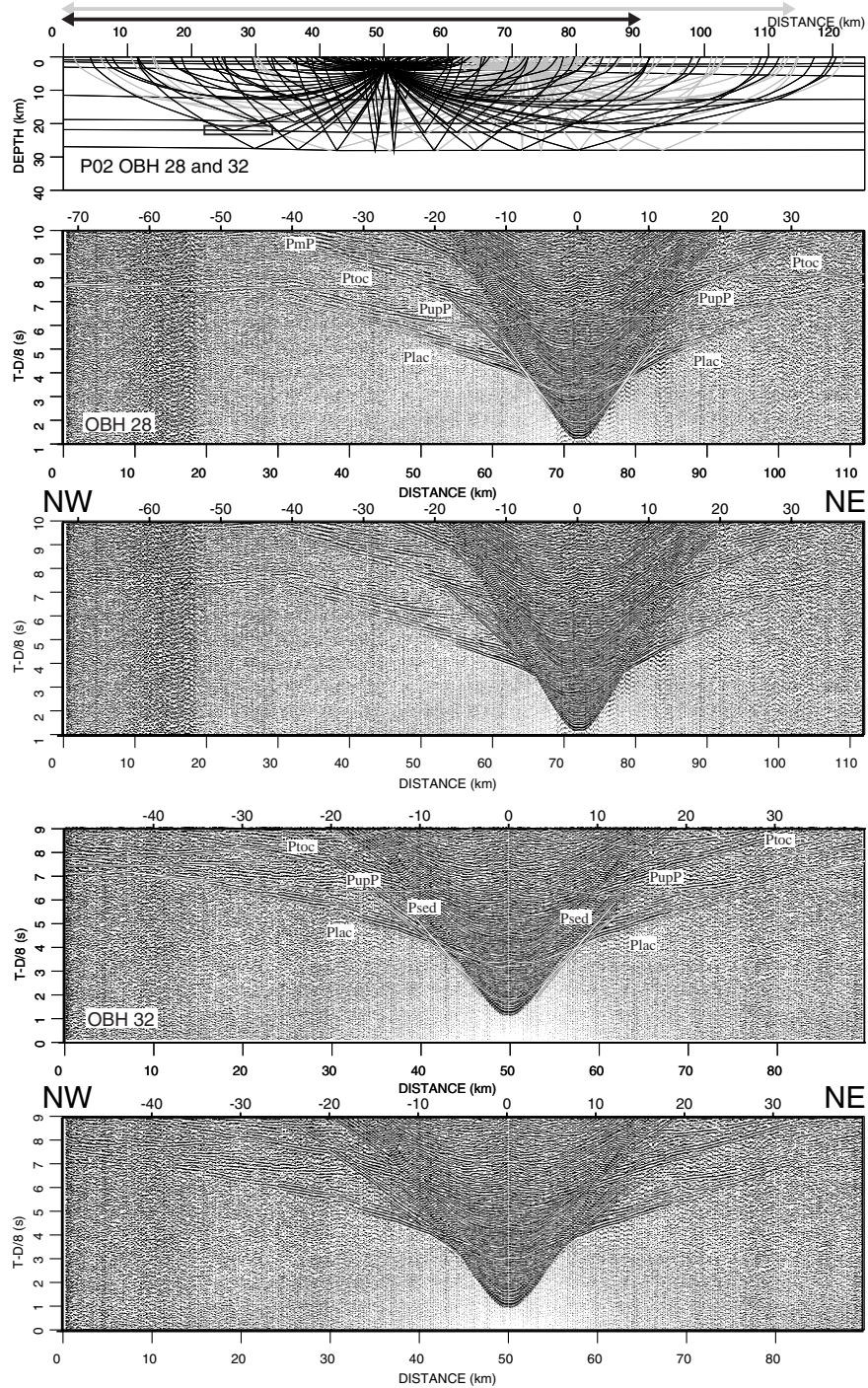


Figure 5.11: Data sections recorded along strike-line S0138-02 by stations 28 and 32. Both stations record the leading edge of the upper plate underneath the outer high as incidents PuP as well as the top of the subducted plate as reflection PtoC. The distinct phase recognized on the section of OBH 28 ca. 0.7 s after reflection PtoC is caused by a discontinuous intracrustal reflector observed here as indicated by the black box in the raypath diagram. This phase is not observed on any other station.

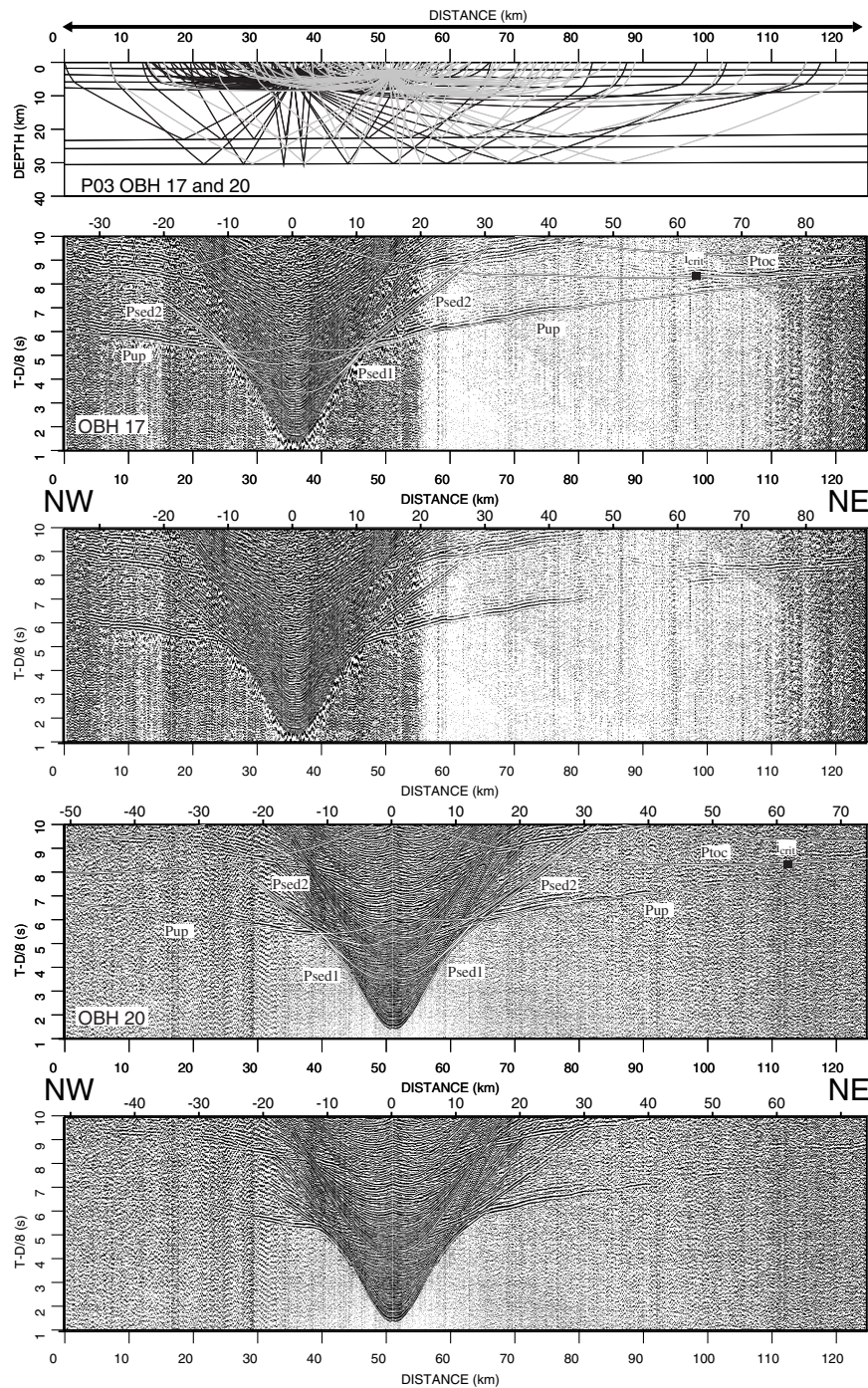


Figure 5.12: Stations OBH 17 and OBH 20 of profile S0138-03 covering the seaward part of the forearc basin off southern Sumatra. The thick sedimentary strata are recorded by phases Psed1 and Psed2. The basement underneath the forearc basin is represented by phases Pup travelling through the upper plate here. The top of the subducted plate was recorded by both stations beyond the critical angle of phase Ptoc. While the downgoing slab was not recorded underneath the forearc basin along the dip line, it is present on the record sections of several stations deployed along the strike line 03.

outer high (represented by refracted waves *Plac*) is bounded at its base by a velocity step from 5.7 km/s to 6.0 km/s (Fig. 5.5). This boundary has been recorded as a clear reflection *PupP* at about 11 km depth (e.g. OBH 28 and OBH 32 in Fig. 5.11). Whereas the top of the subducted plate could not be identified unambiguously underneath this layer by stations deployed along the dip line SO138-01, it is present as a strong incident on several record sections along both strike lines. Stations 28 and 32 which are presented here, record the top of the subducted oceanic crust at 19 km depth as reflection *Ptoc* (Fig. 5.11).

Along strike line SO138-03, which is located 170 km landward of the deformation front, the sedimentary infill of the forearc basin reaches a thickness of 4 km (*Psed1* and *Psed2* in Fig. 5.12). Water depth varies little along the profile and subparallel stratification of the sedimentary units yield a very smooth velocity-depth model (Fig. 5.5). Refracted waves *Pup* through the upper plate basement reveal velocities of 6.0 km/s to 6.6 km/s here. The downgoing plate is only recorded at the southeastern end of the profile, beyond the critical angle i_{crit} . High amplitudes of phase *Ptoc* (OBH 17 and 20 in Fig. 5.12) locate the top of the downgoing slab at 22-23 km depth here. The profile is too short to record the oceanic mantle transition. The depth of the subducted plate found along the strike lines is in perfect agreement with results from the dip line, as seen in Figure 5.5.

5.4.3 Sunda Strait transect

The second transect runs across the subduction complex further southeast, covering parts of the ocean basin, the accretionary complex and ending on the Java shelf within Sunda Strait (Fig. 5.2). Only the part of SO137-42 that is coincident with the wide-angle profile P04 is shown in Figure 5.4. The OBH profile SO138-04 is 330 km long; 13 instruments successfully recorded data. Unfortunately, instrument failure occurred in the vicinity of the trench and therein. Thus the structure of the incoming oceanic plate is deduced only from sections of OBH 35 (Fig. 5.13), which show a 7.5 km thick crust with a typical oceanic velocity-depth distribution. Phases *Poc* travel through the oceanic crust; a *PmP* reflection records the mantle transition at 14 km depth. Immediately seaward of the trench (Fig. 5.4a) a local seafloor elevation not covered by sediment shows some normal faulting. The trench is 20 km wide, carrying an infill with a maximum thickness at the deformation front of 1.5 km, as inferred from the MCS data (Fig. 5.4a).

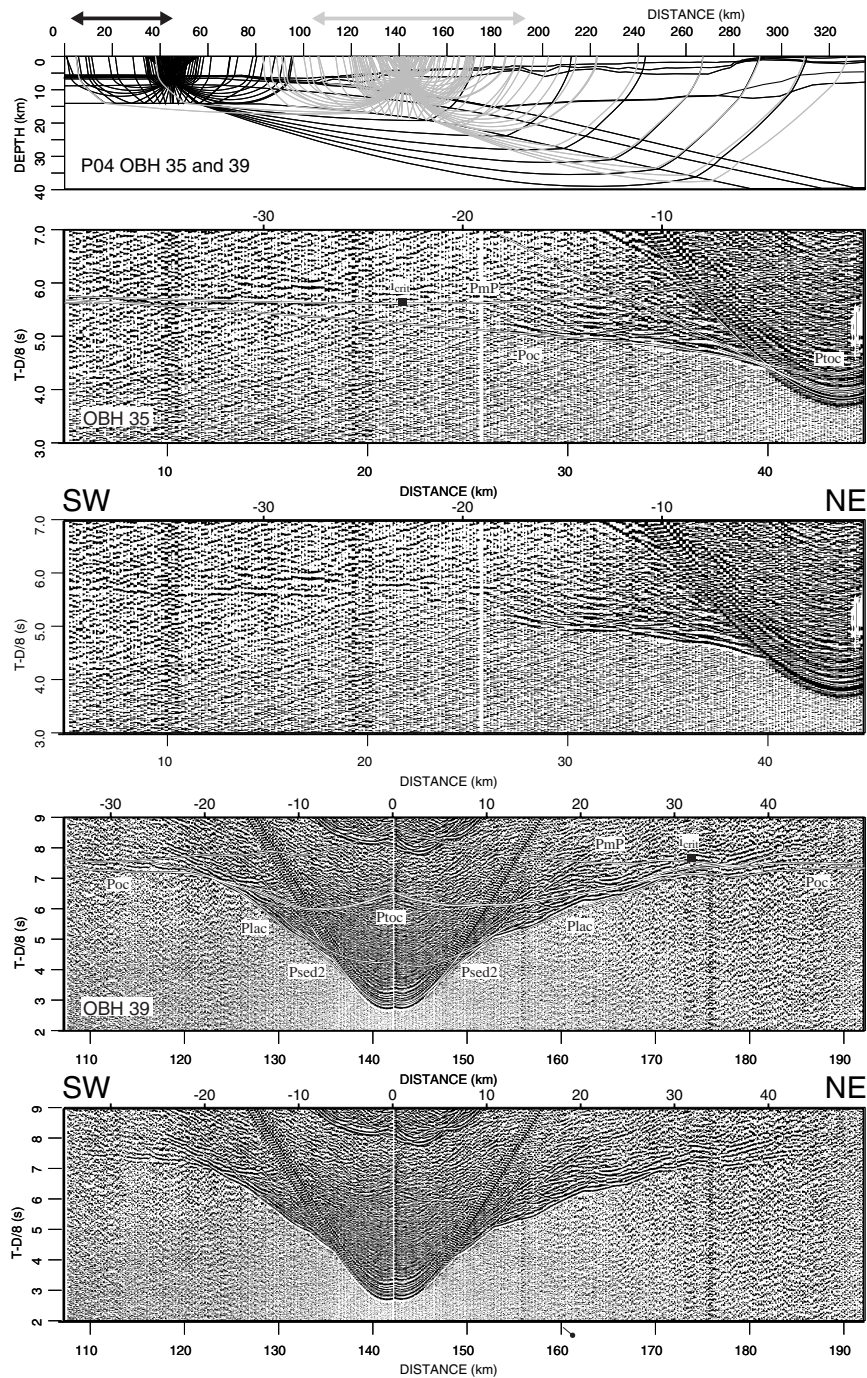


Figure 5.13: Record sections and corresponding raypaths of stations OBH 35 and OBH 39 deployed along the Sunda Strait transect SO138-04. OBH 35 is the only instrument recording data seaward of the trench. A 7.5 km thick oceanic crust showing a normal seismic velocity structure is found here. OBH 39 is the first instrument located landward of the deformation front on the active accretionary domain. The top of the subducted plate appears as a near-vertical reflection P_{toc} and corresponding refraction P_{oc}. The mantle transition is recorded by a landward travelling P_{mP} reflection beyond the critical angle.

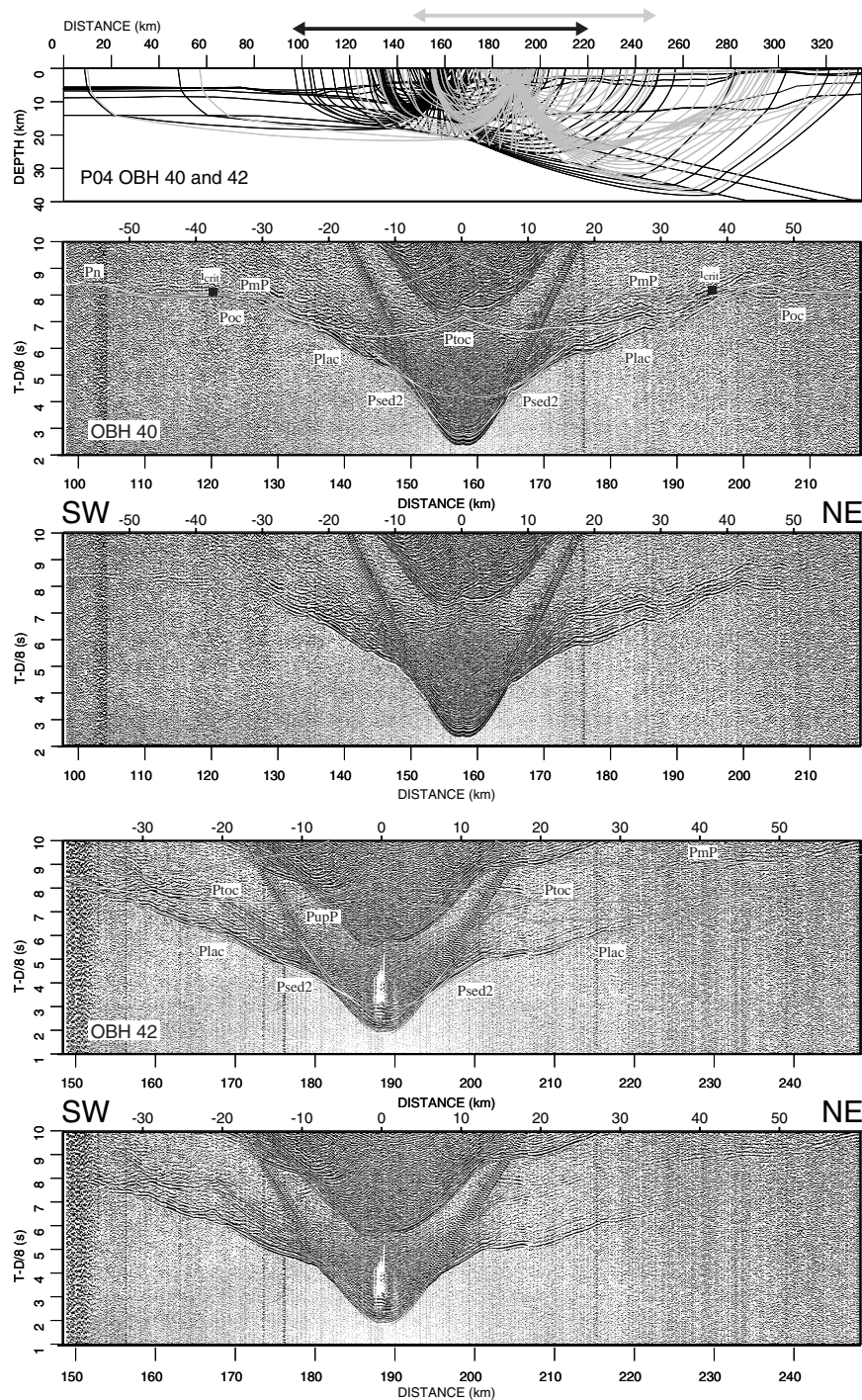


Figure 5.14: OBH 40 and 42 are deployed along the outer high. Station 40 records a Pn mantle phase from the oceanic Moho at negative offsets as well as the corresponding mantle reflection PmP. The top of the subducted plate is recognized as reflections Ploc and refractions Poc. The smooth velocity structure of the outer high domain is documented by phase Plac. OBH 42 records a strong mantle reflection PmP at positive offsets, tracing the oceanic Moho to a depth of over 30 km.

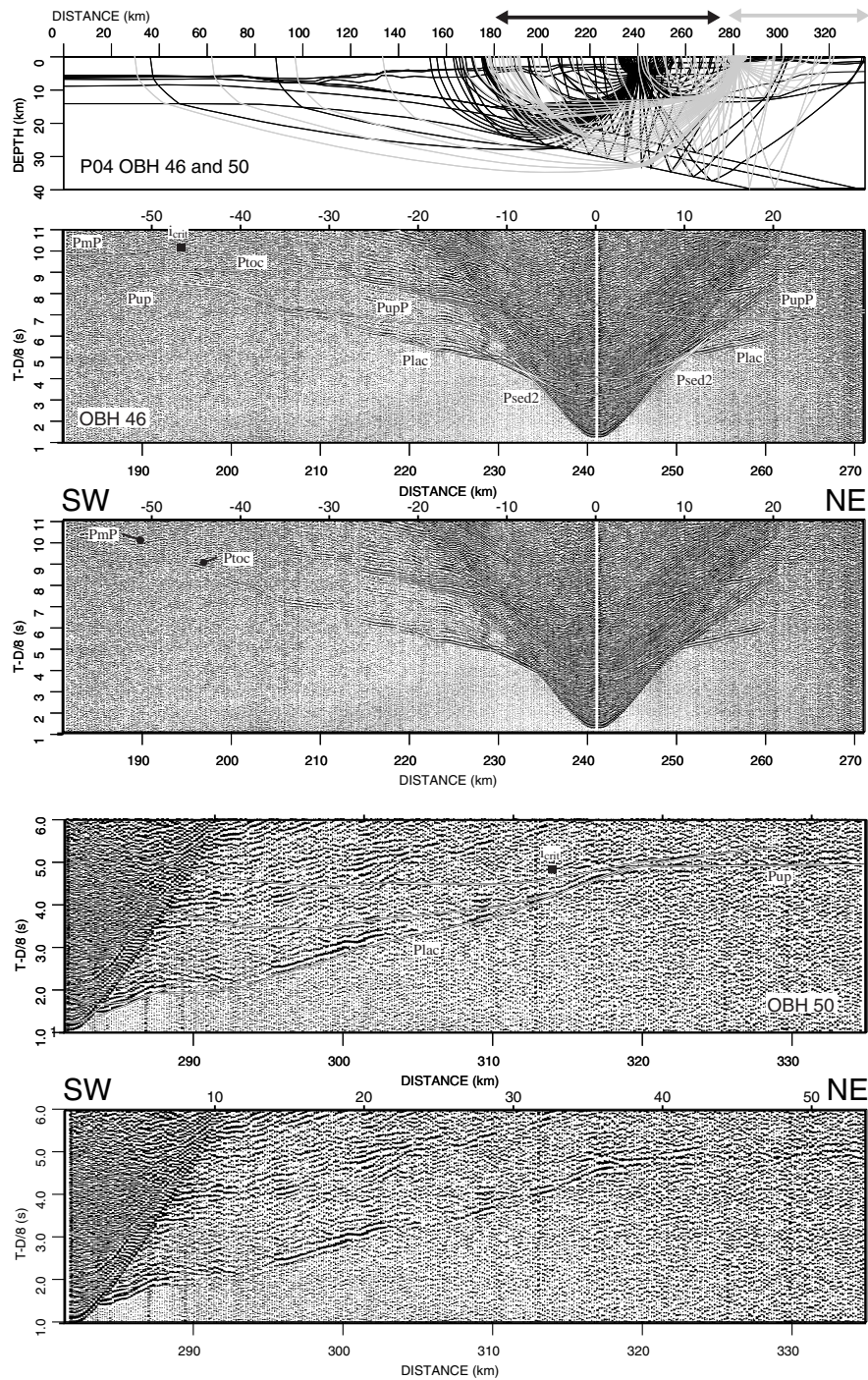


Figure 5.15: Both stations presented here are located within the forearc domain off Sunda Strait. OBH 46 records the leading edge of the upper plate as incidents PupP and Pup as well as the oceanic Moba at offsets beyond -50 km. Station 50 is deployed close to the Java shelf onset and covers the basement ridge at positive offsets. Refraction Pup verifies the elevated velocity values found here as presented in Figure 5.6.

A clear image of the active accretionary domain is presented in Figure 5.4a, in which at least 5 accretionary ridges are recognized, composing an accretionary wedge above the downgoing plate and bounded to the northeast by a sharp backstop structure at the slope break. Imbricate thrust faulting in this frontal part documents the deformation of the accreted sediments as they are pushed against the active backstop. Seismic velocities increase laterally from 3.0 km/s at the deformation front to about 3.9 km/s near the backstop structure (Fig. 5.6), supporting the notion of active accretion here. The upper sedimentary layers have been modelled with the help of the MCS data (Fig. 5.7). Seismic velocities derived from the upper sedimentary units range from 2.0 km/s to roughly 3.0 km/s (Fig. 5.6). Towards the Java shelf, roughly inbetween CDP 13000 through 18000, the sedimentary phases Psed1 and Psed2 are more distinct (e.g. in the record section of OBH 46 (Fig. 5.15)), as the seafloor topography is smoothed by the thicker sediments accumulated here. A bright BSR is identified mimicking the seafloor between CDP 14000 through 17000 approximately 400-500 ms TWT bsf (Fig. 5.4c). No sediment cover is found on the Java shelf onset, where a change in seafloor depth of over 1200 m occurs over a distance of 10 km. Thicker sedimentary sequences are again present at the northeastern end of the profile atop the Java shelf within Sunda Strait (CDP 10000-12000 in Fig. 5.4c).

For the greater part of the profile, inbetween the active backstop and the Java shelf onset, little lateral velocity variation is recognized underneath the upper sedimentary units. The rough surface basement top marks a velocity step from approximately 3.0 km/s at the base of the sedimentary layers to 3.9 km/s (Fig. 5.6). A roughly 9 km thick uniform layer, which shows some thinning below the larger sediment basins immediately seaward of the Java shelf onset, represents the lower accretionary complex. Its smooth velocity field is documented by phases Plac recorded by the various stations positioned along the outer high and forearc domain (OBH 40, 42, 46 in Figs. 5.14 and 5.15). A uniform velocity increase with depth from 3.9 km/s to 5.2 km/s is recognized for the main part of the lower outer high-forearc domain (Fig. 5.6). The frontal most seaward part of this layer thins progressively towards the deformation front as it is bounded at its base by the subducted slab; velocities range from 3.9 km/s to 4.9 km/s here. This is evident from seaward travelling incidents Plac recorded by stations OBH 39 and OBH 40 (Figs. 5.13 and 5.14). The base of this layer is found at a depth of approximately 13 km, except for the aforementioned thinned portion (profile km 250-280 in Fig. 5.6), where the layer boundary

is found at 12 km depth. Velocities increase to 5.9-6.0 km/s, as is deduced from refracted waves Pup and their corresponding reflections PupP ('up' refers to upper plate) of station OBH 46 in Figure 5.15. As OBH 46 also records the top of the subducted plate (P_{toc} in Fig. 5.15) underneath the leading edge of the upper plate, the low velocity-depth gradient is verified here.

A different situation emerges below the Java shelf. A substantial velocity increase is observed and velocity values of 4.3 km/s are recorded close below the seafloor as the recent sedimentary cover here is neglectable. The northeastward phases recorded by OBH 50 (Fig. 5.15) travel through the Java shelf (Plac). Refracted incidents Pup manifest a lateral velocity increase also within the lower portion of the upper plate, where values of 6.3 km/s are detected at 12 km depth.

The downthrusting plate is present in the MCS data as a high amplitude band of energy showing a high degree of coherency, especially underneath the frontal accretionary prism (Fig. 5.4a and b). This event can be followed for about 110 km from the deformation front, though the landward portion is partially inhibited by remnants of the seafloor multiple. Numerous large, landward-dipping faults are recognized in the oceanic crust (e.g. underneath CDP 27000 through 27600). Several OBH stations track the subducted plate: OBH 39 (Fig. 5.13) records a clear vertical reflection P_{toc} of the top of the oceanic plate, as well as the corresponding wide-angle reflection and the refracted wave P_{oc}. The mantle transition is imaged by a P_mP at offsets from 20 km to over 40 km distance down to a depth of over 20 km. The next instrument (OBH 40 in Fig. 5.14) recorded a seaward travelling P_n phase. Station 42 traces the Moho down to 35 km depth beneath the forearc domain (Fig. 5.14), while tracking the top of the plate at southwestern offsets down to 15 km. The deepest response from the downgoing plate was recorded by OBH 46 (Fig. 5.15), which shows elevated amplitudes beyond the critical angle i_{crit} of the P_mP reflection at over 30 km depth and a reflection off the top of the plate P_{toc}. These events allow us to trace the downthrusting plate to a depth of over 30 km.

5.4.4. Gravity modelling

In addition to the seismic data modelling, we also used the gravity field to test the plausibility of our velocity-depth models. Gravity calculations were conducted for both

dip lines, SO138-01 and -04. The gravity model incorporates the structures gained from the wide-angle forward modelling, to which density values as displayed in Figure 5.16 b and d were assigned. Using a priori information of the main geological units is crucial to limiting the number of possible solutions which fit the gravity data. We based our selection of the density values on the relationship between compressional velocities and densities. An average density of 2.23 g/cm^3 and 2.4 g/cm^3 (Ludwig et al., 1970) was assigned to the upper sediment layers which show velocities $<3.0 \text{ km/s}$ and $<4.0 \text{ km/s}$, respectively. For the lower accretionary complex, densities ranging from 2.5 g/cm^3 to 2.7 g/cm^3 correspond to the higher degree of compaction and the greater overburden here. A uniform density value of 2.89 g/cm^3 as suggested by Carlson and Raskin (1984) was assumed for the entire oceanic crust (Fig. 5.16b and d). Lower crustal densities of 2.95 g/cm^3 beneath the forearc domain of the upper plate correspond to values derived from Barton's (1986) relationship. Density values of 3.37 g/cm^3 are associated with the ca. 90 year old lithosphere. The calculated gravity response (black dotted line in Fig. 5.16a and c) was then compared to ship data acquired during the cruise (grey line in Fig. 5.16a and c) (Heyde et al., 2000).

Along line SO138-01 gravity variations of up to 170 mGal occur (Fig. 5.16a); the most pronounced features are the two distinct gravity lows caused by the deep trench and the forearc basin, respectively. The gravity high reaching values of up to 40 mGal seaward of the trench is associated with shallower seafloor observed here. The rugged topography of the rough surface basement top underneath the outer high is expressed in pronounced gravity variations between the trench and the forearc basin (between km 200 and 280 in Fig. 5.16b). The gravity response of the landward part of the forearc basin is already influenced by the higher densities of the upper plate modelled with uniform values of 2.95 g/cm^3 (Fig. 5.16b). Our calculations fit the observed gravity field to within $\pm 10 \text{ mGal}$ (Fig. 5.16a) and thus, to first-order approximation, the 2-D modelling corresponds adequately to the ship survey data. A detailed fit was achieved for the ocean basin and the active accretionary domain, as well as for the forearc basin. Without further efforts to gain a better fit along the outer high, the calculated values match the observed data sufficiently. The main trend of the gravity field across the subduction complex could be matched which yields further information on the geometry of the downgoing slab.

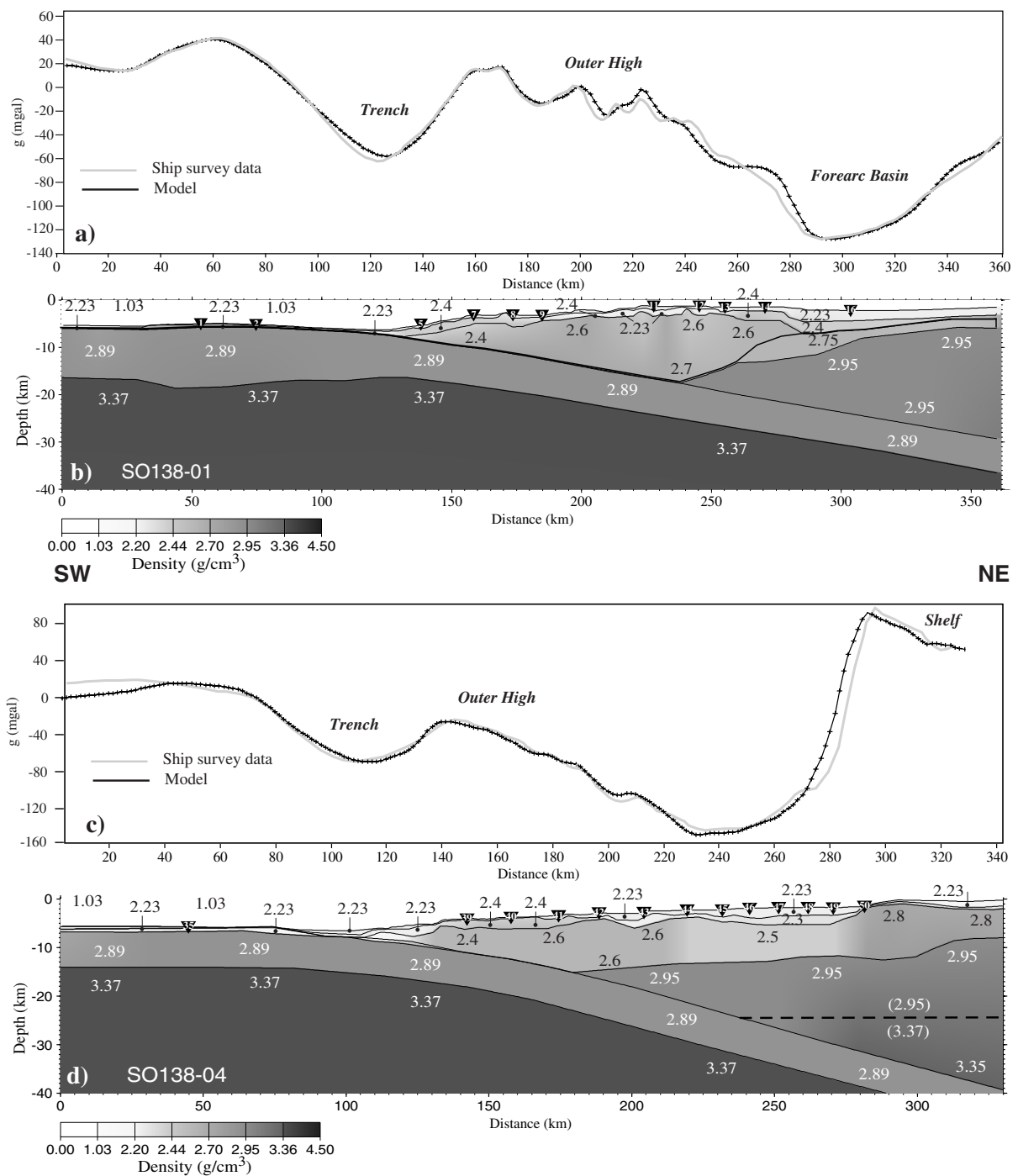


Figure 5.16: Gravity modelling for the dip lines SO138-01 and SO138-04. The ship survey data (black lines in a) and c)) are compared to the gravity response (grey lines in a) and c)) gained from density models shown in b) and d). Density values were assigned to the velocity structures gained from forward modelling of the OBH data. The ship gravity survey during the GINCO project was conducted by the BGR in Hannover, Germany (Heyde, 2000). The gravity calculations presented here sustain the plate geometry across the subduction complex. Along line SO138-04 the approximated upper plate Mobo is indicated by a dashed line.

Gravity variations of up to 250 mGal are present along the Sunda Strait transect, mainly caused by the high positive values associated with the Java shelf (Fig. 5.16c). Comparable to the other line, the trench and forearc domain cause distinct gravity lows around profile km 110 and 240 (grey line in Fig. 5.16c), as is expected from the great depth of the trench and the thick sedimentary sequences observed in the forearc domain. Again, without further efforts to achieve an overall superior fit, a detailed match was nonetheless achieved for the main part of the profile (black line in Fig. 5.16c), except for the seawardmost 40 km and the Java shelf onset. As the rough surface basement top is not as intensely expressed in the MCS data compared to the Sumatra transect, gravity values across the outer high are a lot smoother on the Sunda Strait profile. The lower accretionary complex was modelled with density values ranging from 2.5 g/cm^3 to 2.6 g/cm^3 , except for the more unconsolidated sediments at the frontal part near the deformation front (Fig. 5.16d). The high gravity values found in the Java shelf correspond to the elevated velocities here. Gravity values decline towards the northeastern end of the line at profile distances greater than 290 km (Fig. 5.16d), where a sediment basin is observed in the MCS data (Fig. 5.4c). Though no upper plate Moho phases could be identified in the seismic data underneath the forearc domain, the gravity response allows an estimate on Moho depth, as shown in Figure 5.16d. When the upper plate layer with density gradient ranging from 2.95 g/cm^3 to 3.35 g/cm^3 is substituted by two layers modelling the crust-mantle transition with a density increase from 2.95 g/cm^3 to 3.37 g/cm^3 , the gravity fit remains unchanged. As no corresponding boundary is present in the seismic data, this approximation is solely based on the gravity response. However, the overall fit allows additional constraint on the dip of the subducted plate on this transect, where no wide-angle strike lines are available.

5.5 Discussion

5.5.1 Igneous oceanic crust and subducted slab

The Sumatra line shows a thickening of the incoming igneous crust seaward of the trench. As no similar anomalies have been reported for other parts along the Sunda margin, we interpret this as a local phenomenon. This interpretation is sustained by the recordings landward of the deformation front which show a subducting slab of normal oceanic crustal thickness (7.5 km) (e.g. recorded by OBH 05 in Fig. 5.8). Global satellite gravity (Sandwell and Smith, 1997) is too coarse to resolve this crustal anomaly. The Sunda Strait transect displays a 7.5 km thick crust seaward of the trench. The velocity depth functions

for both domains show a normal velocity-depth structure with values which have also been reported for Pacific oceanic crustal samples older than 29 Ma (White et al., 1992). The closest drilling information from the oceanic basin is available from DSDP Hole 211. It is located at 9.78°S and 102.7°E close to the southwestern end of profile SO137-42. Quaternary pelagic sediment was drilled here before reaching the basement.

Upper mantle velocities of 8.0 km/s are determined from the Pn phases recorded underneath the oceanic basin by several stations along line SO138-01. As no Pn was recorded along the Sunda Strait transect, the mantle velocities are gained from the PmP reflection recorded by OBH 35 and show corresponding values. Seismic investigations off western and central Java (Curry et al., 1977; Kopp et al., 2000) found comparable crustal thickness and velocity values.

The trench fill increases by over 25 per cent from 1.1 km to 1.5 km maximum wedge thickness off Sumatra and off Sunda Strait, respectively. Since the Sumatra reflection line ceases about 20 km seaward of the trench, only the current material input can be determined which lies at approximately 500 m seaward of the trench. A corresponding value is established for recent trench input along the Sunda Strait transect. The Sunda Strait line continues for about 250 km onto the ocean basin (Fig. 5.2). A highly variable basement depth is observed along this segment. In parts the basement crops out above the seafloor, while in other parts it is covered by over 900 m of ocean basin deposits (Reichert, 1999). Judging from this highly variable thickness, a large part of the sediment cover probably originates from turbidites. Hemi-pelagic and pelagic sediment would build a smooth cover, whereas thickness variations and basement outcrops are the results of current-driven sedimentations of turbiditic origin. Judging from satellite gravity (Figs. 5.1 and 5.2), the overall plate structure of the ocean basin within the study area is steady as the large amounts of terrigenous sediment input from the Bengal fan do not cause deviations in the sediment cover this far south. Thus a similar sediment thickness variation on the ocean basin off southern Sumatra as off Sunda Strait can be expected and hence, a difference of 400 m in trench fill thickness is feasible. This is also supported by additional seismic reflection lines collected by the BGR across the trench from north of Enggano island to western Java (Reichert, 1999) and by reflection data collected in 1980 by the Scripps Institution of Oceanography (SIO) off central Java (G. Moore, personal communication).

The trench fill thickness varies arbitrarily up to 1600 m between these lines without showing a regional trend.

The top of the oceanic crust is traced by diverse stations on both dip lines as it starts bending underneath the deformation front. An increase in plate dip along the Sumatra transect from less than 3° near the deformation front to approximately 5° underneath the outer high is observed. The Sunda Strait line shows a corresponding increase in plate dip from a little over 4° to 7° . These trends are supported by the gravity modelling conducted along the dip lines. As no local earthquake or tomographic studies exist, the slab configuration can only be correlated to global data, whose locations however are not detailed enough in this area to yield any conclusive information. For the Sumatran domain some 3D constraint is gained from the two strike lines, which record the downgoing plate at 19 km depth underneath the outer high and at 21 km depth underneath the forearc basin. In order to verify the observed reflections from the leading edge of the upper plate (PupP) and the top of the subducted slab (Ptoc), synthetic data modelling has been attempted using OBH 32 deployed on profile SO138-02 and OBH 20 from profile 03. This dynamic modelling approach is based on the reflectivity method, which uses a homogeneous layer model, for which the reflectivity is calculated analytically from the layers' seismic velocities, densities, and attenuation factors. The resulting synthetic sections are compared to the real data in Figure 5.17. The refraction through the lower accretionary complex (Plac) as well as the reflections from the upper plate and the downgoing oceanic slab (compare Figs. 5.11 and 5.12) could be generated using a velocity-depth model which corresponds to the model derived from forward raytracing shown in Figure 5.5. As the minor inclination of the seafloor and the structural layers in the model for profile 02 as well as the lateral thickness variations of the sedimentary layers of profile 03 cannot be accounted for in the one-dimensional synthetic modelling, some discrepancies in the traveltimes of the real and the synthetic data must be expected. If amplitude variations with offset within each phase of the real data are due to 2D and 3D ray focussing and defocussing effects, they cannot be retrieved with the reflectivity method. Focussing effects are documented along both profiles: the refraction through the upper plate PupP recorded by OBH 20 shows a significant amplitude decrease around profile distance 85-90 km, before higher amplitudes are observed again at approximately 100 km profile distance. The same amplitude pattern is observed on OBH 17 (Fig. 5.12) and OBH 19 (not shown).

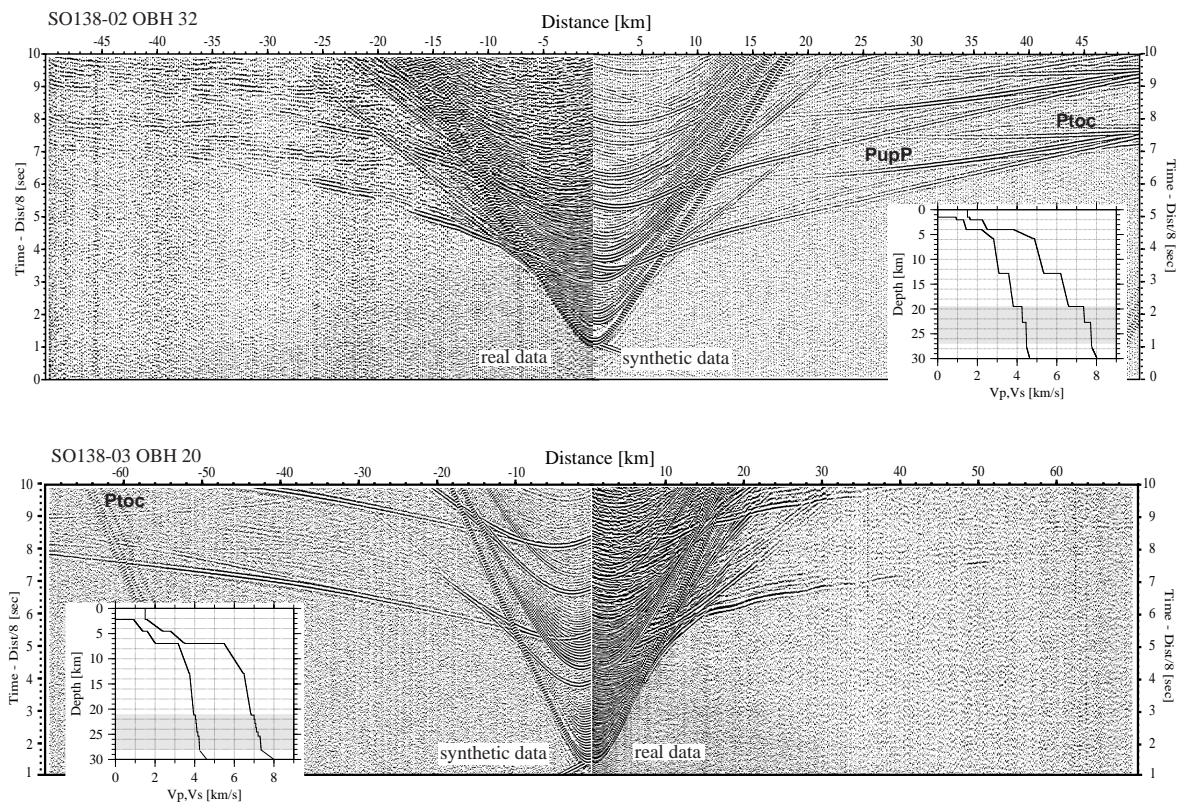


Figure 5.17: One-dimensional synthetic data modelling conducted for two stations deployed along the strike lines SO138-02 and 03 to verify phases recorded from the leading edge of the upper plate PupP and the top of the subducted plate Ptoc. The dynamic modelling procedure employs the reflectivity method and is based on the velocity models derived from kinematic forward modelling. The synthetic seismograms are filtered with identical parameters as the real data to assure compatibility. The corresponding velocity-depth profiles for P- and S-velocities correspond to the velocity-depth structure derived from forward raytracing; the depth of the subducted plate is underlain in grey. The results from two-dimensional raytracing are presented in Figures 5.11 and 5.12.

Similar focussing and defocussing effects influence the phase through the lower accretionary complex (Plac) of OBH 32 (Fig. 5.11), for which the observed amplitude undulations occur at approximately identical profile distances for neighboring stations. The main targets of this synthetic modelling however are the reflection from the upper plate and the subducted oceanic plate (PupP and Ptoc, respectively), for which an adequate amplitude characteristic could be achieved. On OBH 32, reflection amplitudes from the leading edge of the upper plate are increasing from 20 km offset, whereas significant amplitudes from the reflection generated by the top of the subducted slab appear at offsets of around 32 km. The general amplitude decrease of several phases beyond 37 km offset are again due to defocussing effects, as this lack of reflectivity is observed on several stations along this profile. OBH 20 records the subducted plate

underneath the forearc basin at approximately 21 km depth (Fig. 5.17). The amplitudes from the corresponding incident arrive at late times and are strongest at offsets greater than 60 km. This amplitude pattern is also confirmed in the synthetic data. The velocity-depth profile used for the dynamic modelling is shown for both stations in Figure 5.17. The grey shaded area signifies the subducted plate. Minor revisions compared to the velocity field derived from forward modelling have been adapted, but the overall velocity depth structure is consistent with the results presented in Figure 5.5.

5.5.2 Structure of the accretionary domain and outer high

Along both dip lines an active accretionary domain is identified consisting of the material above the subducting slab bordered laterally by the deformation front and the slope break, which is the surface expression of an underlying backstop structure (Figs. 5.3a and 5.4a). Several smaller ridges are the geomorphological indication for active accretion of the trench fill sediment which causes partial stacking and folding between the deformation front and the slope break. Imbricate thrust faulting is recognized on both lines. Whereas the Sumatra transect displays a chaotic seismic signature of the active accretionary domain, the internal structure along the Sunda Strait segment is not completely destroyed, though highly deformed.

Active accretion is also supported by the velocity model. Laterally increasing velocities are characteristic for the frontal prism up to the location of the backstop structure. The low seismic velocities are representative of young accreted sediment. On both lines, the backstop structure marks the transition from the active accretionary domain to the outer high and cuts the entire accretionary units to near the top of the subducted plate. Landwards, tectonic activity is still evident in a number of thrusts on the outer high, but is greatly reduced compared to the active accretionary domain. The reflectivity of the outer high along both reflection lines is limited. On line SO137-12 the rough surface basement top which appears landward of the outer high crest, further inhibits the reflectivity of the lower segments. A similar rough surface is present on the Sunda Strait line, though more internal structure within the basement is resolved which displays a chaotic pattern of thrusting and possible rotation of entire blocks. Velocities show laterally constant values within the outer high, solely increasing with depth due to the greater overburden and material compaction. In view of the large dimensions of the outer high and its great depth,

velocities are fairly low (<5.8 km/s off southern Sumatra and <5.2 km/s off Sunda Strait at approximately 15 km depth). This velocity structure is indicative of a sedimentary composition, possibly including metamorphosed material near the base. The density values used in the gravity modelling for the dip lines which correlate to the seismic velocities and structural model are typical for compacted sedimentary substance.

5.5.3 Forearc domain

The most striking difference between the two transects concerns the crustal structure of the forearc domain and the corresponding lack of a morphological basin off Sunda Strait. In contrast, the forearc basin off southern Sumatra lies at 2200 m seafloor depth. Its lateral extent of over 80 km is bounded by the Sumatra shelf to the northeast (Fig. 5.3c). The seaward part of the basin is highly affected by the presence of the Mentawai Fault anticlinal structure, causing a significant uplift of the seafloor. The Mentawai Fault separates a smaller sub-basin from the main basin; the sub-basin also carries less sediment infill. We still interpret this segment between CDP 16800 to 18700 to form part of the forearc basin complex as the basement top underneath the forearc basin sediment fill continues to below the sub-basin (Fig. 5.3b and c). Nonetheless, the Mentawai Fault poses a structural break here and is possibly related to the uplift of the sub-basin with regards to the main forearc basin.

The lack of an analogue forearc basin off Sunda Strait correlates with the locally concave shape of the trench and deformation front here, resulting from the northwestward motion of the Sumatra sliver plate, for which the area off Sunda Strait acts as a trailing edge (Huchon and Le Pichon, 1984). The forearc domain along the Sunda Strait line (CDP 13100 through CDP 17900 in Fig. 5.4c) shows a comparable lateral extent and sediment accumulation. In contrast to line 12, the sediments here are highly deformed. The intense folding and partial stacking affects mainly the older sequences whereas the younger units are not as strongly altered. The presence of a strong Bottom Simulating Reflection (BSR) observed in the forearc domain along both lines indicates the lower boundary of the gas hydrate stability zone. Unlike most other known occurrences of gas hydrates worldwide, the distribution of gas hydrate and free gas on the central Sunda margin is limited to the forearc domain. The absence of a BSR along the accretionary domain and outer high is probably

due to the intense active faulting observed here (Figs. 5.3a, b and 5.4a, b) which potentially allows the escape of free gas.

Both forearc domains carry a several kilometer thick sedimentary infill (over 4 km on the Sunda Strait transect and over 4.5 km off southern Sumatra). Seismic stratigraphy investigations of the forearc basin north of Nias island (Beaudry and Moore, 1981; Beaudry and Moore, 1985; Izart et al., 1994) were correlated to borehole information and indicate a Neogene history characterized by subsidence and continuous sedimentation. Thus the sedimentary sequences overlying the Paleogene basement are of Miocene age and were deposited after a late Oligocene initiation or rejuvenation of subduction along the margin leading to an uplift of the subduction complex. Off southern Sumatra, the seaward dipping basement top is underlain by a layer ranging from 5.3 km/s to 5.7 km/s velocities (Fig. 5.5), with increasing thickness from 1.5 km underneath the shelf to 4 km underneath the seaward part of the basin. Underneath this layer, velocities increase from 6.0 km/s to over 6.5 km/s within the leading edge of the upper plate. These velocity values correspond roughly to results from earlier refraction studies conducted around Nias island (Kieckhefer et al., 1980). The velocity structure observed within the leading edge of the upper plate (thin black line in Fig. 5.18) closely matches the results compiled by Christensen and Mooney (1995) (thick grey line in Fig. 5.18) for an average continental crustal model including continental arcs.

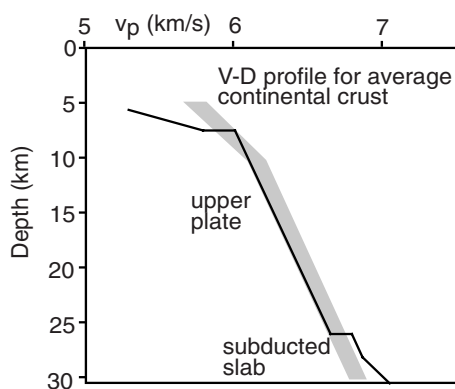


Figure 5.18: Comparison of velocity depth profiles from the forearc domain of line S0138-01 (thin black line) to a two-gradient average continental crust model (thick grey line) after Christensen and Mooney (1995). The velocities found underneath the Sumatran forearc basin, though in the lower range of average values, are indicative of continental type crust.

Off Sunda Strait, a different situation emerges as velocities underneath the basement top range from 3.9 km/s to 5.2 km/s within a 6.5 km to 8.5 km thick unit underneath the forearc domain (Fig. 5.6). These velocities are identical to the velocity structure found underneath the outer high, whereas off Sumatra a significant velocity increase was found. At greater depth, velocities ranging from 6.0 km/s to over 6.5 km/s correspond to the Sumatran results. Further landward, underneath the Java shelf, a substantial velocity increase is observed. Velocities of 4.3 km/s at 2 km depth correspond

to values reported by Lelgemann et al. (2000) on a basement ridge at the southwestern entrance to Sunda Strait. The high gravity values of over 80 mGal observed here also indicate a shallow basement. Further north along the central segment of the Sunda Strait, the ridge is broken into several basement blocks which mark the eastern boundary of the Sunda Strait transtensional basin. This basin or graben formed in conjunction with the northwest motion of the Sumatra sliver plate (Lelgemann et al., 2000).

5.6 Conclusions

An integrative analysis of wide-angle and reflection seismic data provided us with new insights on the structure of the subduction complex off southern Sumatra and off Sunda Strait. Additional 2D gravity modelling and synthetic data further constrain the following results:

1) The configuration of the descending slab is determined along both transects by the MCS and OBH data for the upper 20 km. Near the deformation front, the plate gently dips at about 3° off Sumatra and at 4° off Sunda Strait. Underneath the outer high and the forearc domain, late arrivals from the plate boundary and from the oceanic Moho are identified in the wide-angle data and show a gradually increasing dip to 5° off Sumatra and 7° off Sunda Strait, respectively. The lateral increase in the plate dip to the southeast is supported by the gravity modelling conducted along the dip lines. The Sumatran results are further sustained by reflections observed on the strike lines SO138-02 and SO138-03, which track the subducted plate at 19 km depth and at 21-22 km depth, respectively. These 3D constraints could successfully be modelled with synthetic data.

2) Along both transects an active accretionary prism occupies the frontal part of the subduction complex and is separated from the outer high by a backstop structure. This accretionary domain is characterized by the generation of accretionary ridges and by intense tectonic activity resulting in numerous faults. Seismic velocities show a lateral positive gradient and values typical for young accreted sediment.

3) The extensive outer high domain shows comparable lateral dimensions of 85-90 km along both dip lines: off Sumatra, the leading edge of the upper plate is found in over 16 km depth, whereas off Sunda Strait a shallower upper plate transition (13 km) is consistent

with the velocity structure observed here. The rugged seafloor topography and underlying rough surface basement top of the outer high on both profiles inhibit the reflectivity and little internal structure is resolved. The loss in resolution suggests a higher degree of deformation and compaction of the underlying material, also indicated by the velocity structure of the outer high. Seismic velocities derived from the wide-angle data are moderate along both transects, sustaining a possible sedimentary composition. Metamorphosed material might be present at the base, but in view of the modest velocity values, an overall igneous or ophiolitic composition seems unlikely. Tectonic activity is evident from faults on both sections and ongoing deformation of the ponded sediment in the basins created by the rough surface top is expressed in the ridge and trough morphology.

4) The main difference between the two transects regards the nature of the lower forearc domain and the absence of a distinct forearc basin off Sunda Strait. A typical discrete basin is only observed off southern Sumatra, forming part of the chain of forearc basins along the margin. The velocity structure underneath the basin indicates a continental type crust forming the forearc basement. Several kilometers of sediment fill record the Miocene to Quaternary depositional history of the basin. A similar amount of sediment is found off Sunda Strait, where the clear-cut onset to the Java shelf covers the transition to the morphological features within Sunda Strait, which are related to the transtensional evolution of the Sunda Strait pull-apart basin. The nature of the forearc basement off Sunda Strait remains unclear, as seismic velocities here are lower than off Sumatra.

Barton, P. J., The relationship between seismic velocity and density in the continental crust, a useful constraint?, *Geophys. J. R. Astron. Soc.*, 87, 195-208, 1986.

Beaudry, D., and G. Moore, Seismic Stratigraphy and Cenozoic Evolution of West Sumatra Forearc Basin, *AAPG Bulletin*, 69, 742-759, 1985.

Beaudry, D., and G. Moore, Seismic-stratigraphic framework of the forearc basin off central Sumatra, Sunda Arc, *Earth and Planetary Science Letters*, 54, 17-28, 1981.

Bellier, O. and M. Sébrier, Is the slip rate variation on the Great Sumatran Fault accommodated by fore-arc stretching?, *Geophysical Research Letters*, 22, 15, 1969-1972, 1995.

Carlson, R. L., and G. S. Raskin, Density of the ocean crust, *Nature*, 311, 555-558, 1984.

- Christensen, N. I., and W. D. Mooney, Seismic velocity structure and composition of the continental crust: A global view, *Journal of Geophysical Research*, 100, 9761-9788, 1995.
- Curry, J. R., G. G. Shor, R. W. Raitt, M. Henry, Seismic refraction and reflection studies of crustal structure of the eastern Sunda and western Banda Arcs, *Journal of Geophysical Research*, 82, 17, 2479-2489, 1977.
- DeMets, C., R. G. Gordon, D. F. Argus, S. Stein, Current plate motions, *Geophysical Journal International*, 101, 425-478, 1990.
- DeMets, C., R. G. Gordon, D. F. Argus, S. Stein, Effects of recent revisions to the geomagnetic reversal time scale on estimates of current plate motions, *Geophysical Research Letters*, 21, 2191-2194, 1994.
- Diament, M., C. Deplus, H. Harjono, M. Larue, O. Lassal, J. Dubois, V. Renard, Extension in the Sunda Strait (Indonesia): a review of the Krakatau programme, *Oceanologica Acta Special Volume*, 10, 31-42, 1990.
- Diament, M., H. Harjono, K. Karta, C. Deplus, D. Dahrin, M. T. Zan, Jr., M. Gerard, O. Lassal, A. Martin, J. Malod, Mentawai fault zone off Sumatra: a new key to the geodynamics of western Indonesia, *Geology*, 20, 259-262, 1992.
- Fitch, T. J., Plate convergence, transcurrent faults and internal deformation adjacent to southeast Asia and the western Pacific, *Journal of Geophysical Research*, 77, 4432-4460, 1972.
- Flueh, E.R. and J. Bialas, A digital, high data capacity ocean bottom recorder for seismic investigations, *Int. Underwater Systems Design*, 18, 3, 18-20, 1996.
- Flueh, E.R. (edt) and Shipboard Science Party, GINCO2 (SONNE Cruise SO-138): Geo-scientific investigations along the active convergence zone between the Eastern Eurasian and Indo-Australian Plates off Indonesia, *Cruise Report*, Geomar, Kiel, 1999.
- Hamilton, W., Tectonics of the Indonesian region, *U.S. Geological Survey Professional Paper* 1078, 1979.
- Hamilton, W., Plate tectonics and island arcs, *Geological Society of America Bulletin*, 100, 1503-1527, 1988.
- Harjono, H., Seismicity of the Sunda Strait: Evidence for crustal extension and volcanological implications, *Tectonics*, 10, 17-30, 1991.
- Heyde, I., H. A. Roeser, B. Schreckenberger, Gravimetric measurements and their interpretation, *GINCO Final Report*, Part I, BGR, Hannover, 2000.
- Huchon, P., and X. Le Pichon, Sunda Strait and Central Sumatra fault, *Geology*, 12, 668-672, 1984.
- Izart, A., B. Mustafa Kemal, J. A. Malod, Seismic stratigraphy and subsidence evolution of the northwest Sumatra fore-arc basin, *Marine Geology*, 122, 109-124, 1994.
- Kieckhefer, R. M., Shor, G. G. Jr., Curry, J. R., Seismic refraction studies of the Sunda trench and forearc basin, *Journal of Geophysical Research*, 85, B2, 863-889, 1980.
- Kopp, H., E. R. Flueh, D. Klaeschen, J. Bialas, C. Reichert, Crustal structure of the Java margin from seismic wide-angle and multichannel reflection data, *Journal of Geophysical Research*, submitted, 2000.
- Lelgemann, H., M.-A. Gutscher, J. Bialas, E. R. Flueh, W. Weinrebe, C. Reichert, Transtensional basins in the western Sunda Strait, *Geophysical Research Letters*, 27, 21, 3545-3548, 2000.
- Ludwig, W. J., J. E. Nafe, C. L. Drake, Seismic refraction, in: *The Sea*, 4, 1, A. E. Maxwell (edt), 53-84, Interscience, New York, 1970.

- Luetgert, J., MacRay-Interactive two-dimensional seismic raytracing for the Macintosh, *U.S. Geological Survey Open File Report*, 92-356, 1992.
- Malod, J. A., and B. M. Kemal, The Sumatra margin: oblique subduction and lateral displacement of the accretionary prism, in: *Tectonic evolution of Southeast Asia*, R. Hall and D. Blundell (eds), *Geological Society Special Publication*, 106, 19-28, 1996.
- Malod, J. A., K. Karta, M.O. Beslier, M.T. Zen Jr., From normal to oblique subduction: Tectonic relationships between Java and Sumatra, *Journal of Southeast Asian Earth Sciences*, 12, 85-93, 1995.
- McCaffrey, R., Slip vectors and stretching of the Sumatran forearc, *Geology*, 19, 881-884, 1992.
- McCaffrey, R., Oblique plate convergence, slip vectors, and forearc deformation, *Journal of Geophysical Research*, 97, B6, 8905-8915, 1992.
- McCaffrey, R., Slip partitioning at convergent plate boundaries of SE Asia, in: *Tectonic evolution of Southeast Asia*, R. Hall and D. Blundell (eds), *Geological Society Special Publication*, 106, 3-18, 1996.
- Moore, G. F., J. R. Curray, D. G. Moore, D. E. Karig, Variations in geologic structure along the Sunda fore arc, Northeastern Indian Ocean, in: *The tectonic and geologic evolution of Southeast Asian seas and islands*, D. Hayes (ed), *Geophysical Monograph*, 23, 145-160, 1980.
- Prawirodirdjo, L., Y. Bock, R. McCaffrey, J. Genrich, E. Calais, C. Stevens, S. S. O. Puntodewo, C. Subarya, J. Rais, P. Zwick, Fauzi, Geodetic observations of interseismic strain segmentation at the Sumatran subduction zone, *Geophysical Research Letters*, 24, 21, 2601-2604, 1997.
- Puspito, N. T., and K. Shimazaki, Mantle structure and seismotectonics of the Sunda and Banda arcs, *Tectonophysics*, 251, 215-228, 1995.
- Reichert, C. (ed) and Shipboard Science Party, GINCO1 (SONNE Cruise SO-137): Geo-scientific investigations along the active convergence zone between the Eastern Eurasian and Indo-Australian Plates off Indonesia, *Cruise Report*, BGR, Hannover, 1999.
- Samuel, M. A., N. A. Harbury, M. E. Jones, S. J. Matthews, Inversion-controlled uplift of an outer-arc ridge: Nias Island, offshore Sumatra, in: *Basin Inversion*, J. G. Buchanan and P. G. Buchanan (eds), *Geological Society Special Publication*, 88, 473-492, 1995.
- Samuel, M. A., and N. A. Harbury, The Mentawai fault zone and deformation of the Sumatran forearc in the Nias area, in: *Tectonic evolution of Southeast Asia*, R. Hall and D. Blundell (eds), *Geological Society Special Publication*, 106, 337-351, 1996.
- Sandwell, D.T. and W. H. F. Smith, Marine gravity anomaly from Geosat and ERS1 satellite altimetry, *Journal of Geophysical Research*, 102, B5, 10039-10054, 1997.
- Tregoning, P., F. K. Brunner, Y. Bock, S. S. O. Puntodewo, R. McCaffrey, J. F. Genrich, E. Calais, J. Rais, C. Subarya, First geodetic measurement of convergence across the Java Trench, *Geophysical Research Letters*, 21, 19, 2135-2138, 1994.
- Wessel, P., and W. H. F. Smith, Free software helps map and display data, *EOS Trans. AGU*, 72, 441, 445-446, 1991.
- White, R.S., D. McKenzie, R.K. O'Nions, Oceanic crustal thickness from seismic measurements and Rare Earth Element inversions, *Journal of Geophysical Research*, 97, B13, 19681-19715, 1992.
- Widiyantoro, S., and R. van der Hilst, Structure and evolution of lithospheric slab beneath the Sunda Arc, Indonesia, *Science*, 271, 1566-1570, 1996.

6. BSR OCCURRENCE ALONG THE SUNDA MARGIN AND ITS LINKAGE TO FLUID FLOW: NEW INSIGHTS FROM THE GINCO AND RAMA PROJECTS

6.1 Introduction

In the past decade, the focus of scientific research on the investigations of gas hydrates acknowledged their relevance as a possible form of future energy resource as well as their role in marine geohazards and the global climate change. As a number of geochemical and geological parameters control the occurrence of gas hydrates in nature, it is important to study their global distribution in different environments to better understand the interaction of the controlling factors on the formation of gas hydrates.

Gas clathrates or hydrates are a crystalline form of water molecules which construct a rigid grid around cavities holding a guest gas, most commonly methane. Their generation depends on a number of physical and chemical parameters, mainly temperature, pressure, and composition and is thus restricted to certain geological areas which meet these criteria. Onshore, gas hydrates are found in the permafrost regions. In the ocean, vast areas offer favourable P-T conditions at bottom-water temperatures around 0°C and corresponding depths exceeding about 300 m. However, gas hydrates are mainly found along outer plate margins, most commonly along the slopes of accretionary prisms. This regional limit results from the large amounts of gas (methane)-volume required for gas hydrate formation, which is mainly supplied by sediments found along margin slopes (Kvenvolden, 1998).

6.2 Possible methane sources and BSR formation

The schemes for gas hydrate formation differ in their concepts of methane generation: microbial methane formation from organic matter occurs within the zone of gas hydrate stability (GHSZ), whereas thermogenic generation from deeply buried organic matter at temperatures about 80-150°C produces methane directly (Kvenvolden, 1998). Methane then migrates upwards and forms gas hydrate if the thermobaric conditions are fulfilled (Hyndman and Davis, 1992; Ginsburg, 1998). In both cases, a so-called bottom simulating reflector or BSR marks the base of the stability zone and more or less coincides with its depth as predicted from phase diagrams. This reflector plays a crucial role in seismic data interpretation for identifying marine occurrences of gas hydrates which are inferred from

BSR formation. Seismic characteristics of the BSR generally include a polarity reversal and strong negative reflection coefficient, indicating a velocity inversion from higher velocities of the hydrate-cemented sediment above, to lower velocities from uncemented sediment or free gas trapped below the base of the stability zone (Grevemeyer et al., 2000). Changes in the geological setting, such as tectonic uplift or sedimentation (von Huene and Pecher, 1999), will cause a shifting of the stability zone and result in dissociation of gas hydrate to free gas, which then may migrate back into the stability zone and in turn form gas hydrate (methane recycling).

6.3 The RAMA data acquisition

Along the Sunda margin, extensive BSR occurrence has been identified for the first time in the GINCO reflection data sets. Additional reflection data off central Java were acquired by the Scripps Institution of Oceanography within the scope of the RAMA project (Fig. 6.1).

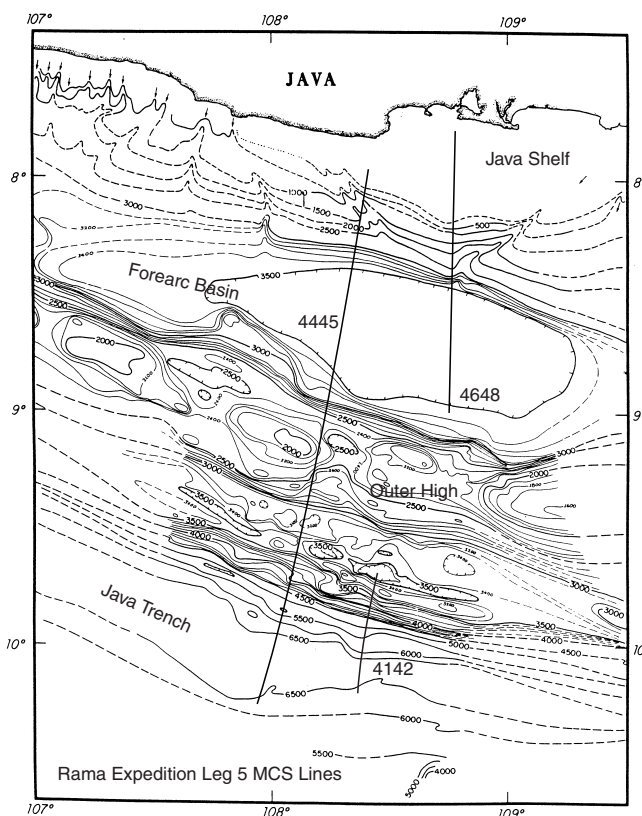


Fig. 6.1: Location map of RAMA expedition reflection profiles off central Java (after Benaron, 1982).

The profiles were acquired in 1980 using RV Thomas Washington. The data were recorded along a 24 channel streamer, using variable airgun sizes as source with a total combined capacity of 890 cu. in. The new migrations of lines RAMA 4445 and RAMA 4648 were conducted at GEOMAR as part of this thesis and are based on the preprocessing accomplished at Scripps (Benaron, 1982).

6.4 Interpretation

Unlike on most other accretionary margins, BSR formation along the Sunda margin is solely restricted to the forearc basin environment. Though the presence of gas hydrates has been suggested for this margin due to its great depth and the large amount of accreted material, no BSR phases were found along the active accretionary domain, the accretionary prism or the outer high. BSRs were identified in the forearc basins off Sumatra and off Java, as well as in the forearc domain off Sunda Strait, where a distinct basin is missing. Figure 6.2 shows the seaward part of the forearc basin off Sumatra, covering the Mentawai anticline. A pronounced BSR is visible crossing the anticline, ranging from 0.5-0.8 s TWT below the seafloor.

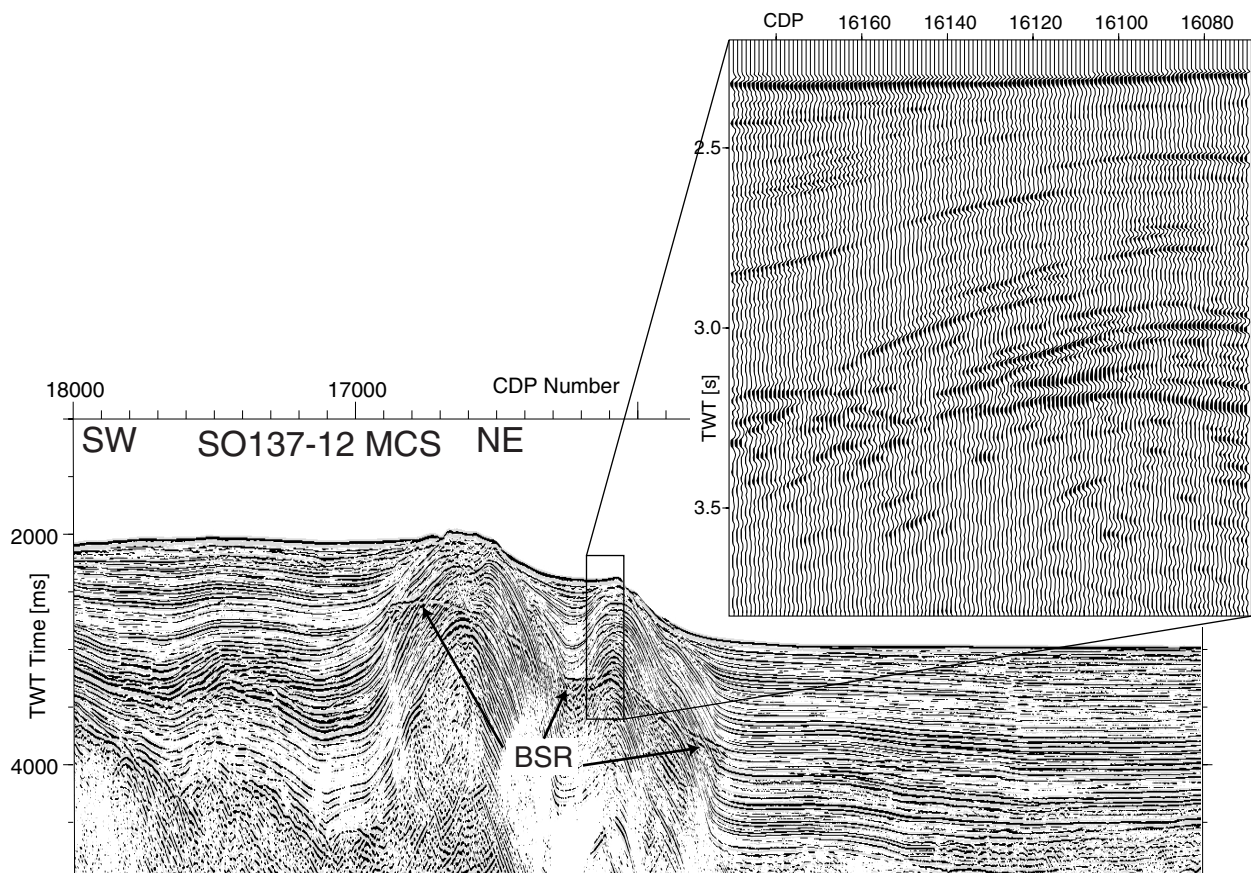


Figure 6.2: Seaward portion of the Sumatra forearc basin across the Mentawai anticline. A distinct BSR is visible cutting stratigraphic layers across the anticline. The BSR disappears in the horizontal layering of the sedimentary strata adjacent to the anticline. A location map is given in Figure 5.2.

The BSR cannot be detected within the sedimentary basins bordering the anticline structure. Even though the sedimentary strata lay mainly subparallel to the seafloor, the stratigraphy is in parts slightly folded and disturbed, so that the diagenetic boundary formed by the BSR, if present, should cut across this layering. Figures 6.3 and 6.4 display discontinuous BSRs on segments of the two strike-lines covered by the ministreamer during SO138 (Fig. 1.2) as well as the short intermediate segment connecting the two profiles at their southeastern ends (SO138-02Q).

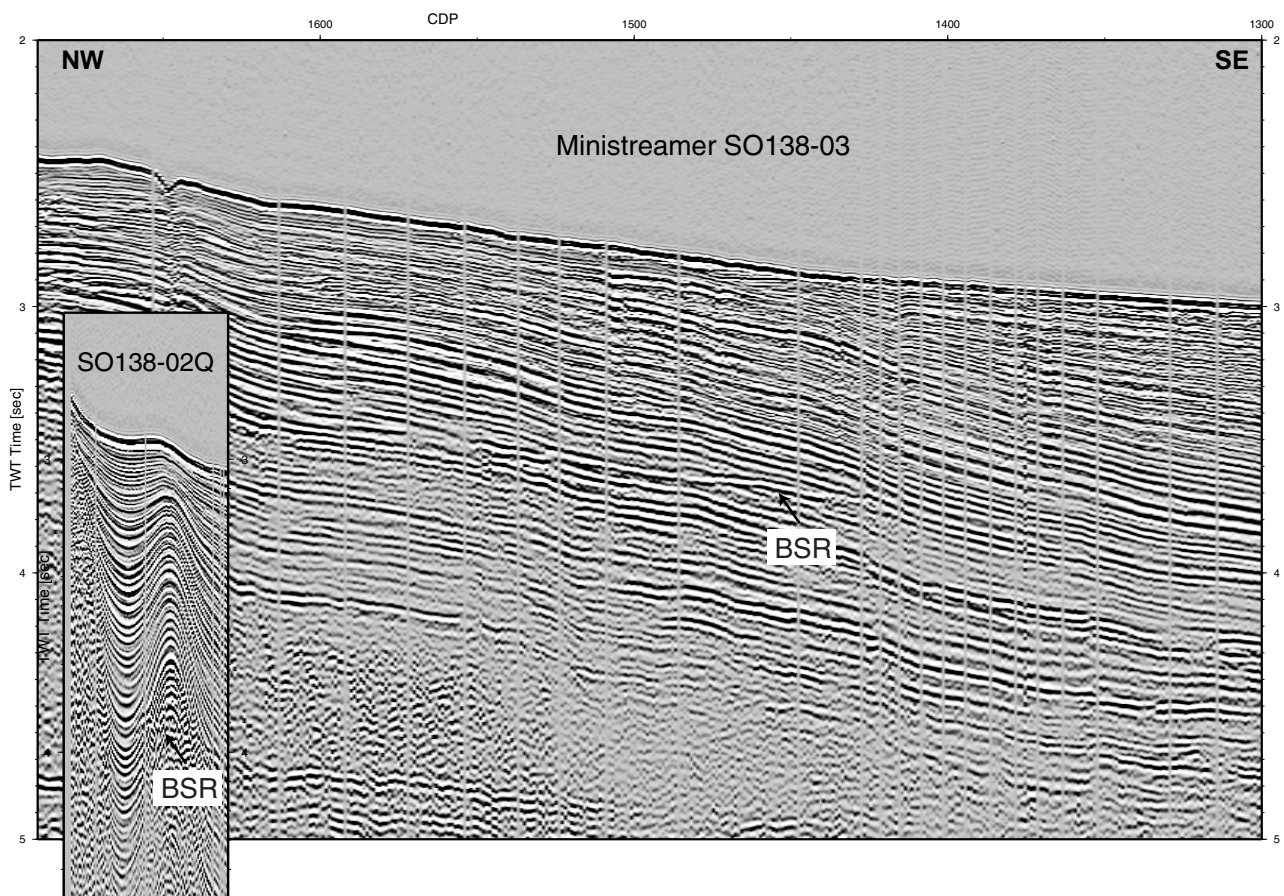


Figure 6.3: Ministreamer reflection line SO138-03 trending along strike of the Sumatran forearc basin. A location map is provided in Figure 5.2. As a diagenetic boundary, the BSR cuts across stratigraphic layering of the sediment. The inlay shows a short profile which was recorded connecting the two strike-lines at their southeastern ends. This profile O2Q covers the Mentawai anticline, where a weaker BSR is visible about 0.7s TWT bsf.

On line 03, the BSR cuts across the sedimentary layers 0.8 s TWT bsf along the northwestern slope of a sedimentary basin. The inset in Figure 6.3 again shows the

Mentawai anticline with a BSR visible 0.7 s TWT bsf. Line 02 shows some topographic variation with a BSR at 0.75 s TWT bsf below a topographic high at the southeastern end of the section. Moving to the Sunda Strait regime (Fig. 6.5), MCS line SO137-42 recorded a BSR along more than 40 km (Fig. 6.5a), displaying the highest degree of lateral continuation of all BSR examples presented here. The corresponding ministreamer data in Figure 6.5b shows the extent of faulting and folding which disturbs the forearc domain. The BSR lies much shallower here at ca. 0.35-0.5 s TWT bsf.

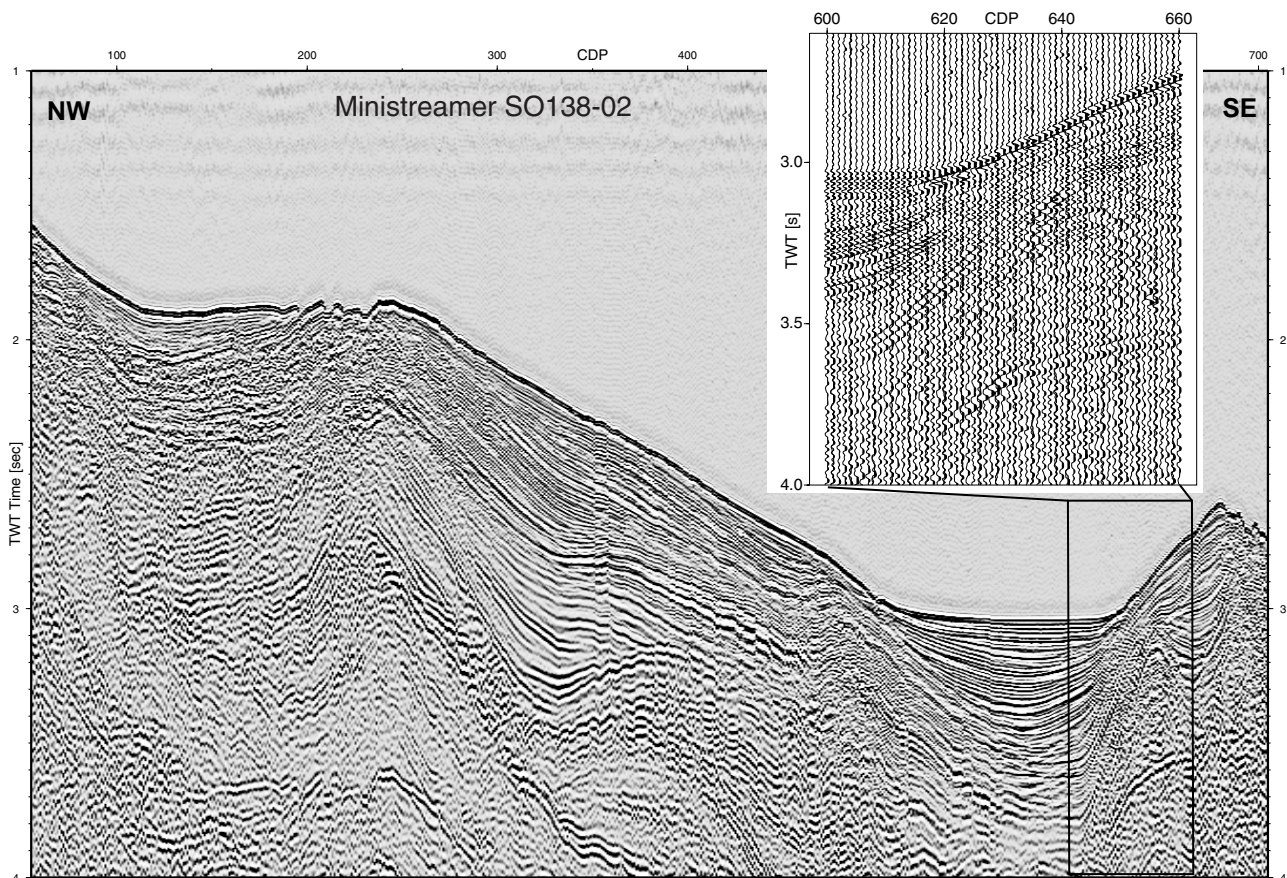


Figure 6.4: Ministreamer line SO138-02 within the Sumatra forearc basin. A strong BSR is found underneath a topographic elevation which displays anticlinal deformation of the sedimentary strata. These structures are likely to show elevated fluid flow.

The characteristic amplitude blankening is only present along this profile, as is visible in the left blowup of the ministreamer line and along large segments of MCS line 42. Blankening is not witnessed where sediment layers have accumulated. Off central Java (Figs. 6.6 and 6.7), the observed BSRs lie deeper than off Sumatra, at 0.95-1.3 s TWT bsf. They are identified along the slopes of the forearc basin, however, not within the center of

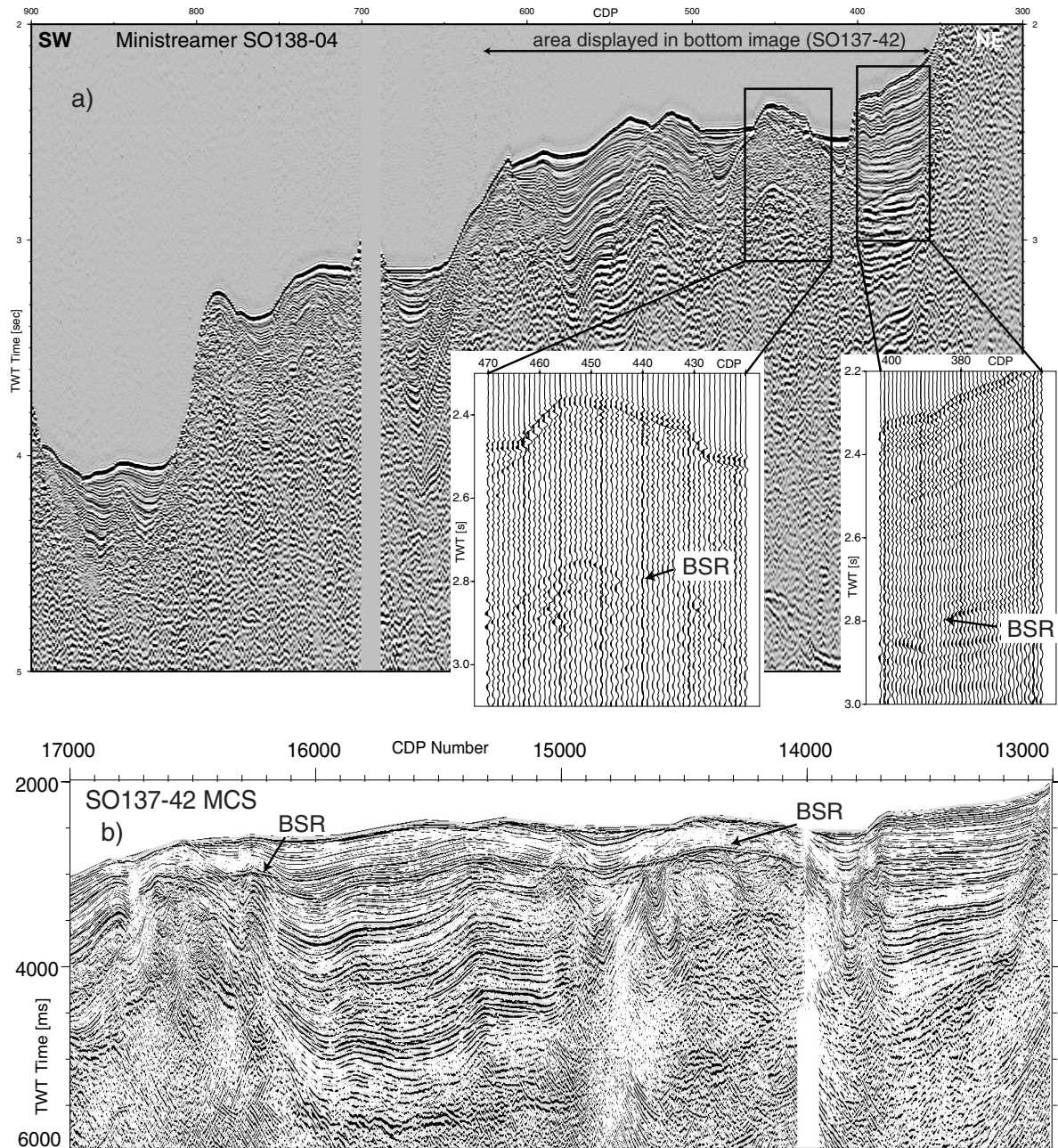


Figure 6.5: MCS Line SO137-42 (b) and corresponding ministreamer profile 04 (a). These data record the forearc domain off Sunda Strait, which is characterized by intense deformation of the thick sedimentary strata. A continuous BSR runs along more than 40 km of the forearc environment (b). In Fig. 6.5a, the BSR is not as easily identified, but appears as a clear reflection underneath topographic elevations.

the basin. On RAMA line 4445 (Fig. 6.6) both seafloor and BSR are followed by a bubble, delayed by 0.15 s.

6.5 Discussion and conclusions

All of the BSR locations mapped along the Sunda margin occur in regions which are likely to represent a focussing of fluid flow. Fluid flow is common along folds and anticlinal structures which show updoming, as is the case for the Mentawai anticline or for the folded strata around the BSR along profiles SO138-02 and 02Q. Within sedimentary basins, fluid migration is likely to occur along layers away from the basin axis or depocenter towards the slopes and higher basin margins (Pecher et al., 2001). It is here that BSR occurrence was identified along the RAMA lines off central Java as well as along profile 03 of the Sumatra forearc basin or the northeastward most sedimentary basin on line 04 off Sunda Strait.

The absence of BSRs (with or without free gas below it) in the basin center could have several causes:

- recognition of a BSR is inhibited by the parallel layering of the sedimentary strata
- the amount of organic matter is not large enough to allow microbial formation of gas hydrates within the gas hydrate stability zone
- free gas at the base of the stability zone migrates towards the basin margins

If microbial generation was taking place within the stability zone, then ongoing sedimentation within the basins will cause an upward motion of the base of the stability zone and dissociation of gas hydrates to free gas at its base to cause a BSR reflection, which however cannot be identified in the seismic data. Should gas migrate underneath the hydrate layer, then it would have to form a tight seal at its base for a migration path exceeding tens of kilometers to the edge of the basin. This concept seems to be fairly unlikely though, leaving the first idea. Identification of a BSR within shallow layered strata is of course difficult, however, even within the Java forearc basin, where sediments show more structure and a higher degree of deformation, no BSR could be identified.

All of the above observations suggest that methane is supplied from greater depth, either dissolved in pore water flows or as free gas flows. This is supported by the observation of BSRs in areas prone for conduits for upward migrating methane-laden fluids. Methane for gas hydrate formation then has been caused by thermogenic or biogenic

generation, neither of which can be ruled out without probes on methane composition. As methane migrates upward into the stability zone, in-situ formation of gas hydrates occurs. Migration of fluids is supported by the detection of an active vent site found in the GINCO study area (Beiersdorf et. al., 1999). Authigenic carbonates were recovered from the so-called 'Snail and Mussel Hill' off western Java (location given in Fig. 1.2 in Chpt. 1), where venting and methane expulsion lead to high methane values in the water probes and surrounding sediment. Though no additional active vent sites were found, methane anomalies in the water column along the forearc basins are indicative of additional active venting.

The complete absence of BSRs along the seaward part of the margin, the outer high and the active accretionary prism, is striking and peculiar compared to most other collision zones. Several factors might influence the absence of a BSR here:

- not enough organic matter is present in the accretionary domain to form adequate supplies of methane for gas hydrate generation
- free gas or fluids are escaping to the seafloor along the numerous faults witnessed here, many of which cut deep into the accretionary prism
- due to the 90 Ma old incoming oceanic crust, heat flow is too low for the formation of thermogenic methane.

The intense faulting along the accretionary domain will provide numerous vertical migration paths for methane-laden fluids or gas, interrupting the lateral extent of BSRs. Lateral seismic resolution may be too low (which is especially true for the Ministreamer data and the RAMA reflection lines) to reveal BSRs (and possibly corresponding free gas) in the close vicinity of the faults. The pelagic sedimentary cover ontop of the outer high is unlikely to contain enough organic matter to form gas hydrates.



Figure 6.6: RAMA line 4445 recorded off central Java in 1980 by the Scripps Institution of Oceanography using RV *Thomas Washington*. The line covers the subduction zone from the Java trench to the shelf. Penetration of this 24 channel recording is limited along the accretionary domain and outer high, but good resolution is achieved below the forearc basin. BSR reflections are recognized along the basin margins, but cannot be identified in the center of the basin despite the structural layering of the sediment infill.

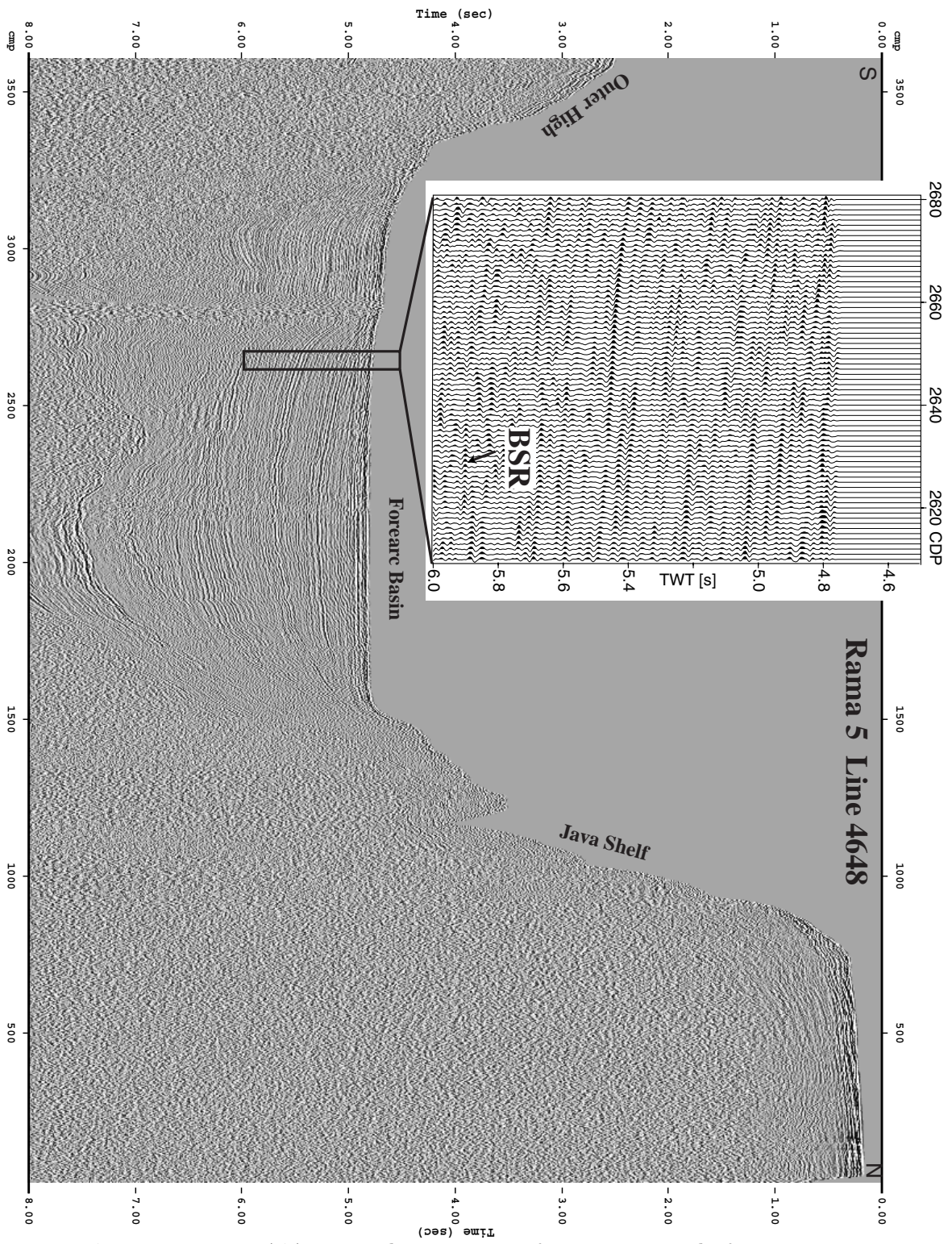


Figure 6.7: RAMA Line 4648 across the central Java forarc basin and shelf. A BSR is recognized in the southern portion of the basin where sedimentary layers are tilted upwards towards a small mound of unknown nature.

- Beiersdorf, H. (edt) and Shipboard Science Party, GINCO3 (SONNE Cruise SO-139): Geo-scientific investigations along the active convergence zone between the Eastern Eurasian and Indo-Australian Plates off Indonesia, *Cruise Report*, BGR, Hannover, 1999.
- Benaron, N., A geophysical study of the forearc region south of Java, Indonesia, Master's Thesis, University of San Diego, 1982.
- Ginsburg, G. D., Gas hydrate accumulation in deep-water marine sediments, in: Gas hydrates: Relevance to world margin stability and climate change, Henriot, J.-P. and J. Mienert (edts), *Geological Society of London Spec. Publication*, 137, 9-30.
- Grevemeyer, I., A. Rosenberger, H. Villinger, Natural gas hydrates on the continental slope off Pakistan: constraints from seismic techniques, *Geophysical Journal International*, 140, 295-310, 2000.
- von Huene, R., and I. A. Pecher, Vertical tectonics and the origins of BSRs along the Peru margin, *Earth and Planetary Science Letters*, 166, 47-55, 1999.
- Hyndman, R. D., and E. E. Davis, A mechanism for the formation of methane hydrate and seafloor bottom-simulating reflectors by vertical fluid expulsion, *Journal of Geophysical Research*, 97, 5, 7025-7041, 1992.
- Kvenvolden, K. A., A primer on the geological occurrence of gas hydrate, in: Gas hydrates: Relevance to world margin stability and climate change, Henriot, J.-P. and J. Mienert (edts), *Geological Society of London Spec. Publication*, 137, 9-30.
- Pecher, I. A., N. Kukowski, C. Huebscher, J. Greinert, J. Bialas, and the GEOPECO Working Group, The link between bottom simulating reflections and methane flux into the gas hydrate stability zone--new evidence from the Lima Basin, Peru margin, *Earth and Planetary Science Letters*, in press, 2001.

7. TRANSTENSIONAL BASINS IN THE SUNDA STRAIT

7.1 Introduction

Sunda Strait, which separates Sumatra from Java, serves as a major boundary between two different geodynamic regimes. The trench itself is curved landward south-west of Sunda Strait, so that the strait appears to be a transition zone between the two different regions (Fig. 7.1). Sunda Strait represents a tectonic as well as a physiographic break in the arc. It is 25 km wide in the east and approximately 100 km wide in the west with the active Anak Krakatau volcano in its center (Fig. 7.1).

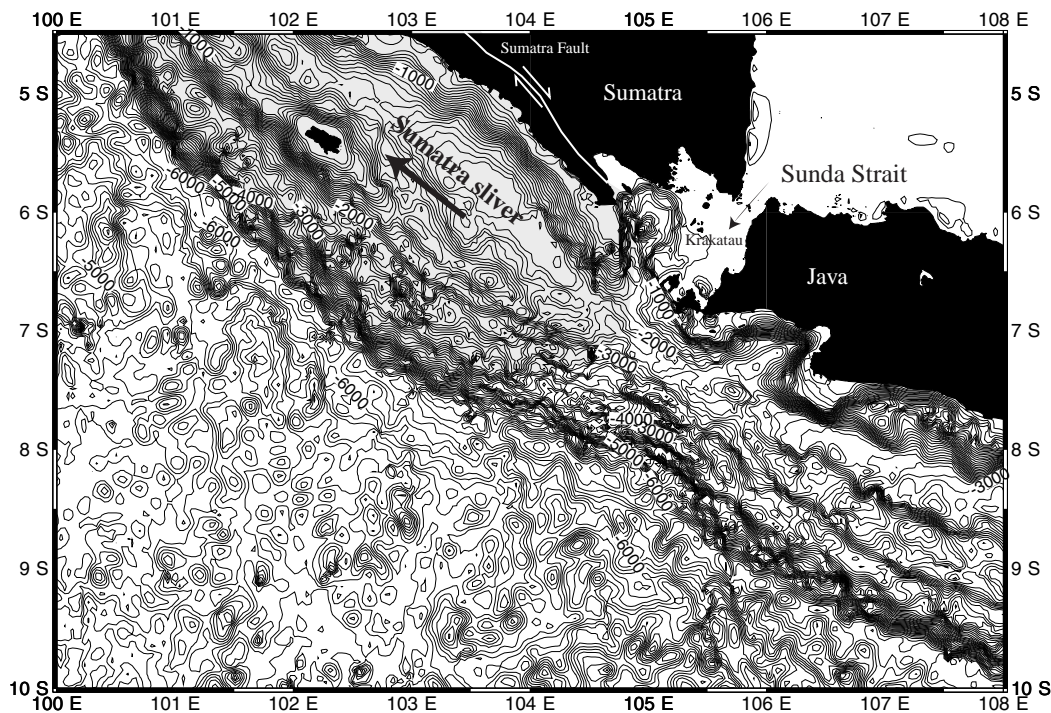


Figure 7.1: Bathymetry of Sunda Strait and the adjacent margin. The trench and forearc region display a concave shape southwest of Sunda Strait and act as a trailing edge for the northwestward moving Sumatra sliver, whose proposed outlines are underlain in grey.

Sunda Strait is thus one of the most active regions in Indonesia in terms of volcanism, seismicity, and vertical motion. A concentration of shallow earthquakes in the Sunda Strait region is further evidence for a tectonic break in this region (Fig. 7.2).

Seismicity in Sunda Strait is not correlated to the bathymetry, but does correlate with the Krakatau volcanic belt (Fig. 7.2). Underneath Krakatau volcano, a cluster of shallow earthquakes exists. It has been proposed that these events are of tectonic rather than volcanic (tremors) origin. Earthquakes associated with a volcanic origin such as magma movements normally have low frequencies as compared to tectonic ones. Also, there is common evidence that volcanic earthquakes are not generated by a double couple as are tectonic ones. The Krakatau events show both high frequencies and up and down first motions. Their vertical distribution and focal mechanisms show that these events correspond to displacement along faults controlled by the deep geometry of the calderas (Hajorno et al., 1991).

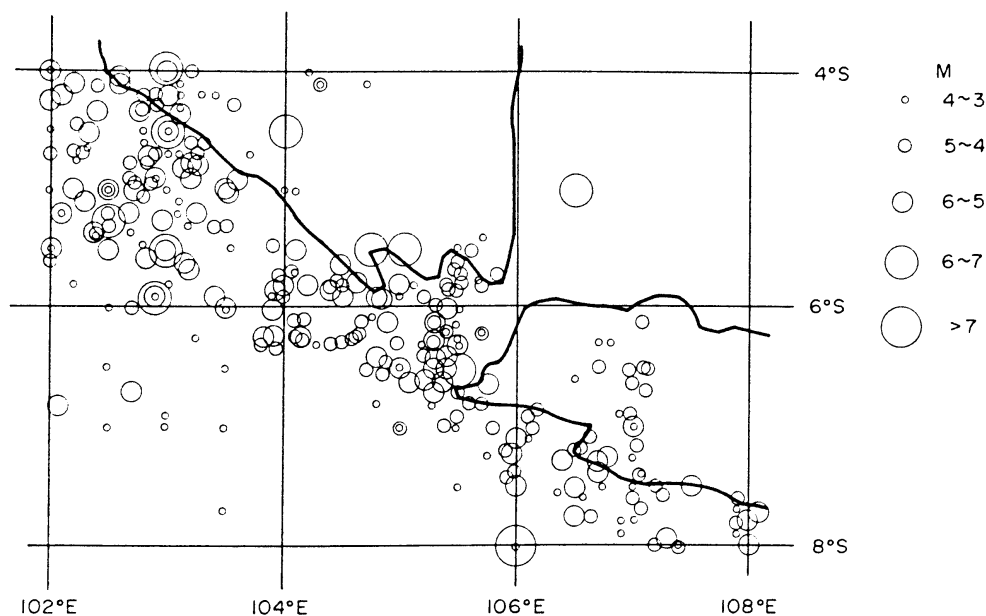


Figure 7.2: Shallow earthquakes ($h < 100$ km) in the Sunda Strait vicinity. Located by the International Seismological Center from 1961-1981. Three clusters of earthquakes are recognized: south of Sumatra, along the eastern flank of the Sunda Strait graben structure and underneath Krakatau volcano.

A second seismicity cluster within the Sunda Strait coincides with the eastern flank of the N-S trending graben found at the western entrance to the strait (Fig. 7.1). It is connected to the Krakatau cluster by a fault striking N50°E-N60°E. Results from focal mechanism

investigations (Hajorno et al., 1991) support the notion that Sunda Strait is under an extensional tectonic regime, the direction of extension being parallel to the Sumatra fault.

A third cluster composed of small magnitude earthquakes has been recorded south of Sumatra. Their centroid moment tensor solutions mostly represent strike-slip faulting with an extensional component (Hajorno et al., 1991). The extension direction is roughly parallel to the Sumatra fault. It has been proposed that the direction of faulting is the one that gives rise to a right lateral fault, in accordance with the dextral movement of the Sumatra Fault. Such a fault, the Batee fault (Fig. 7.3), has been described for northern Sumatra, connecting the Mentawai and Sumatra faults. These faults, transverse to the forearc basin, probably delineate blocks that rotate along the Sumatra fault. The seismic lines presented in Chapter 3 are located south of this earthquake cluster and also transverse to the forearc basin. Thus no evidence for strike-slip faulting across strike of the basin could be found in the GINCO data.

Major tectonic trends, mainly the pronounced forearc basins off Sumatra and off Java and the large faults of Sumatra, are disrupted across the strait. This setting implies that the Sunda Strait region is a key to the understanding of the geodynamic processes involved. It has been proposed that the formation of Sunda Strait results from extension due to the north-westward motion of the Sumatra sliver plate along the Sumatra Fault (as depicted in Figure 7.1), away from the north-east Sumatra and west Java block. However, so far only scarce seismic data exists from Sunda Strait. As part of the GINCO project, a wide-angle line and corresponding ministreamer recordings were acquired within Sunda Strait (Fig. 1.2). These data are complemented by the bathymetry survey. The following chapter discusses a transtensional model for the evolution of Sunda Strait, based on extensional features recognized in the data. Perpendicular trending graben structures, showing normal faulting along their flanks, compose these subsidiary structures, which sustain our evolutionary model.

7.2 Geodynamic Setting

The central Sunda Arc is characterized by a change in orientation of the trench resulting in regimes of normal subduction off Java to oblique subduction off Sumatra (Fig. 7.3). The increasing obliquity gives rise to the Mentawai transpressional fault and the Sumatra strike-slip fault, allowing partitioning of the relative plate motion into a compressional component and a lateral NW displacement of a forearc sliver (McCaffrey, 1991; Prawirodirdjo, 1997). The Sunda Strait is located at the juncture between these two subduction regimes where the increase in obliquity leads to the initiation of partitioning (McCaffrey, 1998) (Fig. 7.3). Huchon and Le Pichon (1984) first proposed that the evolution of the Sunda Strait results from the extension of the forearc sliver as it is entrained northwestward, producing a basin at the southeastern termination of the Sumatra Fault.

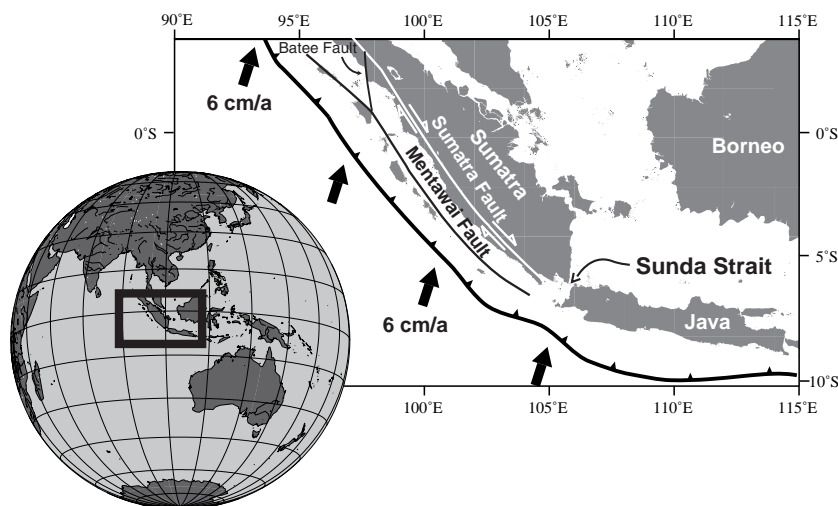


Figure 7.3: Location map displaying the major tectonic features. Plate motion vectors are from the Australia-Eurasia rotation pole.

In this chapter we present new geophysical data collected within the scope of the project GINCO (Geo-scientific

INvestigations along the active CONvergence zone between the eastern Eurasian and Indo-Australian Plates off Indonesia) to constrain the crustal structure of the western and southwestern Sunda Strait which has long been enigmatic (Lassal, 1989; Diament, 1990; Malod, 1995).

7.3 Morphology of the Sunda Strait graben from high resolution bathymetry

High resolution bathymetry data collected in the Sunda Strait reveal two sub-basins separated by a basement ridge, a shallower domain to the east and a deeper graben to the west (Fig. 7.4). These are connected by secondary transverse grabens cutting the basement ridge into discrete blocks. These morphologic highs exhibit positive free-air gravity anomalies of up to 80 mGal (Reichert, 1999), suggesting they are composed of denser arc basement. The deeper western graben trends N-S along 104.8°E and exhibits an average water depth of 1800 m in the central part. It is bounded to the west by a steep flank, which becomes more subdued at 6.5°S and disappears to the south. The eastern flank is more disturbed and cut by several canyons (Fig. 7.4). Both flanks of the graben are tectonically active and display extensional patterns which are also evident in the seismic data.

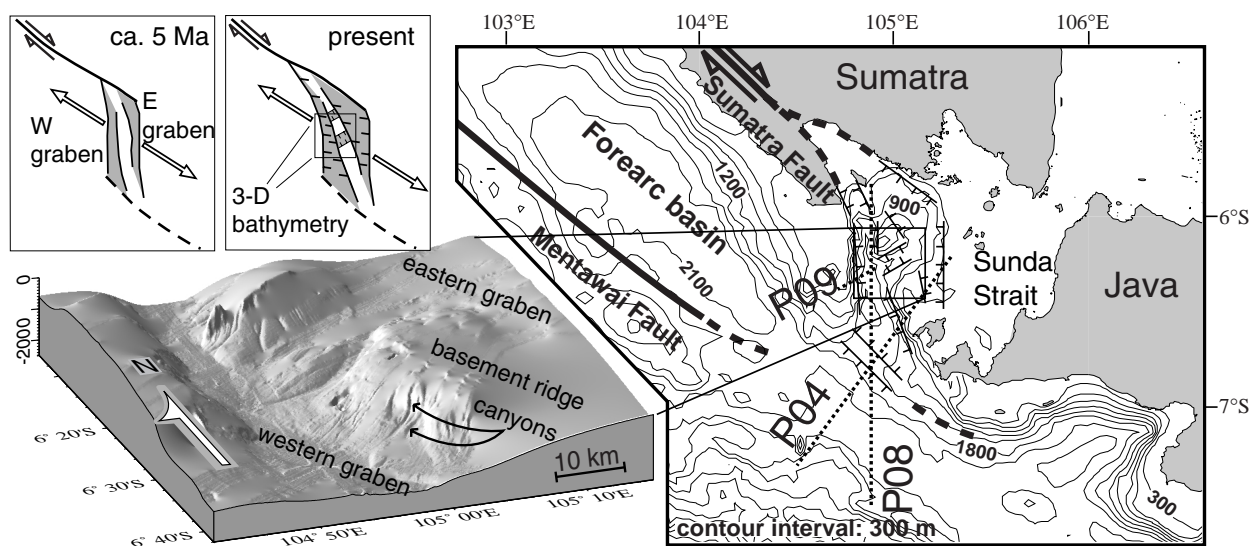


Figure 7.4: Geodynamic setting of the Sunda Strait showing profile locations and major faults. The 3D high resolution bathymetric image displays graben structures and basement blocks in the western Sunda Strait. The N-S trending deep western graben lies at the southern termination of the Sumatra Fault along 104.8°E . The upper inlay displays the evolution of the large scale basin with two sub-basins.

7.4 Stratigraphy of the upper sediment layers

Reflection seismic data were acquired along profiles SO138-04, SO138-08, and SO138-09 using a three-channel streamer (Fig. 7.5). The stratigraphy of the upper sediment layers within the graben has been correlated to well data and stratigraphic interpretations off Sumatra (Beaudry, 1985; Lassal, 1989; Izart, 1994). Six sedimentary sequences can be recognized: the uppermost Pliocene to Pleistocene sediments (Layer A and B) are of pelagic nature, underlain by Miocene sediments (C: Upper Miocene, D: Middle Miocene, E: Lower Miocene). Sequence F has been interpreted as Eocene-Oligocene forarc-basin sediments (Lassal, 1989). The SW-NE striking profile SO138-04 crosses the southern part of the western graben (Fig. 7.5). The basement ridge between SP 350 and SP 300 shows no sedimentary cover. Thick sedimentary infill is again present to the NE between SP 250 and SP 1 in the eastern graben. A number of normal faults dipping roughly 60° can be traced on the flank. The 25 km long profile SO138-09 (Fig. 7.5) crosses the western graben further north at 6.3°S . The steep western flank shows no Pleistocene sedimentary cover and is cut by normal faults dipping 60° .

7.5 OBH Profile SO138-08

Along the 180 km long N-S trending refraction line 16 ocean bottom hydrophone (OBH) and ocean bottom seismometer (OBS) stations were deployed. The data were forward modelled using a ray-tracing technique (Fig. 7.5). The corresponding reflection profile was used to constrain the sedimentary layers. The Pliocene to Lower Miocene sequences display seismic velocities of 1.6-1.9 km/s. This layer is underlain by Oligocene and Eocene volcanoclastic deposits with velocities ranging from 2.2-2.6 km/s. These rocks were also sampled in the Sunda Strait (Mulhadiono, 1987). Pre-Eocene sediments (3.5-3.8 km/s) overlay basement rocks with velocities ranging from 4.5-5.8 km/s. The basement in the southern part of the graben lies at a depth of about 6 km and reaches 7 km depth in the central part. The northern part of the profile shows strong topographic variations which correspond to the morphological units which compose the eastern flank of the graben. These basement highs display velocities greater than 4.3 km/s without any significant sedimentary cover and likely represent faulted blocks of arc basement as is evident from the velocity structure and correlation to the aforementioned strong positive free-air gravity

anomalies. Lower crustal velocities range from 5.8 to 7.2 km/s. A mantle transition was recorded by stations 90, 91, and 92 over a short distance from profile km 35 to 65, indicating a Moho depth of 28 km.

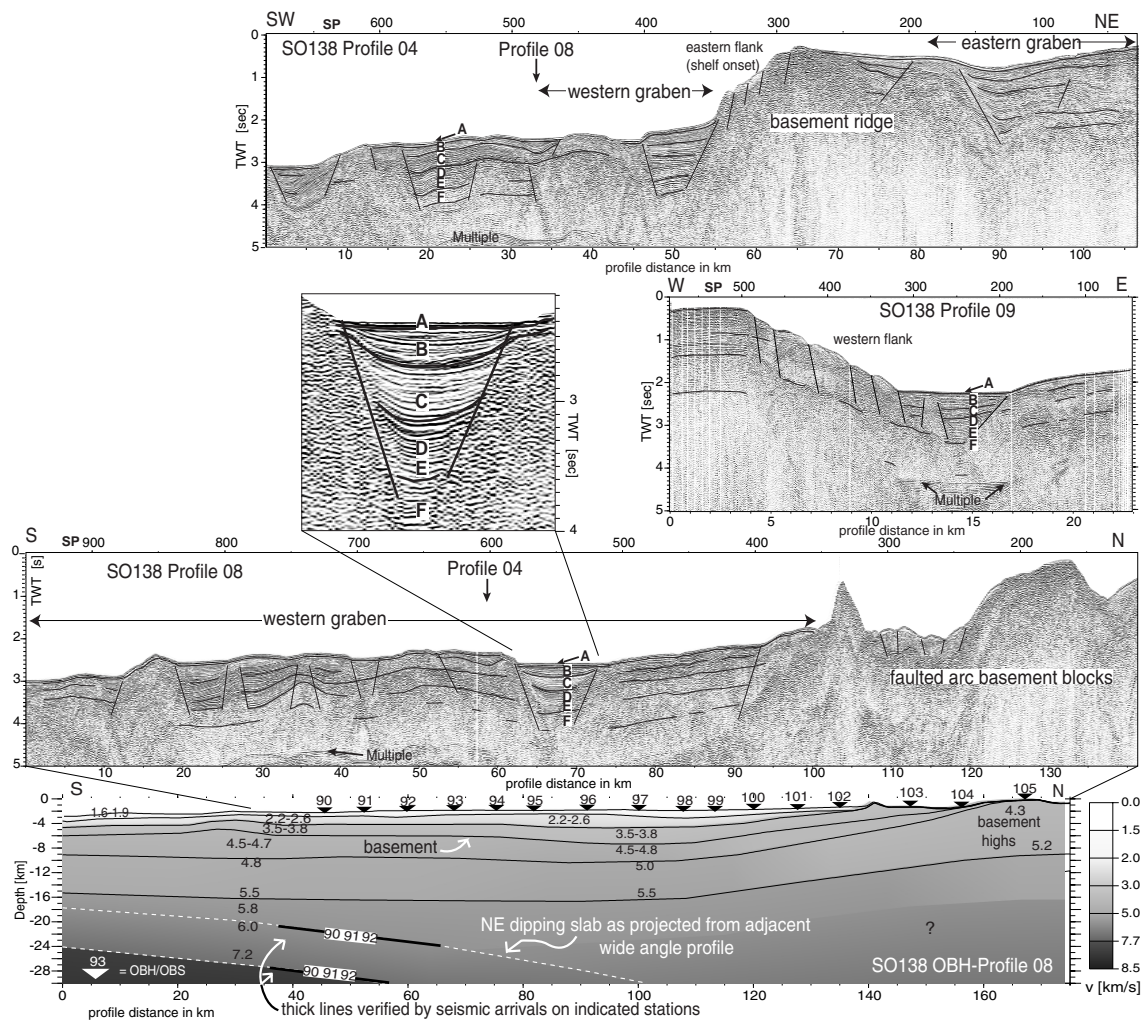


Figure 7.5: Seismic profiles acquired in the Sunda Strait and adjacent areas. 6 sedimentary layers have been identified (blowup) and correlated to earlier stratigraphic interpretations: A and B: Pliocene to Pleistocene; C, D, E: Upper, Middle, Lower Miocene, F: Eocene-Oligocene forearc-basin sediments. Active normal faults on both flanks of the graben are visible on profiles SO138-04 and 09. Faulted arc basement blocks dominate the morphology on the northern third of profile SO138-08. OBH-profile SO138-08 has been forward modelled using the reflection data to constrain the upper sedimentary layers. The basement lies at a depth of 6-7 km. Mantle phases recorded by stations 90-92 are attributed to the downgoing slab, also imaged on an adjacent OBH-profile.

7.6 Discussion and Conclusions

Our data support a transtensional model for the evolution of the Sunda Strait (Huchon and Le Pichon, 1984; Lassal, 1989; Pramumijoyo, 1991; Malod, 1995). Extension caused by the NW motion of the Sumatran plate sliver is focussed in two triangular sub-basins (Fig. 7.4 inset) within a large scale rhomboid region at the southern termination of the Sumatra Fault (Fig. 7.4). Dextral strike-slip motion along the Sumatra Fault has been quantified by GPS studies (Prawirodirdjo, 1997) and geological and geomorphological data (Bellier, 1995). The normal-faulting regime within the Sunda Strait is constrained by earthquake focal mechanisms (Harjono, 1991) as well as by the observation of active normal faults reported here. At the onset of extension, the individual basement blocks identified in the bathymetry (Fig. 7.4 inset) probably comprised a continuous N-S trending ridge which was subsequently stretched and sheared and thus broke into several distinct blocks. While crustal thinning is difficult to quantify without good constraints on Moho depth, the large sedimentary thicknesses (>6 km based on our wide-angle data) support the interpretation of substantial thinning ($\beta > 2$) (Lassal, 1989). Several mantle phases were recorded at the southern end of the refraction profile and are attributed to the downgoing slab. The top of the subducted plate lies at 21 km depth and the Moho at 28 km, which corresponds well to results from the SW-NE trending refraction line SO138-04 (Lelgemann, 1999), covering the forearc domain and the southern part of the Sunda Strait transtensional basin. This interpretation is also supported by free-air gravity values of less than -140 mGal (Reichert, 1999) revealing the strong influence of the downgoing slab.

Beaudry, D., and G. Moore, Seismic Stratigraphy and Cenozoic Evolution of West Sumatra Forearc Basin, *AAPG Bulletin*, 69, 742-759, 1985.

Bellier, O., and M. Sébrier, Is the slip rate variation on the Great Sumatran Fault accomodated by fore-arc stretching?, *Geophysical Research Letters*, 22, 15, 1969-1972, 1995.

DeMets, C., R. G. Gordon, D. F. Argus, S. Stein, Current plate motions, *Geophysical Journal International*, 101, 425-478, 1990.

Diament, M., C. Deplus, H. Harjono, M. Larue, O. Lassal, J. Dubois, V. Renard, Extension in the Sunda Strait (Indonesia): a review of the Krakatau programme, *Oceanologica Acta Special Volume*, 10, 31-42, 1990.

- Flueh, E.R. (edt) and Shipboard Science Party, GINCO2 (SONNE Cruise SO-138): Geo-scientific investigations along the active convergence zone between the Eastern Eurasian and Indo-Australian Plates off Indonesia, *Cruise Report*, Geomar, Kiel, 1999.
- Harjono, H., Seismicity of the Sunda Strait: Evidence for crustal extension and volcanological implications, *Tectonics*, 10, 17-30, 1991.
- Huchon, P., and X. Le Pichon, Sunda Strait and Central Sumatra fault, *Geology*, 12, 668-672, 1984.
- Izart, A. B. Mustafa Kemal, J. A. Malod, Seismic stratigraphy and subsidence evolution of the northwest Sumatra fore-arc basin, *Marine Geology*, 122, 109-124, 1994.
- Lassal, O., P. Huchon, H. Harjono, Extension crustale dans le detroit de la Sonde (Indonesie). Données de la sismique reflexion (campagne KRAKATAU), *C. R. Acad. Sci. Paris*, 309, 205-212, 1989.
- Lelgemann, H., E.R. Flueh, J. Bialas, B. Schreckenberger, GINCO: Structure and geodynamics of the Sunda Arc at the transition from frontal to oblique subduction, Proceedings of the SE Asia Meeting: *Memoires Geosciences-Montpellier*, 14, 115-119, 1999.
- Malod, J. A., K. Karta, M.O. Beslier, M.T. Zen Jr., From normal to oblique subduction: Tectonic relationships between Java and Sumatra, *Journal of Southeast Asian Earth Sciences*, 12, 85-93, 1995.
- McCaffrey, R., Slip vectors and stretching of the Sumatran fore arc, *Geology*, 19, 881-884, 1991.
- McCaffrey, R. and J. Nabelek, Role of oblique convergence in the active deformation of the Himalayas and southern Tibet plateau, *Geology*, 26, 8, 691-694, 1998.
- Mulhadiono, and S. Asikin, 'Pull apart' basin offshore Bangkulu promises attractive exploration ventures, *GEOSEA Conference*, Djakarta, 26-51, 1987.
- Nishimura, S., and H. Harjono, The Krakatau Islands: The Geotectonic Setting, *GeoJournal*, 28.2, 87-98, 1992.
- Pramumijoyo, S., and M. Sébrier, Neogene and Quaternary fault kinematics around the Sunda Strait area, Indonesia, *Journal of Southeast Asian Earth Sciences*, 6, 2, 137-145, 1991.
- Prawirodirdjo, L., Y. Bock, R. McCaffrey, J. Genrich, E. Calais, C. Stevens, S.S.O. Puntodewo, C. Surbarya, J. Rais, P. Zwick, Fauzi, Geodetic observations of interseismic strain segmentation at the Sumatra subduction zone, *Geophysical Research Letters*, 24, 21, 2601-2604, 1997.
- Reichert, C. (edt) and Shipboard Science Party, GINCO1 (SONNE Cruise SO-137): Geo-scientific investigations along the active convergence zone between the Eastern Eurasian and Indo-Australian Plates off Indonesia, *Cruise Report*, BGR, Hannover, 1999.

8. DISCUSSION AND CONCLUSIONS

The Sunda Arc subduction zone has been the target for a number of geophysical and geological research studies in the past decades. Investigations of the central portion of the margin, from southern Sumatra to western Java, have however suffered from the lack of high quality data. The geophysical profiles acquired across the subduction zone and adjacent areas which are discussed here for the first time allow to present a detailed image of the margin.

The results presented in this work have been developed from the application of different geophysical methods to a variety of datasets, as only such an integrative approach employing different types of data allows to draw affirmative conclusions. Whereas migrated reflection seismic data yield a clear image of the subsurface, velocity information covering the lithosphere must be gained from wide-angle observations. Additional geophysical parameters, such as gravity or bathymetry, must in addition sustain the seismic models to arrive at ascertained results.

A combined interpretation of these complementary data sets concurrent with the seismic data contributes the following new insights to the Sunda margin tectonics:

- 1) A detailed velocity-depth model developed from travelttime information of the wide-angle data and from geological horizons identified in the multichannel data is for the first time established for the central Sunda margin and allows to draw the following conclusions:
 - active accretion occurs along the margin inbetween the deformation front and an active backstop structure
 - seismic velocities of the outer high are indicative of a sedimentary composition, probably originating from ancient accreted material
 - continental-type crust is found underneath the Sumatra forearc basin, whereas oceanic-type crust is underlying the Java forearc
 - the configuration of the descending slab is established to a maximum depth of 40 km along the margin.

- 2) the distribution of bottom simulating reflectors (BSRs) is peculiar for accretionary subduction zones, as it is solely restricted to the forearc domain and no BSRs could be identified along the accretionary prism or outer high. A linkage of BSR occurrence to elevated fluid flow is proposed.
- 3) an evolutionary model developed for the Sunda Strait is sustained by seismic and high resolution bathymetry data, tying it to the obliquely convergent setting of the northern Sunda Arc.

These results are indispensable for a better comprehension of the subduction processes as they reveal that the characteristic forearc structures of a convergent plate boundary are present in both collisional domains (frontal and oblique) along this margin. An accretionary wedge and well developed morphological outer high adjacent to a forearc basin are present off southern Sumatra as well as off western Java. Their existence is fundamentally linked to forearc buttress mechanics, as these structures inevitably form from contraction in the presence of a core buttress (von Huene and Scholl, 1991). For the data set presented here, structural effects from the change in orientation of the trench, resulting in an increasing subduction obliquity, cannot be discerned nor separated from the influence of other geological or geophysical parameters changing along strike of the margin (e. g. plate age, composition of the forearc basin basement, fluctuations in trench sediment supply). These parameters cause the variations in forearc structure along the margin, while the main structural features forming as a consequence of buttress tectonics are present all along the convergence zone.

Figure 8.1 displays a comparison of the velocity-depth models for the dip lines, showing the effects of the mechanical role of a core buttress. The term buttress or backstop defines a region within a forearc that is characterized by an increased strength compared to the region lying trenchward of it. It is not linked to a specific composition, as a buttress may consist of arc basement, compacted, well-lithified sediment or features like an allochthonous terrane, all of which represent relatively strong geological material. The definition of a buttress is rather its ability to support larger deviatoric stresses than the

forearc material above or seaward of it due to contrasts in mechanical properties (Byrne et al., 1993).

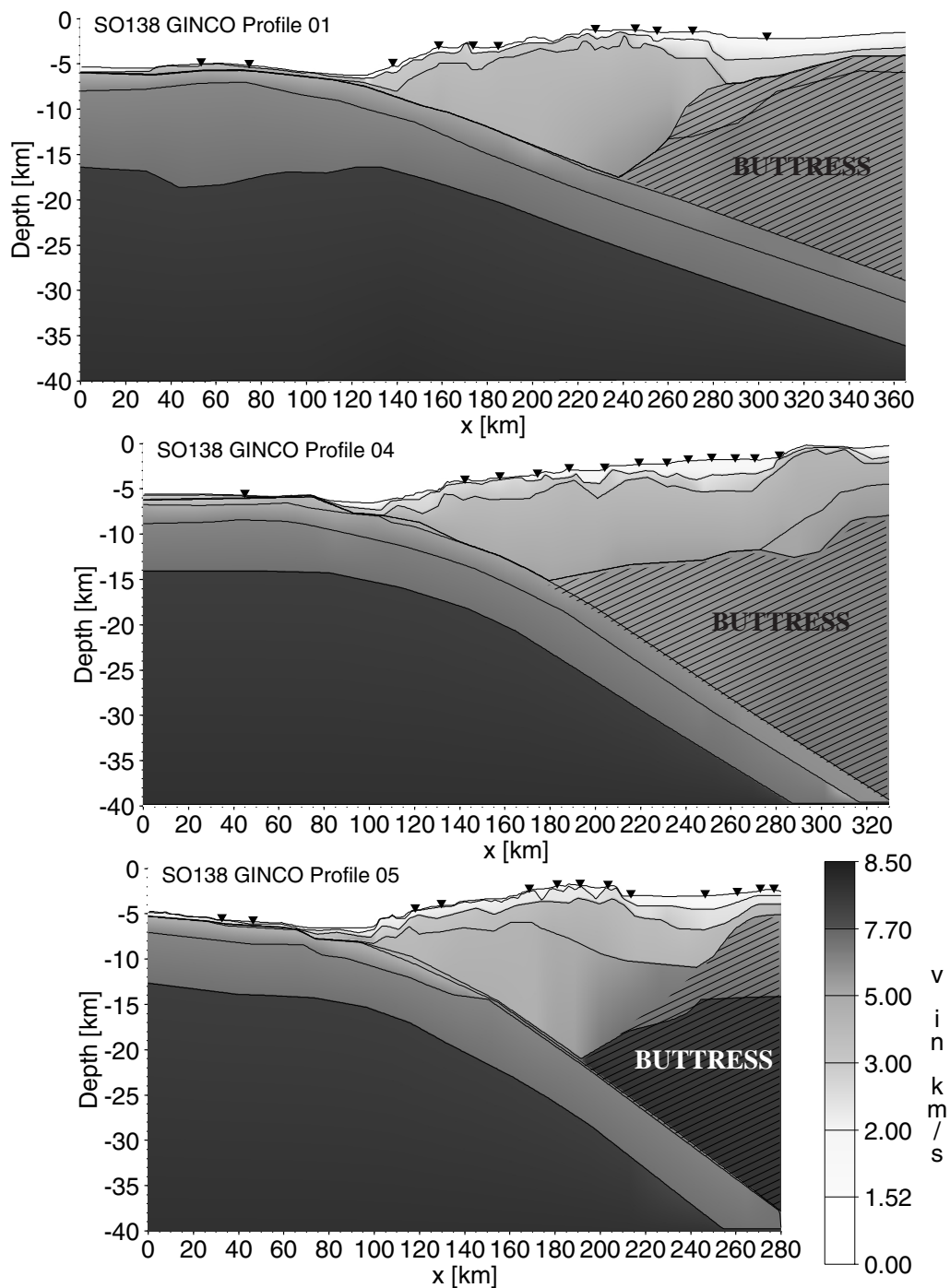


Figure 8.1: Velocity-depth models for the three dip lines presented in this work, scaled to the deformation front. A core buttress is present on all profiles, influencing the development of structural features of the forearc. The main structures (accretionary wedge, outer high, and forearc basin) are present in domains of frontal and of oblique subduction. The crest of the outer high is located above the toe of the core buttress, as predicted from numerical and sandbox modeling.

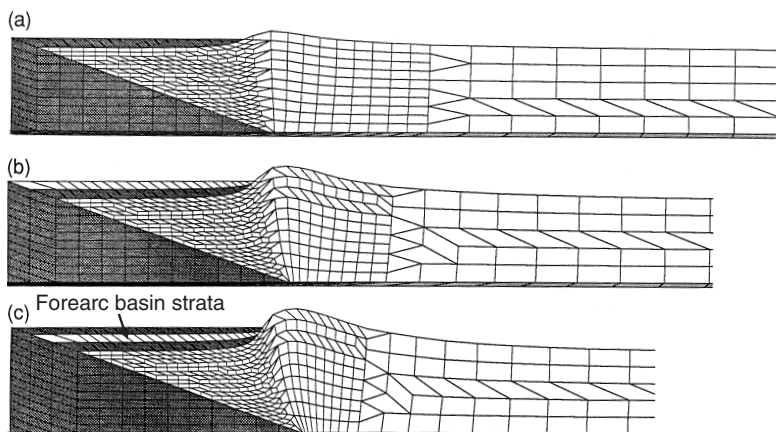
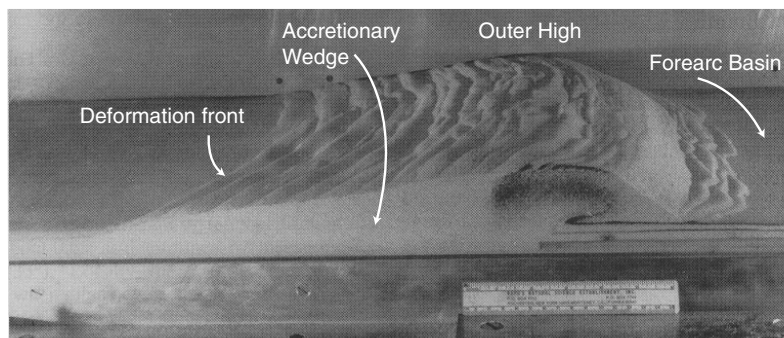
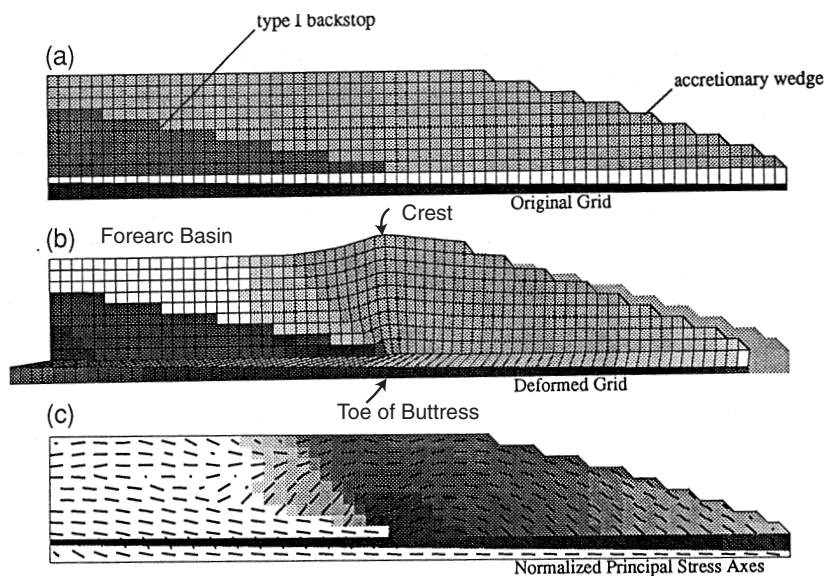


Figure 8.2: a) Numerical modeling of forearc structures. The modeled buttress or backstop dips trench-ward. A structural high will form with its crest above the toe of the buttress, with the area behind it remaining relatively undeformed (after Byrne et al., 1993)

b) Photograph of sandbox modeling using a horizontal buttress. Again, the outer high develops above the toe of the buttress, with a large accretionary wedge seaward and an undisturbed forearc basin arcward (after Wang and Davis, 1996).

c) Development of forearc-basin stratigraphy (after Byrne et al., 1993). Note the uplift and deformation occurring at the right end of the forearc basin with older layers pinching out against the rising outer high.

Numerical and sandbox modeling (e. g. Malavieille et al., 1993; Byrne et al., 1993; Buck and Sokoutis, 1994; Kukowski et al., 1994; Wang and Davis, 1996) has shown that the buttress geometry will influence the development of the associated structural features (Fig. 8.2). The geometry proposed for the central Sunda margin (Fig. 8.1) puts the seaward toe of the buttress near the downgoing plate, such that little or no sediment is thrust beneath the buttress (trenchward-dipping type I geometry of Byrne et al., 1993). The structural effects resulting from this geometry are most pronounced and explain the growth of the outer high as well as the paradoxical seemingly presence of the undeformed forearc basin in close proximity to the highly deformed accretionary wedge (Fig. 8.3), as recognized on the GINCO and RAMA data..

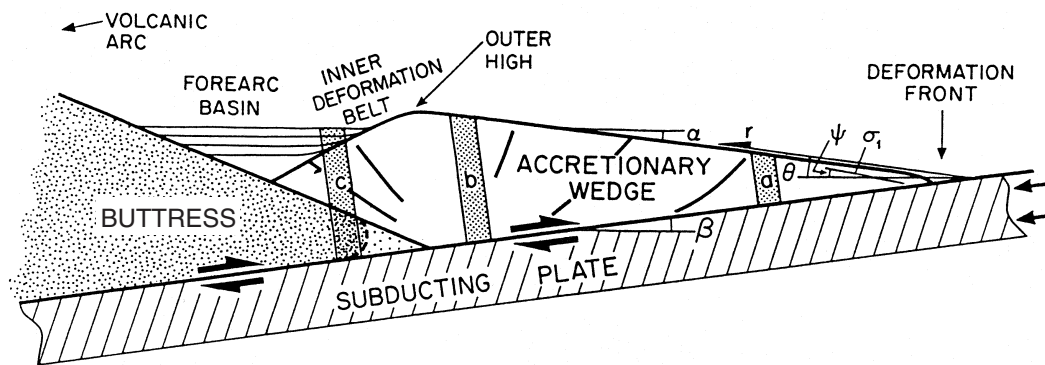


Figure 8.3: Schematic cross section of the forearc region of a typical subduction zone displaying major structural features. In the presence of a buttress, an accretionary wedge, outer high and forearc basin will form as the oceanic plate is subducted (after Byrne et al., 1993).

The deforming wedge will have a stress field consistent with predominantly arcward thrust dips, as established for the MCS data presented in this study. This preferred dip will generally not extend past the active backstop., This explains the area of intense faulting across the active accretionary domain, which is observed on Lines SO137-12, 42, and 03. The outer high then experiences less arcward-dipping faulting. The development of the outer high results from the gradual increase in both strength and bulk density within the accretionary wedge as the material is compacted with depth and distance from the deformation front (Byrne et al., 1993). When this gradual increase in rock strength is replaced by a sharp transition at the buttress, which can support larger loads, the increased net horizontal load is accommodated without further build-up of topography. As a result,

the outer high develops above the seaward end of the buttress, which casts a stress shadow over the area above itself. The buttress thus serves to insulate this area from stress, allowing the presence of a forearc basin which will experience no or little deformation as sediments are deposited within it (Malavieille, 1984; Byrne, 1993). The buttress then supports most of the regional horizontal compressive plate boundary stresses. The models presented in Figure 8.1 show an almost perfect alignment of the crest of the outer high to the toe of the core buttress. This correlation has been predicted from numerical and sandbox modeling as seen in Figure 8.2. As the outer high is uplifted, the seaward part of the forearc basin experiences some uplift and deformation, resulting in landward tilting and pinching out of the older strata near the outer high as seen on line SO137-03.

Modeling by Byrne et al., (1993) suggests that an outer high best develops above a buttress whose contact with the accretionary wedge dips trenchward, as is the case in the data presented here. The growth of an outer high is diminished if the toe of the buttress occurs at shallower depths within the forearc. The influence of an alternate buttress geometry in the transition zone off Sunda Strait on the structural features seen on the Sunda transect (line SO137-42/SO138-04) cannot be resolved completely, as a detailed picture of an underlying buttress may not be determined from the surface information alone. However, the overall structure of this lines would also allow the presence of a buttress of an intermediate geometry (Fig. 8.4), as for example found along the Peru margin (von Huene et al., 1988) or the Alaska margin (Gutscher, 1996).

The presence of a backstop structure as identified at the trench slope break on all reflection dip lines presented in this work indicates the existence of an additional, weaker buttress trenchward of the core buttress. Lithification and compaction of the relatively old sediment above the toe of the core buttress cause it to become stronger than the trenchward sediments. Thus a backstop seaward of the core buttress is produced and rock strength increases successively toward the core buttress. A similar situation has been proposed for the Barbados wedge (Bangs et al., 1990; Byrne et al., 1993; Davis, 1996). Even though several backstops or buttresses may exist simultaneously within a single margin, similar structural features resulting from buttress mechanics are to be expected, even in the presence of a complex or multiple buttress (Byrne et al., 1993).

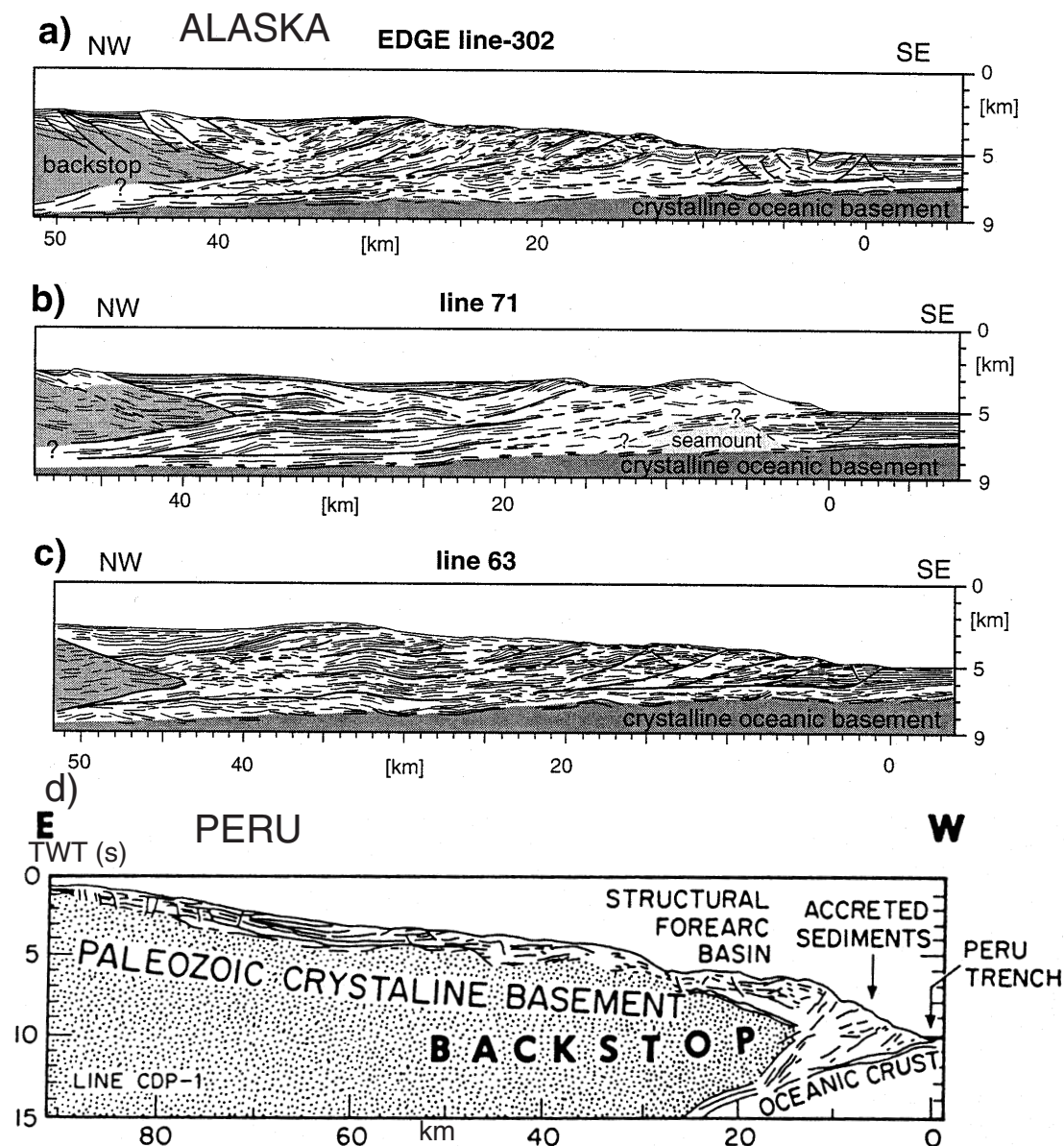


Figure 8.4: Interpretations of reflection lines acquired across the Alaska and Peru margins. The presence of an intermediate buttress, with weaker material accumulating on top and below it, has been inferred for both accretionary zones (after Gutscher, 1996, and von Huene et al., 1988).

A trenchward dipping buttress geometry, as witnessed along the central Sunda margin, has also been proposed for other active plate boundaries, including the Lesser Antilles (e. g. Torrini and Speed, 1989; Westbrook, 1975; Westbrook et al., 1988), the Mediterranean Hellenic arc (e. g. Le Pichon et al., 1982), the Sulawesi margin (Silver et al., 1985) and the Luzon forearc (Lewis and Hayes, 1985). The distinct forearc structure of the Sunda margin however yields by far the best type-example of accretionary mechanics. Sediment input to

the forearc basin is not high enough to cause the basin sediments to diminish the topographic expression of the outer high, as is the case for the Barbados ridge complex (Fig. 8.5), where the forearc basin carries about 10 km of sediment fill (Torrini and Speed, 1989).

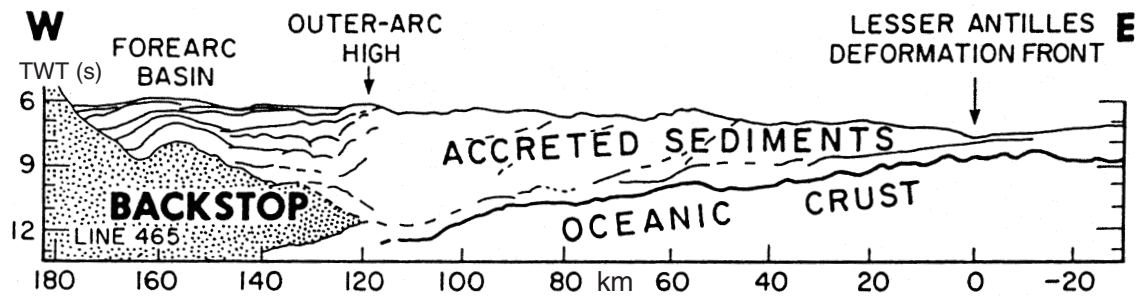


Figure 8.5: Cross section of the Lesser Antilles forearc. A trenchward dipping buttress is present underneath the forearc basin and outer high. The large sediment fill of the basin diminishes the structural elevation of the outer high, however, all main structural units associated with the presence of a backstop are visible (after Westbrook et al., 1988).

A number of other margins probably do not contain a trenchward dipping buttress, as their topographic expressions differ. If the buttress toe is located well above the subducted oceanic plate, weak material may be underplated beneath it (type II buttress of Byrne et al., 1993) and the surface features discussed above are less developed. This geometry has been proposed for the Cascadia margin adjacent to southern Vancouver Island (Davis and Hyndman, 1989). An intermediate geometry, where weaker material is present above and below the toe of the buttress has been described for Peru (von Huene et al., 1988) and Alaska (Gutscher, 1996). This intermediate geometry, which is impossible to discern from a trenchward-dipping buttress from the surface features, might to a certain degree be present along the Sunda Strait transect as discussed above. It remains unclear how the transition from frontal to oblique subduction influences the core buttress geometry.

Outlook:

The investigations presented here demonstrate the need for additional data in the area. A closer profile spacing off Sunda Strait would allow a regional imaging of the buttress geometry and its connection to the transition processes leading from frontal to oblique subduction. An expansion of the study area to central Java, as attempted by incorporating the RAMA profiles, would allow to certify the extent of oceanic-type crust composing the leading edge of the upper plate, as identified off western Java. An extension of the reflection profile grid to central Java and central Sumatra would unravel variations in the accretionary style caused by the increasing obliquity.

Additional bathymetry coverage of the margin would enable an identification of the extent of the numerous fault zones, e.g. the Mentawai FZ or the Ujung Kulon FZ, which are essential for the understanding of the geodynamic processes involved. The nature of both faults zones is yet unresolved, though the difference in the topography level documented on the 2-D seismic images is indicative of strike-slip movement.

The evolutionary model for Sunda Strait is well supported by the seismic and bathymetry data presented here. However, knowledge of the Moho depth is necessary for a quantification of crustal stretching occurring here, which thus remains open for further investigations.

Bangs, N. L. B., G. K. Westbrook, J. W. Ladd, and P. Buhl, Seismic velocities from the Barbados Ridge: Indicators of high pore fluid pressures in an accretionary complex, *Journal of Geophysical Research*, 95, 8767-8782, 1990.

Buck, W. R., and D. Sokoutis, Analogous model of gravitational collapse and surface extension during continental convergence, *Nature*, 369, 737-740, 1994.

Byrne, D. E., W.-H. Wang, and D. M. Davis, Mechanical role of backstops in the growth of forearcs, *Tectonics*, 12, 1, 123-144, 1993.

Davis, D. M., Accretionary mechanics with properties that vary in space and time, in: Subduction top to bottom, *Geophysical Monograph* 96, 39-48, 1996.

Davis, E. E., and R. Hyndman, Accretion and recent deformation of sediments along the northern Cascadia subduction zone, *Geological Society of America Bulletin*, 101, 1465-1480, 1989.

- Gutscher, M.-A., Growth, erosion and material transfer in accretionary wedges: a quantitative analysis based on analog modeling and the implications for the evolution of convergent margins, PhD Thesis, University Kiel, Germany, 1996.
- Kukowski, N., R. von Huene, J. Malavieille, and S. E. Lallemand, Sediment accretion against a buttress beneath the Peruvian continental margin as simulated with sandbox modeling, *Geologische Rundschau*, 83, 822-831, 1994.
- Le Pichon, X., N. Lyb ris, J. Angelier, and V. Renard, Strain distribution over the east Mediterranean ridge: A synthesis incorporation new sea-beam data, *Tectonophysics*, 86, 243-274, 1982.
- Lewis, S. D., and D. E. Hayes, Forearc basin development along western Luzon, Philippines, *Energy*, 10, 281-296, 1985.
- Malavieille, J., Modelization exp rimentale des chevauchements imbriqu s: Application aux chaines de montagnes, *Bull. Soc. Geol. Fr.*, 7, 129-138, 1984.
- Malavieille, J., C. Larroque, and S. Calassou, Mod lization exp rimentale des relation tectonique/sedimentation entre bassin avant-arc et prisme d'accretion, *Comptes Rendues d'Academie des Sciences, S rie II*, 316, 1131-1137, 1993.
- Silver, E. A., M. J. Ellis, N. A. Breen, and T. H. Shipley, Comments on the growth of accretionary wedges, *Geology*, 13, 6-9, 1985.
- Torrini, R., and R. C. Speed, Tectonic wedging in the forearc-basin accretionary prism transition, Lesser Antilles forearc, *Journal of Geophysical Research*, 94, 10549-10584, 1989.
- von Huene, R., E. Suess, and Leg 112 Shipboard Scientists, Ocean drilling program Leg 112, Peru continental margin: Part I, tectonic history, *Geology*, 16, 934-938, 1988.
- von Huene, R. and D. W. Scholl, Observations at convergent margins concerning sediment subduction, subduction erosion and the growth of continental crust, *Reviews of Geophysics*, 29, 279-316, 1991.
- Wang, W.-H. and D. M. Davis, Sandbox model simulation of forearc evolution and noncritical wedges, *Journal of Geophysical Research*, 101, 11329-11339, 1996.
- Westbrook, G. K., The structure of the crust and upper mantle in the region of Barbados and the Lesser Antilles, *Geophysical Journal of the Royal Astronomical Society*, 43, 201-242, 1975.
- Westbrook, G. K., J. W. Ladd, P. Buhl, N. Bangs, and J. G. Tiley, Cross section of an accretionary wedge: Barbados Ridge complex, *Geology*, 16, 631-635, 1988.

APPENDIX A: MCS DATA ACQUISITION AND PROCESSING

Seismic data analysis and interpretation pose the end members of a three stage process, which consists of data acquisition, processing, and interpretation. As the theory of standard processing procedures has been described in a number of works (e.g. Yilmaz, 1987), this appendix concentrates on documenting the acquisition and processing parameters used for the GINCO data. The data examples shown here are all from MCS line SO137-12, however, equivalent processing modules were used for all three profiles. During the processing sequence special attention has been devoted to the multiple attenuation modules, which are described in this appendix. The processing flow is presented in Figure A.1.

The GINCO MCS Lines were acquired during cruise SO137 of RV SONNE, using a 3 km long streamer with a maximum of 120 active channels at 25 m hydrophone spacing. Thus assuming a 50 m shot point increment, a maximum fold of 30 and a CMP distance of 12.5 m were obtained. The demultiplexed raw seismic data was stored in SEG-Y format.

Multichannel processing operations are defined as procedures which operate on several data traces simultaneously in order to suppress noise and enhance signal to gain high temporal resolution. Processing at GEOMAR was conducted using Schlumberger GecoPrakla's SEISMOS processing package and included reformatting and merging of individual profile segments to derive single lines. As the raw seismic geometry was based on the time interval between shots and thus employed the true geographical shot point coordinates, a new geometry installation was conducted to derive a constant offset and shot point interval of 50 m. A constant offset is necessary for multichannel processing as several traces are involved in the operations and thus must be distinguished by their offset. The original geometry was stored on alternate trace headers. After a first velocity analysis, a brutestack was composed after application of a bandpass filter and AGC (Figure A.2). Elimination of several noisy traces was necessary on some profile sections; these were compensated by a subsequent dip interpolation using the adjacent seven traces in the gather. Though these noisy traces would have only a limited effect on a stacked section, balanced traces are necessary for the subsequent demultiple process.

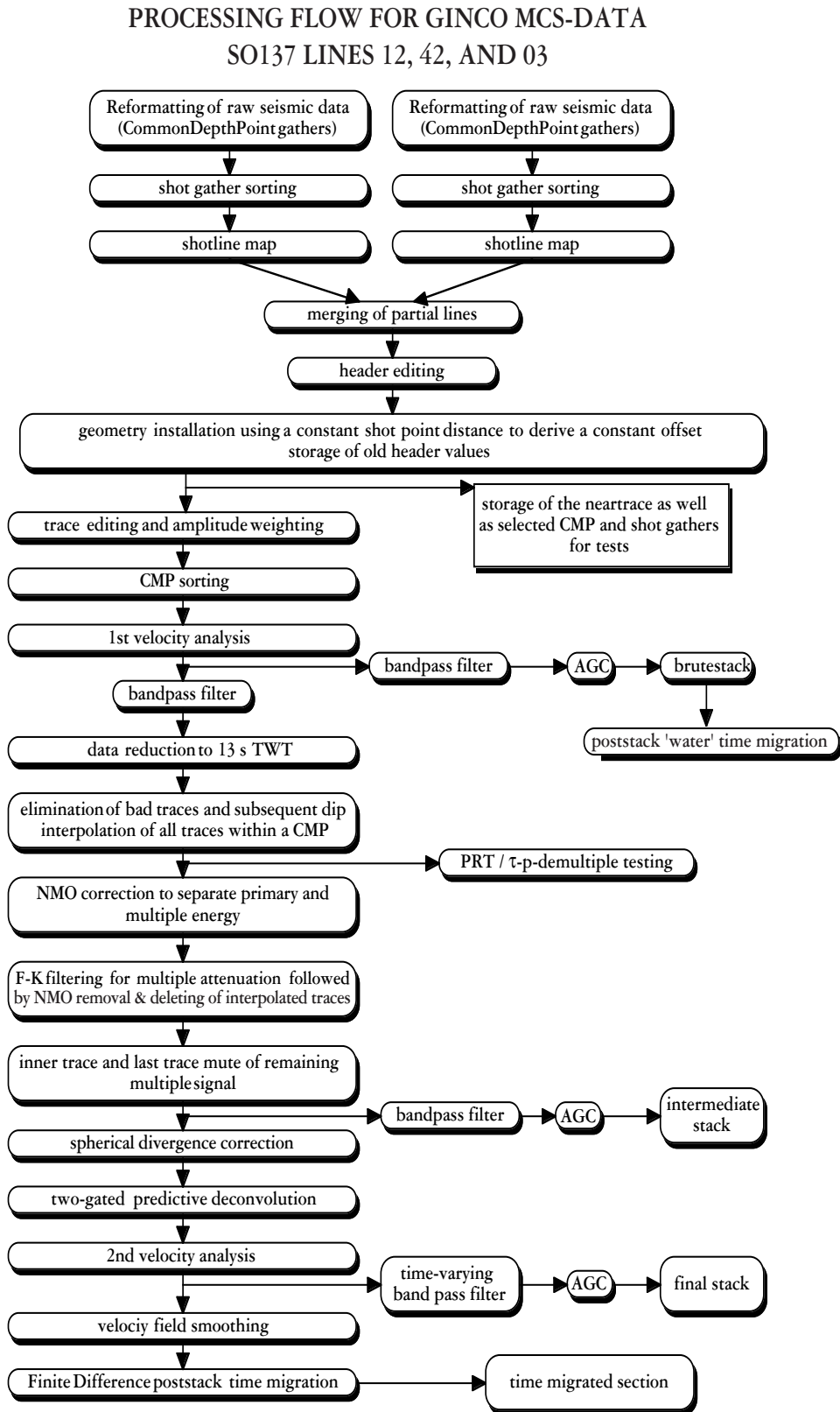


Figure A.1: Flowchart for multichannel processing; AGC=Automatic Gain Control; PRT=Parabolic Radon Transform

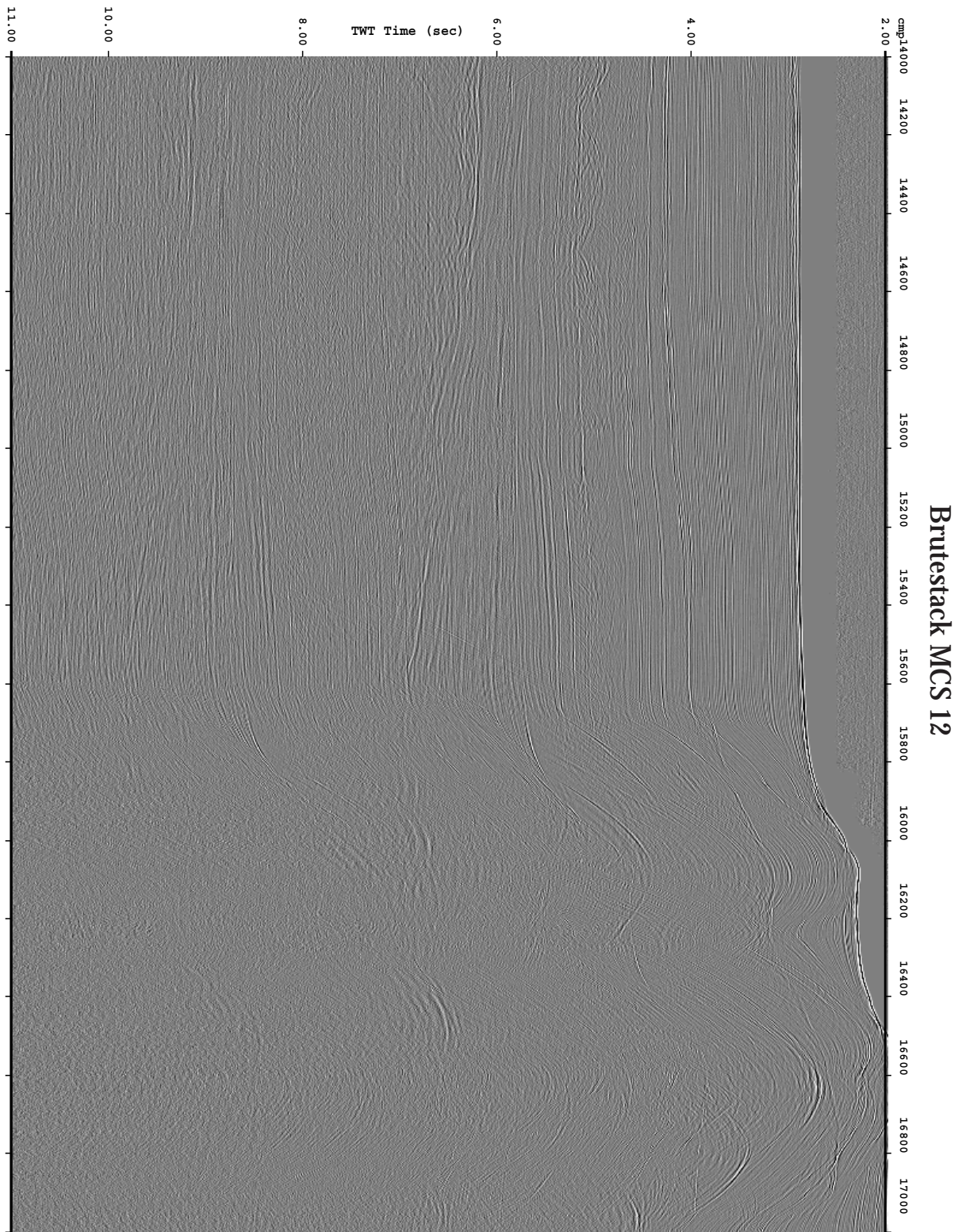


Figure A.2: Brutestack composed after first velocity analysis. Identical amplitude scaling was applied to all three stacked sections presented here (Fig. A.2, A.4, and A.7).

Multiple attenuation was conducted in the F-K domain and is based on velocity discrimination of the multiple energy. As is common with transform methods, spatial aliasing proved to be problematic. Thus a dip interpolation of traces within the CMP gather was carried out to double the fold. The F-K demultiple technique involves NMO correction to split primary and multiple events such that the primary events are over-corrected and the multiples under-corrected. This is achieved by reducing the stacking velocities by a certain percentage (varying between 82%-85% for the primary events and 95%-100% for multiples for the individual profiles).

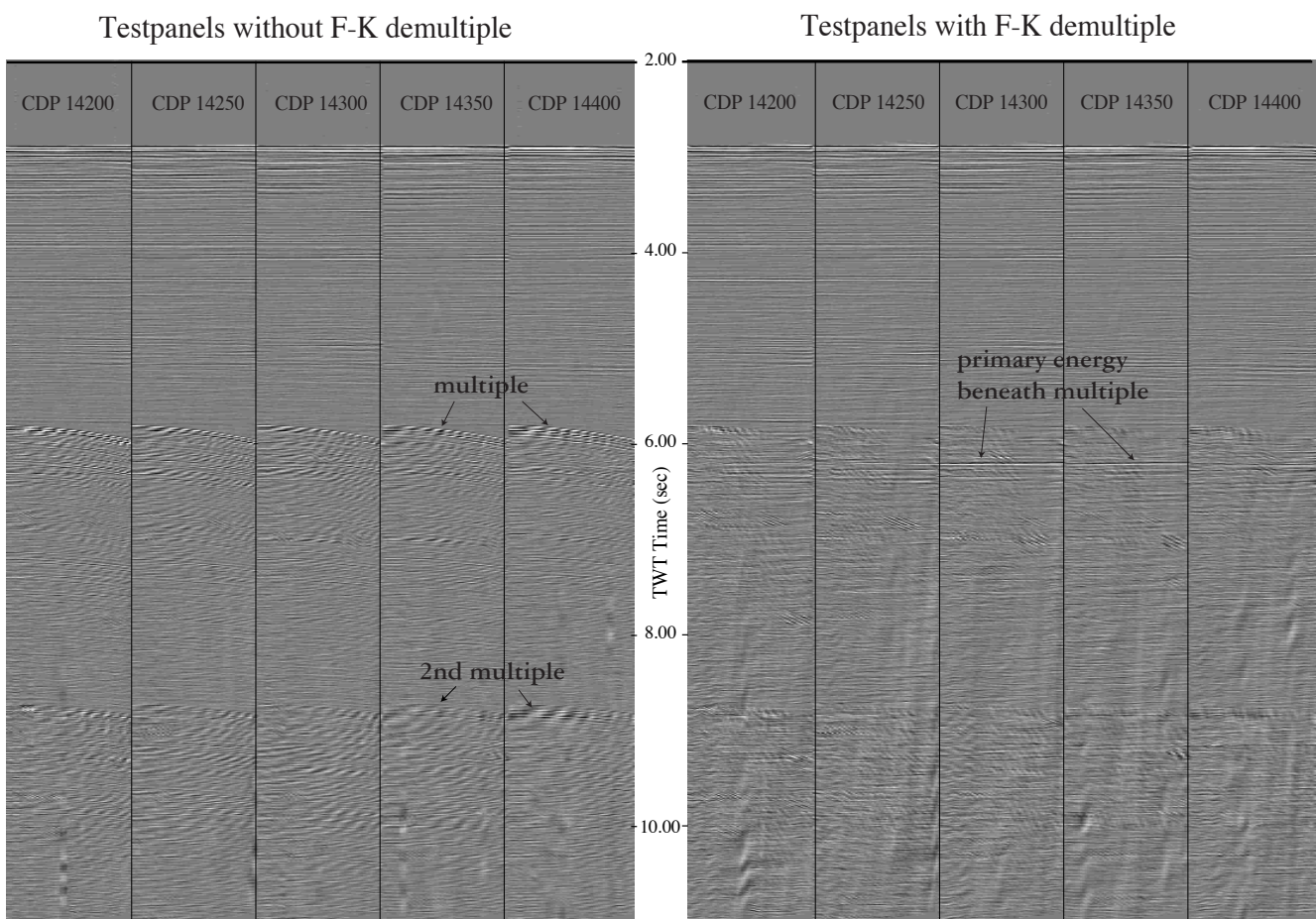


Figure A.3: Testpanels of selected interpolated CMP gathers with a fold of 59 before and after multiple suppression in the F-K domain.

Careful evaluation of the splitting minimizes the possibility to attenuate primary energy. In the F-K domain the multiple energy will now have positive wave number

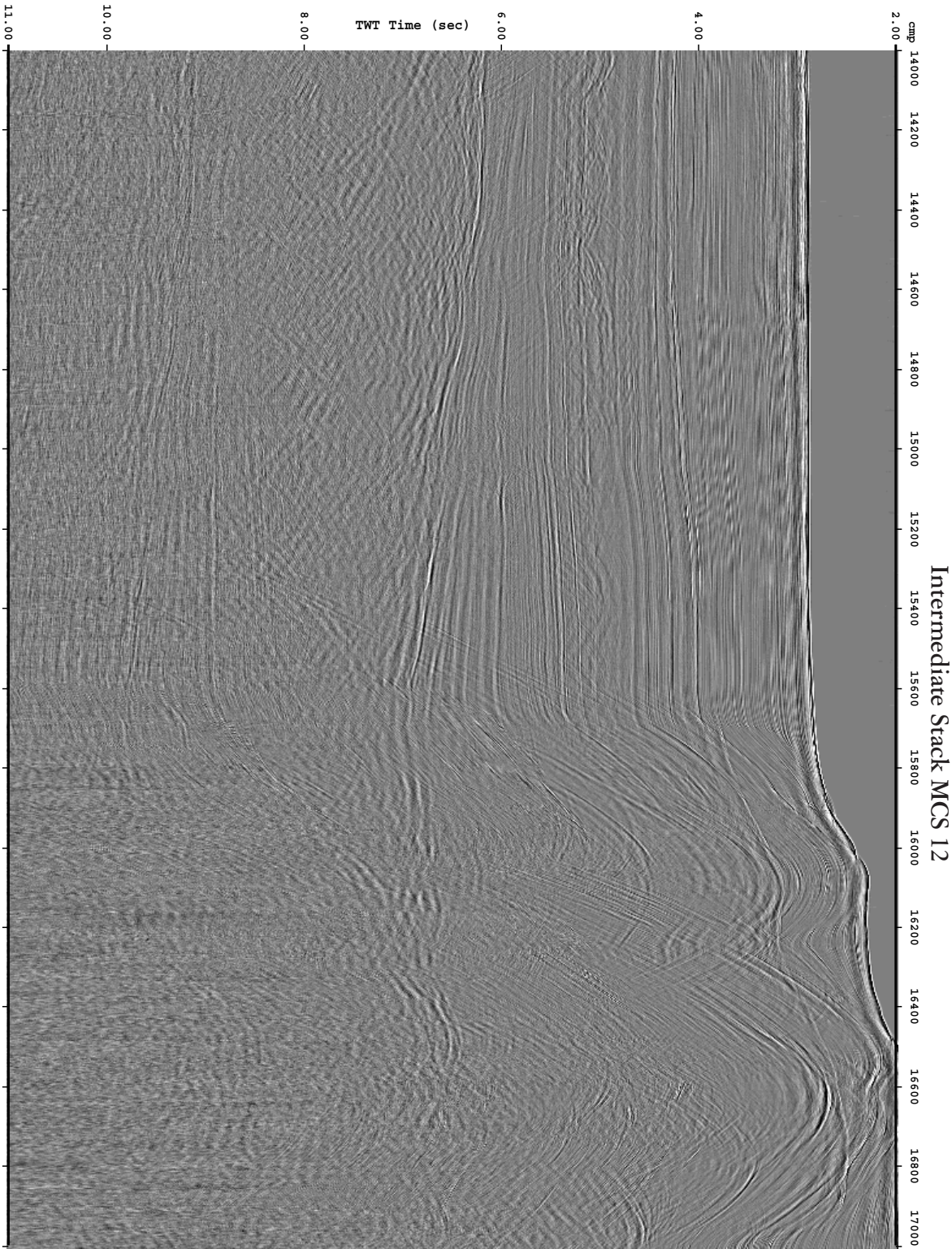


Figure A.4: Intermediate stack conducted after F-K demultiple, deconvolution and additional filtering.

values, which are rejected by the F-K filter. Design of the F-K filter was conducted interactively on the screen. An inner trace and last trace mute around the multiple window round off the demultiple process after removal of the NMO correction and interpolated traces. Application of an AGC before F-K filtering did not improve the results and was thus omitted. Figure A.3 shows selected CMP gathers before and after F-K demultiple application.

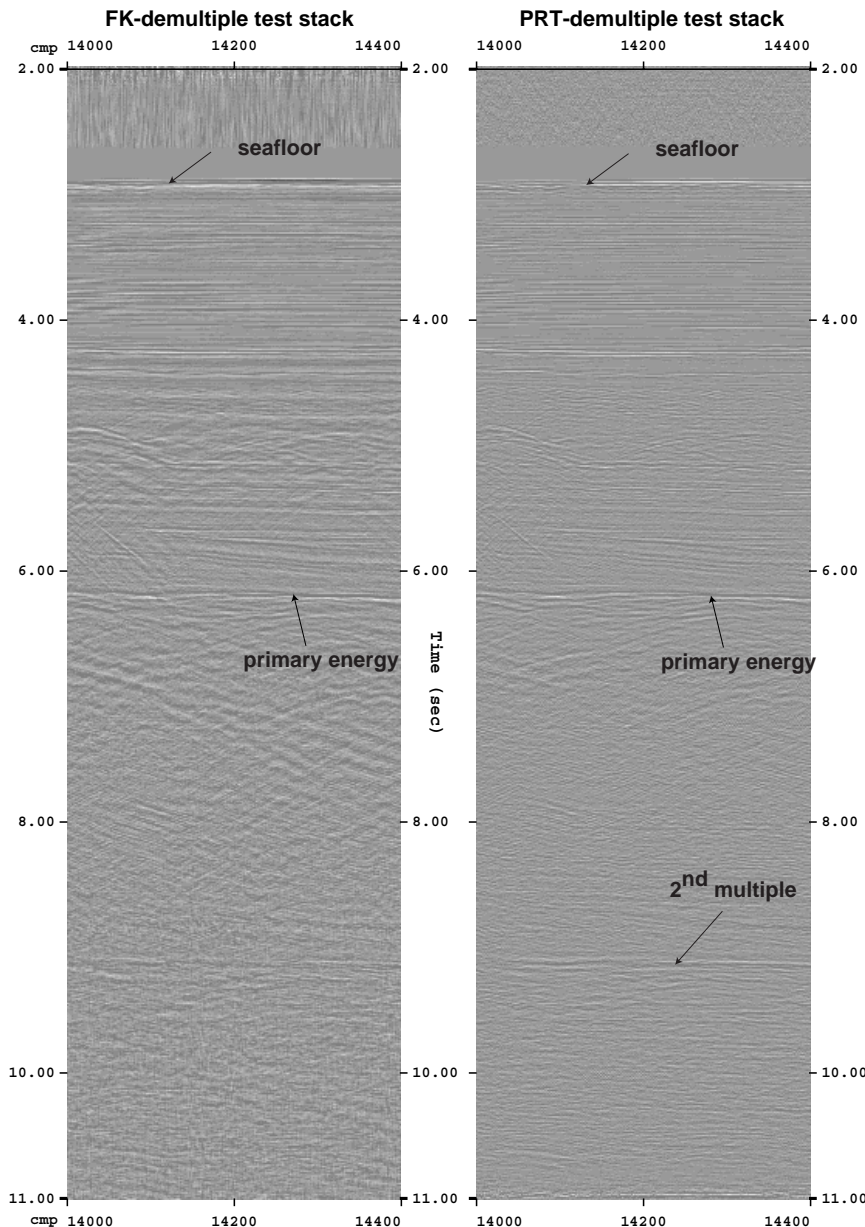


Figure A.5:
Comparison of stacks after multiple removal in the F-K and PRT (parabolic radon transform) domain on CDP range 14000-14400. The first multiple was suppressed successfully, and primary energy is now visible around 6.2 s TWT. The enormous computation time does however not justify the results, which show no improvement to the F-K-demultiple process. Remnants of the second multiple are more distinct after PRT demultiple; better results were achieved in the F-K domain.

Primary events at 6.2 s TWT underneath the multiple are recovered and clearly visible after multiple suppression. Due to aliasing effects, remnants of especially the second multiple still remain underneath the forearc basins.

Underneath the outer high and in areas with highly variable seafloor depth, the F-K demultiple technique is inhibited. This technique is based on the coherency of energy

across traces in order to successfully split primary and multiple energy. This criterion is not met in areas with a low signal-to-noise ratio or where steep dips are common, such as the accretionary prism and outer high. The intermediate stack presented in Figure A.4 shows the status after demultiple processing.

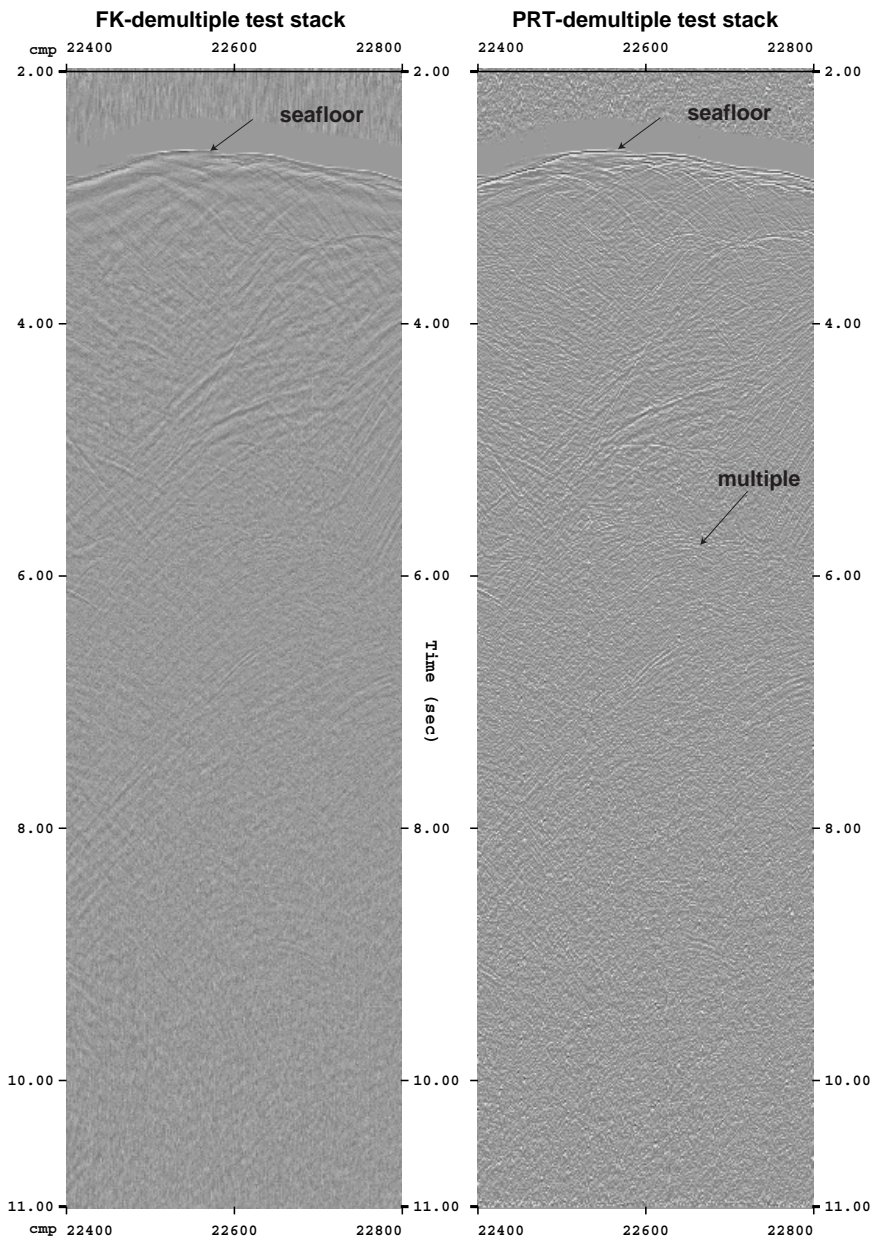


Figure A.6: Comparison of stacks for CDP range 22400-22800. Remnants of the multiple still remain after applying the PRT technique, which shows no substantial improvement to F-K multiple suppression.

A number of other demultiple techniques include the wave equation demultiple, the Tau-P domain predictive

deconvolution and the parabolic radon transform (PRT) demultiple. The latter two were tested on the GINCO data. The Tau-P demultiple process includes application of a predictive deconvolution in the Tau-P domain; however, the technique is especially sensitive to spatial aliasing and thus did not prove successful for the limited fold

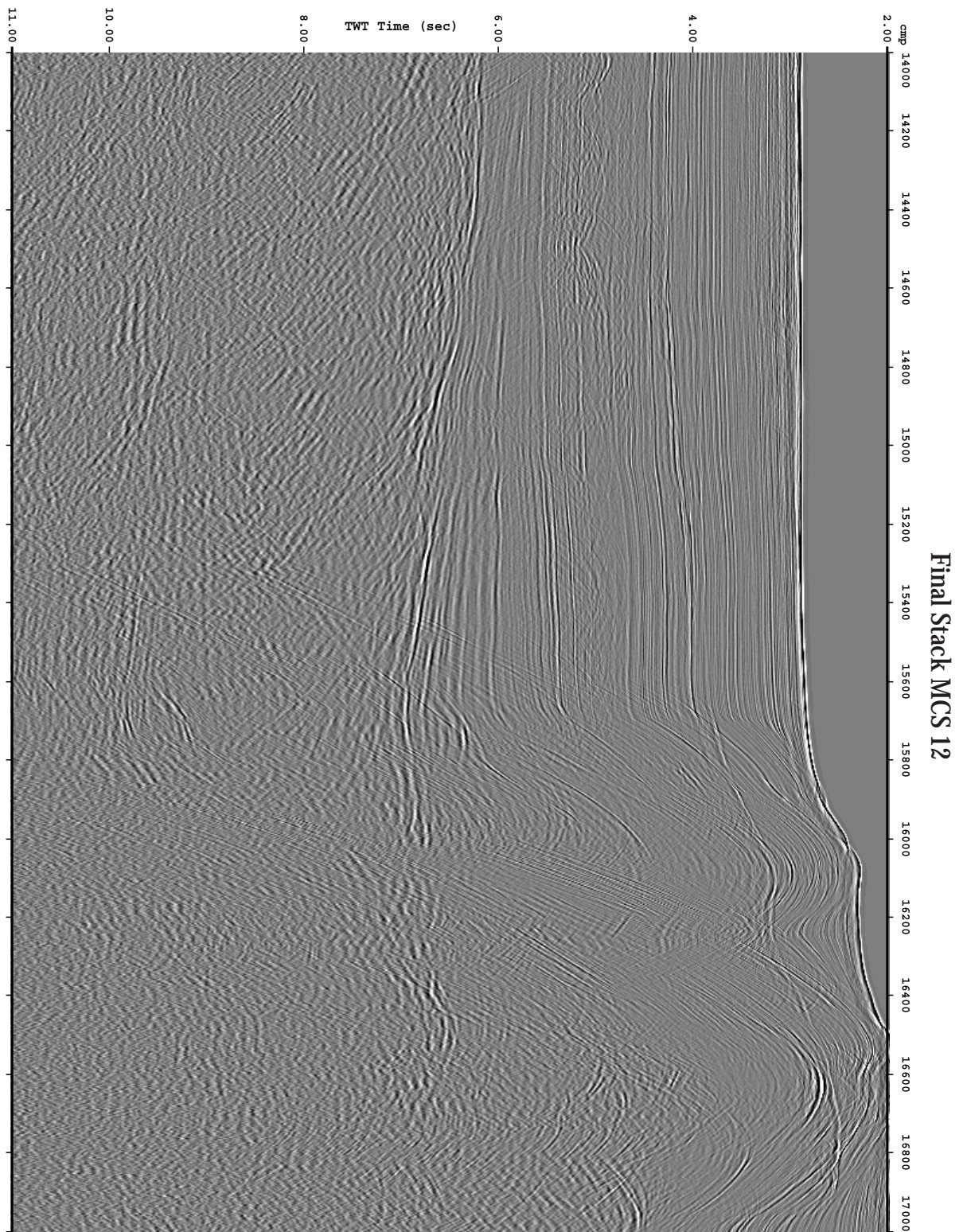


Figure A.7: Final stack after multiple attenuation, deconvolution, and second velocity analysis.

(compared to industry standard) of the GINCO data. The parabolic radon transform takes advantage of the better separation of primaries and multiples in the PRT domain, where the multiples map to higher q values because they are under-corrected after NMO-correction. Muting of the higher q values will then eliminate multiple energy. Testing of this technique showed that the needed computation time would be immense (385 hours on a SUN Sparc Ultra Enterprise 450 with 4 CPUs). 20 for the 22000 CMPs of profile MCS 12, compared to 42 hours needed for the F-K technique) and that no significant improvement compared to the F-K demultiple in the shallow or steep segments of the profile would be achieved. In addition, muting of the primaries in the PRT domain is to a high degree arbitrary, unless the separation between primary and multiple energy is very distinct, which would be true for high-fold industry data. Figures A.5 and A.6 show a comparison of the F-K demultiple stack to results achieved in the PRT domain. In the shallow forearc domain, adequate results are obtained with the PRT technique, as presented for CMP 14000-14400 in Figure A.5, though remnants of the second multiple still remain. The second multiple was better suppressed in the F-K domain, as is true for the first multiple in areas with topographic variations (CMP 22400-22800, Fig. A.6).

After a spherical divergence correction a two-gated predictive deconvolution was applied using the following parameters:

<i>Profile:</i>	<i>prediction length</i>	<i>operator length</i>	<i>pre-whitening</i>
12	12 ms	128 ms	1%
42	20 ms	128 ms	2%
03	16 ms	256 ms	1%

A second velocity analysis was conducted before stacking the data to derive the final stack displayed in Figure A.7, which shows that the multiple was further suppressed by the deconvolution and the additional velocity analysis.

To finish the processing sequence, a finite-difference poststack time migration was applied to the data using a smoothed velocity field derived from the wide-angle recordings. These sections were presented in Chapter 3.

In addition to this pre- and post-stack processing sequence, a pre-stack depth migration was conducted on a short segment of line SO137-42, covering CDP 25800 through 27300 along the seaward part of the accretionary prism and the trench. This migration was carried out to verify the velocity-depth model derived from the OBH data, which was used as an input starting model for the migration procedure. After several iterations the more detailed model displayed in Figure A.8 was derived. Though necessarily the reflection data yield a higher resolution image, the velocity information gained from the wide-angle forward modelling fits even the complex upper parts along the highly deformed accretionary complex. The results gained from the OBH/OBS modelling are sustained by the pre-stack depth migration which is independent of stacking velocities and thus yields some confidence for the wide-angle results.

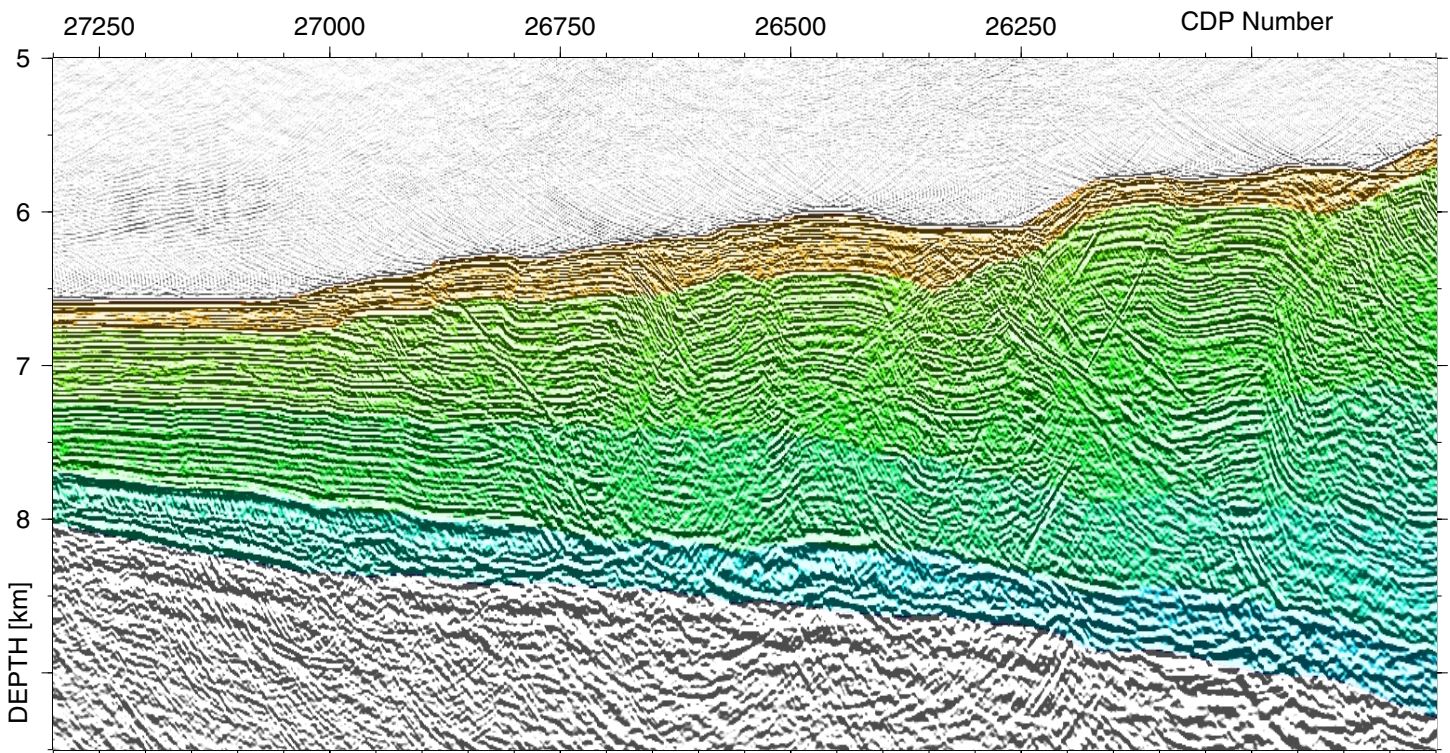


Figure A.8: Pre-stack depth migrated section of profile SO137-42 underlain by the velocity model derived from OBH forward modelling to verify refraction results.

APPENDIX B: MINISTREAMER DATA PROCESSING

During cruise SO138, additional reflection seismic data were acquired along the refraction profiles using a 250 m long three channel unit sampling at 250 Hz. Processing included a frequency filter, a predictive deconvolution, and stacking. Due to the large shot point interval of 60 s and resulting shot point distance of 150 m, any migration technique would be inhibited by spatial aliasing and would thus not yield adequate results.

A gated, time-invariant Wiener deconvolution was applied to the data using gate lengths of 3 s with a 1.5 s overlap. 11 traces were used for averaging the autocorrelation functions from which the operators were computed. Deconvolution tests for the operator length and prediction length are shown in Figure B.1 for a shallow section of profile SO138-03. A prediction length of 80 ms and an operator length of 240 ms were chosen.

The time varying frequency filter was applied after the data were shifted to a fictive plane seafloor at 11 s TWT. The panels for filter testing used frequency bands between 3-5 Hz and 80-90 Hz (Figure B.2). The following filter parameters were selected for all profiles (based on a fictive seafloor at 11 s TWT):

<i>lower stop/pass band</i>	<i>upper stop/pass band</i>	<i>100%-time (TWT in ms)</i>
7/10	90/110	11400
13/17	40/50	11900
13/17	30/40	13500

Following the filtering, a spherical divergence correction based on interval velocities was conducted on the shifted traces, using a water velocity of 1500 m/s at the seafloor and 6000 m/s 2 s TWT below the seafloor. A trace normalization with a 2 s window length was applied before the traces were shifted back to their original travel times. An NMO-correction of 1500 m/s to minimize moveout was carried out before stacking. The stacked data were filtered again using a Butterworth frequency filter characterized by a lower and upper corner frequency of 8 Hz and 90 Hz, respectively. This filtering technique shows only a small amount of ringing compared to other filters.

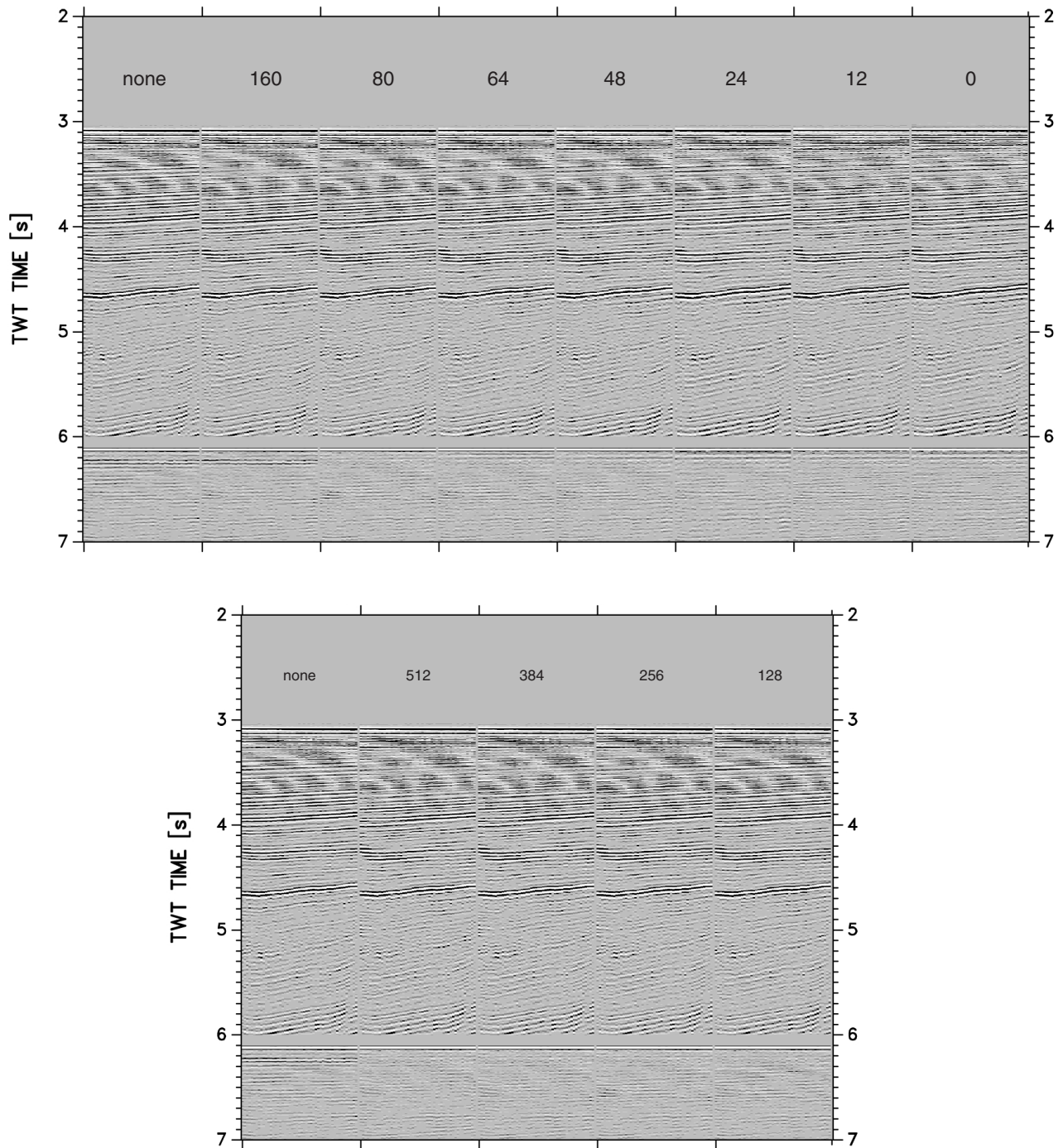


Figure B.1: Test panels to optimize deconvolution parameters. All tests were conducted on traces 1001-1050 of channel 3 along profile S0138-03. Upper image shows panels for different prediction lengths ranging from 0 ms to 160 ms for a constant operator length of 256 ms. Leftmost panel is the original undeconvolved data. The autocorrelation function is displayed in the lower part underneath the data traces. Bottomr panels display testing of different operator lengths for a constant prediction length of 80 ms.

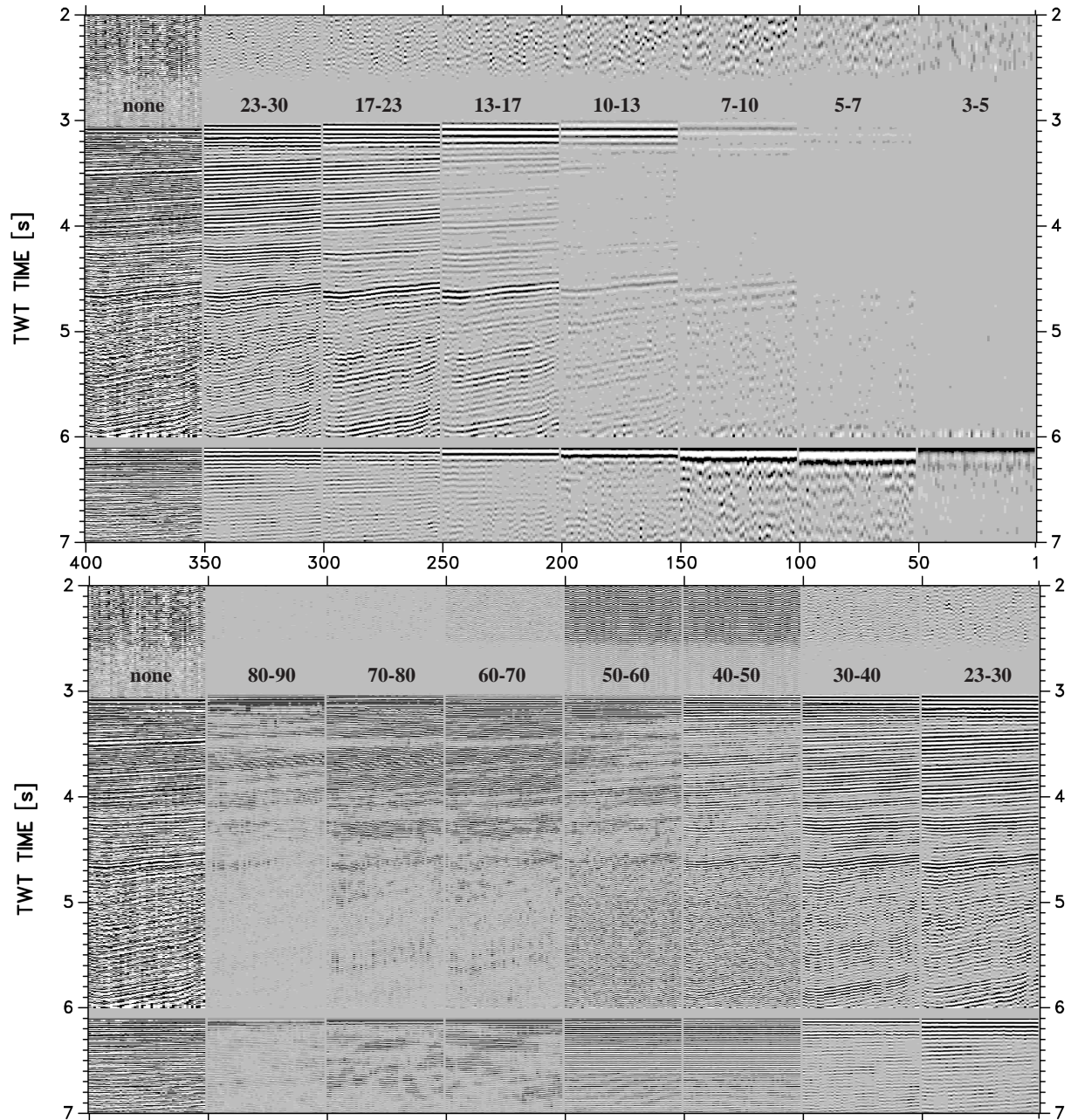


Figure B.2: Bandpass filter testing for different frequency ranges for traces 1001-1050. The leftmost panel is unfiltered.

ACKNOWLEDGEMENTS

First and foremost many thanks to the participants - scientists and crew - of SONNE cruise 138 for their professional help during data acquisition and preprocessing, which made this work possible.

I would like to thank Prof. E. R. Flueh for his continued advice and career guidance and for the many hours spent on board and on land. Numerous trips to scientific meetings and conventions were made possible through his help.

The support of Dr. D. Klaeschen and Dr. C. Kopp during data processing and modeling was essential to this study and is warmly acknowledged.

I thank Prof. W. Rabbel for spontaneously agreeing to act as co-referee.

Prof. G. Moore freely provided the RAMA data set and thus enabled the extension of the study area to central Java.

Numerous discussions with Dr. M.-A. Gutscher, Prof. R. von Huene and Dr. C. Ranero helped clarify many aspects of subduction tectonics.

Many thanks to all members of the Geodynamics Department for their assistance during the last two years, especially to Dr. J. Bialas for providing extended financial support.

Special thanks for his continuing support go to M. Léroç.

CURRICULUM VITAE

Name	Heidrun Kopp
Date and Place of Birth	January 30, 1973 in Kelkheim im Taunus
Citizenship	German
1979-1983	Pestalozzi-Grundschule, Kelkheim im Taunus
1983-1985	St. Angela Gymnasium der Ursulinen, Königstein
1985-1988	Schiller-Oberschule, Berlin
1988-1989	Laurel High School, Laurel, MD, USA
1989-1992	John F. Kennedy Gymnasium, Berlin
1992-1997	Study of Geophysics at Christian-Albrechts-Universität zu Kiel
1998	Visiting Scientist at the U.S. Geological Survey, Menlo Park, CA, USA
since 1998	Research Assistant at Geomar